# MINERALOGICAL AND PALAEOMAGNETIC STUDIES OF THE SULPHIDE - RICH SEDIMENTS OF THE WASH, ENGLAND.

A thesis submitted for the degree

of

Doctor of Philosophy

at

The University of Aston in Birmingham.

by

RICHARD JAMES SUTTILL

February, 1982.

# MINERALOGICAL AND PALAEOMAGNETIC STUDIES OF THE SULPHIDE - RICH SEDIMENTS OF THE WASH, ENGLAND.

A thesis submitted for the degree of
Doctor of Philosophy
at the
University of Aston in Birmingham, 1982.

## SUMMARY

Cores of sediment from the tidal flats of the Wash have been analysed using both mineralogical and palaeomagnetic techniques. The primary objectives were to identify the sulphide minerals and any variations in their abundance, and to determine whether palaeomagnetic dating of the sediments could be achieved and if so, whether it could be used to date any diagenetic changes in the sediments. To achieve these objectives two major fields of research were undertaken, one mineralogical and the other palaeomagnetic.

Mineralogical studies, involving petrography, X-ray diffraction, Mössbauer spectroscopy and atomic absorption spectrometry, have enabled identification of the authigenic iron-sulphides, greigite and pyrite. The presence of mackinawite is also inferred. Mössbauer spectroscopy has permitted the measurement, qualitatively, of the formation of pyrite, with depth, and has allowed the identification of the major iron-bearing minerals in the sediments. These are pyrite, chlorite, greigite, illite, montmorillonite, iron hydroxides and titano-magnetite.

Palaeomagnetic studies of the sediments show the presence of a stable natural remanent magnetization (NRM) which is post-depositional in origin. Experiments involving the natural sediment samples and redeposition experiments show the importance of measuring the water content of unconsolidated sediments, when attempts to interpret their early magnetization are being made. Compaction, resulting in decreased water content, is identified as the principal process involved in the fixation of the NRM.

Analysis of the declination and inclination records from the cores shows the usefulness of palaeomagnetic dating. This is achieved by matching the records from the cores with those of the geomagnetic record for Great Britain. The dating of the sediments can be used to date diagenetic and sedimentological events within the sedimentary sequence and to calculate sedimentation rates.

Finally, rock magnetic experiments and mineralogical observations have identified multidomain titanomagnetite as the principal remanence carrier. Other minor ferromagnetic minerals are greigite, and a "hard" magnetic material (haematite or goethite).

KEYWORDS: Tidal sediments/Sulphides/Palaeomagnetism/
Mössbauer spectroscopy.

RICHARD JAMES SUTTILL.

Acknowlegements.

The author would first like to thank NERC for the receipt of a NERC studentship without which this work could not have been conducted. Assistance from a NERC research grant (GR3/3010) entitled "Sulphides in the sedimentary environment - a mineralogical and palaeomagnetic study" under the direction of D.J. Vaughan and P. Turner is also gratefully acknowledged. Financial support from the University of Aston enabled purchase of equipment for the research.

Assistance from colleagues in other Universities, in the form of practical help involving the use of their equipment and also helpful discussions is also acknowledged. In particular I should like to thank Dr. W.H. Owens, University of Birmingham, for use of the alternating field demagnetization equipment, Prof. D.W. Collinson, University of Newcastle upon Tyne for the use of the palaeomagnetic equipment at the Nuffield Palaeomagnetic Laboratory, and to F. Addison, University of Newcastle upon Tyne for the measurements of magnetic anisotropy.

I would also like to make special thanks to my research supervisors, Dr. D.J. Vaughan and Dr. P. Turner for their invaluable help and encouragement with regard to the planning and execution of this research. The assistance of the other members of the academic staff at the Department of Geological Sciences, University of Aston in Birmingham is also gratefully acknowledged. Finally, I would like to thank my parents for their help and patience during the preparation of this thesis.

CONTENTS

CONTENTS (continued).

CONTENTS (continued).

CONTENTS (continued).

LIST OF FIGURES.

LIST OF FIGURES (continued).

LIST OF FIGURES (continued).

LIST OF FIGURES (continued).

LIST OF FIGURES (continued).

LIST OF FIGURES (continued).

LIST OF TABLES.

LIST OF PLATES.

LIST OF PLATES. (continued).

LIST OF PLATES (continued).

## Chapter 1.

### Introduction.

The Wash embayment is situated on the eastern coast of England between the counties of Lincolnshire and Norfolk. It is roughly rectangular in shape with an area at high-water and with a spring tide of 183000 acres and at low-water with a spring tide its area is 88000 acres (Hydraulics Research, 1958). The present feature (figure 1-1) represents the infilled portion of a much larger depression cut into Jurassic and Cretaceous rocks.

The sediments being deposited in the Wash at the present-day are mainly tidal flat and beach deposits. It is the tidal flat deposits, in which the early formation of diagenetic iron sulphides is taking place (Love, 1967), that are the subject of this project. Surrounding the tidal flat sediments is a plain of earlier Holocene sediments called the Fenland (figure 1-1), the inner parts of which are often below sea-level. Today the present-day tidal flats are seperated from older tidal flat areas, and from the Fenland, by a series of sea defences in the form of artificial earth embankments built in historical times to extend agricultural land use onto the tidal flat areas. The effect of these on the sediment accretion rates has been studied (Inglis and Kestner, 1958; and Amos, 1974) and will be further examined in this project with specific reference to the palaeomagnetic dating of the tidal flat sediments.

The aims therefore of this project are twofold, falling broadly into mineralogical and into palaeomagnetic fields. The mineralogy of tidal flat sediments, and of those in the Wash in particular, has already received the attention of previous workers. The sediments of the Wash were first analysed by Hardy

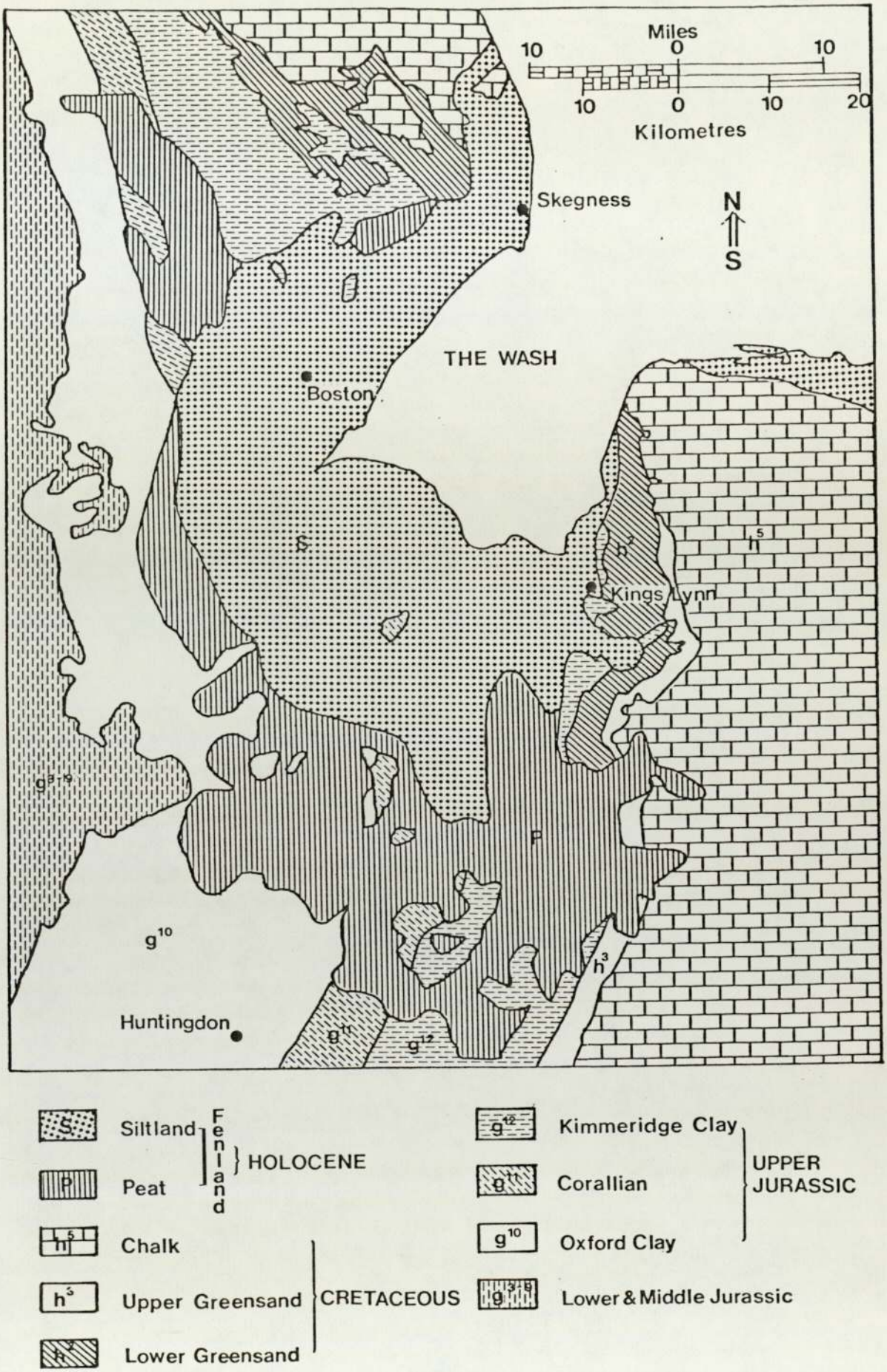


Figure 1-1. Geological map of the Fenland and Wash embayment.

(1920) who studied their whole sediment mineralogy. Later work by Evans (1965) also reported on the whole sediment mineralogy. More recently, studies have been made of the sulphide mineralogy, Love (1967), the heavy minerals Chang (1971), and the clay mineralogy Shaw (1973). In this work one of the major mineralogical aims is to study the iron-bearing mineralogy of the sediments in order to determine its effect upon the magnetic properties of the sediments. This involved first looking at the whole sediment mineralogy of the sediments by standard optical petrography, the scanning electron microscope and by X-ray diffraction (see Chapter 2). The work of Love (1967) has shown that iron sulphide diagenesis is taking place within the tidal flat sediemnts and thus, it is important to determine the effect of this on the bulk magnetic properties of the sediments. One of the factors important in the diagenesis of the iron sulphides is the source of the iron involved in their formation. In order to monitor the distribution of iron, the clay mineralogy of the sediments was studied since, the clay minerals are important iron-bearing minerals in the essentially fine-grained sediments of the tidal flat sediments. The major method of studying the clay mineralogy of the tidal flat sediments used here is X-ray diffraction of clay mineral concentrates discussed in Chapter 3.

Another technique used to study the clay mineralogy of the clay minerals containing iron, and indeed the whole iron-bearing component of the Wash sediments, is Mössbauer spectroscopy. A detailed study of Mössbauer spectral analysis of the samples from the Wash sediments is discussed in Chapter 4. Analysis of the sediments using Mössbauer spectroscopy enables firstly, the identification of the iron-bearing mineralogy of the Wash sedime-

nts (although the technique does in some instances require other mineralogical evidence). Secondly, the location of the iron in different structural sites in minerals can also be determined, as can the oxidation state of that iron. Finally, the magnetic ordering of iron in particular mineral groups can also be determined. Using this knowledge it is possible to calculate the concentrations of iron in individual minerals or mineral groups as a percentage of the total iron in any particular sample, and hence it is possible to monitor changes in the distribution of iron through a sequence of sediments. An example of this is shown in chapter 4 where Mössbauer spectroscopy is used to show the formation of pyrite which is occuring as a result of early diagenesis within the sediments. The possibilities of using this information in measuring the rates of diagenetic processes in these and in other sedimentary sequences will also be discussed.

The principle aim of the palaeomagnetic study of the Wash tidal flat sediments is to establish if palaeomagnetic dating of these sediments is possible, and if so, how it can be used to date events in the history of the sediments, such as changes in the sedimentation rates or diagenetic changes within the sediments.

Before it is possible to attempt to answer these questions, it is necessary firstly, to establish whether the unconsolidated sediments of the Wash are capable of carrying a natural magnetic remanence. In many studies of Recent unconsolidated sediments it has been shown that the sediments do record a stable magnetic remanence. However, only one previous study of the magnetic properties of tidal flat sediments is known to the author, which is a work by Graham (1974), in which it is shown that the sediments of the tidal flat area of San Francisco Bay do record a stable magn-

etic remanence. In the work by Graham (1974) a sequence of sediments was not studied, and hence it was not possible to use the results for palaeomagnetic dating, however, it was implied that this might be attempted in the future.

There have, however, been many palaeomagnetic studies of unconsolidated sediments from other environments of deposition, the most popular of which is the lacustrine environment, which since the early work of Mackereth (1971) who examined the sediments of Lake Windermere, England, has provided a great deal of knowledge on the behavoir of the geomagnetic field during Holocene times (see for example; Creer et al. (1972), Creer et al. (1975), Creer et al. (1976), Creer et al. (1979), Dickson et al. (1978), Noel (1975), Palmer et al. (1979), Stober and Thompson (1977), Thompson and Kelts (1974) and Thompson (1977)). One of the results of these studies is that it is now possible to draw master curves, with which to compare other data, of the secular variation of the Earth's magnetic field, one such master curve compiled by Thompson and Turner (1979) shows the variation of the declination and inclination of the geomagnetic field between 10,000 and 0 yr B.P.. Other environments from which palaeomagnetic dating has been shown to be possible are; the sediments of the abyssal plain, as in the the study of sediments from the Tyrrhenian Sea by Blow and Hamilton (1974), sediments from the Black Sea by Creer (1974), sediments from the partially infilled glacial trough of the Inner Sound, Scotland by Bishop (1975) and even cave sediments (Creer and Kopper, 1976).

Lake sediment studies have remained popular for several reasons; because of their relative ease of sampling, because the finely laminated varve sediments of which they are formed provide

an excellant lithology for recording the stable magnetic remanence, and because the sequences encountered in lake sediments are often continuous and unbroken. There are, however, a number of disadvantages which have led palaeomagnetists to seek suitable sedimentary sequences in other sedimentary environments. Lakes for example, are limited in their geographical extent, large areas may contain no suitable lakes and problems may also arise with correlation between sequences in different lakes. Also many lake deposits show large areas of slumped sediments, especially near to the margins of the lakes, clearly these sediments must be avoided in palaeomagnetic studies.

In this study therefore, it is the aim to show how the sediments of Recent tidal flats may be used in palaeomagnetic studies. This is particularly important in the study of tidal flat sediments since few other techniques are suitable for the dating of these sediments. Tidal flat sedimentary sequences are made up of units deposited at greatly varying sedimentation rates (Amos, 1974) which make the extrapolation back in time of present-day sedimentation rates meaningless, unless careful interpretation of changes in the environments of deposition are taken into account. It will be shown in this study how palaeomagnetic dating of the sediments using secular variation can be used to recognise these changes in sedimentation rates.

The most important priority in interpreting the palaeomagnetism of any sequence of rocks or sediments is to determine the nature and origin of the natural remanent magnetization (NRM). In the studies of lake sediments it has been found that in many instances the natural remanent magnetization of the sediments is carried by detrital grains , usually by magnetite, and that this

remanence is often modified after deposition to give a post-depositional remanent magnetization (PDRM) (see for example, Irving and Major, 1964; Stober and Thompson, 1977). However, in some sequences of unconsolidated sediments it has been suggested that there may be an important component of chemical remanent magnetization (CRM), greigite ($Fe_3S_4$) in sediments from the Mediterranean Sea has been suggested as one carrier of this CRM (Hedley and Vandievoet, 1980) whilst in mud turbidites from Lake Zurich, Switzerland, Giovanoli and Kelts (1980) have suggested that chemically unstable sulphide minerals may be capable of carrying a stable CRM for thousands of years at low-temperatures.

Clearly, therefore, it is necessary at an early stage to; firstly, determine if the tidal flat sediments are carrying a stable magnetic remanence, and if so, what is the nature of this remanence? (for example, is it a DRM, PDRM or CRM?) and finally, to determine the minerals which are the carriers of the magnetic remanence?. The first of these questions is discussed in chapter 6 where data from cores of sediment is used to show that the remanence is stable, and that it is post-depositional in origin, agreeing in part with the conclusions of Graham (1974). The mineralogy of the remanence carriers is discussed in detail in chapter 7. Identification of the remanence carriers has been made by using a variety of rock magnetic experiments, and by using standard mineralogical techniques.

Finally, in chapter 8, it is shown how the mineralogical studies of the tidal flat sediments can be used to interpret some of the palaeomagnetic variations observed. Also there is a discussion of the usefulness of joint palaeomagnetic and mineralogical studies of tidal flat sequences, both in terms of their

mutual benefits and in trying to combine the data to measure rates of chemical processes, in this case, the diagenetic formation of iron sulphides. Mention is also made of the effect of early iron sulphide diagenesis on the magnetic remanence of tidal flat sediments and of what contribution, if any, this makes to the natural remanence recorded by the sediments.

Chapter 2.

## Sedimentology, Mineralogy and Geochemistry of the Recent Sediments of the Wash.

### Introduction.

In this chapter the sedimentology of the areas studied will be described together with a discussion of their whole sediment mineralogy and geochemistry. The sedimentology of the cores collected in this study and of the sites where the cores were collected will be described. Sedimentological features of the tidal flats must be studied because as is shown later they are important in explaining some of the variations observed in the mineralogy and palaeomagnetic properties of the tidal flat sediments. Firstly, we must characterise the tidal flat environment. A sedimentological classification of shorelines by Davies (1964); Hayes (1976) and Hayes and Kana (1976) stresses the importance of tidal range, in which shorelines are divided into three divisions: microtidal, <2 metres; mesotidal, 2-4 metres; and macrotidal, >4 metres. Tidal flats occur in low wave energy, mesotidal and macrotidal settings. The tidal flats of the Wash embayment are deposited within a macrotidal range in which the present tidal variation is 6.3 metres (Admiralty Tide Tables, 1980).

In describing the tidal flat the terminology of Gary et al. (1972) and Rieneck (1975) will be used, in which the tidal flat is subdivided into three zones; above high-water is the supratidal zone; seaward of this is the main part of the tidal flat, the intertidal zone; finally below low-water is the subtidal zone.

The first significant study of tidal flats published in English was a paper by Hantzschel (1955). One of the main features

of tidal flat sedimentation recognised by Hantzschel (1955) is the seaward coarsening in grain-size of the sediment. Hantzschels' (1955) work is also important in identifying some of the major problems in the study of tidal flat sedimentation. Firstly, the source of the mud fraction is identified as a major problem, is it merely a product of reworking? or is new clay material continuously being formed? An attempt to solve this problem using detailed X-ray diffraction analysis of the clay minerals is discussed in Chapter 3. Hantzschel (1955) also identifies the problems involved both in the recognition of criterea for the identification of tidal flat sediments in ancient sequences and also the problem of distinguishing between ancient intertidal flats and those of subtidal origin. Finally, Hantzschel (1955) recognises one of the most interesting problems of clastic tidal flat sediments, the problem of diagenesis and its role in the study of their geochemistry.

Hantzschel (1955) had worked on the tidal flat sediments of the German coast, later work by van Straaten (1961) showed that a similar seaward coarsening sediment distribution can be recognised on the Dutch coast. In describing the source area of the sediments deposited in the tidal flats van Straaten (1961) stresses that the source of all tidal flat sediments is from nearshore, subtidal areas. Only in some parts of the estuaries is a significant fluvial contribution found.

Prior to this work van Straaten (1952a and 1952b) made some important observations on the distinction between vertical and lateral sedimentation processes which occur in the tidal flat environment. Vertical sedimentation is said to result from subsidence which permits a net accumulation of sediments as the

depositional interface remains at a datum corresponding to present environmental processes. Lateral sedimentation is primarily a reworking process involving the migration of meandering channels or creeks, similar to the processes operating on a fluvial flood plain.

Van Straaten (1952a) produced an idealized section through the sediments of the Dutch, Wadden Sea in which he divided the sedimentary sequence of the tidal flat into four units: the marsh deposits, the higher flat deposits, the low flat deposits and the channel deposits. Another important feature which van Straaten (1952a) recognises is the significance of the variation in colour with depth of the sediments, and the dependance of this colour on the oxidation state of the sediments. These zones van Straaten (1954) assigned to represent, from top to bottom, hydroxidic, monosulphidic and bisulphidic zones.

An extensive series of publications in the late 1950's and early 1960's by Rieneck discussed the sedimentary structures of tidal flat sediments, these works are readily summarized in Reineck and Singh (1975). Also summarized in Reineck and Singh (1975) are the physical parameters needed for the development of a tidal flat sequence, these are a gently dipping sea with marked tidal rhythms where there is a source of sediment and strong wave action is absent. These conditions are met by the Wash embayment which is formed on a shallowly dipping sea coast with a macrotidal, tide range and low wave activity due to the protected nature of the embayment.

The next major work concerning the study of tidal flats was an analysis of the environments of deposition of intertidal sediments in the Wash, by Evans (1965). In the tidal flat sediments

of the Wash, Evans (1965) was able to recognise seven sub-environments of deposition, the first six of which are arranged parallel to the shoreline. These are, begining with the most landward: the salt marsh, the higher mud flat, the inner and Arenicola sand flats, the lower mud flat, the lower sand flat, and finally, the creeks and bordering areas which cross all the other sub-environments of deposition. Using the nomenclature of Gary et al. (1972) the salt marsh sub-environment of deposition belongs to the supratidal zone whilst the remaining sub-environments are found within the intertidal zone.

In this study the sediments belonging to the salt marsh, higher mud flat and Arenicola sand flats have been studied. The salt marsh is the most landward of the sub-environments of deposition and is only flooded at high-water spring tides, which means that it is able to support a cover of marsh plants. At Freiston Shore, and at Leverton (areas studied here) the salt marsh passes seaward into the higher mud flats, but in some areas it is bounded by a small cliff (Kestner, 1962). Crossing the salt marsh are the creeks which degenerate inland into a series of shallow elongate depressions. Evans (1965) has termed these bare muddy depressions as salt pans, they are derived from degenerated creeks or are inherited from depressions in the original mud flat. An interesting feature of these salt pans is the development of mud cracks as a result of desication during long periods of exposure. If a trench is cut through such a salt pan it can be seen that the mud cracks break through the fine parallel lamination of the sediments, and that, the polygonal mud flakes that they produce are preserved at depth, often still with their upturned edges intact. Thus a mudcrack-conglomerate or breccia deposit is formed. The deposits

of the salt marsh are laminated silty clays and clayey silts with small amounts of sand. Evans (1965) records that in the outer part of the salt marsh, laminae of sand and mud alternate, further inland the sandy laminae decrease.

The higher mud flat sub-environment of deposition occupies a zone which projects seawards along the creeks giving its seaward edge a cuspate form. The surface is generally irregular showing a series of elongate depressions and shallow drainage channels seperated by raised areas vegetated with the alga Enteromorpha sp. In the depressions the eel-grass Zostera sp. is found.

Evans (1965) has described the sediments of the higher mud flat as consisting of laminated or thinly laminated silty sands and sandy silts with less than one per cent of the sand belonging to the fine sand grade and the remainder to the very fine sand grade. The sandy laminae decrease in number and thickness when traced inland, with a complementary increase in the proportion of mud. Trapping of the sediment by the matted filaments of the alga Enteromorpha sp. is an important process in building up the higher mud flat which produces a sediment with a banded structure that is often preserved when the algal material has decayed.

The final environment studied in this work consists of the inner and Arenicola sand flats which extend seawards from the outer edge of the higher mud flats to the begining of the slope upon which the lower mud flats are deposited. Immediately to the seaward of the higher mud flats, the inner sand flats occur and are characterised by either a smooth or a rippled muddy surface. The Arenicola sand flats have a distinctive surface morphology consisting of weel-rippled sand with abundant casts of the worm Arenicola marina. Evans (1965) has described the inner sand flats

as consisting of sands and silty sands containing more fine-grained material than those of the Arenicola sand flats. Five to ten percent of the sands belong to the fine sand grades and the remainder to the very fine sand grades. The sorting of the sediment grain-size is poorer than that of the Arenicola sand flats, and the median grain-size is slightly smaller. The deposits generally show a less well-developed stratification than those of the higher mud flats and those of the salt marsh. Symmetrical ripple-marks are common and are aligned parallel to the coast. The main feature of the inner sand flats is the abundant evidence of burrowing activity by the crustacean Corophium sp.

The Arenicola sand flat also is strongly bioturbated and little of the initial stratification is preserved, indeed the deposits are named after the main organism responcible for this bioturbation, Arenicola marina. Evans (1965) has described the sediments of the Arenicola sand flats as being composed of sands with minor amounts of finer-grained material, between 8 and 18% of the sand belonging to the fine sand grades. The sands are the best-sorted sediments of the intertidal flat area. The remaining subenvironments of deposition on the tidal flat, the lower mud flat and lower sand flat are not studied here but are described in Evans (1965).

As described briefly in the introduction, (chapter 1), one of the main aims of this work is to examine the early diagenesis of iron sulphides in the tidal flat sediments, since this may have an important role in modifying the natural magnetic properties and remanence of the sediments. In order to do this a broader examination of the whole sediment mineralogy of the Wash sediments has been carried out (section 2-2) with a more detailed

examination of the clay mineralogy in chapter 3 and of the iron-bearing mineralogy in chapter 4. Firstly, a review of the previous work on the mineralogy of the Wash tidal flat sediments is provided.

A study of the mineralogy of the Wash sediments was first published by Hardy (1920) who described the sediments as containing a majority of sub-angular quartz grains with a few grains of feldspar and approximately twelve percent of heavy minerals. The similarity of the sub-angular quartz grains to those found in boulder-clay deposits was observed by Hardy (1920) and gives an important clue to the source area of the sediments as is discussed later. Hardy (1920) also listed the heavy minerals in approximate order of abundance as; blue-green hornblende (arfvedsonite), magnetite, glauconite and chlorite, aragonite (in the form of shells and broken ooliths), dolomite, ferriferous chert, augite and tourmaline. Lesser amounts of rutiles, muscovite, biotite, staurolite, epidote, zircon, kyanite, apatite and garnet are also recorded.

Evans (1965) also records that the heavy minerals constitute twelve percent of the sediment. In addition to the heavy minerals recorded by Hardy (1920), Evans (1965) includes sillimanite, zoisite and clinozoisite. The light fraction of the sands, Evans (1965) observes as consisting of quartz, mica, orthoclase (0-15%) and plagioclase (2-3%).

The carbonate mineralogy of the sediments is described by Hardy (1920) as consisting of aragonite in the form of shell fragments and prisms possibly derived from echinoids, oolitic grains described as highly ferriferous and altered by iron and magnesium, also observed are "fresh" looking crystals of dolomite. Hawker

(in Hardy, 1920) suggests a diagenetic origin for these. Evans (1965) records the carbonate content of the sediments as between 1.5 to 10.5 percent (expressed as $CaCO_3$) and being greatest in the finer-grained sediments.

The clay mineralogy of the tidal flat sediments, is studied in more detail in chapter 3, however, a brief review of the literature is included here as the clay minerals form an important part of the mineralogy of the sediments, particularly of the finer-grained sediments. In the study of the sediment sample from Friskney, Hardy (1920) examined the "finer fraction of the silt" using transmitted light microscopy and was able to identify only quartz, muscovite, zircon, and calcareous matter (probably miss-identified clay minerals). A much later work using X-ray diffraction techniques (Shaw, 1973) is the first detailed study of the clay minerals of the Wash tidal flat sediments. In the work of Shaw (1973) the major clay minerals present in the Wash intertidal flat sediments are identified as; illite, kaolinite, mixed-layer illite-montmorillonite, montmorillonite and chlorite. In the present study a more complete analysis of the clay mineralogy of the tidal flat sediments is made (see chapter 3).

The other important mineralogical aspect studied in this work is the sulphide mineralogy of the tidal flat sediments (chapter 5). Love (1965) has described the formation of pyrite in the intertidal flat sediments at Freiston Shore (grid reference, TF 397425) and how the sedimentary pile has a colour zonation dependant on the oxidation state of the sediment. The work by Love (1965) uses optical methods (of glycerine mounts) and geochemical methods to show the formation of the iron sulphides. In this work the sulphide mineralogy of the sediments is analysed

using optical methods and Mössbauer spectroscopy (discussed in chapters 4 and 5 respectively). The contribution of the iron sulphide minerals to the magnetic properties of the sediments is also examined.

Finally a geochemical study (see section 2-4) of the Wash tidal flat sediments analysed here is described. The objective of the geochemical study is to provide quantitative data on the distribution of the major elements and to determine the variation of these major elements with respect to changes in lithology (arising from changes in the environments of deposition). The variations in the geochemical data are compared, with the help of statistical analysis, to the variations observed in the mineralogy of the different lithologies encountered in the three subenvironments studied here.

## 2-1. Sedimentology and whole sediment mineralogy of the tidal flat sediments of the Wash.

### 2-1-1. Collection and Sampling.

The collection of the samples used in this study was largely determined by the requirements of sampling for the palaeomagnetic measurements. This has meant that nearly all of the sampling has been from cores of sediment. The specific methods used for coring and the restrictions imposed when sampling for palaeomagnetic measurements are, therefore, explained in the chapter on palaeomagnetism (chapter 6). Naturally the need for cores of sediment, particularly for the longer cores, also brought about further restrictions on the choice of sampling area (also discussed in chapter 6).

Initially, sampling was undertaken on the tidal flat at Freiston Shore, grid reference TF 408421, (figure 2-1) where four one-metre cores of sediment were collected from the higher mud flat subenvironment, forming together a composite sequence through the upper part of the modern tidal flat. The location of Freiston Shore was chosen because it has in the past been studied by several workers (Evans, 1965; Amos, 1974) and in addition it has good access. The rate of deposition at Freiston Shore is more rapid than at areas lying further to the east, and so for comparison, a further one-metre core of sediment was collected from the the tidal flat at Wrangle Flats, grid reference TF 457486.

Because of the relatively fast sedimentation rates in the Wash (Amos, 1974 gives an average sedimentation rate for the whole of the tidal flat as 8mm $yr^{-1}$) and because of the need for a core of sediment deposited over a longer period of time than that represented by a one-metre core it was decided to try to collect a

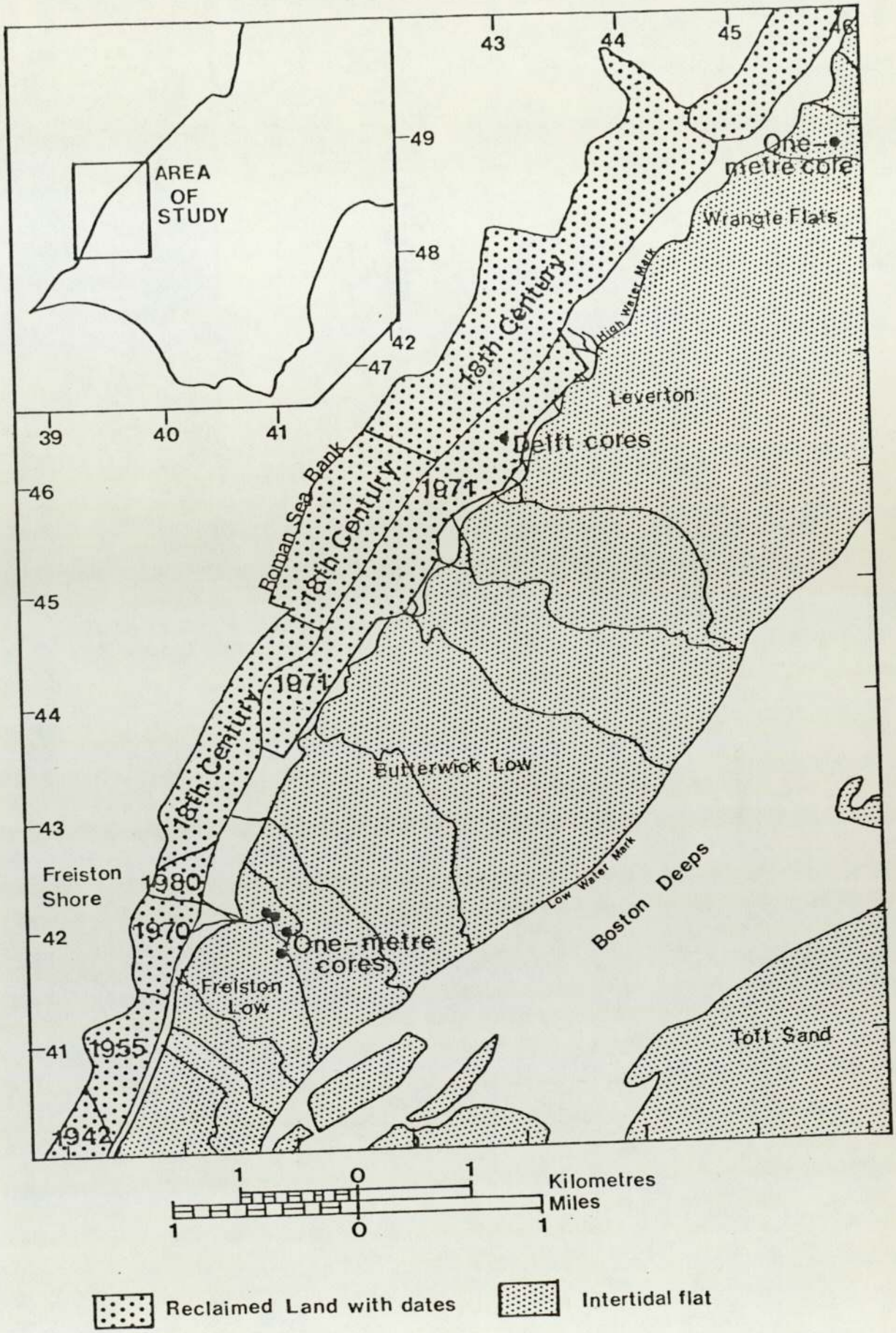


Figure 2-1. Location map for the cores of sediment used in this study.

complete sequence of sediment representing the total sequence of the tidal flat. This it was hoped would penetrate to the underlying Holocene Clay (presumed to occur at a depth of 7 metres (Evans, 1965)) marking the initiation of tidal flat sedimentation in the Wash. The method used here, the Delft corer, is again described in chapter 6. The choice of site was at Leverton, grid reference TF 429463, shown on figure 2-1. By this method a total depth of 9 metres of core was recovered in each of two parallel cores from the tidal flat sediments at Leverton, penetrating the salt marsh, higher mudflat and Arenicola sand flat sub-environments.

In addition to using cores of sediment in sampling, a small number of surface sediment samples were collected from the present day tidal flats at Freiston Shore and at Leverton for use in studies of the clay minerals (chapter 3) and in the study of the magnetic fabric of the sediments (chapter 6).

## 2-1-2. Sedimentology at the sampling locations, and sedimentological description of the cores.

The first area to be examined was at the well documented present-day tidal-flat at Freiston Shore (Evans, 1965 and Amos, 1974), (see figure 2-2). The present-day tidal flat at Freiston Shore extends from the 1970 and 1980 sea banks 1500 metres seaward to the mean low-water mark. Only a narrow (0-100 metres) salt marsh is present because of the recent reclaimation work, leaving most of the tidal-flat, at Freiston Shore, within the intertidal zone. An interesting feature of the history of the tidal-flat at Freiston Shore is reported by Preston (1921) in which evidence is given from an old report that mentions that the

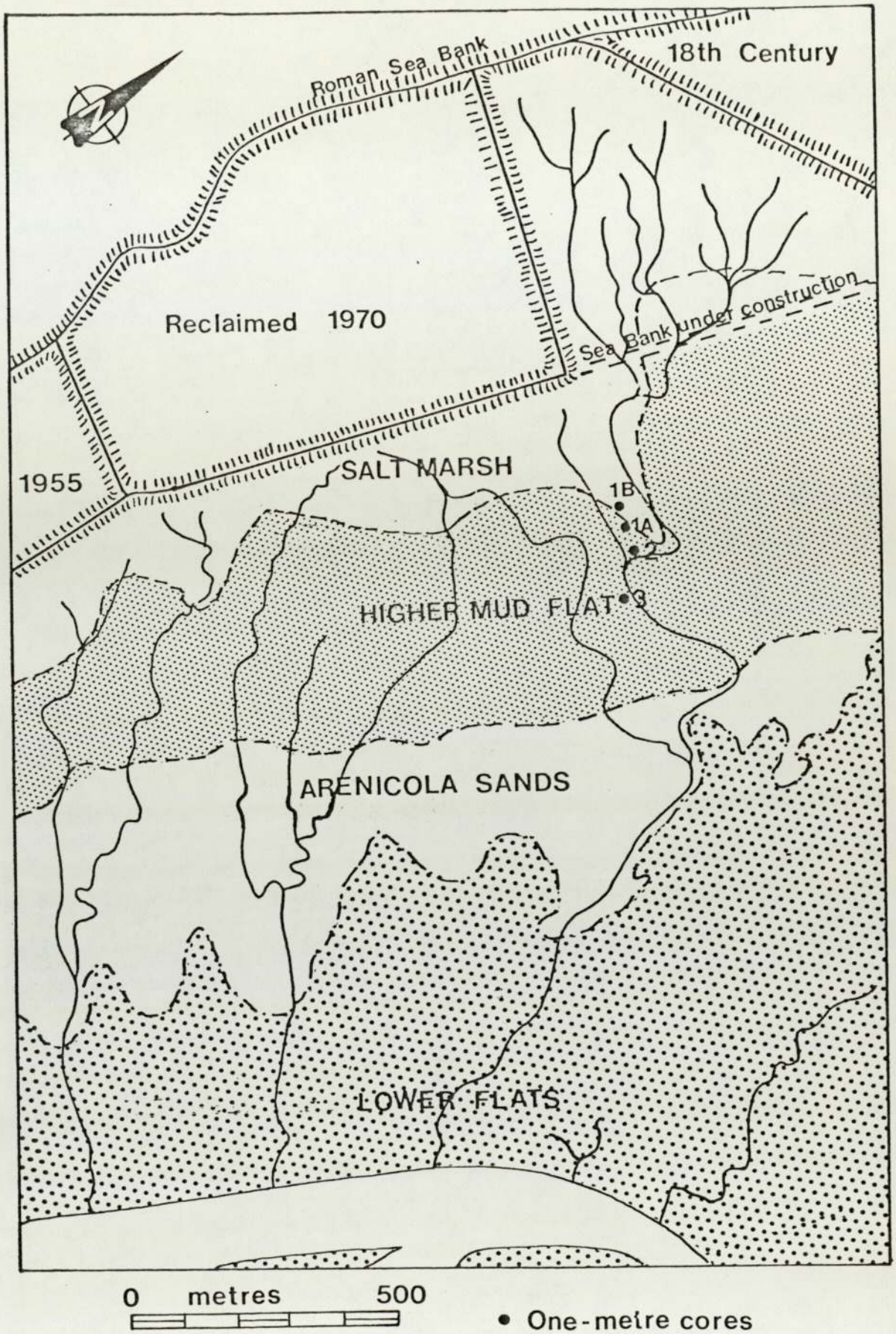


Figure 2-2. Location map for the one-metre cores collected from Freiston Shore.

shore at Freiston was used for Pony racing and that "eighty or one hundred" years ago the shore at Freiston was a "clean, white, hard sand, quite suitable for sea-bathing". Using this evidence Preston (1921) suggests that the shore at Freiston was a sea-side resort, with a good sandy beach and the reason for the change to tidal-flat sedimentation took place as a result of the building of the Witham Cut which Preston (1921) dates as being made "some time during the last Century". The result being that silt was brought down by the river Witham and its tributaries covering the sandy beach to a depth of "several feet".

The Witham outfall cut was made in 1884, and was an attempt to both straighten the river downstream of Boston and in so doing reduce the risk of flooding. The effect of this cut on salt marsh advancement rates is shown in the data of Kestner (1962) (figure 2-3). The graph shown in figure 2-3 deals specifically with the flats at Butterwick, some 1.83 Km to the northeast of Freiston Shore. The contrast between the rates of advancement of the salt marsh from between 1828 and 1871 and between 1887 and 1903 is clearly due to the Witham Cut, the only major outfall work of the period between: the area embanked in 1872 close to the site of the future cut is not considered of sufficient size to have brought about such a radical change in hydrodynamics. Kestner (1962) considers that the rate of advancement at Butterwick between 1828 and 1871 was significantly affected by the emplacement of reclaimation embankments during the 18th Century (figure 2-1) and to the 1809 enclosures further north.

Kestner (1962) concludes from a careful study of old salt marsh edges that the advancement of the salt marsh is not a continuous process, but that foreshore saltings tend to become

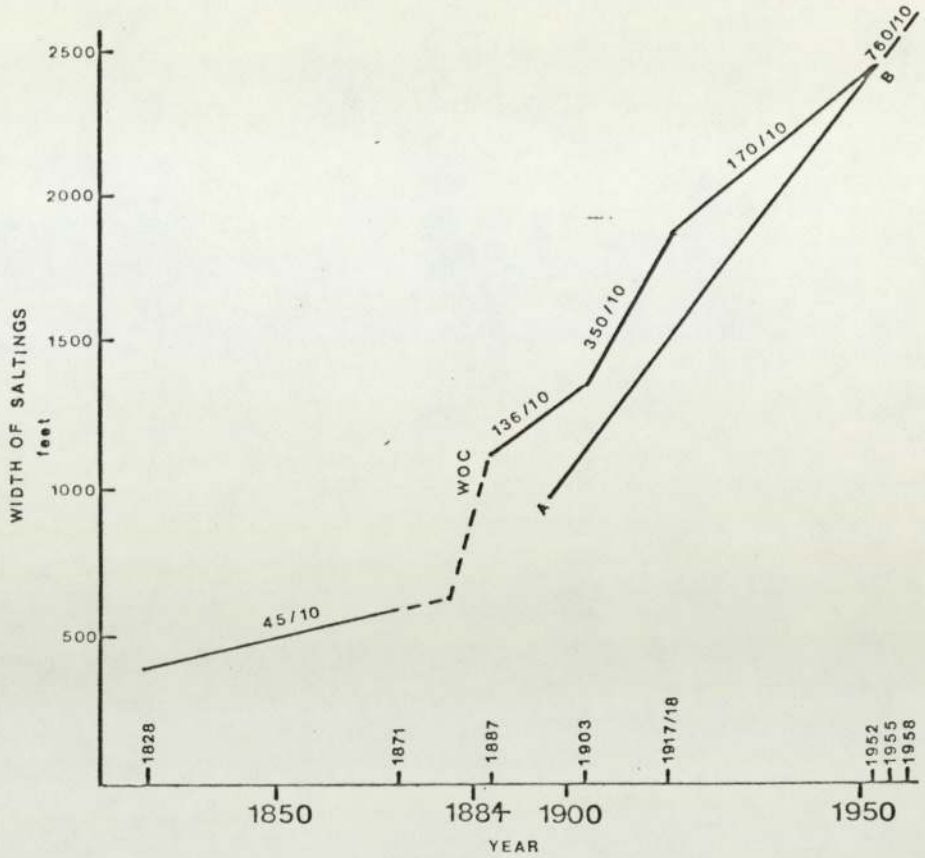


Figure 2-3. The rate of advance of saltings at Butterwick during the period 1828 - 1958. After Kestner (1962).

KEY:

45/10 = 45 ft. per 10 years. (rate of advance of saltings).

WOC = Witham Outfall Cut, completed 1884.

A——B = Mean rate of advance of saltings as calculated from core sampling experiments.

stabilized when they are 0.5 - 0.8 kilometers wide, with a wider belt of mud flats in front of them. In the mudflat areas accretion, caused by continuous deposition from suspension, is balanced by side erosional processes. Salt marsh advancement takes place only when this balance is upset, either by man-made processes, such as the straightening of river outfalls and the reclaimation of the salt marsh, or by natural catastrophe.

Prestons (1921) view that the Witham Cut was the cause of the change in depositional environment at Freiston Shore thus is disproved. An event occuring between 1828 and 1871 appears to have been the real cause. Kestner (1962) considers that the rate of advancement at Butterwick between these dates (approximately 1.4 m $yr^{-1}$) as having been considerably affected by the 18th Century reclaimation embankments and by the 1809 enclosures further to the north. The nearly three times greater rate of advancement to the south of these constructions, south of Freiston, argues for another, more major change.

The only major change to the Wash environment during the required time period was the entrainment of the river Welland Outfall in 1838, which caused the flood and ebb channels of the Witham - Welland system to occupy courses closer to the Lincolnshire shore, thus increasing sediment input to the area.

Clearly further examination of the history of sedimentation at Freiston Shore would be aided by excavations and/or coring. Dating of the sediments encountered would greatly aid the understanding of such processes.

As explained in the introduction to this chapter, Evans (1965) has described the shore at Freiston as being made up of six morphological zones arranged parallel to the coastline. Each of

which provides a recognizable sub-environment of deposition characterized by distinctive deposits and organisms. A seventh sub-environment of deposition is provided by the network of drainage channels or creeks that cross the tidal-flats. Also mentioned in the introductory chapter (chapter 1) is the fact that for palaeomagnetic purposes only the three landward deposits, the salt marsh, higher mud flat, and the Arenicola sands, are studied in this work.

At Freiston Shore sampling took place using four one-metre cores of sediment, the upper one of which penetrated the salt marsh, and the remainder form a sequence through the higher mud flat sub-environment. The cores were collected near to one of the major creeks (figure 2-2) which are a feature of the shore at Freiston. Care was taken to select coring sites on the erosional sides of the creeks, avoiding reworked (laterally deposited sediments) sediments and also avoiding sediments affected by slumping, such areas being marked on the surface by cracks indicating the presence of shear planes at depth.

The sedimentology of the cores (cores 1B, 1A, 2 and 3) is shown in figures 2-4, 2-5, 2-6, and 2-7. As can be seen from these logs, two of the cores (cores 2 and 3) are affected by minor shear planes. In core 2 the shear plane almost bisects the upper part of the core vertically and then reappears at a depth of about 48cms to cut the core at an angle of about $15^{o}$ off the vertical. However, as no marked displacement of the sediments on either side of the shear plane could be detected, it was decided that the core could still be used for palaeomagnetic purposes.

The total thickness of sediment represented by the sequence of cores could not be determined accurately because of the

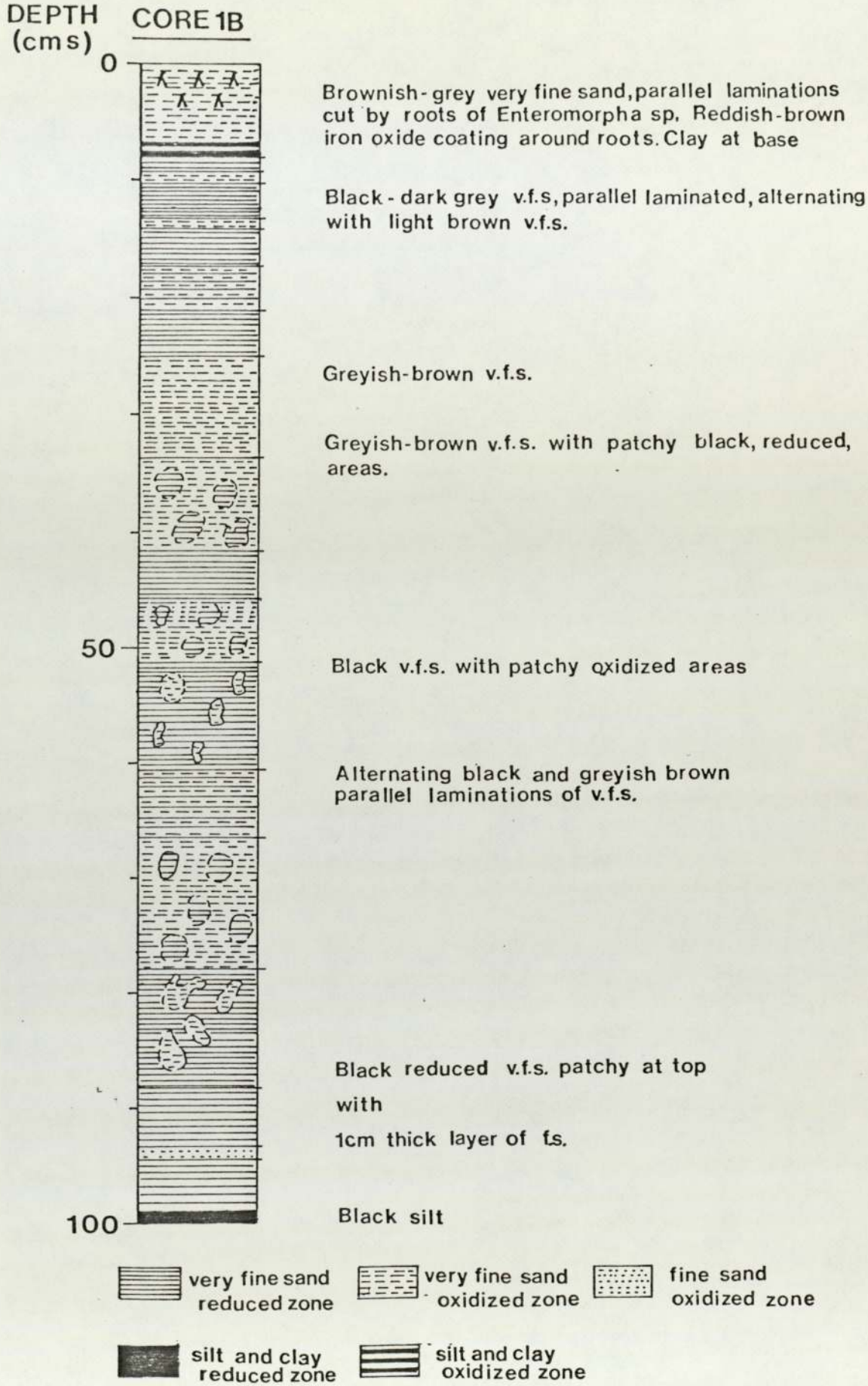


Figure 2-4. Lithological log of core (1B) from Freiston Shore.

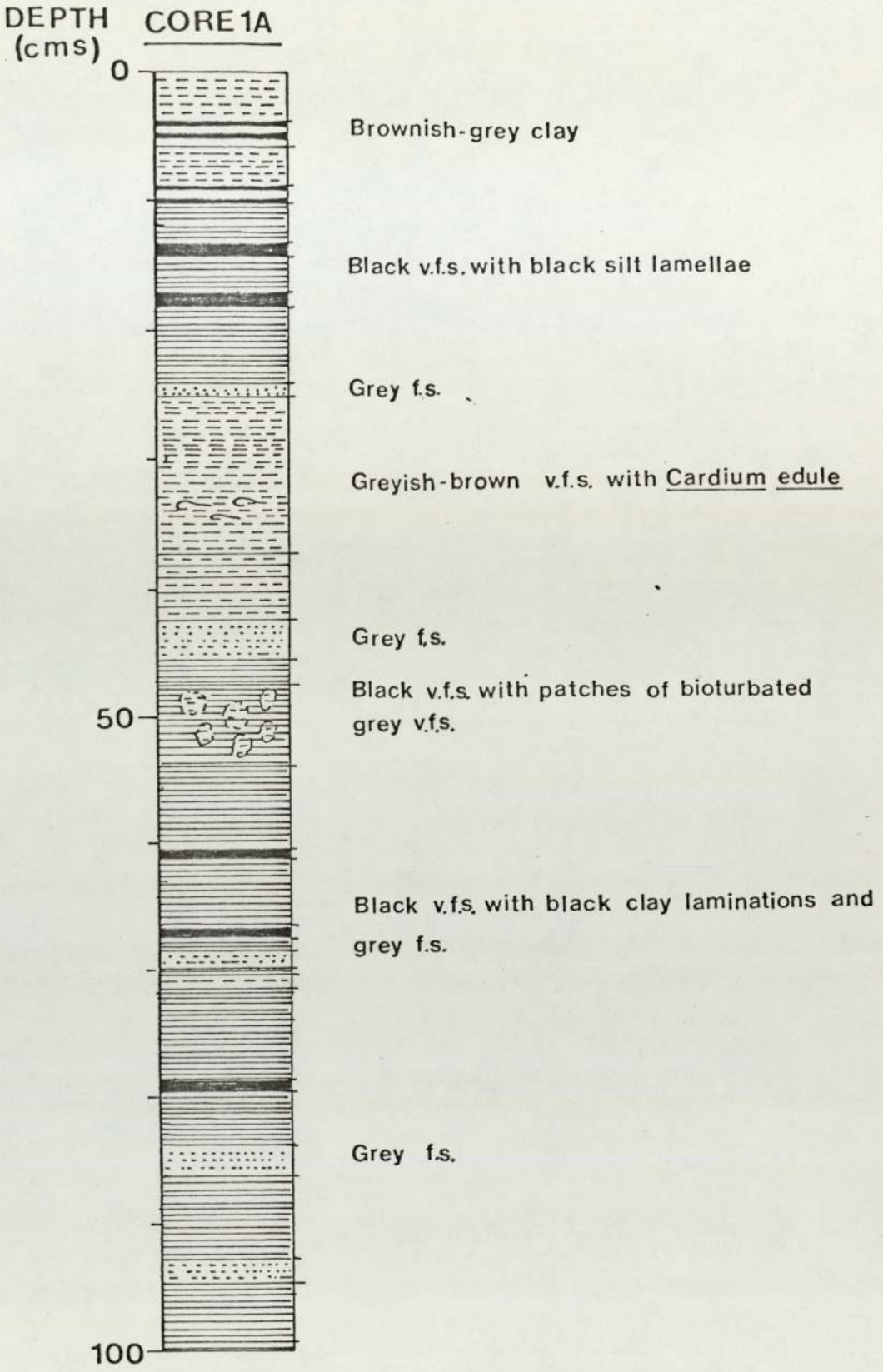


Figure 2-5. Lithological log of core (1A) from Freiston Shore.

See figure 2-4 for key.

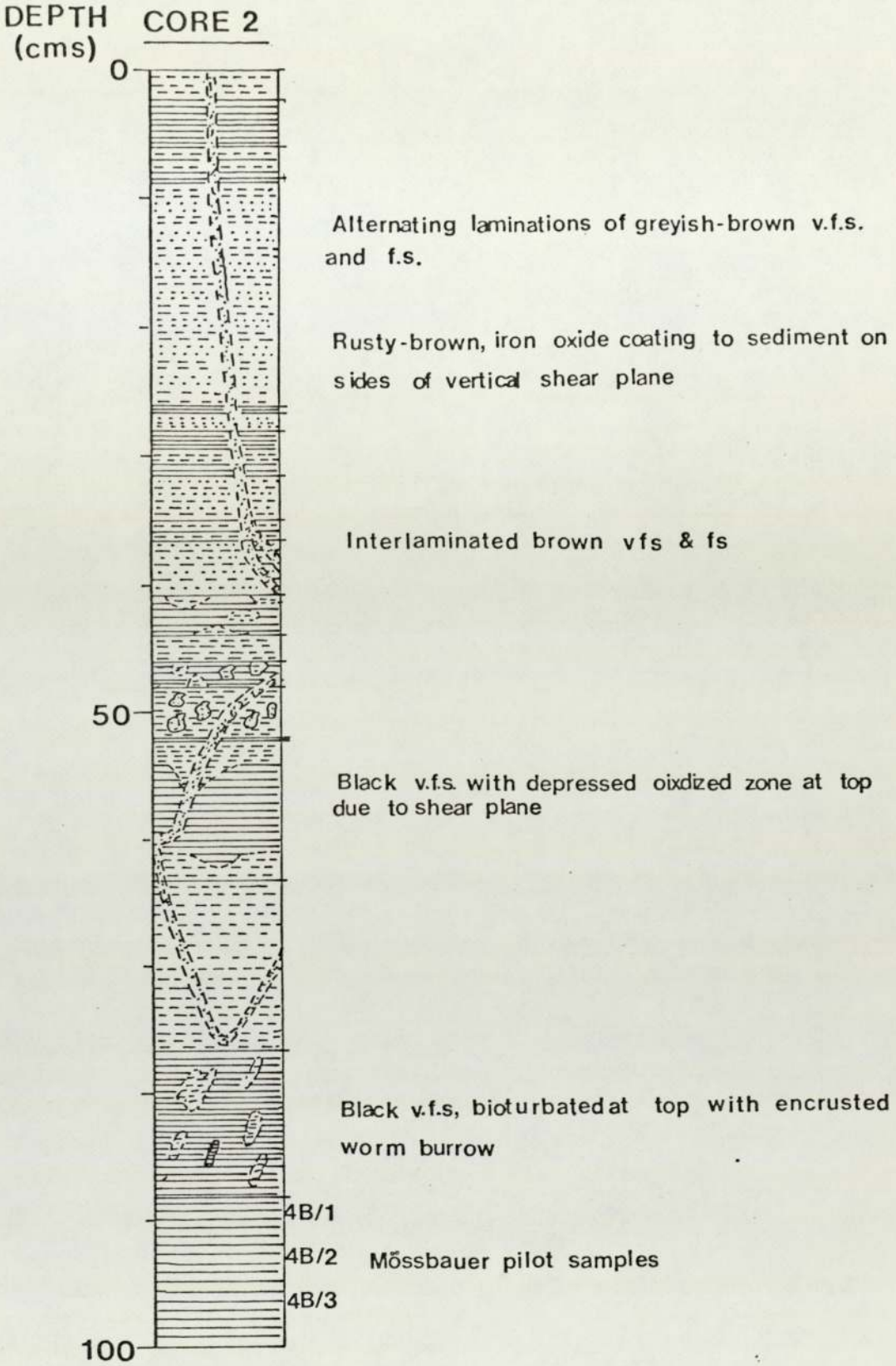


Figure 2-6. Lithological log of core (2) from Freiston Shore.

See figure 2-4 for key.

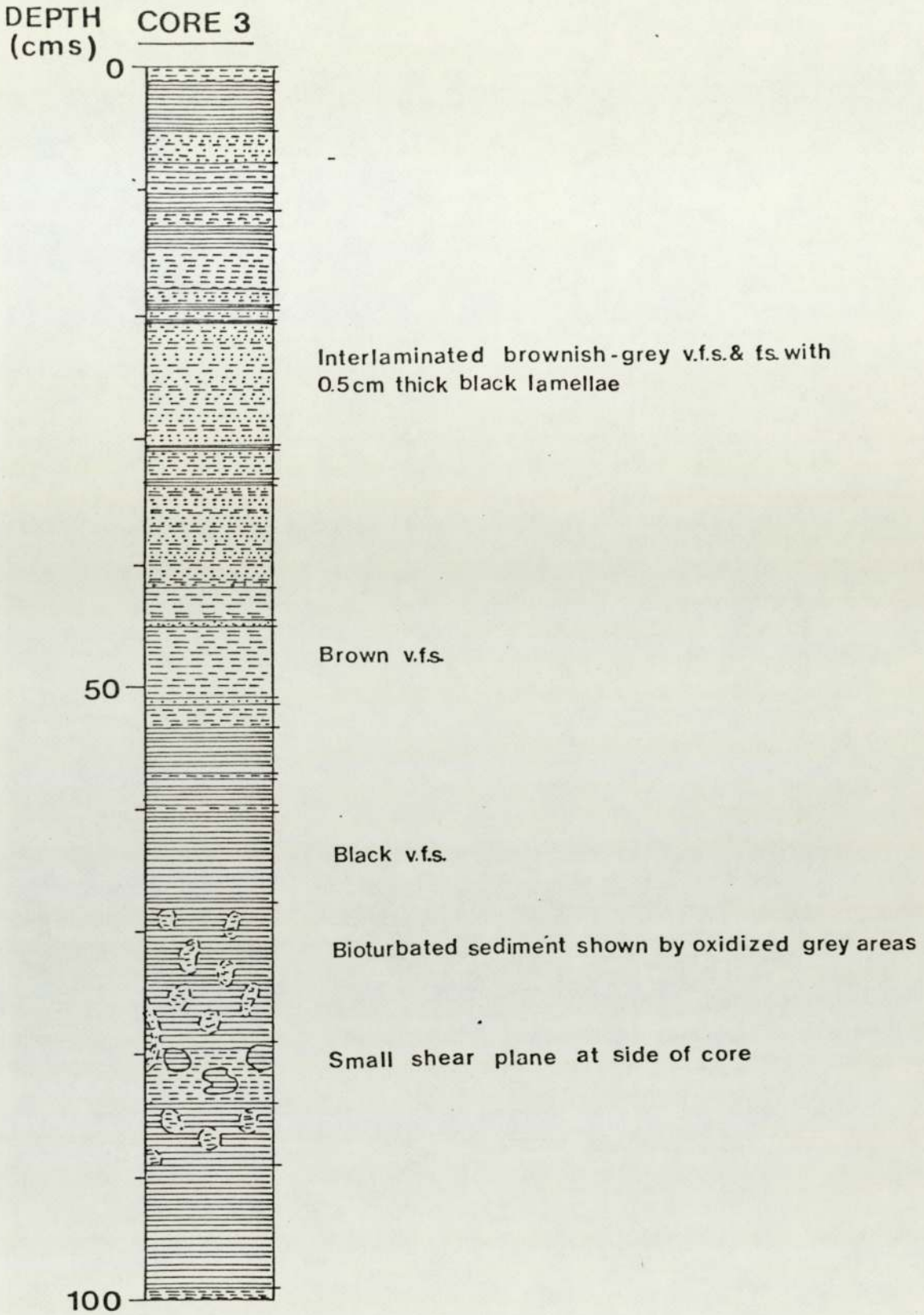


Figure 2-7. Lithological log of core (3) from Freiston Shore.

See figure 2-4 for key.

absence of any useful marker horizons, but it is estimated that the sequence is 2.40 metres thick. The juxtaposition of the cores with respect to one another is studied in more detail in chapter 6 where it is shown how palaeomagnetic features assist in correlation.

The uppermost core in the sequence, core 1B, passes through the upper surface of the salt marsh, near to its boundary with the higher mudflat sub-environment. The top part of this core consists of brownish-grey coloured very fine sand (v.f.s.) which is very finely parallel laminated (less than 0.5mm), these laminations are cut by the roots of plants belonging to the Enteromorpha species. Around the rootlets iron oxide coating of the sediment occurs giving the sediment a deep reddish-brown colour. After only 8 cms this marginal salt marsh sediment passes quickly into sediments composed of parallel laminated greyish-brown and and black or dark-grey very fine sand, with minor amounts of clay and silt lamellae. The sediments apart from their parallel lamination show a complete absence of other sedimentary features, except for occassional minor current laminations in units less than 5 mm thick. The brownish-grey and greyish-brown sediments belong to the oxidized zone (Love, 1967) in which reduction of iron is not yet taking place, whilst the dark-grey or black sediments belong to the reduced or monosulphidic zone (Love, 1967) in which iron monosulphides are forming. The sequence from oxidized to reduced sediment is not a simple one, but a complex repetition of reduced and oxidized horizons exist, probably due to the oxidation of sediments at depth by the movement of oxygenated water through slightly more permeable units of sediment. Some of the sediments which are predominantly of either the oxidized or

reduced zones show patchy occurences of, respectively, reduced or oxidized sediment, such sediments occur in the lower half of the core. In addition the reduced-oxidized sediments may alternate, often on a very fine scale corresponding to the fine laminations of the sediment, such as occurs in the unit of sediment between depths of 61 and 66 cms.

Towards the base of the core, below 87 cms, the black reduced very fine sand begins to be dominant, and the only oxidized sediment is a thin (1 cm) layer of fine sand (f.s.). At the base of the core is a thin unit of black, reduced, silt.

Core 1A is estimated to begin at a depth approximately 20 cms below that of core 1B and, thus it is completely within the higher mudflat sub-environment of deposition. However, a thin 3 cms zone of brownish-grey clay near the top of the core again gives evidence of the proximity of the salt marsh, and of a possible early encroachment of the salt marsh. This clay is underlain by parallel laminated black very fine sands, together with black silt lamellae, extending from a depth of 10 cms to 25 cms. Below this, two units of grey fine sand at 25 - 26 cms and at 42 -45 cms bound a unit of parallel laminated, oxidized, greyish-brown very fine sand, in which occur shells of the bivalve Cardium (Cerastoderma) edule.

Immediately below the grey-coloured fine sand at a depth of 45 cms occurs a zone of black very fine sand in which oxidation of patches of bioturbated sediment has taken place, returning the sediment to a grey colour. The lower 47 cms of the core are dominated by black parallel laminated very fine sand in which black clay and silt laminations occur, and in which grey fine sand lamellae begin to become more abundant.

Core 2 was collected about 25 metres further seaward along the side of the same creek, and penetrates the higher mud flat approximately 80 cms from its surface and 90 cms below the level of the top of core 1B. As mentioned earlier, the most pronounced feature of this core is the shear plane which bisects the core, however, since there is no evidence of displacement on either side of the shear plane, it was decided that the core could still be used for palaeomagnetic studies. In contrast to core 1A and 1B and also to core 3, this core shows a smaller proportion of black or dark-grey reduced sediment. It is thought that this is due to oxidation of the sediment at depth associated with the presence of oxygenated waters travelling down the shear plane. The upper 40 cms of the core contain almost equal proportions of fine sand and very fine sand, continuing the trend, observed in core 1A, of an overall coarsening of sediment grain-size. This may be a factor in accounting for the paucity of reduced sediment in the upper part of the core. Where the shear plane re-enters the core at a depth of of 48 cms there is again evidence to show its effect on oxidizing the surrounding sediment. This is particularly well shown by the unit of reduced, black-coloured very fine sand which occurs between depths of 54 and 61 cms. At the point where the shear plane crosses its upper surface, oxidized sediment forms a funnel-shaped depression in the surface of the black sediment below. Below this reduced zone the sediment again becomes oxidized again due to the presence of the shear plane. The walls of the shear plane are themselves encrusted by a thin, 1 mm, thick layer of reddish-brown iron-oxide. Finally, below 78 cms the sediment reverts to its fully reduced state consisting of black very fine sand, the upper part of which shows some evidence

of bioturbation in the form of patches of grey-coloured very fine sand, and also by the presence of encrusted worm burrows.

The lower core in the sequence, core 3, was collected again further to the seaward, approximately 110 metres from the landward edge of the higher mud flats. This core is largely unaffected by slumping, except for the occurence of a minor shear plane at the side of the core, which occurs between a depth of 75 cms and 81 cms. The upper 10 cms of core 3 continues with very fine sands, similar to those encountered at the base of core 2, except that more of the oxidized laminations occur in core 3. Below this, to a depth of 53 cms, the sediment consists mainly of parallel laminations of very fine sand and fine sand, thus being slightly coarser-grained than the more landward part of the sequence. The presence of fine sand lamellae means that little of the sediment belongs to the reduced zone of sulphide formation. Below a depth of 53 cms the sediment in the lower part of the core consists of black parallel laminated very fine sand broken only by a zone in which oxidized grey patches of very fine sand occur, which can be attributed to the oxidizing effect of burrowing organisms.

To summarize, the sequence of sediments, represented by the four one-metre cores of sediment from Freiston Shore, show a sequence through the lower (seaward) part of the salt marsh and through most of the higher mudflat sub-environments. The salt marsh is thin consisting of brownish-grey very fine sand and clay, with rootlets of the alga Enteromorpha sp.. Beneath this the deposits of the higher mud flat are characterized by parallel laminated sediments, chiefly of the very fine sand-grade but also containing minor amounts of fine sand, silt and clay laminations.

A trend of coarsening overall grain-size is indicated by the increased concentrations of fine sand found in the lower sections of the sequence, and also by the presence, only in the upper part of the sequence, of thin silt and clay laminations. These observations compare well with those of Hantzschel (1955) who studied the sediments of the German coast, and with the observations of the sediments of the Dutch coast examined by van Straaten (1962).

Finally, although there is a general tendancy for all of the cores to show increased reducing conditions with depth, the pattern of oxidized and reduced sediment is also controlled by the activity of burrowing organisms, which may cause oxidation of the sediment within the reduced zone, and also by the introduction of oxygenated waters along lines of high permeability, such as along shear planes and along coarse-grained beds. This oxygenation of the sediment along preferential horizons is greatly aided by the movement of tidal waters over the sediment surface.

One further one-metre core was collected. This core, core W1, was collected at Wrangle Flats (grid reference TF 459488) see figure 2-1. The location of the core is also shown in plate 1, which illustrates the side of the trench from which the core was recovered. The site is on the present-day surface of the Arenicola sand flats approximately 620 metres from the present-day sea-bank. At Wrangle flats the width of the tidal flats is much greater (approximately 3.1 kilometers) than at Freiston Shore. The result of this is that the gradient of the flats is smaller and hence vertical sedimentation is much slower. Hence, shorter cores of sediment will represent longer periods of time - an advantage when collecting material for palaeomagnetic purposes. Another

Plate 1. Wrangle Flats, showing the location of the trench from which core W1 was recovered. Note the small current ripples on the sediment surface. The colour zonation of the sediment is also illustrated. Zone 1 is the reddish-brown fine-grained sand belonging to the oxidized zone. Zone 2 is the black or dark grey sediment of the monosulphidic zone and the third zone, zone 3 consists of a sequence of grey-coloured sediments belonging to the bisulphidic zone.

Plate 2. Wrangle Flats, showing the subdued creek profile and the extensive development of the salt marsh. The photograph is taken from the side of the creek where vertical accretion through reworking of the salt marsh sediments is taking place. On the far side of the creek there is active erosion of the salt marsh sediments.

Plate 1.

Plate 2.

feature which suggests that the tidal flats at Wrangle are closer to achieving equilibrium with the marine environment than those at Freiston Shore is the low number of creeks. The creeks which are present also tend to have much shallower profiles than the ones at Freiston Shore (see plate 2). Also evident from Plate 2 is the fact that the sub-environments of deposition at Wrangle Flats cover larger areas, this being due to the lower gradient of the intertidal area at Wrangle. This is in turn due to the areas distance from the erosional effects of large fluvial outfalls, and their seaward extensions. As a result the salt marsh at Wrangle Flats is 30 - 150 metres wide, the higher mud flat is 100 - 400 metres wide and the Arenicola sands extend some 2 - 2.5 kilometres.

As can be seen from plate 1 and from the log of core W1 (figure 2-8), the upper surface of the Arenicola sand flats is marked by small current ripples and by abundant worm casts of the worm Arenicola marina. Beneath the surface, however, the sediments are devoid of sedimentary structures because of the almost complete bioturbation by Arenicola marina and thus the sediments are a marked contrast to the parallel laminated higher mud flat sediments described above. Another difference is that the sediments of the Arenicola sand flats are coarser grained being composed of fine-grained sands in contrast to the very fine sands and silts of the higher mud flats. Another feature is the colour zonation of these sediments (see plate 2). The upper 15 cms of the core consists of reddish-brown fine-grained sand belonging to the oxidized zone. Beneath this the sediment is black or dark-grey in colour, representing the monosulphidic zone within which Love (1967) has suggested the iron sulphides, greigite and mackinawite are forming. The boundary between the oxidized and monosulphidic zones here is a sharp

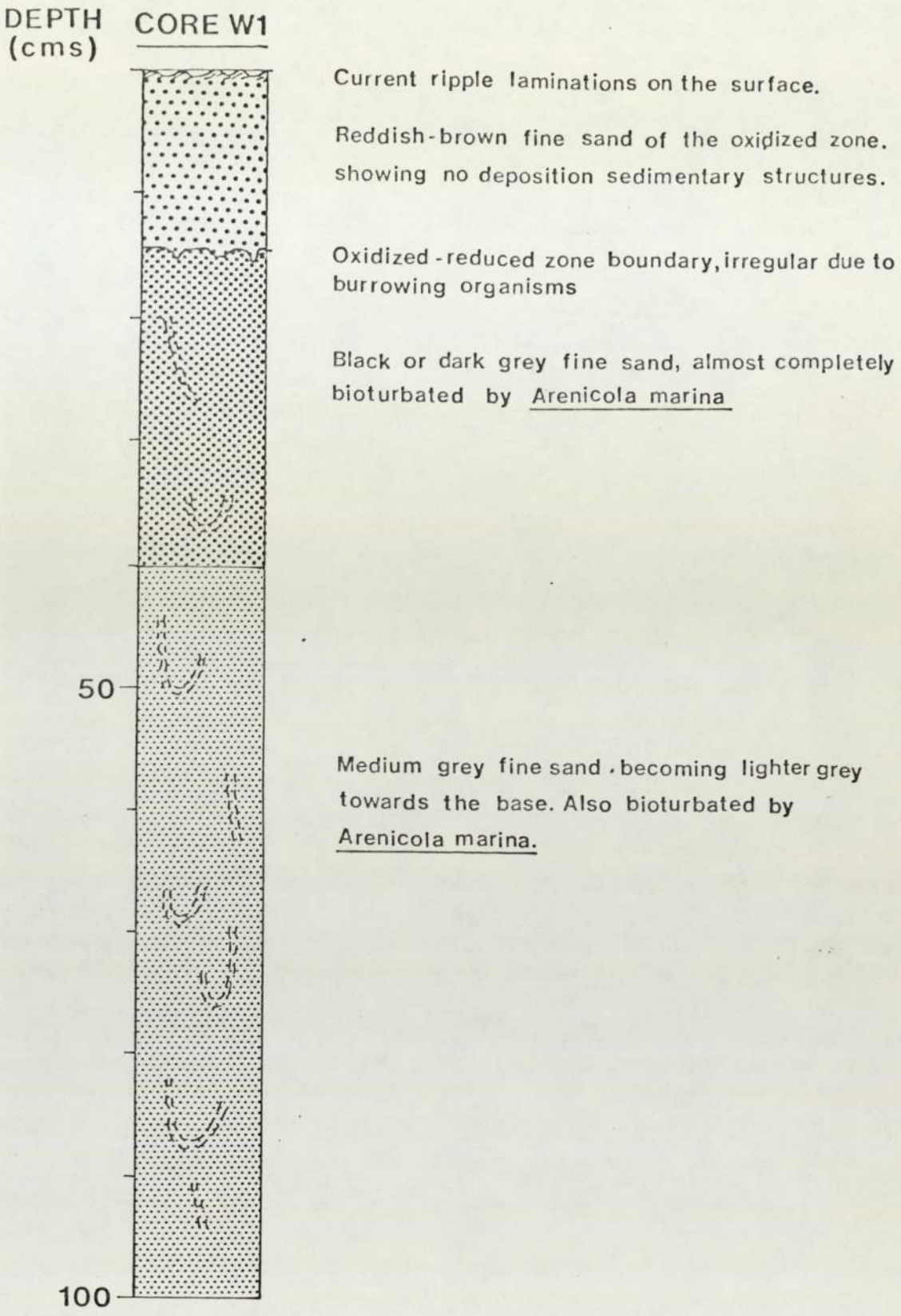


Figure 2-8. Lithological log of core (W1) from Wrangle Flats.

one, which picks out an irregular surface caused by the burrowing activity of worms. This situation contrasts with the higher mud flat subenvironment where the boundary consists of alternating reduced and oxidized zones.

The sediments of the reduced monosulphidic zone extend to a depth of 40 cms, at which point they grade into a medium coloured sequence of sediments consisting of fine sands. These sediments are typical of the pyritic or bisulphidic zone of sulphide formation. Unlike the overlying monosulphidic and oxidized zones the sediments of this bisulphidic zone show areas or patches of darker coloured sediment more typical of the monosulphidic zone. Such patchy sediment indicates areas where the formation of pyrite from monosulphide minerals is still incomplete.

The final sampling location was at Leverton, on the area of salt marsh reclaimed during 1971 (see figure 2-1). Here two parallel cores were collected using the Delft corer (for a full description see Chapter 6). The cores were collected only 10 metres appart and subsequent inspection of them revealed a high degree of similarity in their sedimentology. The cores were designated core D1 and core D2. The majority of the results presented here are from examination of core D1, the exceptions being from those samples of sediment taken for low-temperature Mössbauer spectroscopy.

The following system was used in the numbering of samples: the first figure of the sample number refers to the core, D1 or D2. The second figure refers to the core section from which the sample was taken, since in both cores the top section was empty the uppermost samples come from core sections D12 and from D22. The final figures refer to the depth of a particular sample within the core section. As an example, a sample labelled D110.45 [illegible]

would refer to a sample from core D1, from core section 10 and from a depth within that core section of 45 cms. The sample would thus have originated from a depth below the present sediment surface of 8.45 metres.

Examination of core D1 shows three main lithological units. The first of these, unit 1, occuring in the top 36 cms of the core consists of a unit of dark-brown clay (plate 3) which near the top contains small plant rootlets. With increased depth thin silt and very fine sand lamellae occur, these are light-brown in colour (plate 3). The bases of the clay units show load casts indicating early compaction of the sediments. The lower part of this unit also shows the effects of bioturbation by worms. This upper part of the core can be interpreted as having been deposited in the salt marsh sub-environment of deposition.

Unit 2, consists of 1.50 metres of silts and very fine sands containing some shells, mainly of Cardium (Cerastoderma) edule. The upper part of the sequence forming the top 44 cms of this unit is also strongly bioturbated. The absence of bioturbation in the lower part of the sequence indicates that bioturbation may have occured as a result of the advancing salt marsh edge. The lower part of unit 2 extends into core section D12, and consists of very finely laminated silts and very fine sands. The laminations are mostly parallel laminated, however, some minor current laminations are also present. The silts and very fine sands are dark- and light-brown in colour, the darkest horizons are those with the highest proportions of clay-grade sediment. Also present in unit 2, are the bivalves, Cardium edule, Littorina littorea and Mytilus edulis. Using the characteristics defined by Evans (1965) unit 2 can be assigned to the higher mud flat depositional sub-

CORE D1

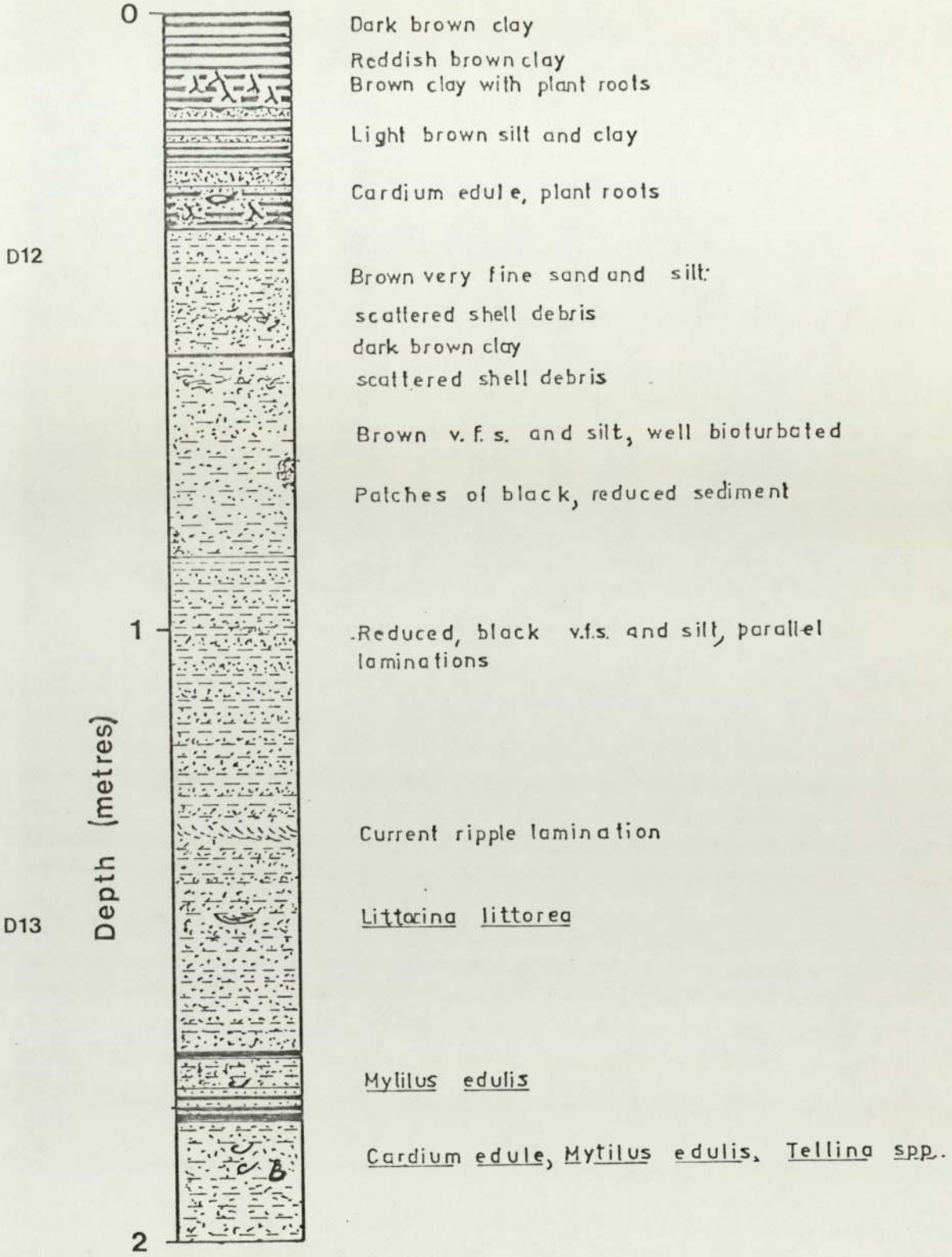


Figure 2-9. Lithological log of the Delft core (D1) from Leverton showing the upper 2 metres of sediment.

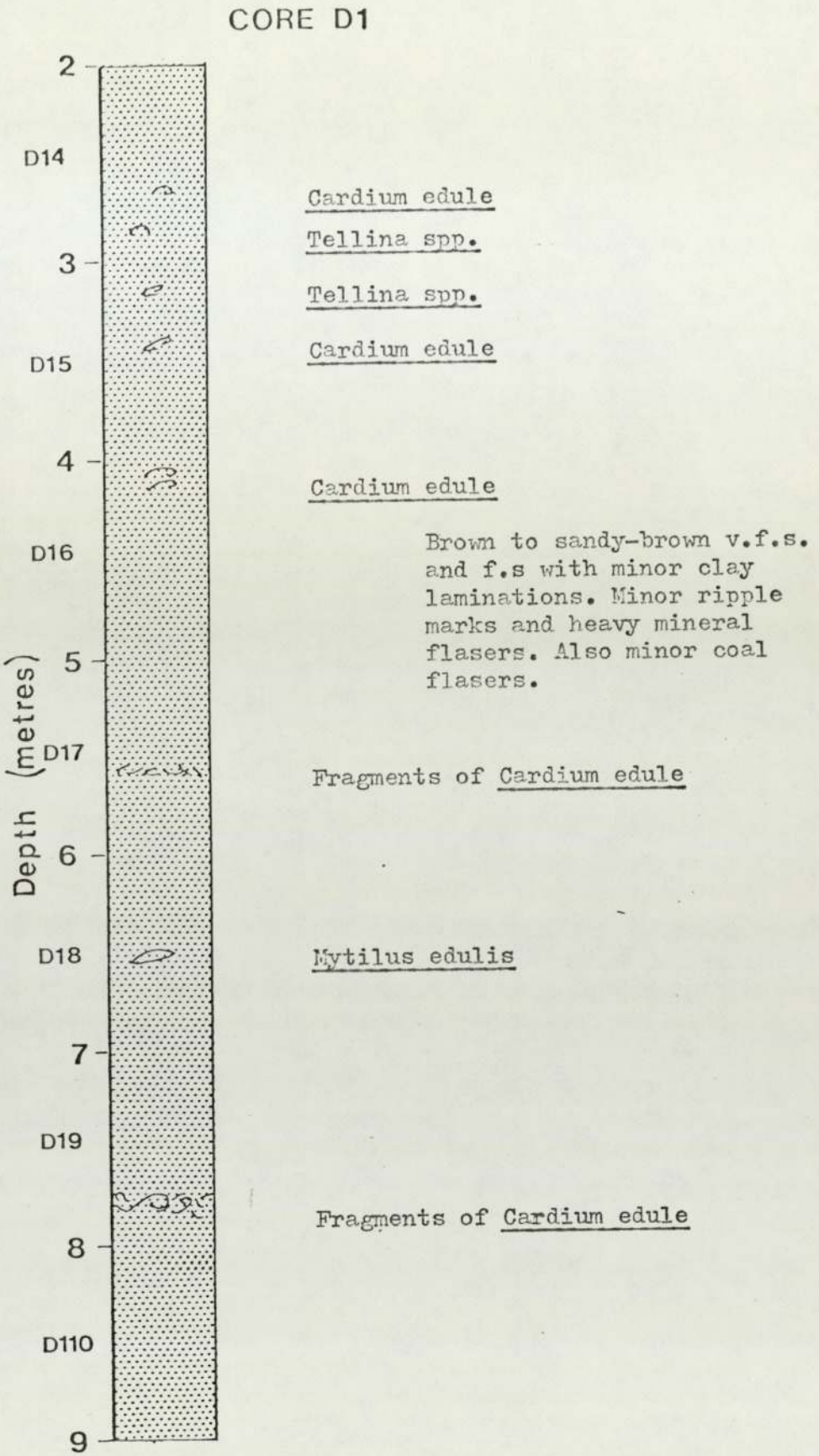


Figure 2.10. Lithological log of the lower seven metres of Delft core D1, from Leverton.


A A'

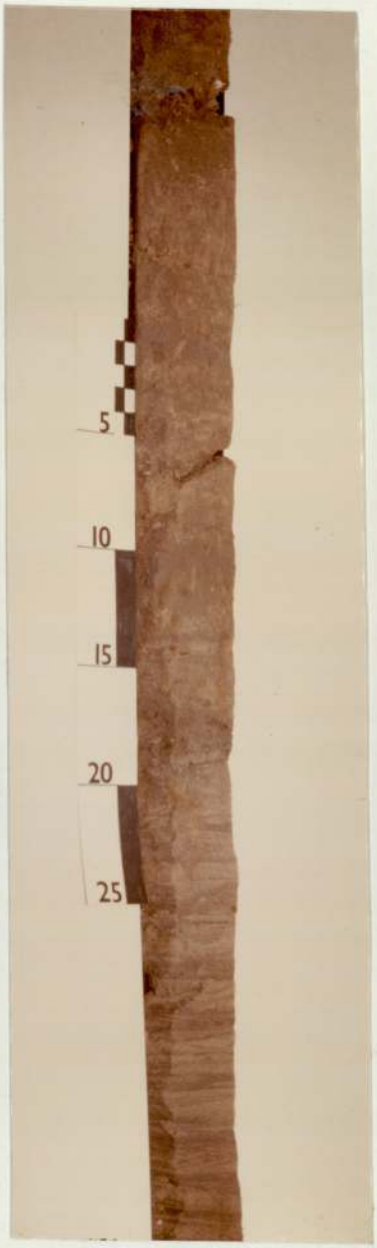


A A'

Plate 3. Core Section D12.

environment.

The final unit recognised, unit 3, in core D1 consists of 7 metres of " clean" well sorted fine-grained sands. These sands show few sedimentary structures because of the almost complete bioturbation by the worm Arenicola marina. Occasionally some sedimentary features such as heavy mineral flasers, and cross lamination were observed. At the top of the core the bivalves Cardium edule and Tellina sp. are found as is shown in the log (figure 2-10). However, towards the base of the core, in the lower 4 metres of sediment, the occurence of bivalves tends to be in the form of fragments of shells. This fragmentation of the shells indicates a higher energy depositional regime. Three distinct horizons of shell debris were encountered, two consisting of fragments of Cardium edule and one composed entirely of fragments of the bivalve Mytilus edulis. Unit 3 can be interpreted as belonging to the Arenicola sand sub-environment of deposition. However evidence in the lower part of the core for a higher energy depositional regime may be indicative of a fourth style of deposition, possibly a beach style of deposition. This problem will be discussed further in chapter 6.

## 2-2. Petrography of the Tidal Flat Sediments.

The preparation of thin sections from unconsolidated sediments requires that the sediments are first impregnated. Impregnation of the sediments is required to give sufficient physical strength to the sediments so that they can be cut into thin sections. The method used here is to impregnate the sediments (sample size, approximately $4cm^2$), under vacuum, with a mixture of "araldite" resin and hardener (100 parts CY212 resin, 9 parts HY951 hardener and 150 parts acetone). After being impregnated and after allowing the resin to harden, thin sections can then be prepared in the normal way.

The use of this method of impregnation was found to cause the minimum disturbance to the sedimentary fabric of the samples as will be shown in the accompanying photomicrographs. It has been found that the best results are obtained when the samples are impregnated whilst they are still slightly damp. If the samples are first allowed to dry completely, they become too friable and break-up during specimen preparation.

A second method of analysing the sediments using optical microscopy is to prepare mounts of dispersed sediments in glycerine on glass slides. This method of preparation has advantages in that it is; inexpensive, provides samples for analysis quickly, and that preservation of unstable minerals (by isolating them from the atmosphere) is possible. Another advantage is that the glycerine mounts can be analysed in both transmitted and in reflected light, using oil immersion. This is particularly useful since it allows examination of both opaque and transluscent minerals. The disadvantage is that no relationships between minerals can be observed, nor can the original

sedimentary fabric be observed. A combination of the two methods of optical microscopy described above has been used to obtain the observations discussed below.

Because of the similarities between samples from different cores, the descriptions of the sediments are grouped according to their environment of deposition, rather than repeating the descriptions for each core.

The petrology of the salt-marsh sediments is dominated by the abundance of detrital clay minerals. These are arranged in very fine laminations interspersed with very fine laminations of silt and very fine sand consisting of detrital quartz grains (often only one or two grains thick) (plate 4). This preservation of primary sedimentary lamination, indicated by the prefered alignment of platy grains is particularly well preserved in the lower parts of the salt marsh. The abundance of the silt and very fine sand laminations increases towards the salt-marsh - higher mud flat boundary. Disturbance of the primary lamination occurs both by the action of burrowing organisms and by plant rootlets (plate 5 ). Primary lamination may also be interupted and deformed by desication cracks (plate 6). Infilling of the burrows and dessication cracks then occurs (plate 6), this may be by further sediment from above or as is illustrated by the formation of authigenic pyrite. In the quartz-rich layers deformation of the detrital clay minerals occurs as a result of compaction (plate 7).

As inferred earlier, the salt marsh sediments contain varying amounts of quartz and clay minerals, tending to be more clay-rich further inland. In the example shown in plates 4,5,6, and 7, which are from sediment in the lower part of core 1A, the

Plate 4. Photomicrograph of very fine laminated salt marsh sediment, consisting of alternate laminations of silt and very fine sand. Plane polarized light.

Plate 5. Photomicrograph showing bioturbation of the primary current laminations in the salt marsh sediments. Plane polarized light.

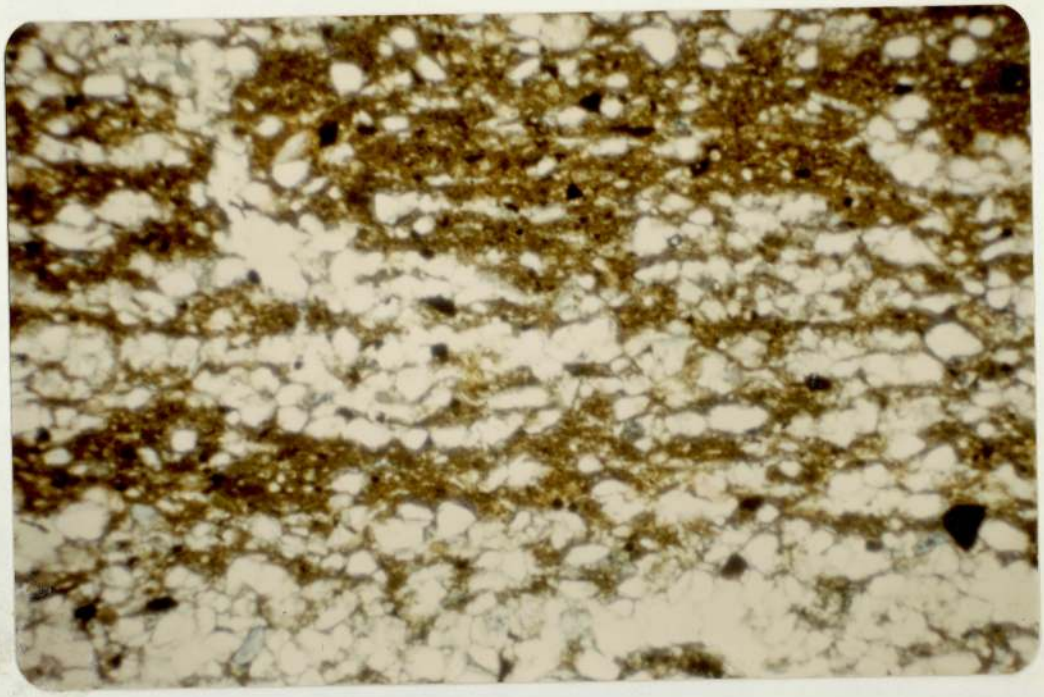

Plate 4. 1000µm

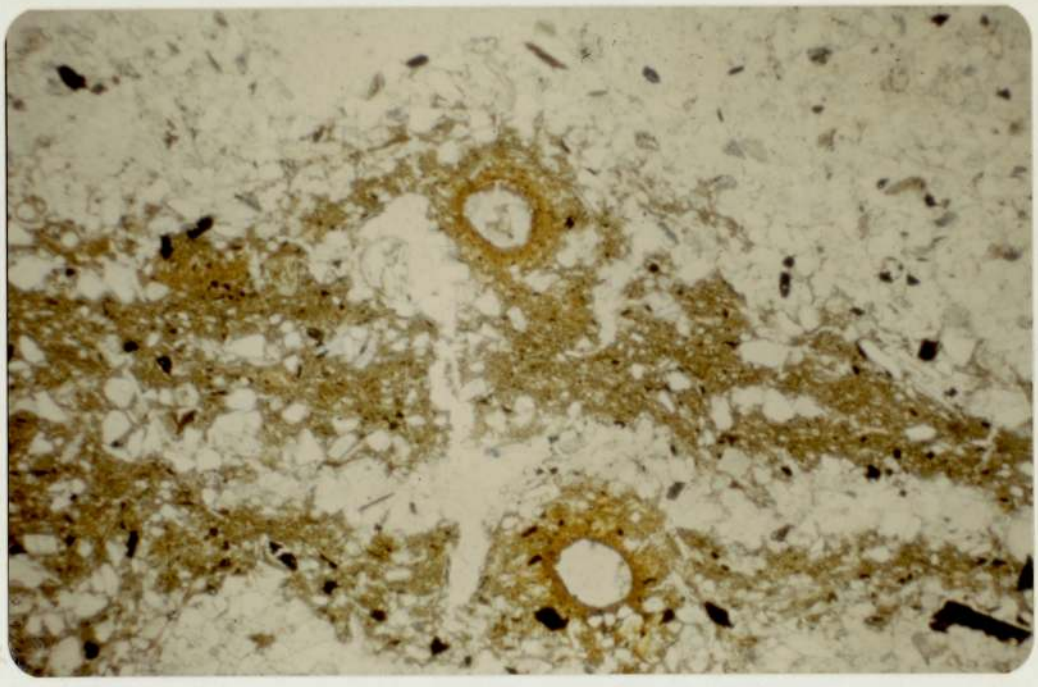

Plate 5. 1000µm

Plate 6. Photomicrograph showing disruption of primary laminations in the salt marsh sediments soon after deposition as a result of the development of mudcracks. Later infilling by quartz grains has been accompanied by the formation of authigenic pyrite (black, opaque grains). Plane polarized light.

Plate 7. Photomicrograph showing early evidence of compaction in the sediments of the salt marsh through deformation of a clay pellet (right centre) between quartz grains. Note also the irregular distribution of the clays and their poor crystallinity, indicating their allogenic origin.

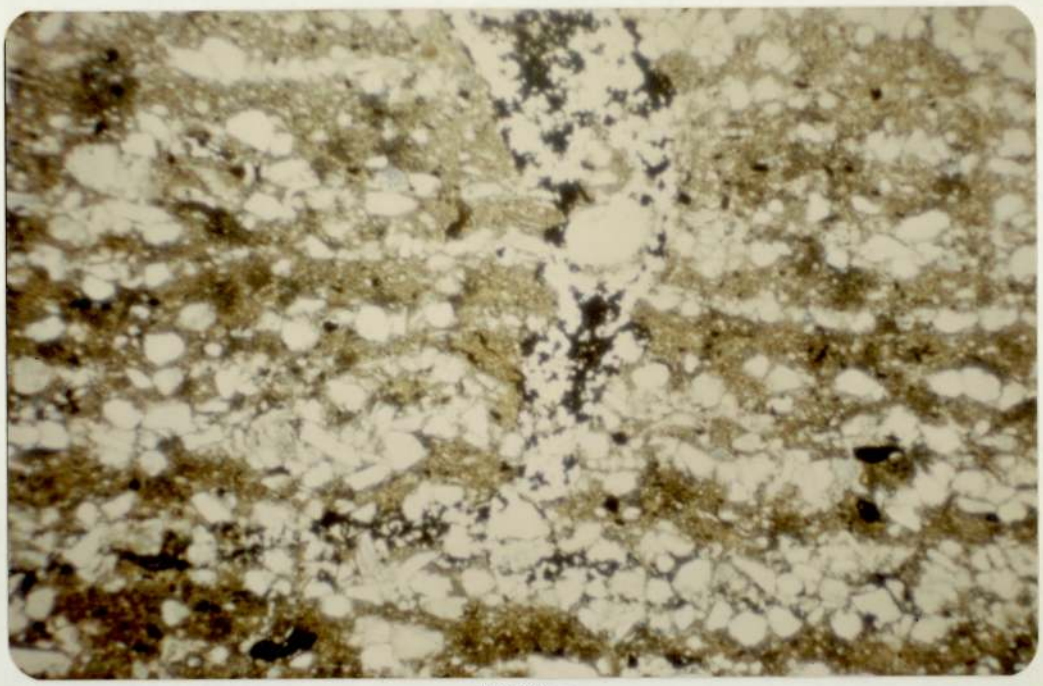

1000μm

Plate 6.

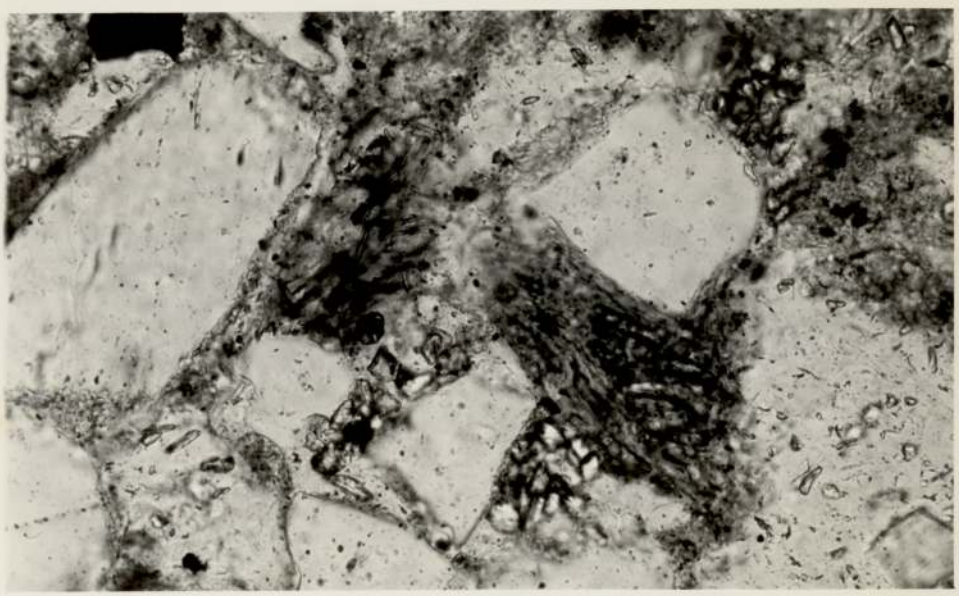

100μm

Plate 7.

sediments are composed of approximately equal proportions of clay and coarse silt grading to very fine sand, thus giving a bimodal grain-size distribution. The quartz grains are angular to sub-rounded in shape and fall into the coarse silt to very fine sand grain size range (Wentworth, 1922). The clays are allogenic in origin showing poor crystallinity. Continued breakdown of unstable detrital grains such as micas and feldspars is supplying further clay minerals. Many of the micas can be seen to be partially altered to clay minerals (plate 8), this is typified by "unpeeling" of the cleavages at the edges of the grains. Analysis of the clay mineralogy using optical microscopy is made difficult by their poor crystallinity and therefore, X-ray diffraction of clay mineral concentrates has been used for a more accurate determination of the clay minerals present (chapter 3).

Other minerals present in lesser quantities in the salt-marsh sediments include ferroan calcite, authigenic pyrite and detrital opaque minerals.

The petrology of the higher mud flat sediments differs from that of the salt marsh in that it is coarser grained and contains greater quantities of quartz. The sediments range in grain-size from coarse silt to very fine sand. The mean grain-size of the quartz grains is approximately 100 μm. Some 60 - 80% of the sediment is made up of quartz grains which are sub-angular to sub-rounded in shape with generally high sphericity. Some 80% of the quartz grains have single straight extinction (using the empirical classification of quartz types (Folk and Ward, 1957)) with about 8% having semi-undulose extinction and the remainder consisting of composite grains.

In some of the sediments of the higher mud flats the next most abundant mineral is calcite, which can form 0 - 15% of the total sediment. The calcite is almost entirely micritic with less than 5% sparry calcite. Approximately 60% of the calcite is ferroan calcite. The calcite occurs in the form of irregular rounded grains or in the form of shell fragments and foram tests. A small amount of calcite also occurs in the form of ooids and calcispheres.

Opaque minerals form approximately 5% of the sediment and are disseminated throughout the sediment, although they do tend to be concentrated in the clay-rich and organic-rich laminations. The opaque minerals can be divided into two groups; firstly, there are a group of sub-hedral to euhedral mineral grains, some of which appear to have a cubic habit. These minerals have a grain-size range from 60 - 180 μm (plate 9). Whilst some of these grains may be euhedral crystals of pyrite, subsequent concentration and analysis by X-ray diffraction and observation using the scanning electron microscope has shown that they are composed of titano-magnetite. A feature of some of these grains, in thin section, is the occurence of "cherry" red oxidized margins to the grains. Such alteration will be further discussed in section 7-7. The second group of opaque minerals, occur as small (5 - 30 μm) circular grains in thin section. However, analysis of these grains using glycerine mounts shows that they are composed of pyrite with a framboidal texture. These pyrite framboids occur in several different positions within the sediment, they are most commonly located in the fine-grained organic-rich laminations where they occur as clusters sometimes totalling several hundred individual framboids. Some are found on the margins of quartz and glauconite grains, these tend not to be clustered, but occur as

Plate 8. Photomicrograph showing the decomposition of detrital muscovite leading to "unpeeling" along the cleavages at the margins of the grain giving a "bow-tie" section to the grain. Plane polarized light.

Plate 9. Photomicrograph showing paralled laminated very fine sands of the higher mudflat subenvironment. Note also the alignment of opaque grains parallel to the laminations. Analysis of heavy mineral concentrates and magnetic mineral concentrates has shown that these grains are primarily composed of titanomagnetites. Plane polarized light.

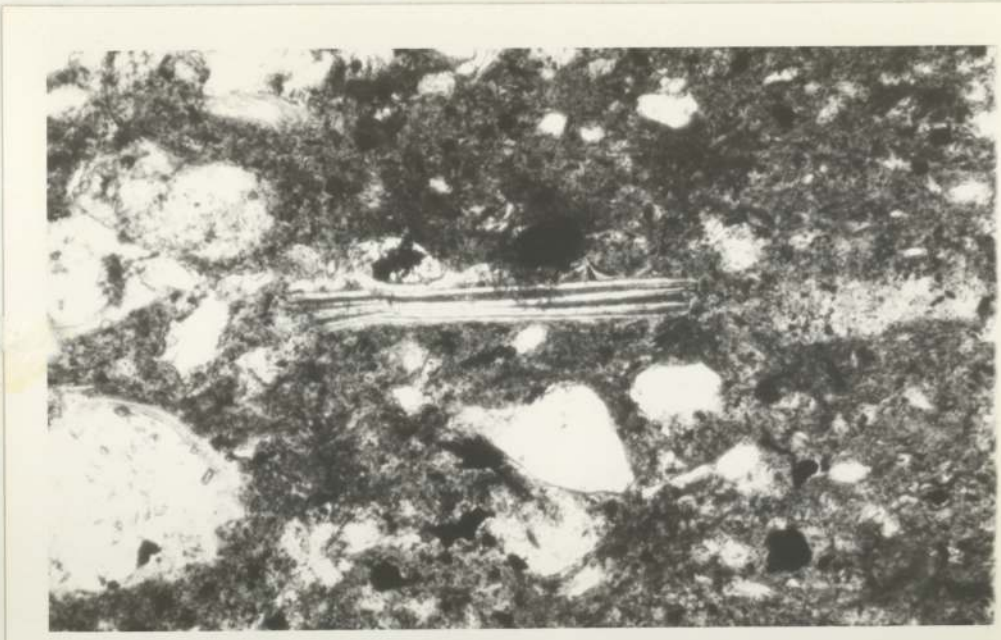

Plate 8. 100μm

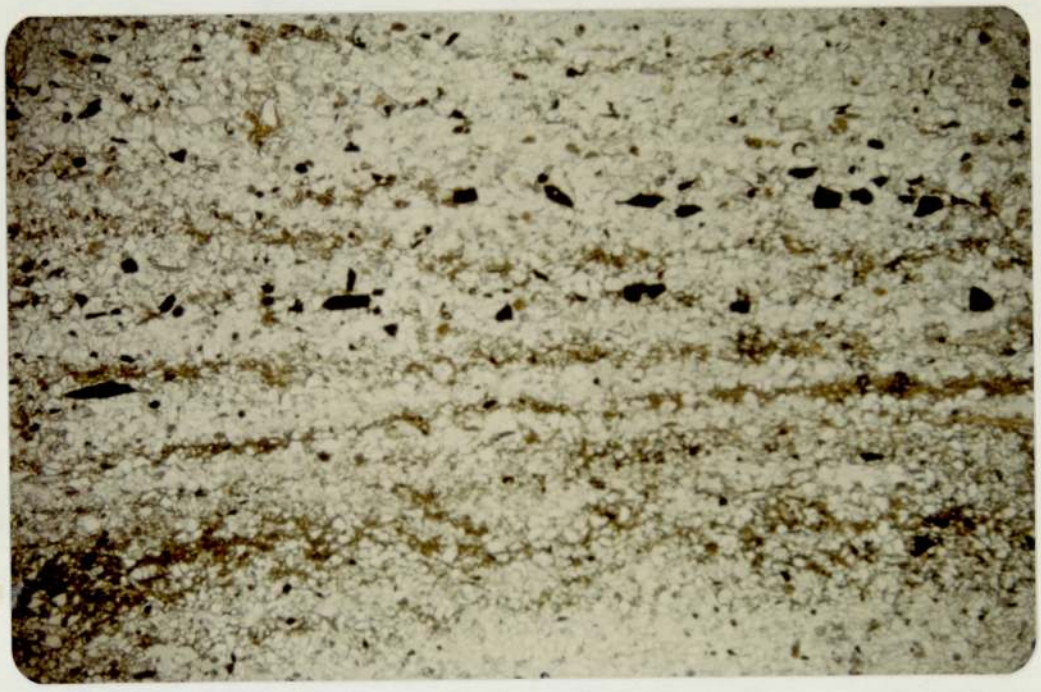

Plate 9. 1000μm

Plate 10. Photomicrograph showing the preservation of primary current lamination in the very fine sands and silts of the higher mud flats. Preferred alignment of large magnetite grains (opaques) can also be seen. Plane polarized light.

Plate 11. Photomicrograph showing section through a foraminiferid test which shows partial infilling of its chambers by pyrite framboids (opaque circular grains). Note that the lowest parts of the foram have been infilled first. Plane polarized light.

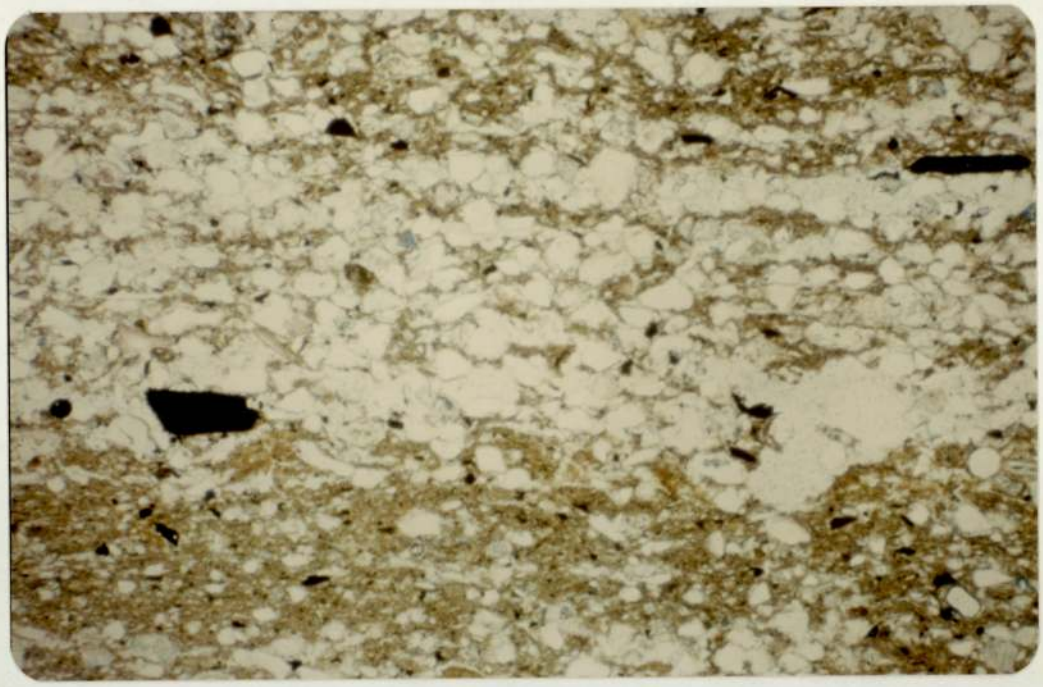

1000μm

Plate 10

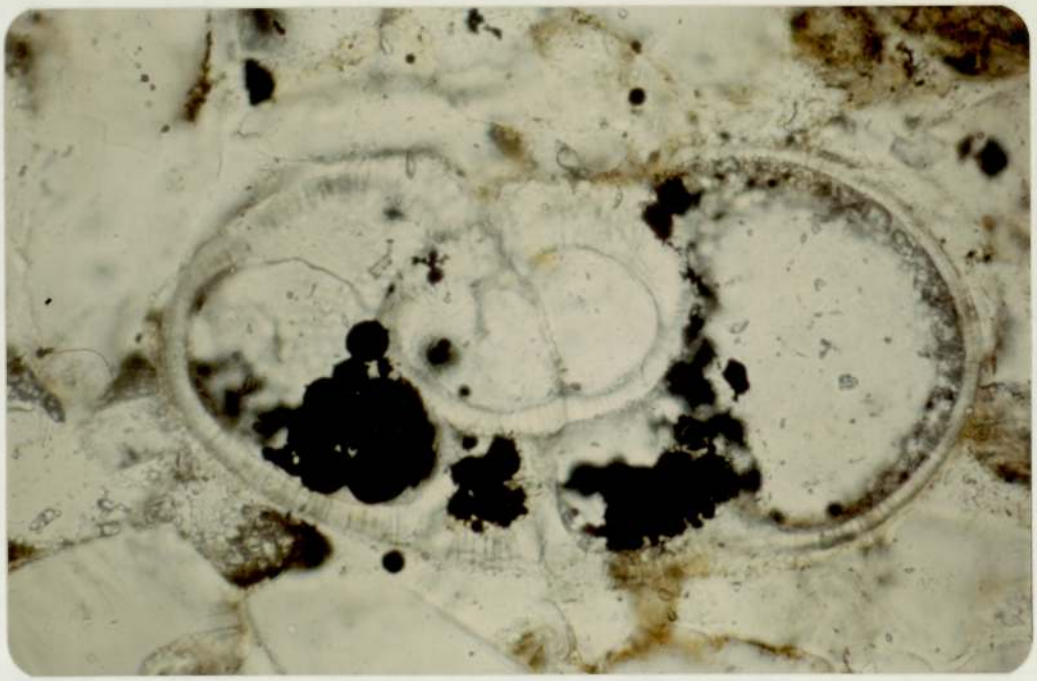

100μm

Plate 11

Plate 12. Photomicrograph showing section through a foraminiferid test, which shows almost complete infilling of its chambers by authigenic pyrite framboids (opaque circular grains). Plane polarized light.

Plate 13. Photomicrograph showing the same view as above except using crossed nicols.

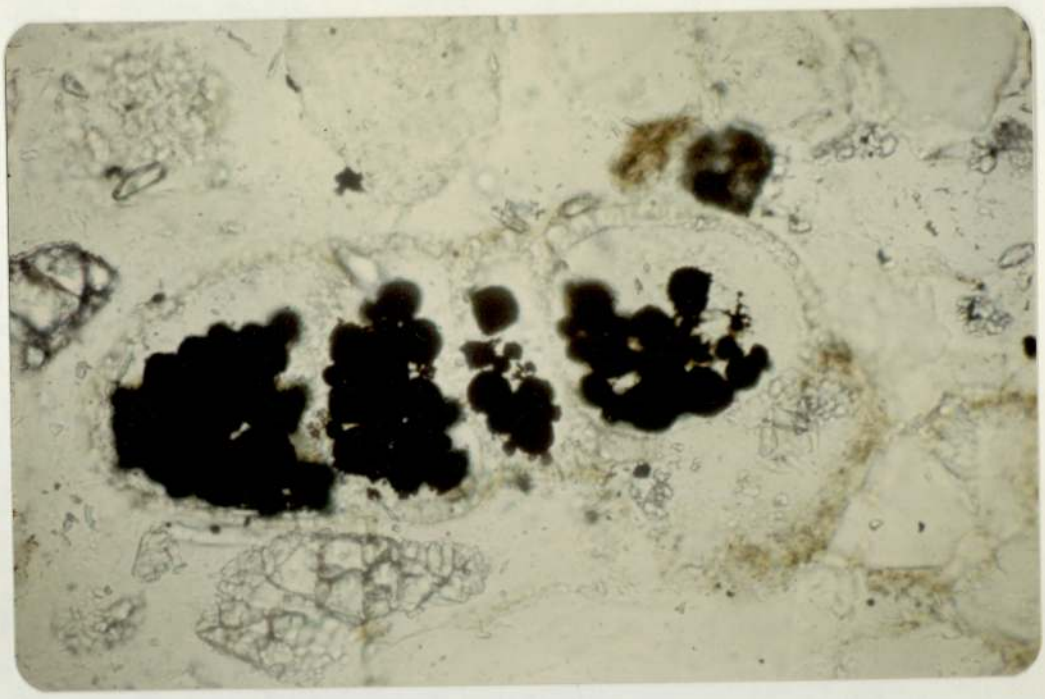

Plate 12

100µm

Plate 13

100µm

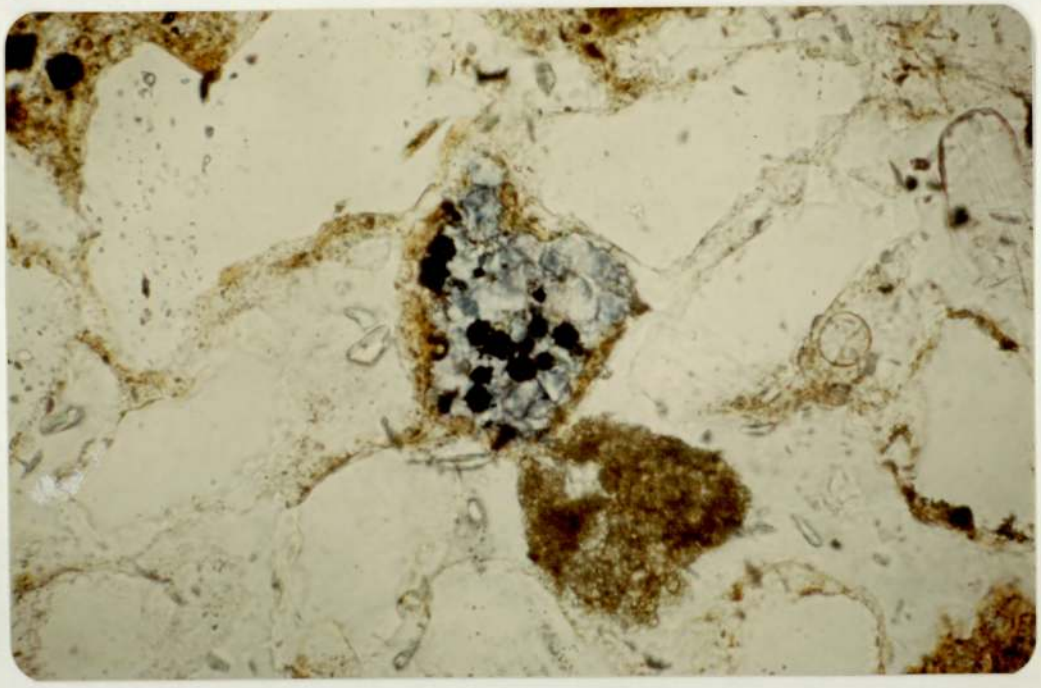

Plate 14.

100μm

Plate 14. Photomicrograph showing a detrital ferroan calcite grain (stained blue) on which authigenic pyrite framboids (black opaque grains) have formed. Plane polarized light.

Plate 15. Photomicrograph showing a detrital chlorite pellet (green grain at centre) showing the typical spherical shape. Plane polarized light.

Plate 16. Photomicrograph of the chlorite grain shown above using crossed nicols. Note the typical patchy extinction.

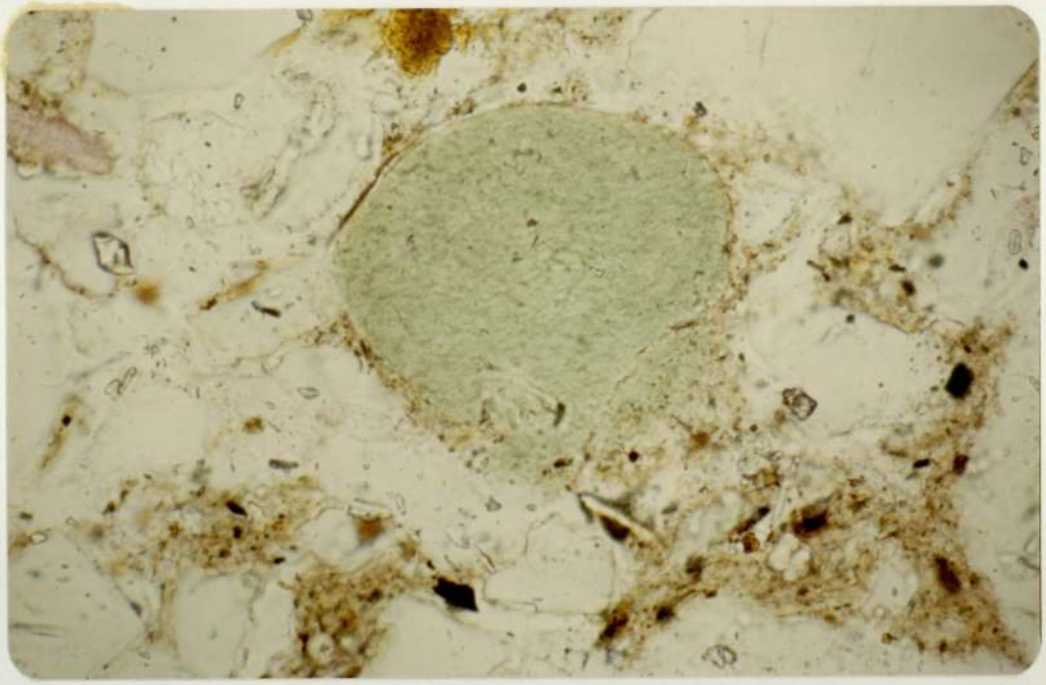

Plate 15

100µm

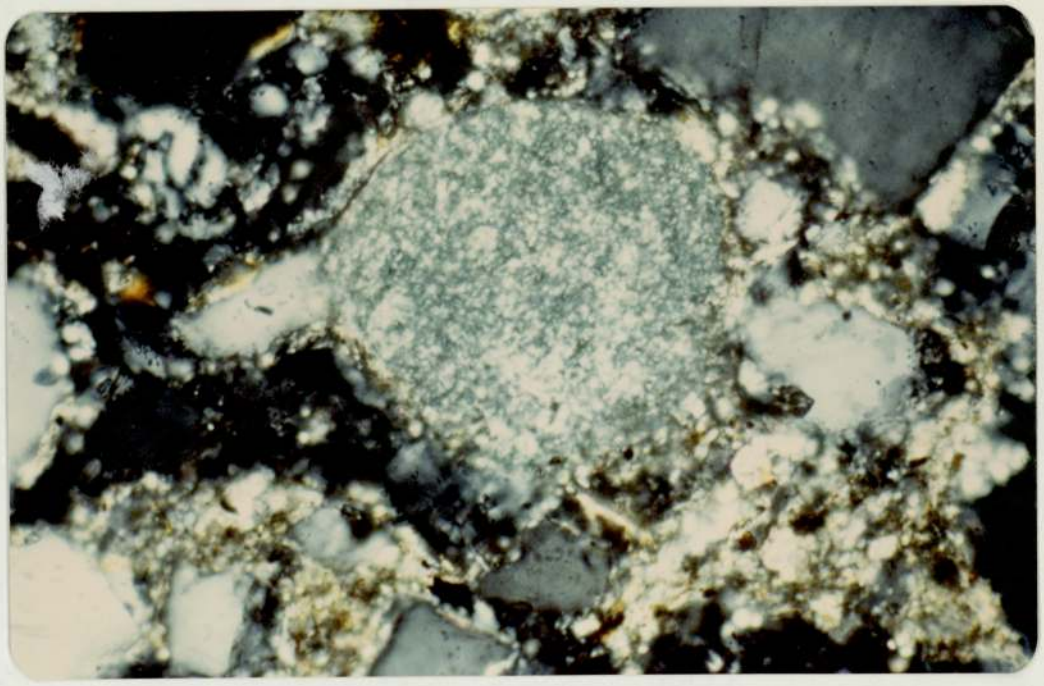

100µm

Plate 16

Plate 17. Photomicrograph showing chlorite pellet (green grain at centre) which has been deformed between quartz grains during early stages of compaction in the sediments. Plane polarized light.

Plate 18. Photomicrograph showing the same chlorite pellet as shown above except using crossed nicols.

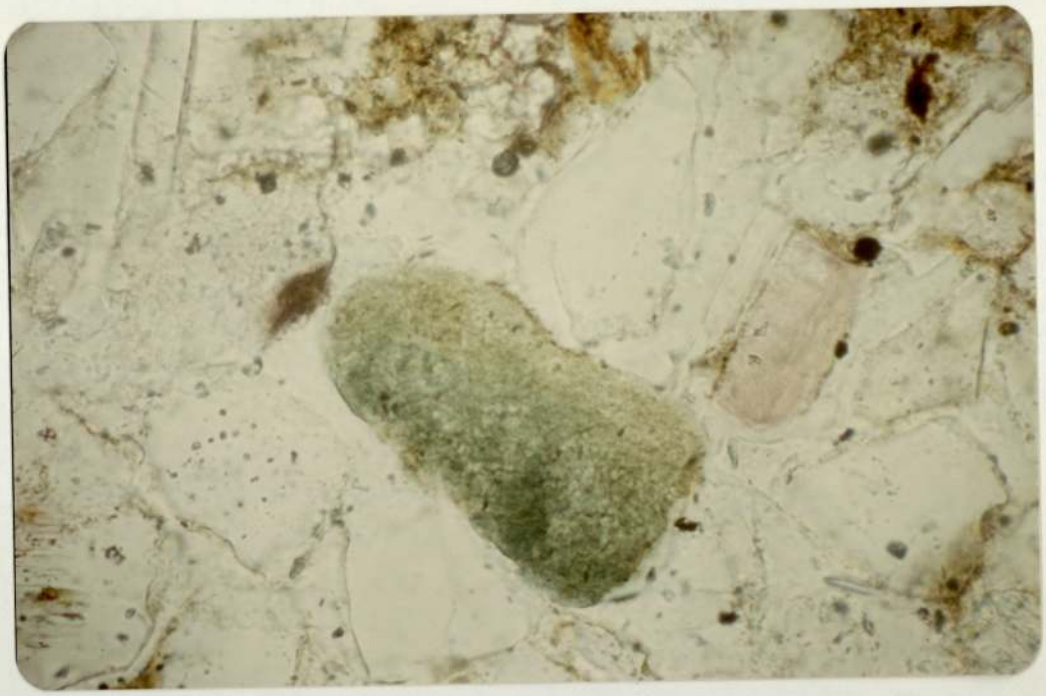

Plate 17

100µm

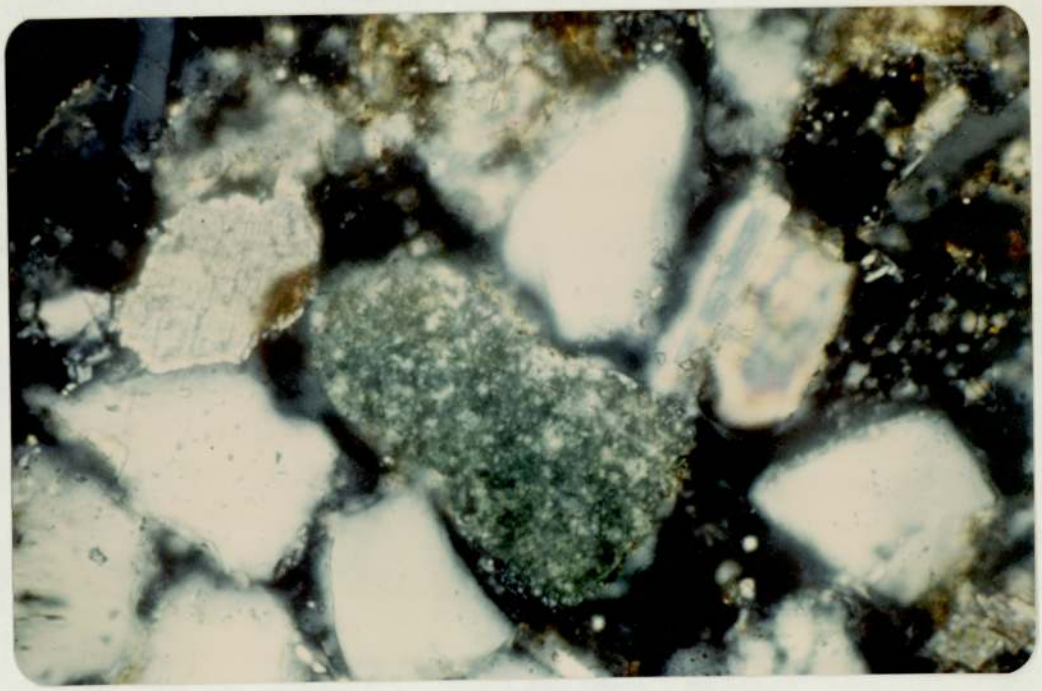

Plate 18

100µm

individual framboids or in smaller groups of 2,3, or 4 framboids. Other framboids are found partially or totally infilling foraminiferal tests (plates 11, 12 and 13). Some of these foraminifera also show partial infilling by radially cemented micritic calcite. A final occurence of pyrite framboids is in association with ferroan calcite, where the framboids can be seen partially replacing the ferroan calcite (plate 14).

The clay mineralogy of the sediments again is dominated by allogenic clays with poor crystalinity, and, reference is again made to chapter 3 where their mineralogy is analysed using X-ray diffraction.

Less than 2% of the sediment consists of feldspars, which are mostly of plagioclase often exhibiting the characteristic Carlsbad twinning.

Accessory minerals include glauconite pellets, chlorite, zircon, pyroxenes, amphiboles, dolomite, siderite, kyanite and tourmaline. The chlorite pellets are shown in plates 15, 16, 17 and 18, they are commonly round in shape but may show partial deformation due to compaction between quartz grains.

A feature of many of the detrital quartz and calcite grains is a red surface coating of iron oxide, this is possibly hematite although it has not been possible to obtain any other mineralogical data on it, due to its low concentration within the sediment and its inferred poor crystalinity.

Primary lamination is often well preserved in the sediments of the higher mud flats, indicating their potential as good sediments for use in palaeomagnetic studies (plates 9 and 10). Even using the relatively crude technique of coring employed in the collection of the one-metre cores, primary lamination is

preserved to within 2 mm of the core edge, (plate 19) where a zone of disturbed sediment 2 mm thick occurs. Evidence of minor compaction in the sediment is provided by the presence of dewatering structures in the form of micro "boudinage" (plate 20) where coarse sediment has compacted into horizontal cylinders of sediment around which are finer (darker) laminations. Another minor deformational structure seen in some of the sediments of the higher mud flats is the occurence of small scale flame structures again indicating compaction. These tend to occur as irregular cuspate upward surfaces within the sediment (plate 21 and 22). Finally, minor bioturbation is also found in the sediments of the higher mud flat resulting from the burrowing activity of the worm Nereis diversicolors, evidence of which is shown in plate 23. Despite these influences, the primary lamination is often well preserved in the sediments of the higher mud flat, as evidenced by laminated sediments (plates 9 and 10), and by prefered alignment of platey grains and foraminifera (plate 24).

In a study of the differences in grain-size distributions between the sub-environments of deposition on the tidal flats of the Wash, Amos (1974) was able using the parameters; mean grain-size, sorting and skewness to define a series of fields for each sub-evironment. Grain-size analysis, using the standard seive and pipette methods, was performed on samples taken from core 2, representing the higher mud flat sediments at Freiston Shore. The results (see Table 2-1 ) when plotted on the charts of Amos (1974) show good general agreement with the fields outlined for the higher mud flat sub-environment, (figures 2-11 and 2-12) although some enlargement of the fields seems necessary.

By contrast the sediments of the Arenicola sand flats, the

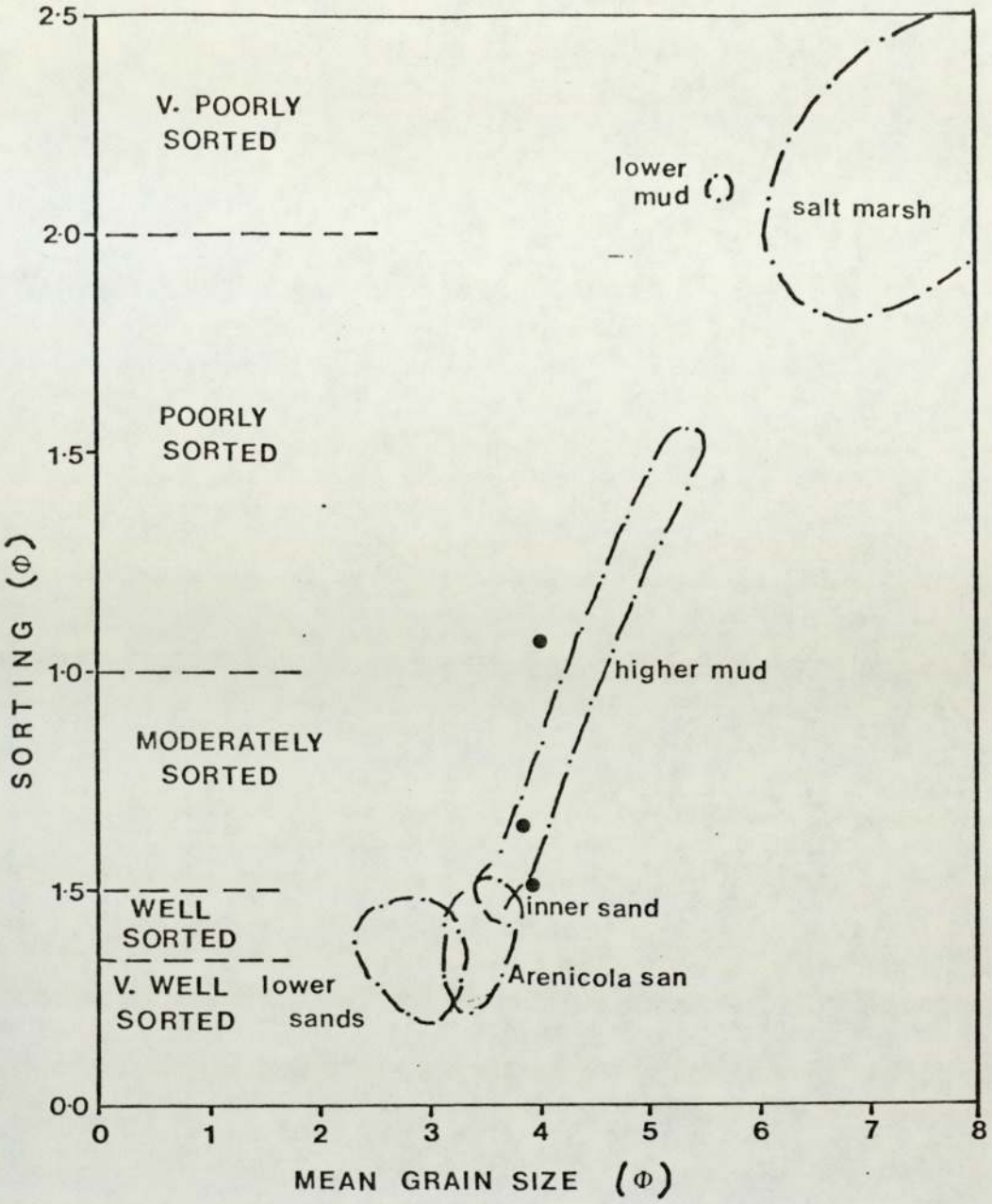


Figure 2-11. Mean grain-size verses sorting for sediments from the sub-environments of deposition recognised by Evans (1965). Data is also plotted for sediments studied here (•). Modified after Amos (1974).

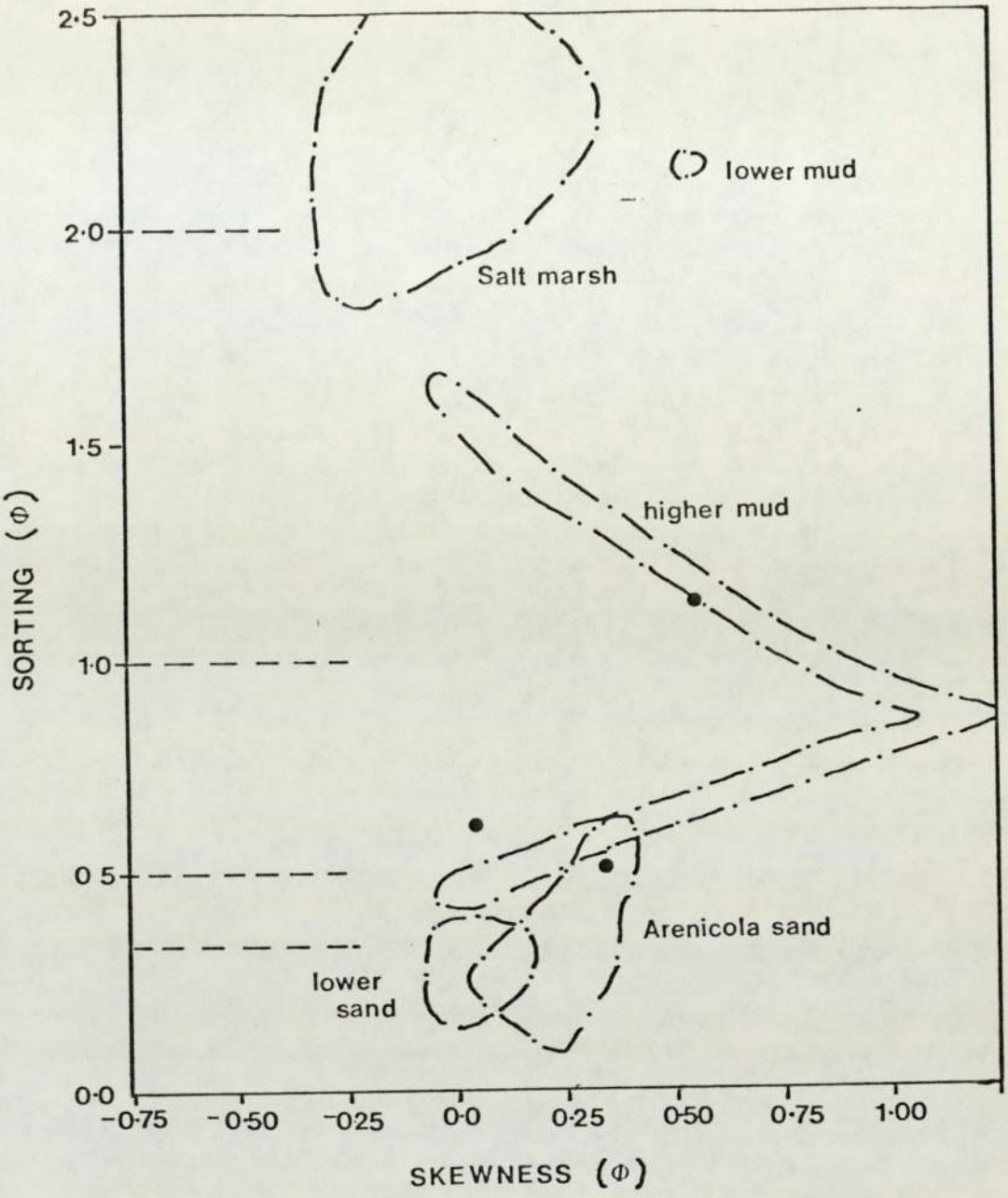


Figure 2-12. Sorting verses skewness (after Amos, 1974) showing data from sediments studied here, plotted as (•).

Plate 19. Photomicrograph showing the thin zone (2mm thick) of disturbed sediment at the margin of the core (lower left). Note that primary laminations are preserved right up to the edge of this disturbed zone. Plane polarized light.

Plate 20. Photomicrograph showing the development of dewatering structures in the form of micro "boudinage". Plane polarized light.

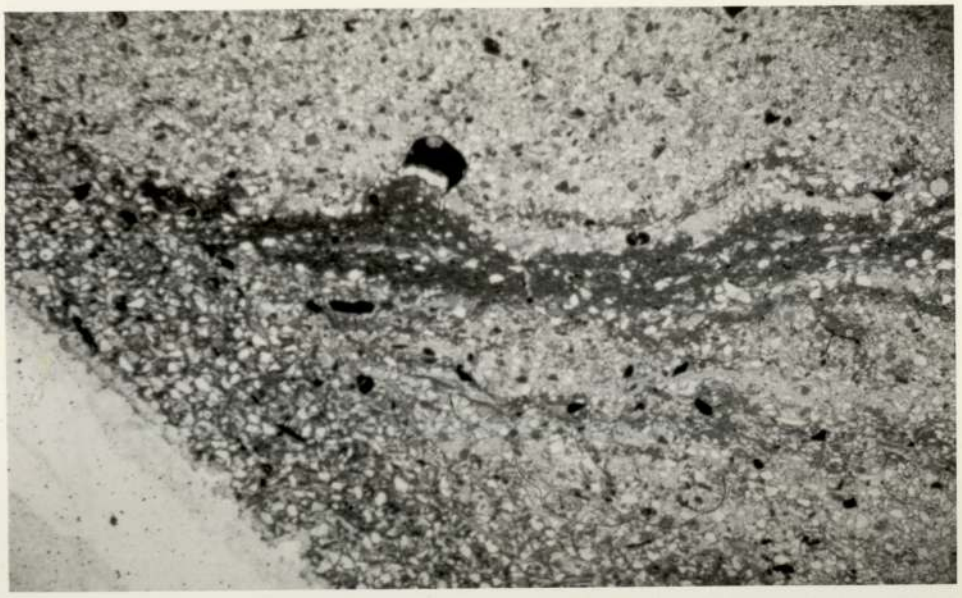

1000µm

Plate 19.

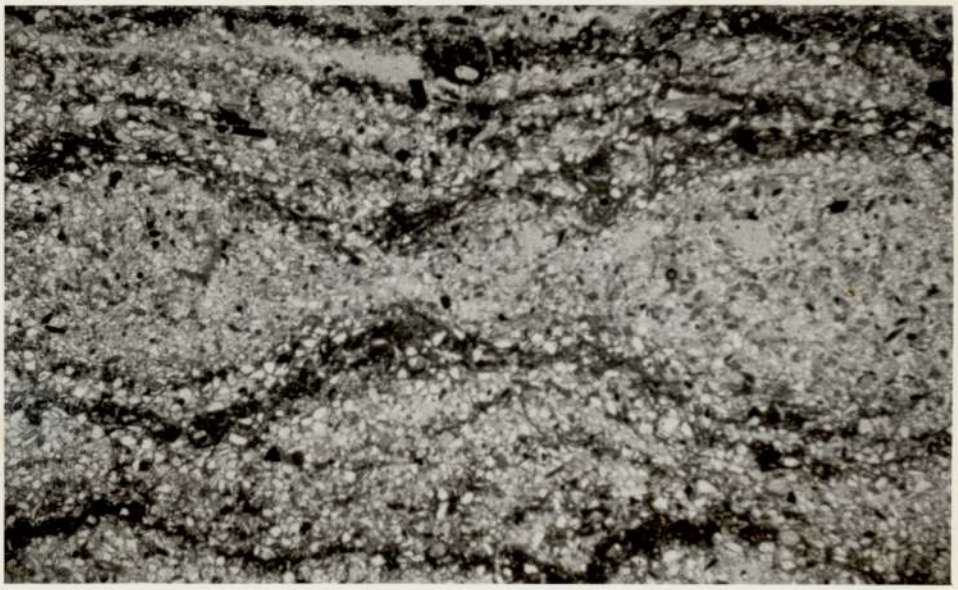

Plate 20.

1000µm

Plate 21. Photomicrograph showing the development of cuspate upward pointing dewatering structures in the sediments of the higher mud flats. Plane polarized light.

Plate 22. Photomicrograph showing a close up of the upward pointing cuspate structures shown above. Note that the primary lamination is quite strongly distrupted in this part of the sediment. Plane polarized light.

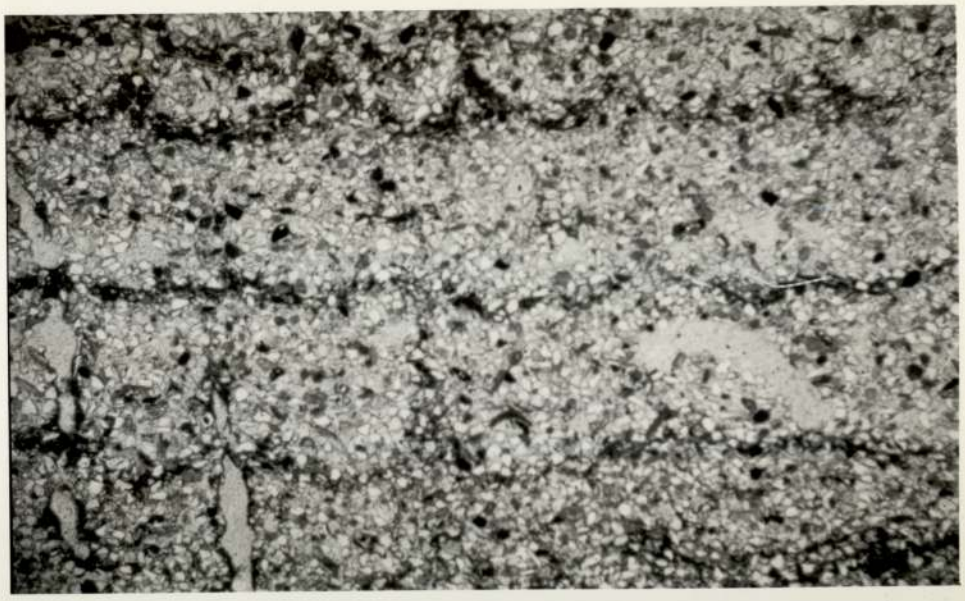

Plate 21. 1000μm

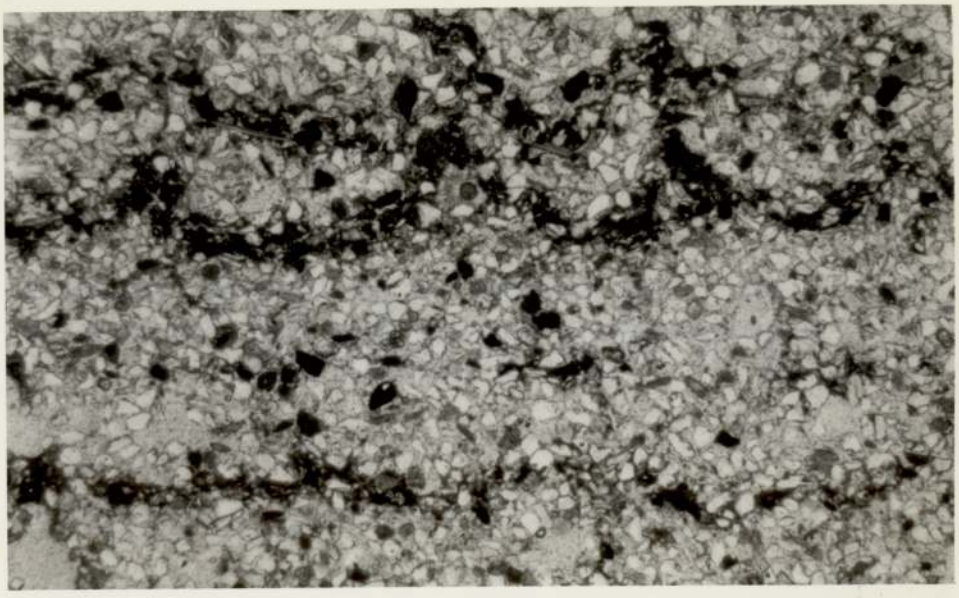

Plate 22. 1000μm

Plate 23. Photomicrograph showing a burrow probably caused by the worm Nereis diversicolors. Plane polarized light.

Plate 24. Photomicrograph showing the preferred alignment of platey grains and foraminifera. Plane polarized light.

Plate 23. 1000µm

Plate 24. 100µm

third and final sub-environment examined here, show little evidence of primary current laminations due to the almost complete bioturbation by the worm Arenicola marina. The sediments also differ in having greater concentrations of quartz and lesser concentrations of clay minerals. The quartz grains fall in the very fine sand to fine sand grain-size range and are sub-angular to sub-rounded in shape. A similar distribution of quartz extinction types to those recorded for the higher mud flats occurs in the sediments of the Arenicola sand flats.

Calcite is present in minor quantities (0-6%) and occurs mainly in the form of shells and foraminifera, with rare ferroan calcite and sparry calcite grains of the type found in the sediments of the higher mud flats. The occurence of pyrite is also much reduced in the Arenicola sand flat sediments due to the coarser grain-size, which promotes more oxidizing conditions prior to deep burial, and also to the lower initial concentrations of organic matter found within the Arenicola sands.

Finally, since only rare sedimentary structures can be observed in the Arenicola sands it is not possible to gain a visual appraisal of the extent to which the sediments have suffered from compactional deformation. However, the extensive bioturbation of these sediments has probably aided the initial loss of depositional porosity, leading to early compaction. It is suggested that once the sediment is buried below the reach of bioturbating organisms, that compactional processes will slow down. This is important with regard to the dating of the magnetization of these sediments and will be discussed further in subsequent chapters.

| Sample | Median | Mean | Dispersion | Skewness | Kurtosis |
|---|---|---|---|---|---|
| 2,8 | 3.85 | 4.00 | 1.11 | -0.56 | 4.02 |
| 2,24 | 3.85 | 4.00 | 0.40 | 0.35 | 1.67 |
| 2,48 | 3.75 | 3.85 | 0.64 | 0.07 | 5.82 |

TABLE 2-1. Grain-size statistics (Folk and Ward, 1957) for sediments from the higher mud flat subenvironment at Freiston Shore (Core 2).

## 2-3. X-ray Diffraction of Whole Sediment Samples.

In order to verify the results of optical microscopy a series of samples from core D1 were subjected to analysis using X-ray diffraction (Table 2-2). The method used was to crush asample of the sediment to a powder and then to mount it as an unoriented powder for X-ray diffraction analysis. In all of the samples analysed in this way the whole sediment mineralogy was found to include quartz and clay minerals. Other minerals present in some of the samples are calcite and feldspar and also minor dolomite. These results agree with those of Shaw (1973) who also found quartz, calcite, clay minerals, feldspar and dolomite to be the chief minerals identifiable by X-ray diffraction.

As a result of these determinations it was decided that no systematic study of the whole sediment mineralogy of the tidal flat sediments, using X-ray diffraction, need be attempted. However, it was decided that the analysis of the clay mineralogy by X-ray diffraction warranted further study. This would enable accurate identification of the clay minerals which could not be achieved from the traces made of whole sediment samples. The analysis of the clay mineral concentrates is discussed in chapter 3.

| Specimen | Quartz | Calcite | Clay Minerals | Feldspar | Dolomite |
|---|---|---|---|---|---|
| D12.50 | P | P | P | P | A |
| D13.50 | P | P | P | A | P |
| D14.50 | P | P | P | A | A |
| D15.50 | P | A | P | A | A |
| D16.50 | P | P | P | P | A |
| D17.50 | P | P | P | P | A |
| D18.50 | P | P | P | A | A |
| D19.50 | P | P | P | P | A |
| D110.50 | P | P | P | A | A |

P = Present

A = Absent

Table 2-2. X-ray diffraction results showing the occurence of quartz, calcite, clay minerals, feldspar and dolomite in whole sediment samples from core D1.

## 2-4. Geochemical Analysis of the Tidal Flat Sediments From Core D1.

A sequence of seventeen samples were selected from the Delft core D1 for geochemical analysis of their major elements. The samples analysed are spaced at 20 cm intervals in the upper 2 metres of the core, in the section which shows greatest lithological variation, and at one-metre intervals in the lower severn metres of the core. The samples correspond to those used in the study of the clay mineralogy, chapter 3; and to some of those used in the study of Mössbauer spectroscopy.

The samples were prepared by first washing them in distilled water prior to analysis so that any precipitated salts (deposited from evaporated sea-water), particularly salts of sodium and magnesium, were removed. The method of analysis used in this study is atomic absorption using a Perkin Elmer Atomic Absorption Spectrophotometer. The method of analysis was that described by Van Loon and Parissis (1969), which is a standard method of silicate analysis based on a lithium metaborate fusion technique. Analysis was performed to determine the concentrations of the following cations; aluminium, silicon, magnesium, manganese, calcium, iron, sodium, and potassium. The results of the analyses are shown in figure 2-13 and in table 2-3, where the concentrations are expressed as the weight percentage oxide. Measured and actual values are also given for a standard rock sample (internal standard AGV-1, a granodiorite).

The results of the analyses show that, as expected from optical and X-ray diffraction studies, silicon is the most abundant element forming between 59.8 and 95.6% oxide of the sediments. Most of this silicon can be assigned to silica ($SiO_2$) although a proportion of it also occurs in the clay minerals and

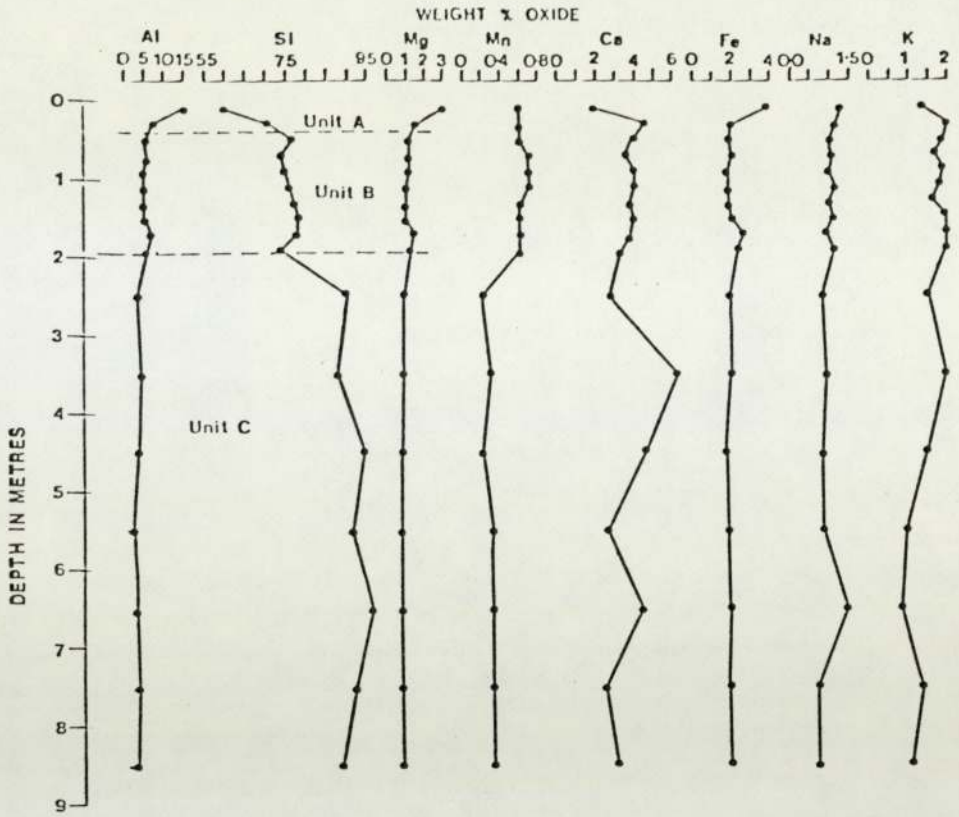


Figure 2-13. Results of the geochemical analyses, showing the distribution of the weight percent oxide of the major elements present in the sediments from core D1.

| SAMPLE | WEIGHT PERCENT OXIDE | | | | | | | |
|---|---|---|---|---|---|---|---|---|
| | Al | Si | Mg | Mn | Ca | Fe | Na | K |
| D12.10 | 14.86 | 59.84 | 3.03 | 0.06 | 1.97 | 3.93 | 1.30 | 1.36 |
| D12.30 | 7.49 | 71.77 | 1.66 | 0.06 | 4.52 | 2.05 | 1.16 | 1.98 |
| D12.50 | 5.17 | 77.20 | 1.19 | 0.06 | 3.86 | 1.79 | 1.03 | 1.87 |
| D12.70 | 5.86 | 73.93 | 1.24 | 0.07 | 3.59 | 2.11 | 1.10 | 1.67 |
| D12.90 | 5.21 | 74.51 | 1.10 | 0.07 | 4.03 | 1.85 | 1.07 | 1.89 |
| D13.10 | 4.78 | 76.04 | 1.00 | 0.07 | 4.07 | 1.80 | 1.14 | 1.83 |
| D13.30 | 4.91 | 77.20 | 1.04 | 0.06 | 3.73 | 1.94 | 0.97 | 1.62 |
| D13.50 | 4.84 | 78.33 | 0.99 | 0.06 | 3.99 | 1.94 | 1.06 | 1.95 |
| D13.70 | 6.74 | 77.94 | 1.40 | 0.06 | 3.77 | 2.65 | 0.92 | 1.94 |
| D13.90 | 6.27 | 73.50 | 1.24 | 0.06 | 3.25 | 2.32 | 1.11 | 1.95 |
| D14.50 | 3.37 | 90.11 | 0.84 | 0.02 | 2.63 | 1.87 | 0.84 | 1.52 |
| D15.50 | 3.55 | 87.69 | 0.82 | 0.03 | 6.22 | 1.86 | 0.89 | 1.91 |
| D16.50 | 3.11 | 94.14 | 0.70 | 0.02 | 4.51 | 1.60 | 0.77 | 1.44 |
| D17.50 | 2.07 | 90.82 | 0.76 | 0.03 | 2.50 | 1.78 | 0.76 | 0.92 |
| D18.50 | 2.64 | 95.59 | 0.78 | 0.03 | 4.30 | 1.89 | 1.45 | 0.77 |
| D19.50 | 2.43 | 91.59 | 0.71 | 0.03 | 2.40 | 1.73 | 0.67 | 1.28 |
| D110.50 | 2.47 | 88.38 | 0.69 | 0.03 | 3.05 | 1.79 | 0.65 | 1.06 |
| AGV.1m | 16.74 | 59.82 | 1.78 | 0.05 | 5.99 | 5.91 | 4.99 | 1.69 |
| AGV.1e | 17.01 | 58.99 | 1.49 | 0.09 | 4.98 | 6.80 | 4.33 | 2.89 |

TABLE 2-3. Geochemical results of whole sediment samples from core D1. Concentrations are expressed as weight percent oxide. AGV.1m are the measured values for the standard sample, whilst AGV.1e shows the established values for its composition.

in detrital feldspars. It is also the silicon which shows the most marked variation throughout the core. At the top of the core, in unit 1, the silicon content shows an increase from 59.8 to 71.8 weight percent oxide. This increase is continued through units 2 and 3, in unit 2 the silicon content rises to approximately 75 weight percent oxide, and in unit 3 it rises again to form 87.5 - 95.5 weight percent oxide.

The distribution of aluminium, magnesium, and iron each show an inverse relationship to that of silicon. This indicates that their variation is mainly attributable to variations in the total clay fraction present in the samples, agreeing with the data from petrographic observations. Of these three elements, aluminium is the most abundant with a peak concentration of 14.9 weight percent oxide in unit 1, decreasing to a minimum concentration of 2.1 weight percent oxide in unit 3. The concentration of iron in the core falls in the range 1.6 - 3.9 weight percent oxide (expressed as $Fe_2O_3$) whilst magnesium is slightly less abundant with a concentration of 0.7 - 3.0 weight percent oxide.

The distribution of calcium throughout the core shows a somewhat erratic variation, probably because of its occurence mainly in the form of shells and shell debris. The concentrations of calcium lie in the range 2.0 - 6.2 weight percent oxide. Sodium shows little variation throughout the core, its concentration falling in the range 0.70 - 1.3 weight percent oxide. What variation there is in the distribution of sodium appears to follow the trends of the aluminium, magnesium, and iron distributions indicating that most of the sodium occurs in clay minerals. In view of the analyses carried out on the clay mineralogy (chapter 3) it is probable that the sodium is mostly concentrated within the

clay minerals; montmorillonite, and illite-montmorillonite.

The variations in the distribution of these elements show a marked dependance upon the particular lithological type in which they occur (Figure 2-13). This dependance is better displayed if the geochemical data are clustered. Figure (2-14) shows a Q-mode dendrogram using the average pair-group method with the distance coefficient as a similarity measure. Units 1, 2, and 3 have clearly dissimilar chemical compositions.

The variations in the compositions of the samples may also be clustered to show which elements show similar variations. Figure (2-15) shows an R-mode dendrogram using the correlation coefficient as a similarity measure. The diagram clearly shows the similar distribution of aluminium, magnesium, and iron indicating that these elements mostly occur together, probably in clay minerals. Sodium is also grouped with Al, Mg, and Fe, also indicating its chief occurence in the clay mineral montmorillonite.

The variation in silicon and calcium shows virtually no similarity, due to the scattered nature of the occurence of calcium in shell material. Silicon and calcium together show a negative correlation with the other elements, indicating an inverse relationship with them. Hence, clay-rich sediments are low in silicon (dominantly in the form of quartz grains) and vice versa.

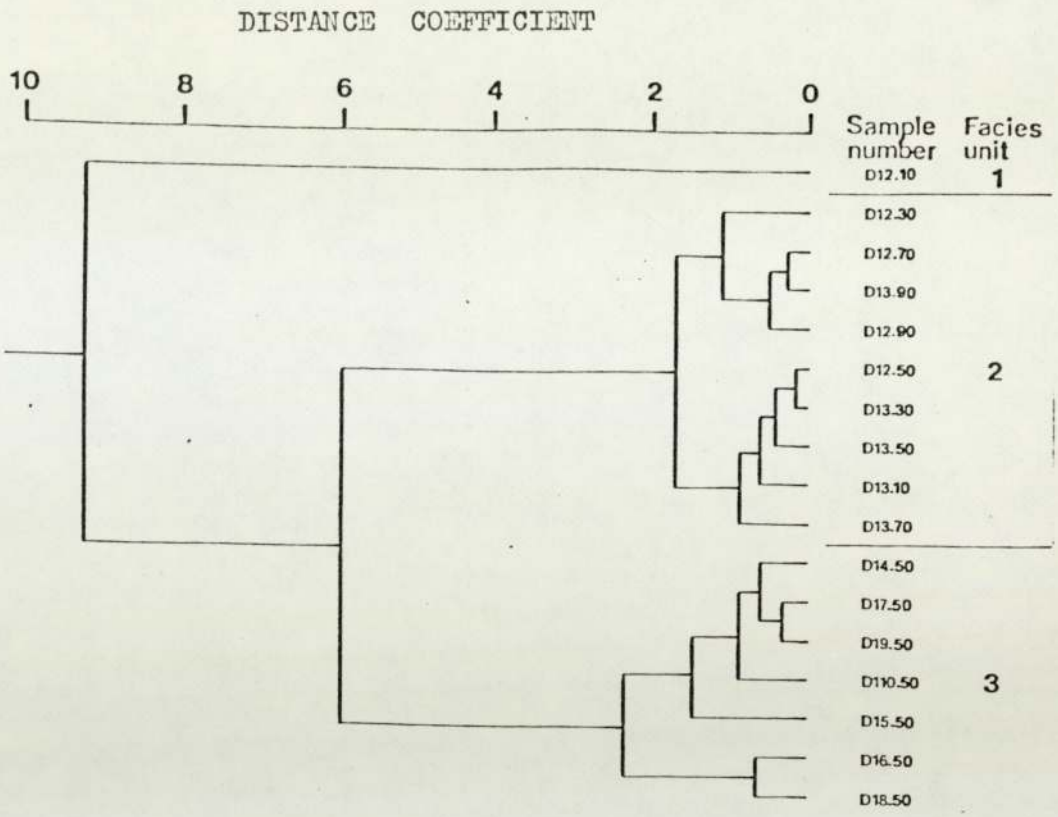


Figure 2-14. Q-mode dendrogram using the distance coefficient as the similarity measure. The diagram shows the clustering of the samples, using geochemical data, into the three major lithological units recognised in Delft core D1.

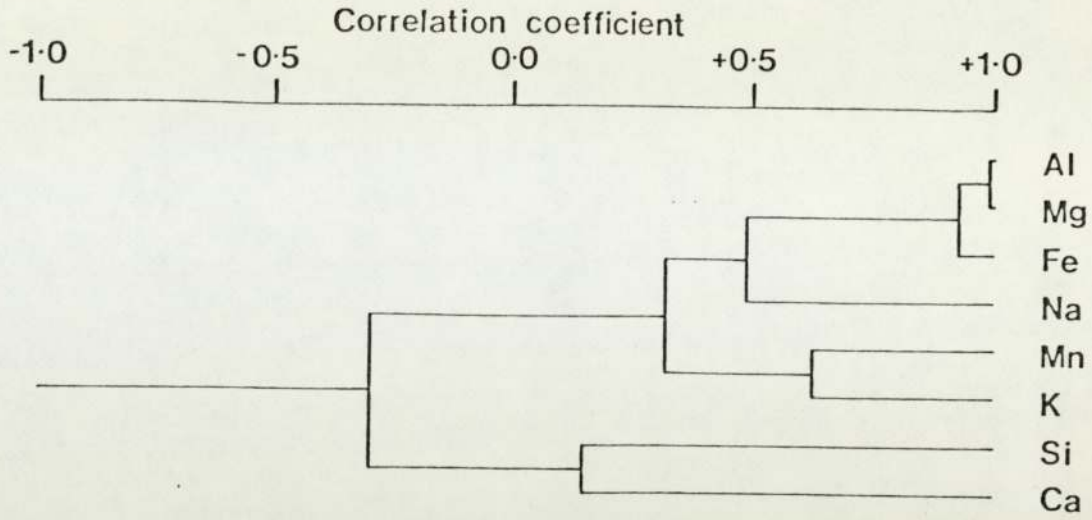


Figure 2-15. R-mode dendrogram using the distance coefficient as the similarity measure. The diagram shows the clustering of the major elements found in the clay minerals in core D1, which are; Al, Mg, Fe and Na. An inverse relationship between the elements in the clay minerals and the presence of silicon in the samples is also indicated.

## 2-5. Conclusions

In this study, sampling of the salt marsh, higher mud flat and *Arenicola* sand flat sediments has been achieved using both one-metre and nine-metre Delft cores. These techniques enabled examination of a sequence 2.40 metres thick at Freiston Shore, one metre thick at Wrangle flats and 9 metres thick at Leverton. All the cores were found to end still within the tidal flat deposits, giving a minimum thickness of these deposits of 9 metres. This disproves Evans (1965) estimate that the tidal flats were approximately 7 metres thick.

The sediments from the cores have been analysed initially in terms of their whole sediment mineralogy and geochemistry. The most important observations, relevant to the objectives of this study, are the occurences of iron sulphides, chiefly as authigenic pyrite framboids, and also the occurence of opaque euhedral grains, thought to be magnetite grains aligned parallel to the primary laminations in the sediment. Also important with regard to the studies of the paleomagnetic properties of the sediments, which are discussed later, are the observations of the sedimentary fabric. Most importantly, the primary laminations present in the salt marsh and higher mud flat sediments show good preservation and are unaffected by the coring process. In contrast the sediments of the *Arenicola* sand flats show almost complete bioturbation with few primary sedimentary structures preserved. It is thus concluded that the sediments belonging to the salt marsh and the higher mud flats will probably give the best results in the palaeomagnetic studies.

Mineralogically the sediments are composed chiefly of quartz, calcite, clay minerals, feldspars and minor dolomite.

These observations have been confimed by X-ray diffraction analysis of whole sediment samples. Apart from variations in the ratio of quartz to clay minerals no major variations were found in the whole sediment mineralogy.

Geochemical studies of the sediments show them to be composed dominantly of silicon, ranging in abundance from 59.8 - 95.6 weight percent oxide of the sample. The next most abundant element is aluminium, followed by calcium, iron magnesium and potassium, which are all present in proportions of 0.5 to 4 weight percent oxide. Sodium and manganese are present only in minor concentrations.

Finally, cluster analysis of the geochemical data shows that the distribution of the major elements is dependant on the lithology of the sediments, itself a result of the sub-environment from which the sediments come.

The mineralogical studies have shown the need for accurate identification of the clay minerals, since these may be an important source of iron for the formation of the authigenic iron sulphides. Therefore, the next part of this study is an examination of the clay minerals using X-ray diffraction of clay mineral concentrates.

Chapter 3.

## X-ray Diffraction Studies of the Clay Minerals.

### Introduction.

The aim of this aspect of the work was to investigate the nature of the major clay minerals in the Delft core D1 and their distribution throughout the core. X-ray diffraction alone does not permit conclusive identification of clay minerals which, thus have been also studied using thin sections, the scanning electron microscope and, in the case of iron-bearing clays, Mössbauer spectroscopy.

A previous study of the clay mineralogy of the Wash sediments by Shaw (1973) shows that the major clay minerals in the $< 2\mu m$ fraction are illite, kaolinite, mixed-layer illite-montmorillonite, montmorillonite and chlorite. Shaw's (1973) study, however, was part of a wider study of the origin of the clay minerals in the Wash and involved examination of samples from the intertidal sediments, the offshore bottom sediments and also some of the Early Holocene and Pleistocene deposits. Shaw (1973) did not specify the exact location of the specimens within the intertidal flat. In the present study it was possible to determine the variations in clay minerals in the upper three sub-environments recognised by Evans (1965); the salt marsh, higher mudflat and the Arenicola sand flat.

3-1. Preparation of the samples and X-ray techniques.

The X-ray identification of clay minerals is largely based on differences in their basal interplanar spacings. In order to obtain strong basal reflections it is necessary to orient the clays. Two main advantages arise from using oriented mounts; firstly, the diagnostic basal reflections are emphasised and the non-basal reflections are suppressed, simplifying the overall pattern; secondly, the sensitivity is increased many times, allowing the detection of small amounts of poorly crystalline materials.

Several methods have been developed for the orientation of clay minerals parallel to the mount, most of which involve a sedimentation process. Gibbs (1965) has pointed out that in such sedimentation techniques, a segregation of large from small grains occurs, giving the mount a thin surface layer of fine particles. Since different clay mineral species may be of different mean grain size, large errors can occur in quantitative estimations of mineral abundance (Gibbs, 1965). This arises because 90% of the diffracted X-rays originate from the top 5 - 12$\mu$m of the sample. It is thus necessary to prepare mounts which are oriented but have no grain size seggregation. Gibbs (1971) has found two techniques to be acceptable in these respects. They are the "smear on a glass slide technique" (Gibbs, 1965) and the "suction onto ceramic tile method".

The "smear on glass slide technique" involves the smearing of a paste of clay across a slide using a flexible plastic spatula. The mount is then allowed to dry prior to being X-rayed. The "suction onto ceramic tile method" has several advantages over the "smear on glass slide technique"; the mounts can be heat-

treated without damage, solutions such as acids can be passed through the tile, and the tile can act as a reservoir for excess organic swelling agents during glycolation, preventing relaxation of expandable layers in the clays whilst diffraction traces are being recorded. The "suction onto ceramic tile" method is also preferable since it provides an even coat of clay and it is easy to build up a suitably thick layer of clay on the mounts, from samples which have a low proportion of clay material, by applying successive coats of clay. The "suction onto ceramic tile method" was therefore used throughout this study.

The following method was used to prepare the ceramic tile mounts used in this study. Sediment samples of approximately 40 grams were dispersed overnight in 200 mls of distilled water. After being thoroughly shaken, a sample was pipetted from the stock suspension and a $<2\mu m$ fraction was seperated out using a centrifuge. Circular sample mounts were cut from unglazed ceramic tiles using a 2.54mm (1") diamond drill. The tile was then clamped in position between two rubber seals in a stainless steel funnel. This assembly was attached to a buchner flask and a vacuum was applied. After checking the seal by dripping distilled water onto the tile, the $<2\mu m$ suspension was pipetted from the centrifuge tube and placed on the tile. The water was then drawn through the tile by the vacuum leaving a coat of clay on the upper surface of the tile. It is important to note that since the suspension on the tile is only a few millimeters thick, and that $2\mu m$ particles will fall 1mm in 4.8 minutes, care must be taken not to exceed 10 - 15 minutes for the preparation of one layer of clay. Of course, it is possible to build up a thick coat of clay by repeating this proceedure.

When all of the distilled water has been drawn through the tile and a satisfactory layer of clay deposited, the tile is removed and placed in a vacuum desiccator in order for it to dry completely.

One complication that can arise from the use of the ceramic tile method is that the tile itself may contribute to the diffraction trace particularly if the clay layer is thin or if exposed parts of the tile occur in the area analysed. To compensate for this possible source of interference, a number of blank tiles were themselves run on the X-ray diffractometer. In all cases, the tiles were found to be composed of quartz and feldspar and gave peaks within the range of interest at 4.272Å and 4.054Å which can be subtracted from the diffraction traces of the specimens.

Following sample preparation, three diffraction traces were run for each sample. Initially, a sample was run after drying in the vacuum desiccator and prior to any other treatment. Next, the sample was subjected to an organic swelling agent, ethanediol (ethylene glycol). Glycolation of the samples was carried out in an oven at 80°C. The most successful method of glycolation involved actually standing the tile in ethanediol, taking care not to cover the top of the tile since this might cause floatation of the clay particles and their disorientation. The third trace was run after heating the tile at 180°C for one hour in a furnace. This served to vapourise all theethanediol and also to remove any remaining interlayer water molecules in the expandable clays. Traces were then run immediately after cooling to prevent re-absorption of water from the atmosphere. All of the diffraction data were obtained using iron-filtered cobalt - Kα radiation

produced from a Philips X-ray Diffractometer operated at a current of 30Ma and a voltage of 30kV. Iron-filtered cobalt - Kα radiation was used in preference to copper - Kα radiation in order to minimise possible fluroescence from iron-bearing clay minerals.

3-2. X-ray diffraction results and their interpretation.

Initial interpretation of the X-ray diffraction traces reveals that illite, kaolinite, chlorite and mixed-layer and expandable clay minerals are the major clay species present in all of the samples examined. In order to calculate the abundance of each clay mineral species the method described by Griffin (1970) was used. The method requires that three basic conditions are met. Firstly, that the reported clay minerals (in this case; illite, kaolinite, chlorite and expandable clays) comprise 100% of the sample. Secondly, that the diffracting ability of each of the clay minerals is equal. This condition is not always met since the diffracting ability is dependant on the composition, polytype and degree of crystallinity of each individual clay mineral. Finally, since the chlorite (004) and kaolinite (002) basal reflections are used in the determination of the relative proportions of these two minerals, the assumption is made that if kaolinite and chlorite are present in equal proportions, the intensities of these two peaks will be equal.

The method requires that the three diffraction traces described earlier are available; that is, the trace obtained after drying the sample, one after glycolation, and one after heating to 180°C for one hour. A modification of the method described by Griffin (1970) used here was to employ the areas of the diffraction peaks rather than their heights in estimating intensities. This is particularly important if the crystallinity poor and a broad peak is produced. This modification is critical in the interpretation of the traces obtained in this study because marked variation occurs in the degree of crystallinity of the samples, (for example, between mixed-layer and expandable clays with low

crystallinity and illite which has better crystallinity, see figure 3-1).

Calculation of the percentage abundance of each clay mineral is undertaken as follows. Firstly, the total percentage of kaolinite and/or chlorite is found using the diffraction pattern obtained at 180°C. The notation used is as follows; K,C,I, and M refer to kaolinite, chlorite, illite and mixed-layer and expandable clays respectively. The symbol "a7Å(180°C)" refers to the area of the 7Å peak on the 180°C diffraction pattern; similar symbols being used for other peaks. The formula for the total percentage of kaolinite and chlorite is thus:

$$\%K+C = \frac{(a7Å(180°C)/2.5)}{(a7Å(180°C)/2.5)+a10Å(180°C)} \times 100$$

The constant "2.5" is used to correct for the difference in the diffracting ability of the (001) kaolinite diffraction peak and the (001) illite diffraction peak. The relative proportions of kaolinite and chlorite are then calculated as follows:

$$\%K = \frac{a3.58Å(180°C)}{a3.58Å(180°C)+a3.54Å(180°C)} \times \%K+C$$

and

$$\%C = (\%K+C)-\%K$$

The percentages of illite and the expandable clays are then determined as follows:

$$\%I+M = \frac{a10Å(180°C)}{(a7Å(180°C)/2.5)+a10Å(180°C)} \times 100$$

Finally, the relative proportions of illite and the expandable clays are determined as follows:

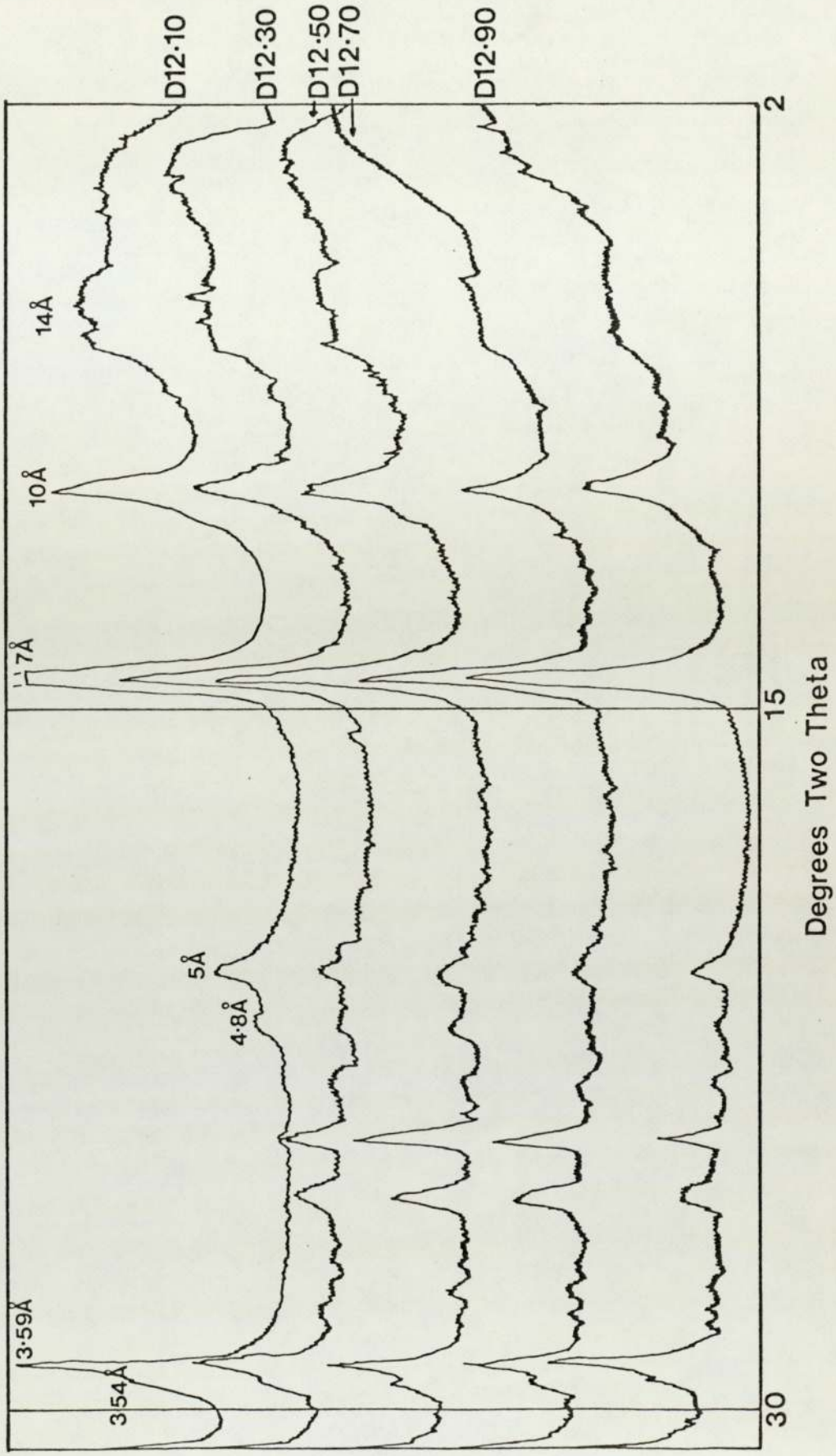


Figure 3-1. Examples of the X-ray diffraction traces for samples of the<2$\mu$m fraction of sediment from core D1. The traces shown are for those taken prior to treatment with ethylene glycol

$$\%I = \frac{a10\text{Å}(E.G.)x(a7\text{Å}(180^{\circ}C)/a7\text{Å}(E.G.))xI+M}{a10\text{Å}(180^{\circ}C)}$$

$$\%M = (\%I+M)-\%I$$

An example of a typical calculation is shown in appendix 1 The unit of area used on the diffraction traces in the measurement of peak intensities, is $25mm^2$. The fraction labelled expandable clays is made up of both montmorillonite and mixed-layer illite-montmorillonite. In the fractions studied by Shaw (1973) the data were rounded to the nearest 5%. However, in the duplicate determinations made in this study, the repeatability of results was found to be of the order of 2%. For this reason the data have been presented to the nearest 1% since further round ing would mask minor, but real, variations in the clay mineralogy.

Seventeen samples were analysed from core D1, the samples being spaced at twenty centimetre intervals in the upper two metres of the core, where the greatest variation in lithology occurs, and at one-metre intervals in the lower seven metres of the fine sands. The results of the analyses are presented diagrammatically in figure 3-2 and the data are tabulated in appendix 2.

The results show that throughout the core, illite is the most abundant clay mineral with a mean concentration of 48.0% of total clay in the $<2\mu m$ fraction. The next most abundant clays are those of the expandable (montmorillonite and mixed-layer illite-montmorillonite) group which show a mean concentration within the core of 25.1%. Kaolinite forms 20.0% of the total clay in the $<2\mu m$ fraction. The only other clay identifiable by X-ray diffraction is chlorite with a mean concentration of 6.9%.

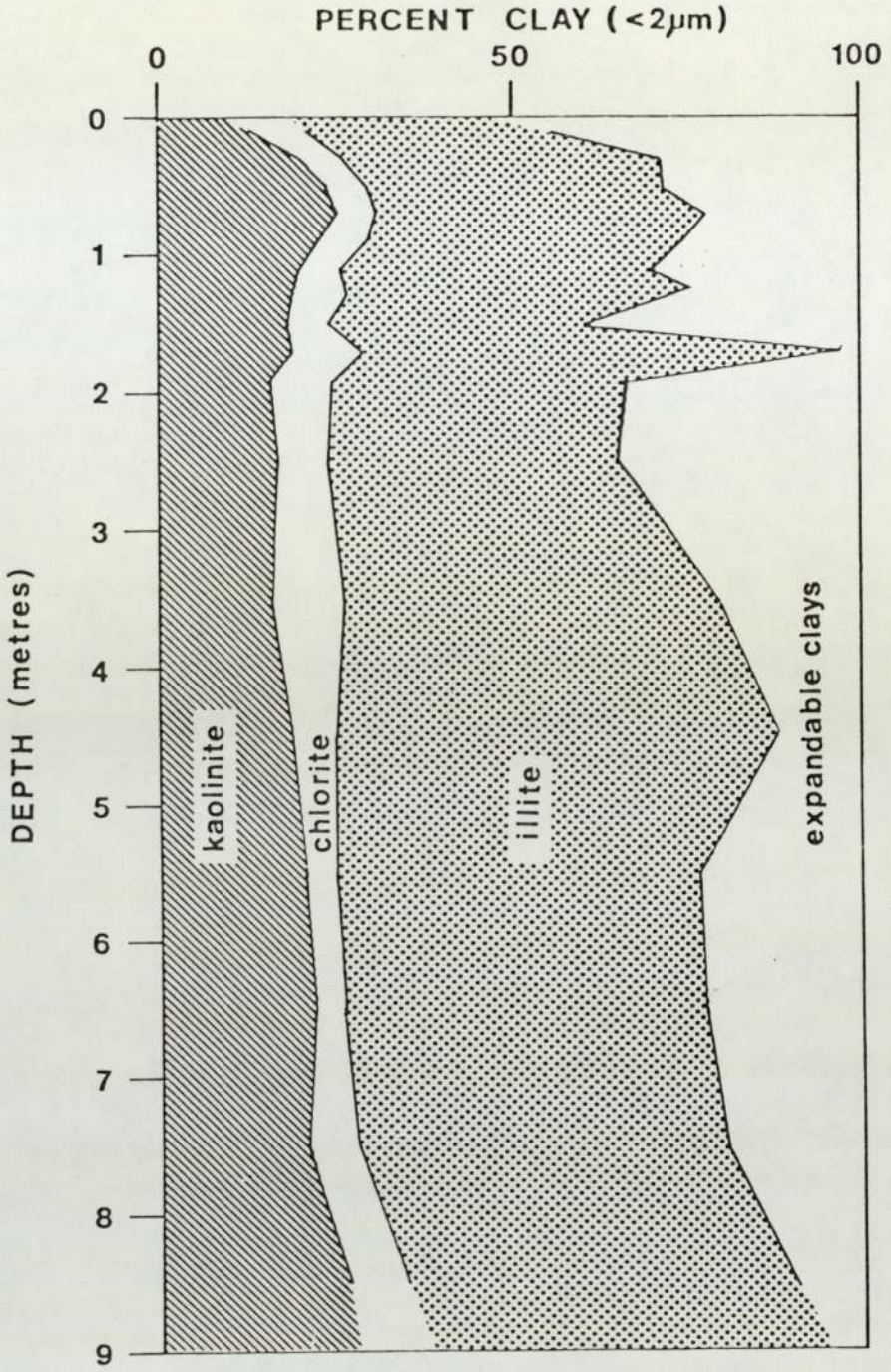


Figure 3-2. Clay mineral variations of the <2μm fraction of sediments in Delft core D1.

These figures agree well with those obtained by Shaw (1973) which show illite to comprise 40 - 45% of the total clay in the $<2\mu m$ fraction, mixed-layer illite-montmorillonite 25 - 35%, kaolinite 15 - 20%, and chlorite 5 - 10%.

The most pronounced variation in the clay mineralogy in core D1 is the decrease in expandable clays (illite-montmorillonite and montmorillonite) with depth from 44% at the top of the core to 10% at the base. Most of this variation is taken up by a corresponding increase in the abundance of illite from 35% at the top of the core to 55% at the base. In part, this variation can be explained by the increased montmorillonite in the salt marsh deposits of unit 1. In unit 2, the higher mudflat sediments, the expandable clays show little variation (a mean of 26% of the total clay) except for sample D12.70 (at a depth of 0.70m) which is greatly depleted in montmorillonite. In the sands of unit 3, the mixed-layer and expandable clays show a depletion with depth from 35% at the top to 10% at the base.

It is most unlikely that this depletion of mixed-layer and expandable clays with depth can be explained by burial diagenesis as proposed in older sequences such as the Eocene sediments of the Gulf Coast (Burst, 1959; Burst, 1969, and Perry and Hower, 1970). However, Millot (1970) considers that burial diagenesis is the best explanation to explain the common observation of decreasing montmorillonite concentration with depth in Recent sediments. Millot (1970) was, however, considering environments in which the clay minerals were introduced into the marine environment from fluvial sources. Powers (1957) suggested that the loss of montmorillonite with depth in the sediments of Chesapeake Bay could be explained by a process involving conversion to illite

by substitution of $Mg^{2+}$ for $Al^{2+}$ in the silicate structure, with the consequent fixation of interlayer potassium. In the Wash embayment, the major source of sediment is not fluvial (although this plays a small part) but is from the glacial deposits of the North Sea and from longshore movement along the coasts to the north and the south of the Wash (Evans and Collins, 1975 and Amos, 1974). It is expected that montmorillonite would also have been derived from the North Sea and would already have achieved equilibrium with the marine environment and would not be affected by burial diagenesis with a layer of sediment only nine metres deep.

An alternative mechanism is that of differentiation of the clay fractions, particularly montmorillonite from illite, as a result of their relative densities, resulting in differences in their settling velocities. Since the source of sediment on the tidal flat is from the seaward, it might reasonably be expected that montmorillonite, having the lowest settling velocity, would be carried furthest and be enriched in the most landward subenvironments of deposition. This appears to be the case in core D1 in which montmorillonite is concentrated in the sediments that have been identified as representing the salt marsh and higher mudflat subenvironments, and depleted in the coarser Arenicola sands.

Kaolinite also shows significant variations in abundance throughout the core. There is a general tendency for variations in kaolinite to be the inverse of those observed in the mixed-layer and expandable clays. This is particularly well illustrated in the top one-metre of the core, where there is a large and progressive increase in kaolinite from 13% in unit 1, to a peak

value of 26% near the top of the higher mudflat sediments (unit 2). A progressive decrease then follows throughout unit 2 and into unit 3, until values of 16% are reached. In the lower four metres of unit 3, kaolinite begins to increase again until it forms 26% of the sample at the base of the core.

There is no evidence for alteration of kaolinite from variations in its degree of crystallinity or any other features observed using the scanning electron microscope (see chapter 2). It is concluded that the variations in kaolinite distribution are also best explained by differential sedimentation since the shape of the kaolinite grains (thin platy flakes) will have a significant effect upon their hydrodynamic properties. Since kaolinite generally forms large flakes, often upto 20$\mu$m in diameter, its concentration in the coarsest part of unit 3 may also be explained by differential sedimentation. The increase in abundance at the top of unit 2, the higher mudflat sediments, is more difficult to explain. However, since this part of the core represents a palaeo-mean high-water mark, it suggests that a sedimentation process associated with this particular horizon is responsible for the increase in kaolinite concentration. One possible explanation is an enrichment of very fine-grained kaolinite at this level. It is concluded that differential sedimentation is the most important process in explaining the observed variations in the distribution of kaolinite.

Chlorite is the least abundant of the clay minerals in the core, although it is the major iron-bearing clay mineral species. There is little significant variation in the distribution of chlorite (which falls in the range 4 - 10% total clay), probably because the minor amounts of chlorite present are close to the

detection limit of the X-ray diffraction technique.

Measurements of the abundance of the clay grade quartz, feldspar and calcite in these sediment fractions were not made since experimental difficulties are caused by the use of ceramic tiles, which themselves contain both quartz and feldspar. Shaw's (1973) data showed that quartz was detected in only three out of twenty four samples. It is of interest to note that these three samples (using the notation of Shaw (1973) samples; HS.24, HS.12 and HS.30) all lie at points of fluvial input into the Wash, on the Witham, Welland and Nene outlets respectively. Hence, it is concluded that the prime source of this $< 2\mu m$ quartz on to the tidal flats is from fluvial input.

From the shapes of the diffraction peaks (figure 3-1) it is possible to estimate the relative degree of crystallinity of the clay particles. All of the samples examined show the same trend with the degree of crystallinity decreasing in the order; kaolinite, chlorite, illite, mixed-layer illite-montmorillonite. It must be noted that broadening of the X-ray diffraction peaks is also a function of the grain-size of the respective clay minerals, and since the trend observed in the degree of crystallinity is similar to that for the variations in grain-size, it is concluded that both effects interact to produce the differences in the shapes of the diffraction peaks observed here.

3-3. Glycolation, thermal treatment and acid dissolution.

The X-ray identification of the clay minerals using dried oriented samples can be substantiated by further treatment of the sample involving the use of organic swelling agents, heating, and acid dissolution. The use of ethylene glycol as a swelling agent for the identification of montmorillonite and mixed-layer clays has already been discussed briefly in the section on quantitative analysis (section 3-2). Initially these clay minerals were merely identified as the expandable clays or as montmorillonite and mixed-layer illite-montmorillonite. However, further inspection of the data indicates the presence of other "swelling" clay minerals.

In many of the samples, glycolation results in the development of a broad peak extending from the 14.4Å peak to peaks indicating larger basal spacings of upto 18.7Å. Heating of the samples reverses this process leaving the 14.4Å peak as shown in the diffraction traces of sample D12.30 (figure 3-3). Associated with the production of this broad peak is a diminution in the size of the 10Å peak on glycolation and an increase again on heating (figure 3-3, and appendix 3 ). This is characteristic of the swelling of the interlayer spacings between the (001) basal plane of montmorillonite. However, since the 14.4Å peak also shows a diminution on glycolation and growth after heating, it is probable that another mineral species is contributing to this broadening. Brindley (1961) has described the swelling of labile chlorites which show a swelling from 14Å to 17.8Å. It is suggested that labile chlorites may also contribute to this broadening. These features are evident in all of the samples studied (appendix 3).

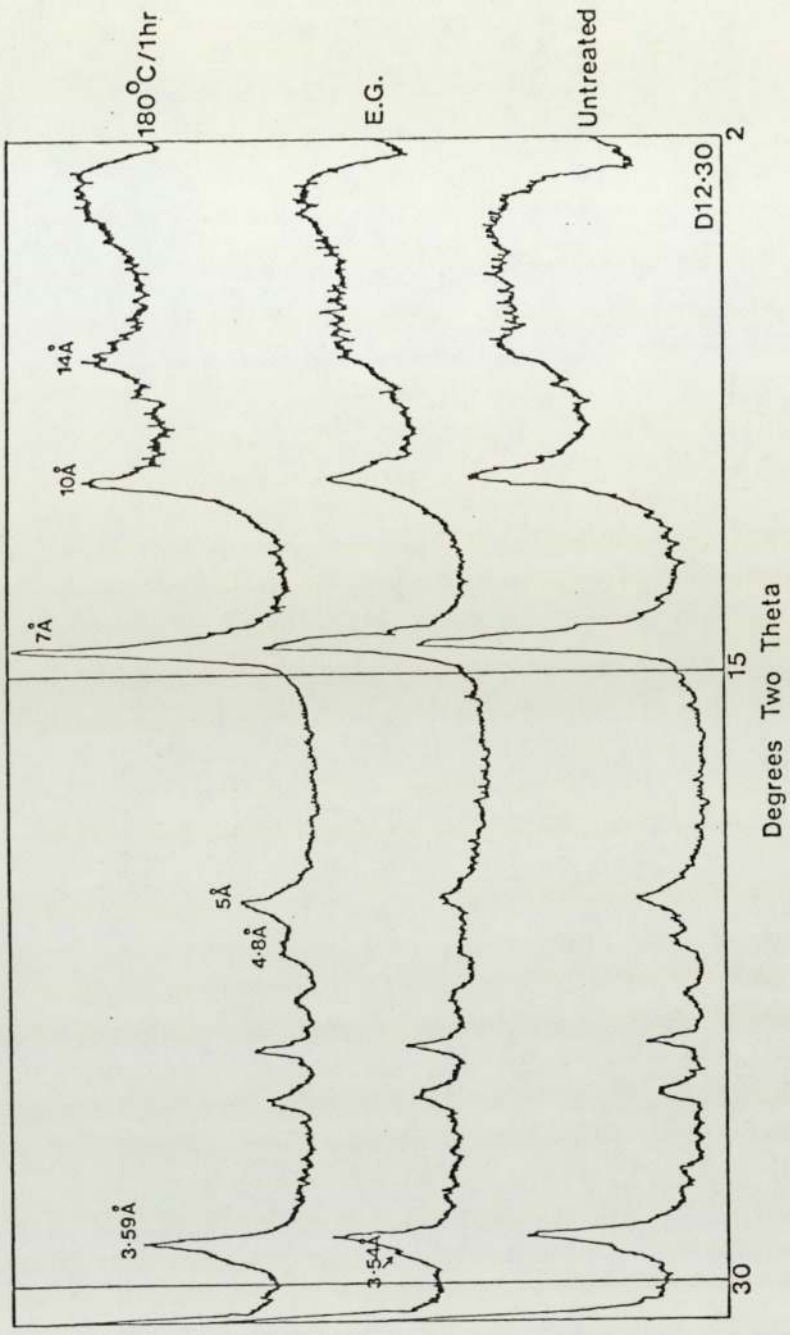


Figure 3-3. Typical example of the three X-ray diffraction traces (untreated, after treatment with ethylene glycol, and after heating to 180°C for one-hour) used in the quantitative study of the clay mineralogy. The grain-size of the fractions analysed is 2 m. The traces shown here are for specimen D12.30.

In most of the samples (D12.50 to D110.50) the background of recorded X-rays is high at low Bragg angles (2 - 4°2θ) due to scattering of X-rays at low angles and also possibly due to slight imperfections in the orientation of the clay particles on the ceramic tiles. However, in samples D12.10 and D12.30, a broad band of low angle basal reflections are observed from 2°2θ in sample D12.10, and 2.75°2θ in sample D12.30, to about 6°2θ. The main characteristic of this feature is the rapid increase in the intensity from 2°2θ to 3°2θ . In sample D12.10, this broad band has a poorly defined peak at 3.5°2θ corresponding to an interplanar spacing of 29.35Å. After glycolation, this peak is reduced in intensity and is more diffuse. Heating of the specimen to 180°C for one hour results in the complete disappearance of this peak and, presumably, the decomposition of the clay mineral concerned. The diffraction trace for the untreated specimen D12.30 also shows the maximum of this broad band of low angle reflections to be centered at 3.5°2θ (an interplanar spacing of 29.35Å). However, on glycolation, these low angle reflections are not reduced as in specimen D12.10, but intensify slightly and also expand to give an interplanar spacing of 31.2Å. Heating of the specimen at 180°C for one hour does not result in any noticeable change in the shape or intensity of this peak.

The additional clay mineral present in samples D12.10 and D12.30 is identified as the clay mineral corrensite. Corrensite is a mixed-layer clay mineral containing regular mixed-layers of chlorite and montmorillonite. The large basal spacing of the (001) plane is caused by the additive effect of the two interstratified layers of chlorite and montmorillonite producing a basal interplanar spacing of 29Å. This spacing of 29Å expands to 32Å in

corrensite on treatment with glycerol (Millot, 1970) and this agrees well with the swelling to 31.2Å observed in specimen D12.30 using ethylene glycol as the swelling agent. Specimen D12.10, on treatment with ethylene glycol, shows reduction in the intensity of this peak, although some swelling is evident. As noted earlier, heating of the samples causes disappearance of the (001) basal reflection of corrensite suggesting that the products are seperate chlorite and montmorillonite. Hence, it appears that sample D12.10 contains a structurally less stable form of mixed-layer chlorite-montmorillonite (corrensite).

Since the mineral corrensite is found as a significant component only in the X-ray traces from the upper two samples of the core, it appears that it breaks down on burial probably to form seperate chlorite and montmorillonite. Alternatively, it may be that the conditions prevailing in the salt marsh sediments lead to the growth of this clay mineral. The fact that the lowermost of the samples (D12.30) appears to contain a more stable form of corrensite suggests that the later process is more important. Close inspection of the remaining diffraction traces shows that minor amounts of a clay with 29Å basal interplanar spacings, probably corrensite, occur in samples D12.50, D13.50, D13.90, D14.50 and D15.50.

Further information regarding the clay minerals may be obtained from examination of X-ray diffraction traces made after thermal treatment of the samples at successively higher temperatures. Specimen D12.50 was treated in this way and the diffraction traces obtained after each heating stage are shown in figure 3-4. Traces were recorded after heating for one hour at 400°C, 500°C and then at 50°C intervals upto 750°C. The intensities of some of

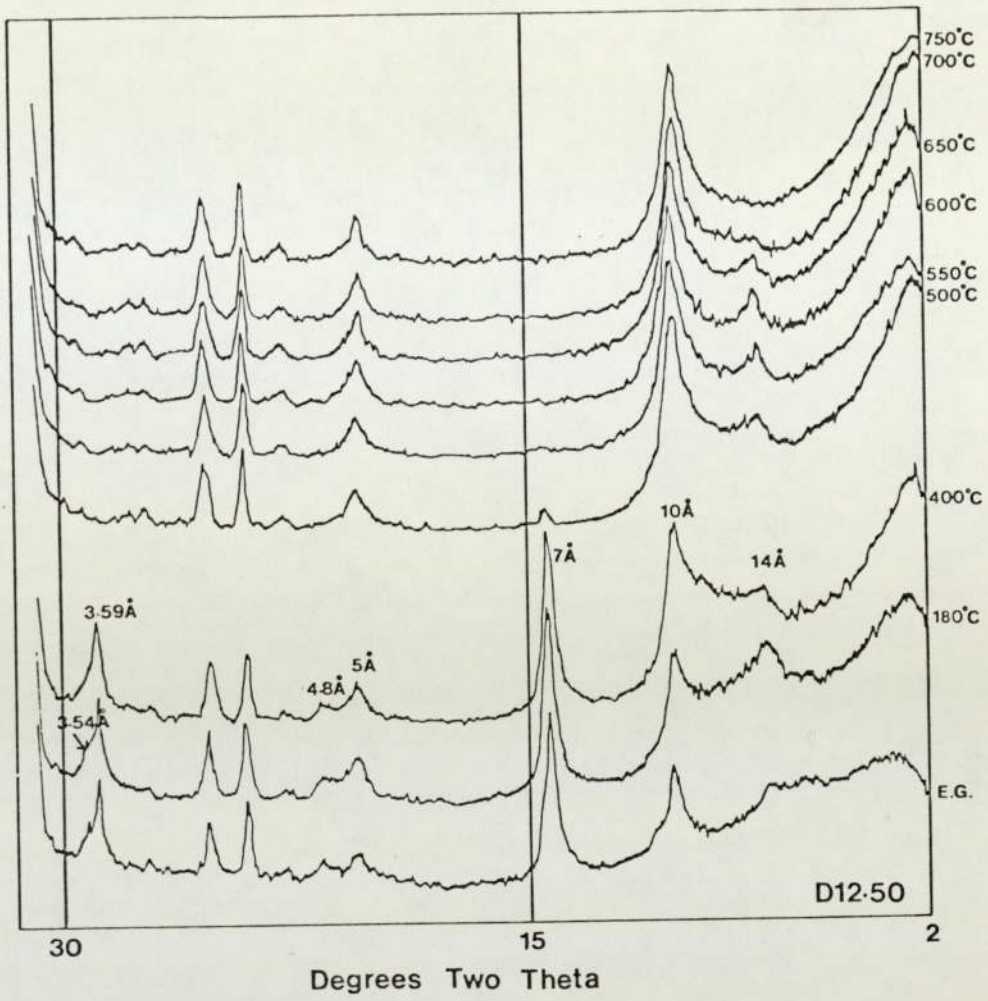


Figure 3-4. X-ray diffraction traces taken after heating sample D12.50 at successively higher temperatures. The sample was heated at the given temperatures for one-hour prior to making each diffraction trace.

the major peaks plotted against increasing temperature are shown in figure 3-5.

The most significant variation on heating to 400°C is the two-fold increase in the intensity of the 10Å peak which continues to increase in intensity upto 500°C. Above 500°C, the intensity of the 10Å peak decreases slightly and from 550°C to 750°C it remains constant in intensity. There is no change in position of the 10Å peak, indicating that no change occurs in the "c" unit cell parameter in illite. However, examination of the behavoir of the (002) reflection for illite reveals an expansion in the "c" cell parameter above 550°C from 5.009Å to 5.033Å after heating to 600°C for one hour, and then to 5.045Å for temperatures in the range 650 - 750°C. This phenomenon cannot be caused through interference by the (003) chlorite reflection since the chlorite peak disappears after heating to 550°C for one hour before the expansion in the illite "c" unit cell parameter is observed.

The behavoir of the kaolinite basal reflections is simpler; they indicate a characteristic decomposition of kaolinite after heating to 500°C for one hour, leaving only a minor (001) peak which is completely removed on heating to 550°C for one hour. The collapse of the kaolinite structure to an X-ray amorphous metakaolin on heating above 550°C has been described previously by Brindley (1961). The sharp (001) reflection observed prior to any thermal treatment is typical of well crystallised kaolinite (Carroll, 1970). Disappearance of the (002) reflection of kaolinite occurs after heating to above 500°C.

Analysis of the variations in the behavoir of chlorite after thermal treatment is partly complicated by the overlap of the (001) reflection of chlorite with the (001) reflection of mont-

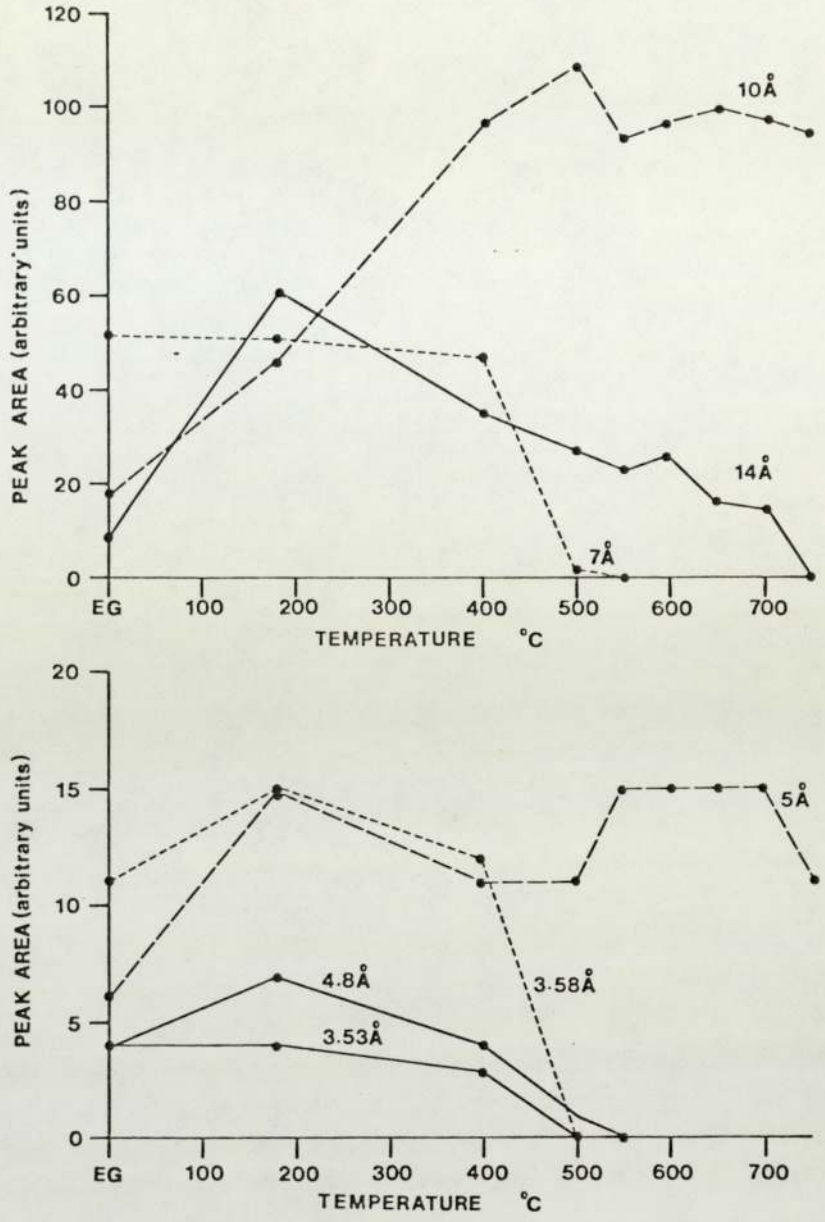


Figure 3-5. Diagrams showing the behavoir of the areas of each of the major clay mineral peaks on heating of specimen D12.50 to 750°C.

morillonite. A general decrease in intensity with increased temperature is shown by the (001),(003) and (004) basal reflections which disappear after heating to 750°C, 550°C and 500°C respectively. The (002) chlorite basal reflection is completely masked by the more intense (001) peak of kaolinite. It is possible that the small peak with an interplanar spacing of 7.15Å which remains after heating to 500°C for one hour is the (002) peak of chlorite and not a remanent peak resulting from the incomplete decomposition of kaolinite to metakaolin. Further evidence for this is provided by a change in the peak position, since below 500°C the (002) peak is typical of kaolinite, having a slightly larger interplanar spacing of 7.17Å.

Heating of the specimen to 550°C for one hour results in a slight sharpening of the (001) chlorite peak and a contraction of the "c" unit cell parameter to 14.06Å; after heating to 600°C a further contraction of the unit cell occurs to 13.78Å. Brindley (1961) records a transition in chlorite at 600°C which results in an increase in intensity of the (002), (003) and (004) reflections. This results from a dehydration reaction which occurs in two stages, the first of which corresponds to the decomposition of the brucite-layer and produces the small changes in the lattice parameters and the large changes just described in the reflected intensities (Brindley, 1961). As already seen, small changes, particularly in the (001) reflection, are observed in the cell parameters. Also inspection of figure 3-5 shows that after heating to 600°C for one hour, there is an increase in the intensity of the (001) reflection. This is also indicated by the sharper (001) peaks produced in the traces at 550°C and 600°C (figure 3-4).

Brindley (1961) has also recorded that X-ray clay mineral studies of chlorites in Recent sediments often show reflections which are broad, and show poor or no resolution of (004) chlorite and (002) kaolinite peaks. This, however, is not the case in the samples studied here as is well shown in the diffraction traces of figure 3-4. Here, a distinct shoulder is seen, on the larger (002) kaolinite peak. The shoulder, with an interplanar spacing of 3.53Å is the (004) chlorite reflection. This suggests that the chlorite in the Wash samples is of a well-crystallized variety. Complete decomposition of the chlorite occurs after heating to 750°C for one hour. However, even after heating at 700°C for one hour, only a much flattened broad band of reflections is observed. Heating at 750°C for one hour thus leaves illite as the only stable clay mineral.

Finally, acid dissolution of clays prior to X-ray diffraction may also be used as an aid to their identification. Acid dissolution is particulary useful in determining whether the chlorites are magnesium or iron-rich. A second sample of specimen D12.50 was made up for this purpose. In figure 3-6 diffraction traces of the clay mount before and after acid dissolution in a 10% hydrochloric acid solution at 80°C for twelve hours are shown. It can be seen that acid dissolution results in the breakdown of the chlorite leaving only weak (001) and (003) reflections. The (004) reflection is almost completely removed. Again, the (002) reflection is masked by the strong kaolinite (001) peak. Brindley (1961) has shown that iron-rich chlorites are more susceptable to acid dissolution than magnesium-rich chlorites and it is concluded that the chlorites in the Wash sediments are iron-rich chlorites. Further evidence for this is provided by Mössbauer

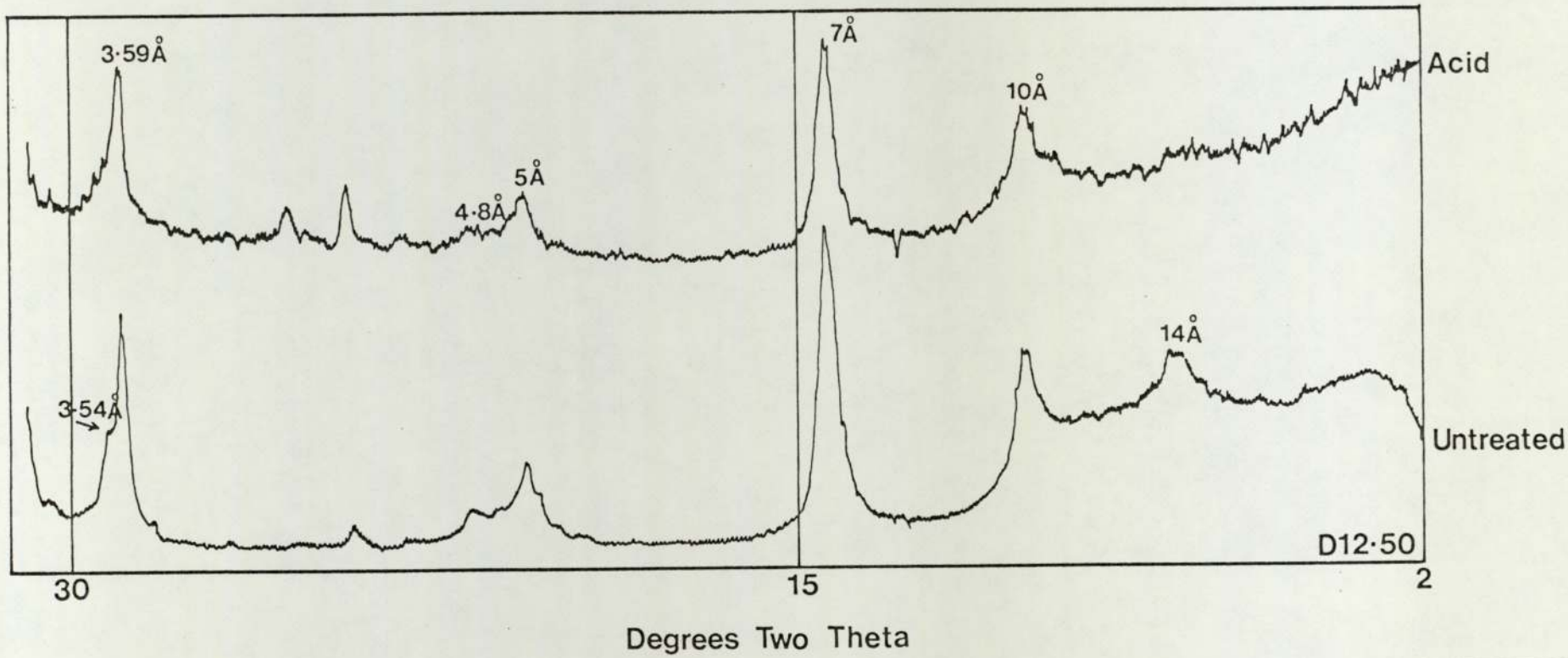


Figure 3-6. X-ray diffraction traces for a specimen from sample D12.50 taken before and after treatment with a 10% hydrochloric acid solution at 80°C.

spectroscopy (see chapter 4).

3-4. Surface sediment clay studies.

Studies of the clay mineralogy of the samples from the Delft core D1 have shown that there is good evidence to suggest that differential sedimentation of the clays occurs. This differential sedimentation results in subtle variations in the concentrations of the clay minerals so that each lithological unit in core D1 is characterised by a particular clay mineral assemblage. Studies of the clay minerals using the SEM have shown that none of the clays are authigenic. X-ray diffraction studies have shown no variation in the degree of crystallinity of the clays which would suggest diagenetic alteration of the clays. The only possible exception to this is provided by corrensite, in the salt marsh deposits, which, as discussed earlier in section 3-3 occurs in two forms; a stable one which does not breakdown on heating to 180°C for one hour, and an unstable one which appears to undergo a structural breakdown into its constituent, montmorillonite and chlorite components.

In order to test the hypothesis that the observed variations in the clay mineralogy could be explained by differential sedimentation, it was decided to collect surface sediment samples from the present-day tidal-flat. Four of these samples were collected from a traverse at right-angles to the shore at Leverton (see figure 3-7). The remaining two samples were collected at Freiston Shore (TF 40254195). The sample locations were selected so that a variety of subenvironments of deposition were represented, these are as follows; sample number 1, lower (seaward) Arenicola sands; sample number 2, strongly bioturbated Arenicola sands; sample number 3, upper (landward) Arenicola sands near to a creek; sample number 4, the higher mudflat; sample number 5,

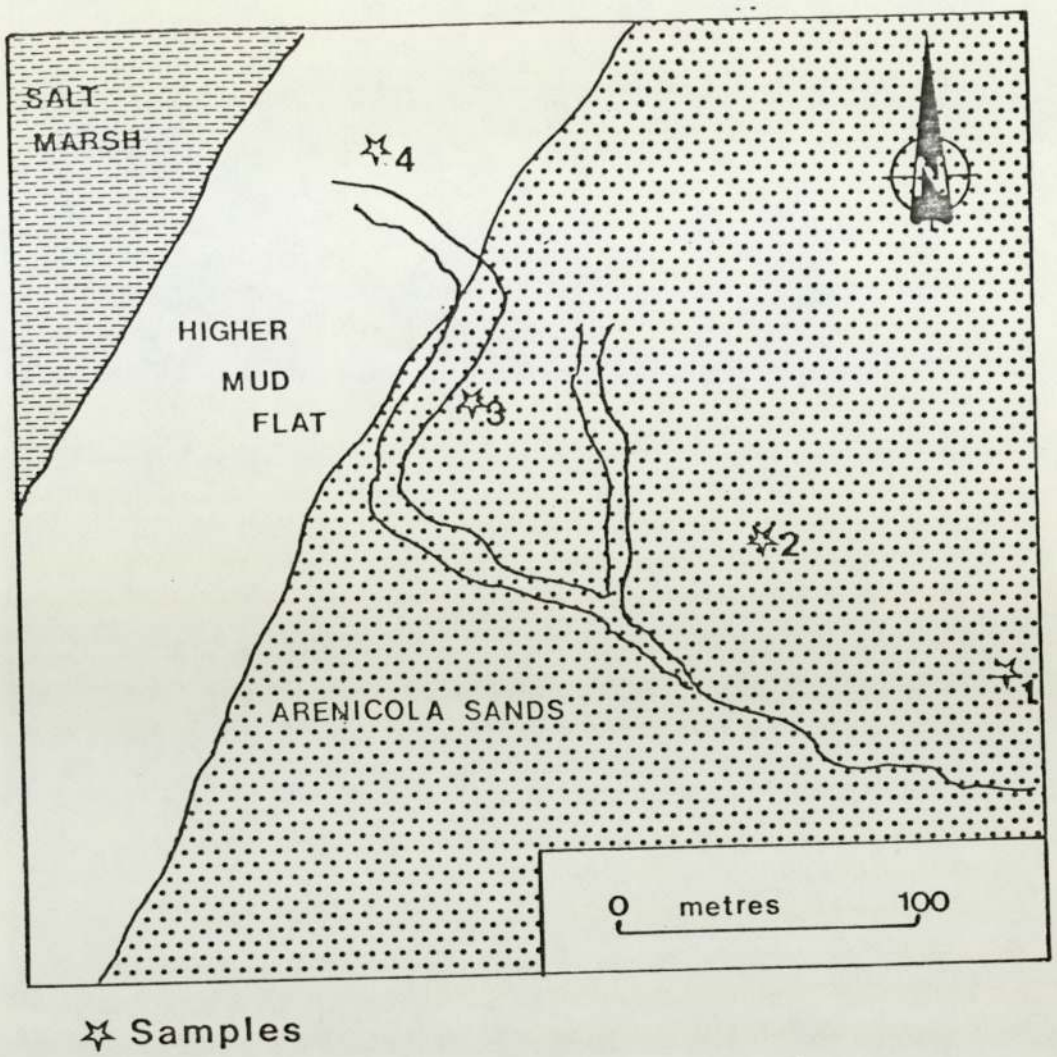


Figure 3-7. Location map for the surface sediment samples from Leverton (sketch map only), used in the surface sediment study.

the salt marsh; and sample number 6, reworked higher mudflat sediment in a creek bottom.

Analysis of the samples was made, by X-ray diffraction, using the modification of the technique described by Gibbs (1965) discussed in section 3-1. The results of these analyses are shown in figure 3-8. Kaolinite, chlorite, illite and expandable and mixed-layer illite-montmorillonite are again the major clay minerals present. The mean concentrations of the surface samples may be compared with those of the sample from core D1 as shown in table 3-1.

The figures show that there is little difference between the mean clay mineral concentrations of the surface samples and those from core D1. The major differences occur in the mean concentrations of illite and the mixed-layer and expandable clays. Illite is less abundant in the surface sediments and also shows less variation between different subenvironments in the surface samples. The mixed-layer and expandable clays are more abundant in the surface sediments than in the core sediments and again show less variation between different subenvironments of deposition. In figure 3-8 the concentrations of the clay species from both core D1 and the surface samples are plotted with respect to the subenvironments of deposition within which they occur. It can be seen that the variations in clay minerals between different subenvironments of deposition are reflected in both the data from surface samples and from samples taken from core D1. The relatively low illite, and high mixed-layer illite-montmorillonite and montmorillonite, concentrations in the Arenicola sand flat surface sediments compared to the core samples requires explanation. Diagenesis, as discussed in section 3-3, is unlikely

TABLE 3-1. Mean clay mineral concentrations of the samples from core D1 and from the surface sediments.

| | Kaolinite | Chlorite | Illite | Mixed-layer and expandable clays |
|---|---|---|---|---|
| Core D1 | 20.0 ±3.6 | 6.9 ±1.7 | 48.0 ±8.6 | 25.1 ±10.2 |
| Surface sediments | 20.2 ±1.5 | 6.9 ±1.2 | 44.8 ±2.4 | 28.2 ± 3.7 |

Note: Concentrations are expressed as percentages of the total clay in the <2μm fraction.

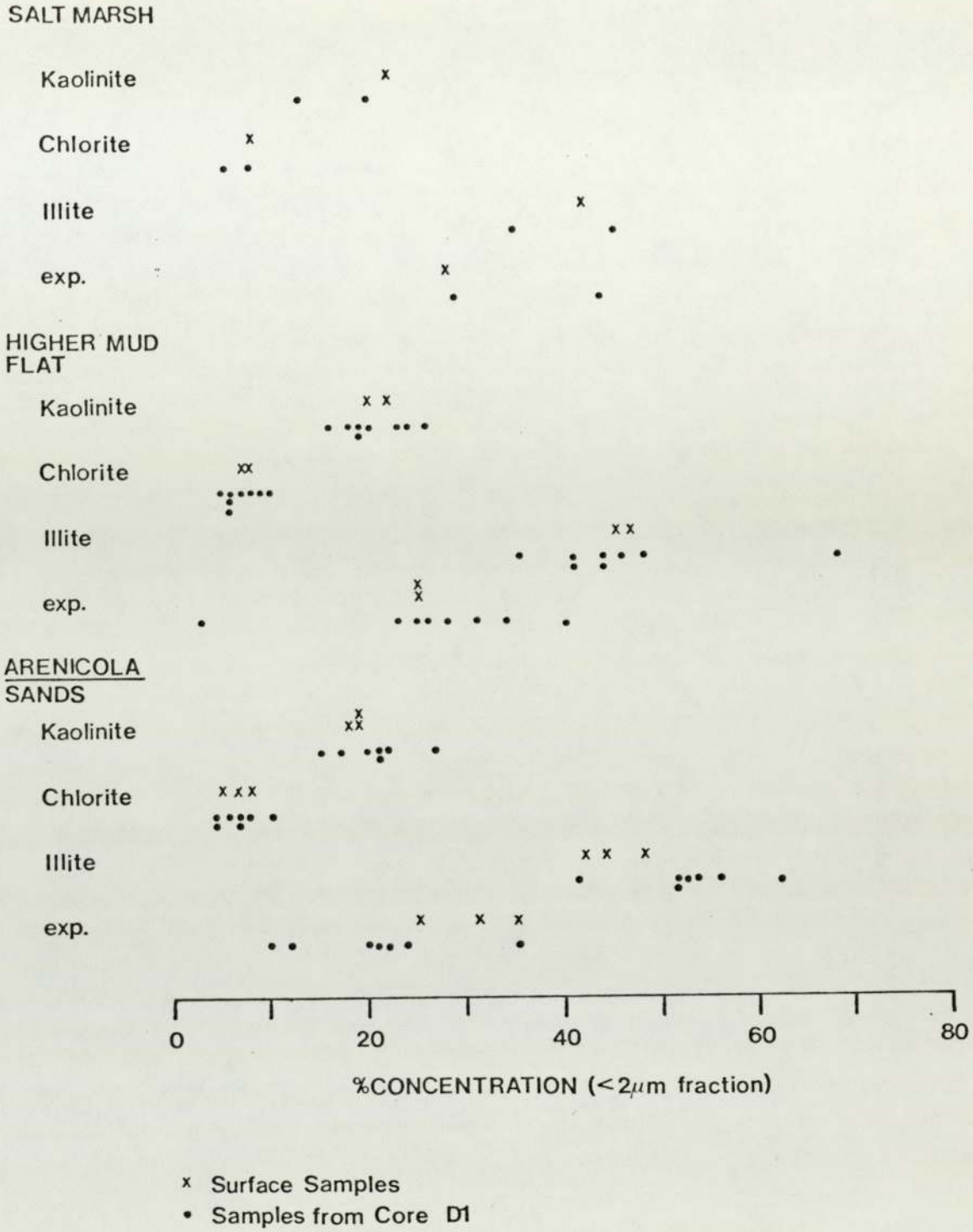


Figure 3-8. Distribution diagram showing the concentrations of clay minerals, from three sub-environments of deposition, both from surface samples and from the samples from core D1.

to be the cause of this anomaly. Two other possible explanations are; either the clay entering the Wash has changed, or, that the entrainment of the salt marsh has lead to a modification of the sediment sorting pattern on the present-day tidal-flat. The former process might be explained in terms of larger scale sorting, perhaps as a result of winnowing, of the sediment entering the Wash, however it is unlikely that this would lead to an increase in montmorillonite and mixed-layer illite-montmorillonite since these phases have the lowest settling velocities. The second process, modification of the surface sediment mineralogy as a result of entrainment work, seems more likely. Inglis and Kestner (1958) have shown how the reclaimation of the salt marsh by the building of sea banks leads to lateral migration of the tidal-flat seawards. It is thus likely that this situation could result in an imbalance in the sorting of the sediment and then lead towards mixing and homogenisation of the sediment mineralogy before equilibrium is reached again.

Finally, no corrensite was detected in any of the surface sediment samples. This therefore, adds evidence to support the idea that the corrensite is an early diagenetic mineral.

## 3-5. Conclusions.

Through X-ray diffraction studies of clay concentrates on ceramic tiles it has been possible to confirm that the principal clay minerals in the Wash sediments are; illite, montmorillonite and mixed-layer illite-montmorillonite, kaolinite and chlorite, together with subordinate mixed-layer chlorite-montmorillonite (corrensite) present in some samples. The presence of corrensite was not reported in the study by Shaw (1973). Quantitative analysis of the clays in samples taken from Delft core D1 have shown variations in the clay mineralogy which are caused by differential sedimentation rather than by burial diagenesis. This is substantiated by the fact that the distribution of the clay minerals shows a relationship to the facies variations in the sediments within which they occur. Analysis of surface samples taken from the present-day tidal-flat has shown similar variations. The data from surface samples however suggests a further complication possibly resulting from the extensive reclaimation works which affect sedimentation in the Wash embayment. The effect of the reclaimation work is to cause the whole tidal-flat to prograde causing mixing of the surface sediments, and thus, reducing the variations in clay mineralogy between different subenvironments of deposition.

The data from both sets of samples (samples from core D1, and samples from the present-day tidal-flat) have been combined in figure 3-9 which shows the mean and standard deviation of the concentration of each clay mineral in the three subenvironments of deposition studied in this work. The main feature shown in figure 3-9 is the variation in the concentration of illite, which increases with depth, and the corresponding decrease in the conc-

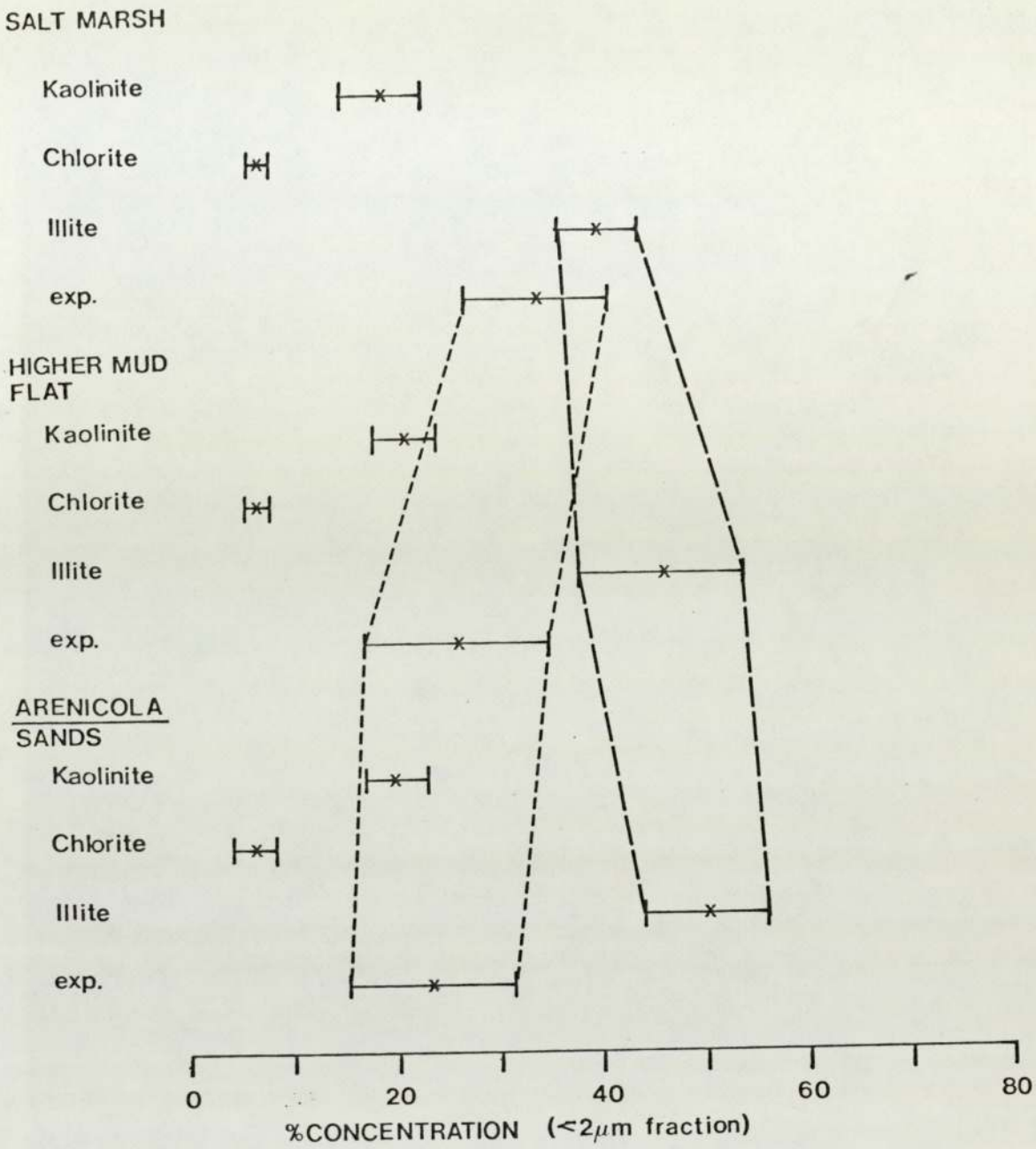


Figure 3-9. Distribution diagram showing the mean (marked by an 'x') concentrations of each of the clay minerals encountered in the samples from core D1 and from the surface samples. The bars represent the standard deviation about the mean for each clay mineral in each of the three sub-environments. Dashed lines indicate major trends.

entration of mixed-layer illite-montmorillonite and montmorillonite. There is little apparent variation in the mean concentrations of chlorite and kaolinite between different subenvironments of deposition. However, in the more detailed variations plotted in figure 3-2 a major feature occurs at the transition from the salt marsh to higher mudflat lithofacies. Here, there is a marked increase in kaolinite and decrease in the expandable clays. This transition occurs at a point in the core representing a palaeomean high-water mark and, if differential sedimentation can be established as a universal process on modern tidal-flats, it is possible that variations in clay mineralogy can be used to interpret conditions of sedimentation in ancient tidal-flat sequences.

Thermal treatment of the clay minerals in the range 180°C - 750°C prior to X-ray diffraction has confirmed the presence of kaolinite and chlorite. Kaolinite decomposed to an X-ray amorphous phase after heating to 400°C for one hour. Chlorite showed a two stage decomposition, the first being dehydration which results in a contraction of the basal cell parameter to 13.78Å, and secondly total decomposition occurs after heating to 750°C for one hour. Finally acid dissolution has been used to show that the chlorites are iron-rich chlorites.

Chapter 4.

# Mössbauer Spectroscopy.

## Introduction.

The mineralogical and geochemical applications of Mössbauer spectroscopy have developed rapidly in recent years. In this study $Fe^{57}$ Mössbauer spectroscopy has been used as a finger-print technique to identify the major iron-bearing minerals in the sediments of the Wash and also as a semi-quantitative method to monitor the changes in the concentrations of these minerals. Mössbauer spectral studies also enable the characterisation of the oxidation state of iron, the electronic configuration of iron (eg., high-or low-spin), the coordination symmetry about the iron atom (eg., tetrahedral or octahedral), assignment of the peaks to structurally distinct cation positions and also the observation of magnetic ordering of iron in minerals. Bancroft et al. (1977) have also shown the advantages of Mössbauer spectroscopy in determining the ferrous/ferric ratios of bulk rock samples.

Analysis of the samples from core D1 was made on the whole sediment fractions obtained from the core, either on "fresh" or freeze-dried material. The interpretation of the resulting spectra is thus complicated by the presence of a variety of iron-bearing minerals. However, by using knowledge obtained from optical, geochemical and X-ray studies of the sediments and by comparing the resulting Mössbauer parameters with those published for single mineral specimens, it is possible to assign a number of peaks, which contribute to form the spectrum, to particular minerals or mineral species. This is easily achieved with the good quality Mössbauer data which are obtained from specimens containing proportionally large amounts of iron. The Mössbauer

analysis of whole sediment or whole rock samples has understandably received less attention than the analysis of monominerallic specimens and hence there are few studies with which to compare the data. Recently "whole-rock" analyses have been reported (Andersen et al., 1975; Coey et al., 1974; Coey, 1975; Durrance et al., 1978; Manning and Ash, 1978, and Manning et al., 1979) which demonstrate the application of Mössbauer spectroscopy to materials containing assemblages of minerals. In one of these studies (Manning et al., 1979), it was also possible for the authors to propose a diagenetic relationship between pyrite and chlorite in lake sediments in which pyrite forms from the reaction of hydrogen sulphide with ferrous ions located in finer-grained chlorite or in amorphous silicate and with ferric ions in mainly amorphous hydrated oxides.

The theory of Mössbauer spectroscopy will not be discussed here as it is adequately covered in standard texts (see, for example; Greenwood and Gibb, 1971; and Bancroft, 1973). The method of fitting used however is discussed more fully in section 4-2-1. Initially a pilot study of samples from one of the one-metre cores was made to see if satisfactory spectra could be obtained from the sediments, and also to identify the major iron-bearing phases present in the samples; this work is discussed in the next section.

4-1. Pilot study.

Prior to obtaining the Delft cores, a pilot study of samples from one of the one-metre cores (core 3) was undertaken. The objectives of this study were, firstly, to establish that the sediments could be suitably analysed using Mössbauer spectroscopy. The main factor controlling this is the percentage of iron contained in the specimen, since if this is low, then the count rates will be slow and the signal to noise ratio will be high leading to poor resolution of the spectra. Bancroft (1973) suggests that a sample be prepared with less than 5mg $cm^{-2}$ of mineral in the absorber. $Fe^{57}$ occurs in only about two percent natural abundance, thus in samples with low iron content more material will be required in order to obtain a suitable sample.

Three pilot samples were prepared from core 3 (samples; 4B/1, 4B/2, and 4B/3). The samples were prepared by taking "fresh" unoxidised sediment from the core and freeze-drying it prior to specimen preparation. The dry sediment was then mounted on cello-tape covering a 20mm diameter (12.6$cm^2$) circular aperture cut into a card mount giving a randomly oriented sample. The exposed side of the absorber was then covered with thin aluminium foil which had been coated on one side with vacuum grease. The grease serves two purposes; firstly, it helps to prevent reorganisation of the sample, and secondly, it helps to seal the sample, protecting it against oxidation and absorption of water.

The three pilot samples were then analysed using the Mössbauer Spectrometer at the University of Birmingham. Collection of the spectra was made at room-temperature using 256 channels of a multichannel analyser. Analysis of the resulting spectra was made using the computer fitting program of A.J. Stone described

in Bancroft et al. (1967), discussed in more detail later. The spectra have been fitted with two pairs of peaks and are illustrated in figures 4-1,4-2, and 4-3. For each of the pairs of peaks the values of quadrupole splitting, isomer shift and half width have been calculated (table 4-1).

The outer doublet with a quadrupole splitting of 2.51-2.57 mm $s^{-1}$, and an isomer shift of 1.10-1.13 mm $s^{-1}$, is characteristic of high-spin ferric iron in a silicate framework with a co-ordination number of six, that is in an octahedral site (Bancroft, 1973; and figure 4-4). The doublet with the smaller quadrupole splitting of 0.59-0.66 mm $s^{-1}$, and isomer shift in the range 0.36-0.47 mm $s^{-1}$, may be assigned to high-spin ferrous iron occuring in a variety of environments (most probably clay minerals and iron hydroxides) and to the low-spin ferrous iron which occurs in pyrite (Imbert et al., 1963; Temperley and Lefevre, 1966; and Vaughan, 1971).

As a result of the rather poor resolution of the data, because only 256 channels were used in its collection further interpretation of these spectra has not been attempted. However, it was concluded from the pilot study that the sediments are suitable for analysis by Mössbauer spectroscopy and that valuable information may be obtained about the site distribution, oxidation state, and spin state, of the iron in these sediments.

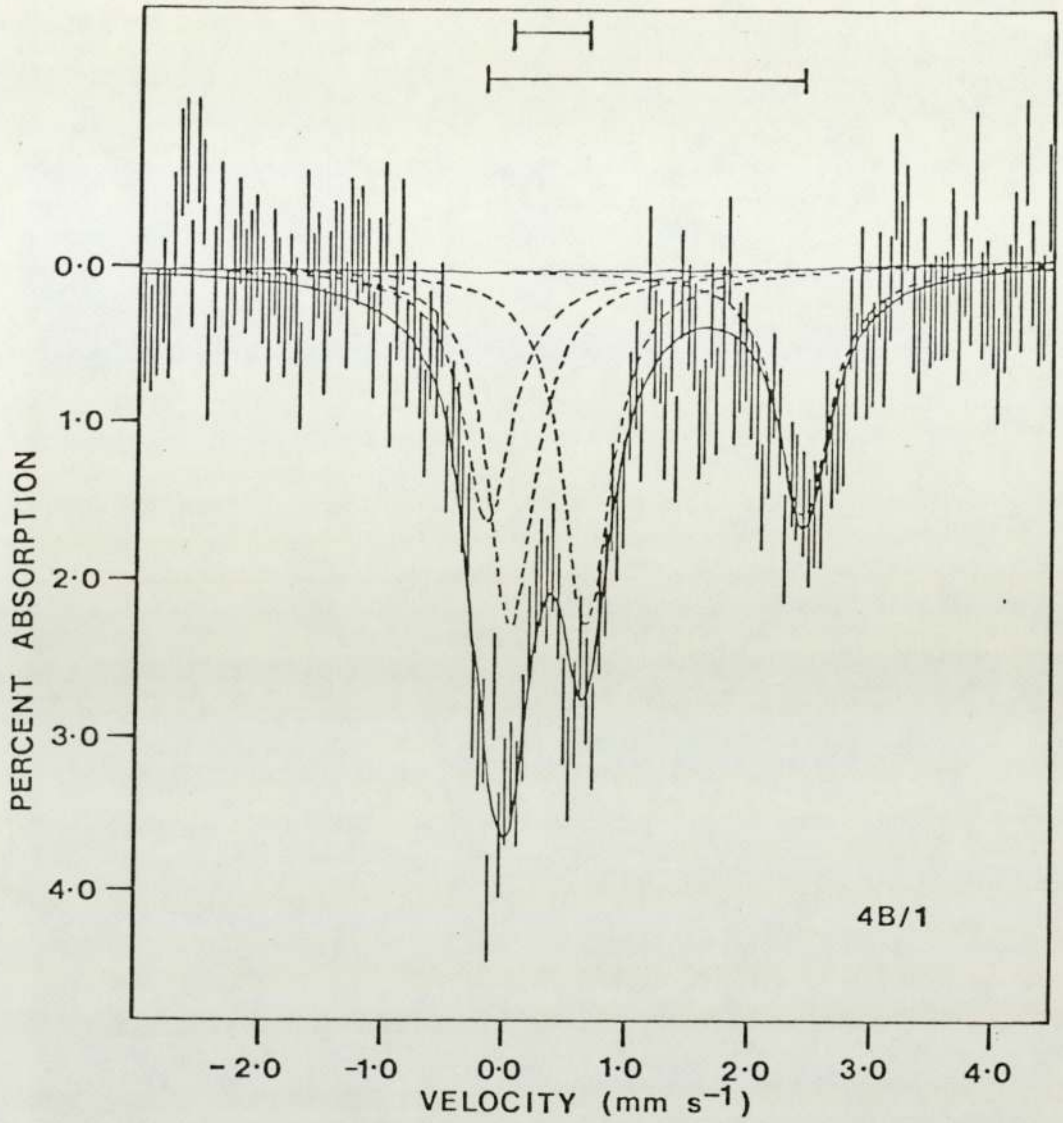


Figure 4-1. Pilot Mössbauer spectrum for specimen 4B/1 showing a two doublet computer fit. Spectrum was collected with the absorber at room-temperature (297°K).

NOTE: In this and all subsequent figures of Mössbauer spectra, the solid vertical bars represent the raw data. The component peaks fitted by computer are represented by dashed lines and the resultant fitted curve is shown by a solid line. Peaks in the figures and tables are numbered conventionally from '1' upwards begining on the left of the spectra.

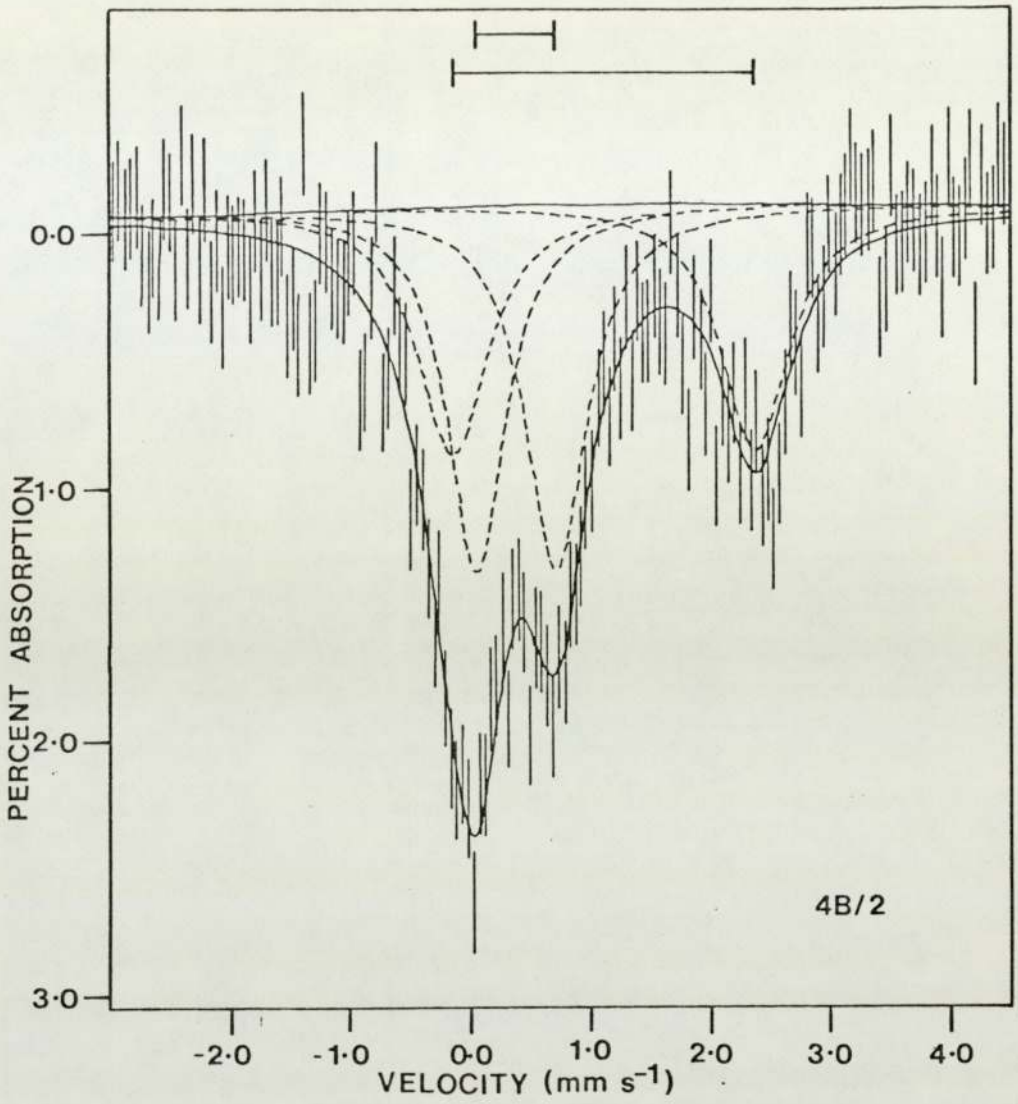


Figure 4-2. Pilot Mössbauer spectrum for specimen 4B/2 showing a two doublet computer fit. Spectrum was collected with the absorber at room-temperature (297°K).

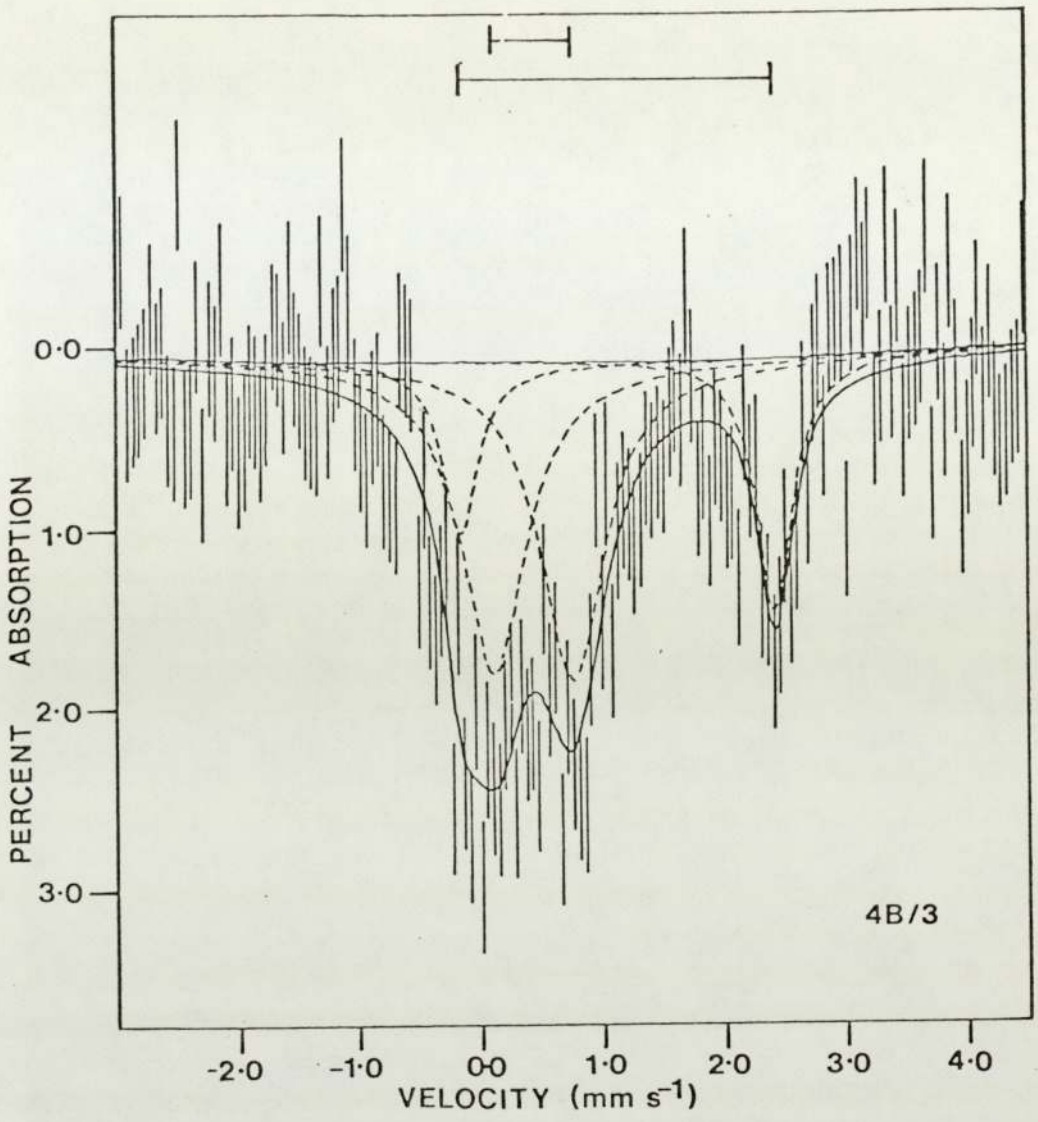


Figure 4-3. Pilot Mössbauer spectrum for specimen 4B/3 showing a two doublet computer fit. Spectrum was collected with the absorber at room-temperature (297°K).

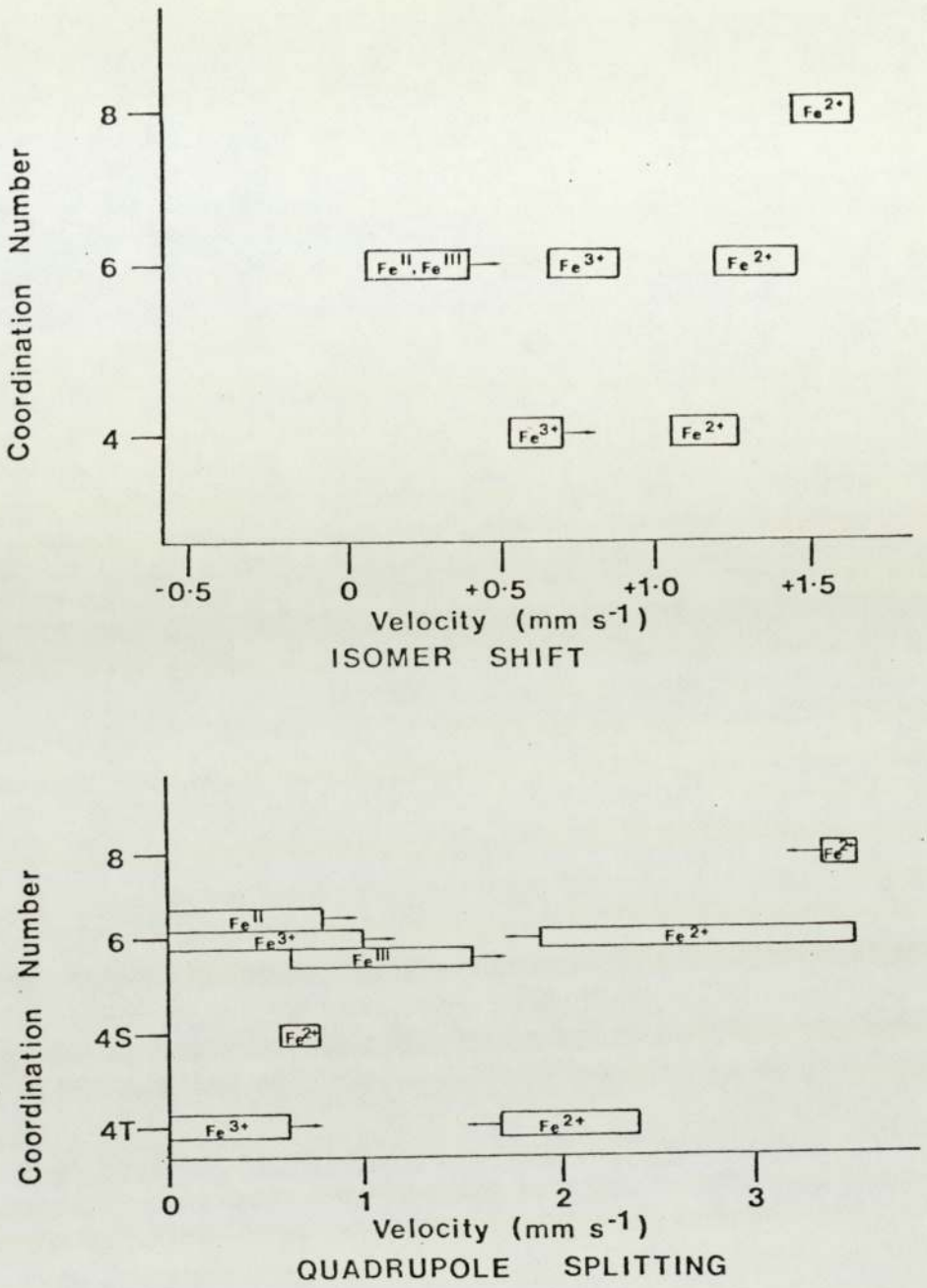


Figure 4-4. $^{57}Fe$ Isomer shifts (top) and Quadrupole splittings (bottom) plotted verses coordination number for "ionic" high-spin and low-spin compounds and minerals. Arrows indicate that values outside the boxed areas have been observed. (modified from Bancroft, 1973).

| Specimen | Quadrupole splitting (mm $s^{-1}$) | Isomer shift (mm $s^{-1}$) | Half width (mm $s^{-1}$) | Intensity | Outer/ Inner ratio |
|---|---|---|---|---|---|
| 4B/1 Outer doublet | 2.57±0.04 | 1.13±0.04 | 0.51±0.08 | 22150. | 0.77 |
| Inner doublet | 0.61±0.02 | 0.36±0.02 | 0.47±0.05 | 28907. | |
| 4B/2 Outer doublet | 2.51±0.05 | 1.10±0.05 | 0.58±0.11 | 54339. | 0.85 |
| Inner doublet | 0.66±0.03 | 0.37±0.03 | 0.69±0.06 | 64204. | |
| 4B/3 Outer doublet | 2.55±0.03 | 1.10±0.03 | 0.37±0.07 | 11662. | 0.50 |
| Inner doublet | 0.59±0.04 | 0.45±0.04 | 0.61±0.09 | 23262. | |

| Goodness of fit<br>Specimen | $\chi^2$ | degrees of freedom |
|---|---|---|
| 4B/1 | 250.98 | 243 |
| 4B/2 | 220.26 | 243 |
| 4B/3 | 240.80 | 243 |

TABLE 4-1. Mössbauer parameters obtained from the two doublet computer fits applied to the pilot specimens; 4B/1, 4B/2 and 4B/3. Units of intensity are arbitrary units (related to the height of the peak in counts and to the width of the peak in channel numbers on the multichannel analyser). The lower table shows the "goodness of fit" in terms of the $\chi^2$ and the number of degrees of freedom for each fit.

## 4-2. Room-temperature studies of samples from core D1.

### 4-2-1. Sampling and Experimental Methods.

During sampling of core D1 for palaeomagnetic specimens, sediment samples were taken from the "fresh" core and were immediately placed into centrifuge tubes in which they were freeze-dried using a Speedivac High Vacuum Centrifrugal Freeze-dryer. The samples were placed on a centrifuge mounted within a vacuum chamber which was then evacuated. A charge of phosphorus pentoxide ($P_2O_5$) was used as a drying agent, and was placed in a stainless steel tray beneath the vacuum chamber. Once evacuated, the centrifuge was switched on, to freeze the water contained in the samples, this usually took 10 to 15 minutes. The centrifuge was then switched off while the samples were left under vacuum for 2 to 3 hours so that sublimation of the ice could occur. The samples were then sealed in their centrifuge tubes under vacuum to prevent oxidation and reabsorption of water. The main purpose of the freeze-drying of the sediments was to prevent oxidation of any unstable iron minerals present in the samples, such as mackinawite and greigite, after their removal from the core. The freeze-dried samples in their evacuated centrifuge tubes were not opened until just before being run on the Mössbauer spectrometer. A series of nine freeze-dried samples, spaced at one-metre intervals down the core were analysed using the Mössbauer effect. The samples were mounted on card holders in which a 20mm diameter circular aperture had been cut. The sample was spread onto a piece of cellotape covering the aperture and a cover of greased aluminium foil was then attached in the same way as described in the pilot study.

The equipment used to collect the spectra in this study

consisted of the Harwell Spectrometer drive and counter systems coupled with the Ino-tech 5200 Multichannel Analyser utilizing 512 channels, of the 1024 available, for data collection. The source used was $^{57}Co$ in a palladium matrix with an initial activity of 50 mi Curie. Calibration of the spectra was made using an iron foil standard (all isomer shifts are quoted relative to iron). Each sample was run for between 40 and 60 hours in order to obtain a satisfactory spectrum. The relatively long time required for these runs was a result of the low concentrations of iron in the samples (1.19 - 2.93 wt.%Fe).

Computer fitting of the spectrum data was undertaken using the program written by A.J. Stone (described in Bancroft et al., 1967). The program fits a number of Lorentzian peaks to the Mössbauer spectrum using the Gauss non-linear regression proceedure with a facility for constraining any set of parameters or linear parameters. The success of the method depends greatly on the sensible use of constraints. Constraints applied in the early stages of computer fitting may be released during later stages. The choice of suitable constraints depends on the spectrum and what may already be known about the crystal chemistry of the material under investigation. For example, two peaks may be constrained to be the same intensity if they are known to form a quadrupole doublet, or a particular line position may be constrained because the line arises from a species of known isomer shift. Bancroft (1973) describes examples of fitting proc edures, the fundamentals of which may be applied to fitting other spectra. A "good fit" or the "goodness of fit of a spectrum" are expressions used to describe confidence in the fitting of a spectrum (Bancroft, 1973). This relies on three main criteria; 1) the $\chi^2$

value must be statistically acceptable, 2) the number of sites in which iron is found must be consistent with what is known from other evidence, such as X-ray or petrographic, and 3) the Mössbauer parameters for iron must be consistent with previous Mössbauer studies on similar coordination sites. The computer used in this study was the ICL. 1904S at the University of Aston in Birmingham. The use of the computer fitting program on the Aston computer system is described in a guide by Vaughan and Linskill (1979).

4-2-2. Results and Interpretation of Spectrum D16.75.

In addition to the nine equally spaced samples from core D1, a sample (D16.75) was taken from a thin black coloured clay layer in core D1. It is a common feature that such fine-grained sediment layers tend to be richer in iron (Blatt et al., 1972) and, as a result, the spectrum obtained from this sample showed much better resolution than those from the more representative sediment samples. The spectrum from sample D16.75 was therefore used as a key to interpreting the other spectra. Computer fitting of the spectrum for sample D16.75 was undertaken in a number of stages; the Mössbauer parameters obtained for each stage are shown in Table 4-2. The first stage was to fit two pairs of peaks to the central part of the spectrum as shown in figure 4-5a. Comparison of the Mössbauer parameters obtained for the two doublet fit of specimen D16.75 with those from the pilot samples shows good agreement. As discussed in the pilot study, the inner of these two doublets may be assigned to the high-spin ferric iron occuring in a variety of environments (most probably clay minerals and iron hydroxides) and to the low-spin ferrous iron

TABLE 4-2 Stages in the fitting of spectrum D16.75. The Mössbauer parameters; quadrupole splitting, isomer shift, and the half widths of the peaks are given together with the percentage contribution to the total iron content of each fitted doublet. Also the goodness of fit is given in terms of the chi-squared ($\chi^2$) value and the number of degrees of freedom. (Overleaf).

Specimen D16.75.

| | Quadrupole splitting ($mm\ s^{-1}$) | Isomer shift ($mm\ s^{-1}$) | Half width ($mm\ s^{-1}$) | %Contribution to total iron | Goodness of fit | |
|---|---|---|---|---|---|---|
| | | | | | $\chi^2$ | degrees of freedom |
| Two doublet fit (central part of spectrum). | | | | | | |
| Outer doublet | 2.60±0.01 | 1.14±0.01 | 0.46±0.01 | 41% | 769.3 | 500 |
| Inner doublet | 0.61±0.00 | 0.35±0.00 | 0.47±0.01 | 59% | | |
| Three doublet fit (Pyrite constrained). | | | | | | |
| (1,6) | 2.60±0.00 | 1.14±0.00 | 0.46±0.01 | 42% | 378.0 | 236 |
| (2,5) | 0.60±0.02 | 0.31±0.02 | 0.35±0.05 | 21% | | |
| (3,4) | 0.61±0.03 | 0.41±0.03 | 0.52±0.04 | 37% | | |
| Three doublet fit (Two high spin ferrous sites + one ferric). | | | | | | |
| (1,6) | 2.60±0.00 | 1.18±0.00 | 0.39±0.01 | 33% | 264.4 | 236 |
| (2,5) | 2.41±0.01 | 0.94±0.01 | 0.27±0.03 | 7% | | |
| (3,4) | 0.62±0.00 | 0.36±0.00 | 0.47±0.01 | 60% | | |
| Two doublet + magnetic pair of peaks | | | | | | |
| (1,6) | peaks of magnetic part spectrum | | | 4% | 639.3 | 497 |
| (2,5) | 2.60±0.01 | 1.14±0.01 | 0.48±0.01 | 40% | | |
| (3,4) | 0.62±0.00 | 0.35±0.00 | 0.47±0.01 | 56% | | |

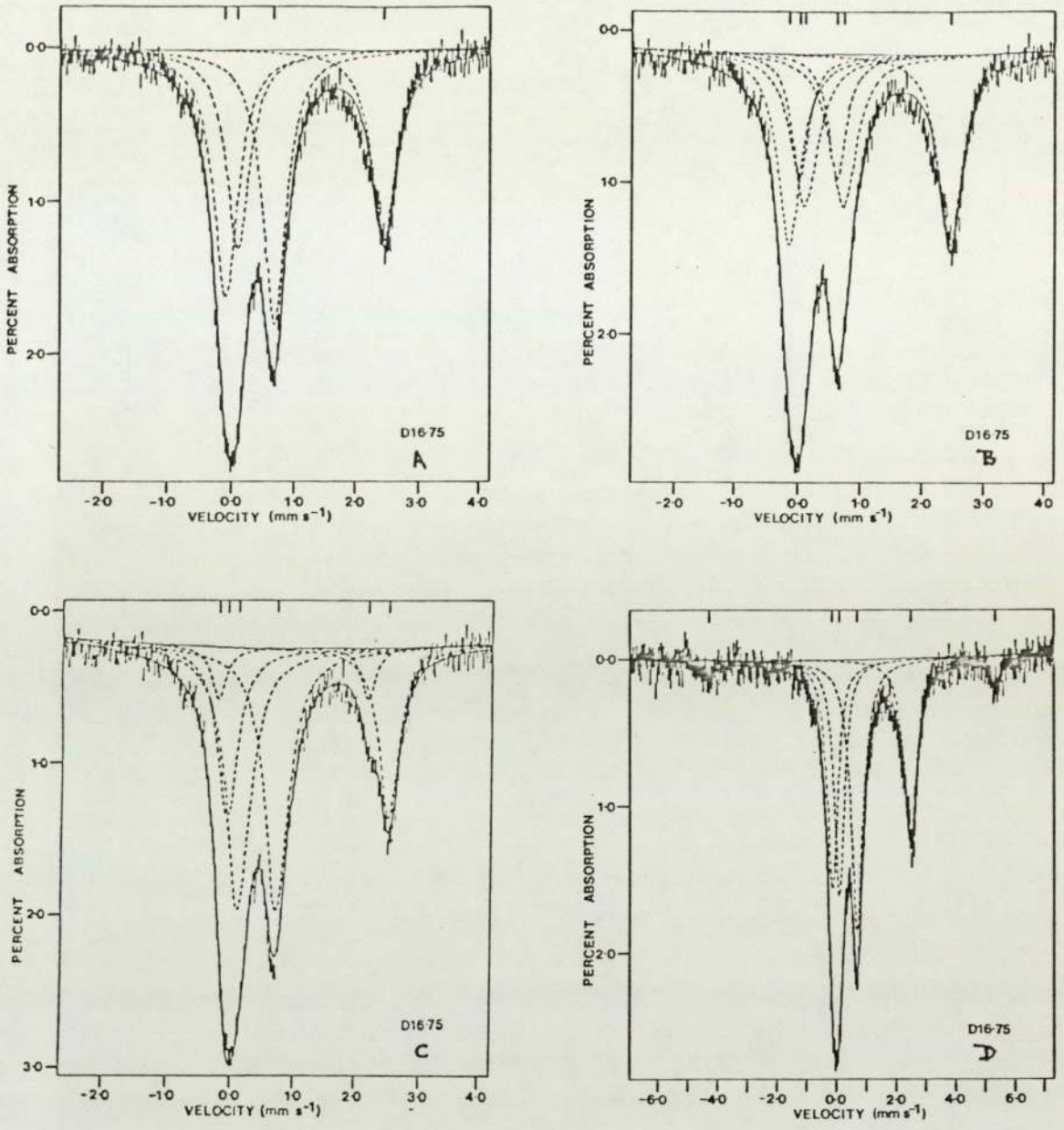


Figure 4-5. Computer fitted Mössbauer spectra showing the stages involved in resolving the high resolution spectrum from specimen D16.75. (a) shows the initial two doublet fit. (b) shows the two doublet fit with the addition of a further pair of peaks included to represent pyrite. (c) shows the two doublet fit of stage (a) with the addition of a further pair of high-spin ferrous peaks. Note the improved fit to the low velocity side of the high velocity peak. (d) shows the whole of spectrum D16.75 with the two doublet fit of stage (a) together with peaks fitted to the two magnetically ordered peaks.

which occurs in pyrite.

The next stage in the computer fitting of spectrum D16.75 was to attempt to further resolve the components of the inner doublet. The Mössbauer parameters for natural and synthetic pyrite have been well documented (Imbert et al., 1963; Temperley and Lefevre, 1966; and Vaughan, 1971). It was thus decided to constrain the Mössbauer parameters for the low-spin ferrous iron in pyrite into the program and to use 0.31 mm $s^{-1}$ for the isomer shift and 0.60 mm $s^{-1}$ for the quadrupole splitting values of this species. In addition, a pair of peaks corresponding to a ferric doublet, and the high-spin ferrous peaks were also fitted at this stage. The component peaks fitted to the spectrum are illustrated in figure 4-5b. No variation in the quadrupole splitting or isomer shift of the outer high-spin ferrous doublet took place as a result of the fitting of the pyrite peaks. However, the problem, of asymmetry in the areas of the two peaks of the inner doublet, encountered in the first stage, is overcome by the inclusion of the pyrite data. At this stage there was no improvement in the goodness of fit of the spectrum, mainly due to the poor fit of the high velocity, high-spin ferrous peak and also to the outermost parts of the spectrum at very low and very high velocity where a further pair of peaks is located.

The third stage of fitting was to improve the fit of the high-velocity, high-spin ferrous peak which has a pronounced shoulder on its low-velocity side. This was achieved by fitting a further high-spin ferrous doublet in addition to the doublet which was fitted in the first stage. The improved fit to the high-velocity, high-spin ferrous peak can be seen in figure 4-5c and is shown by the overall improvement in the chi-squared value

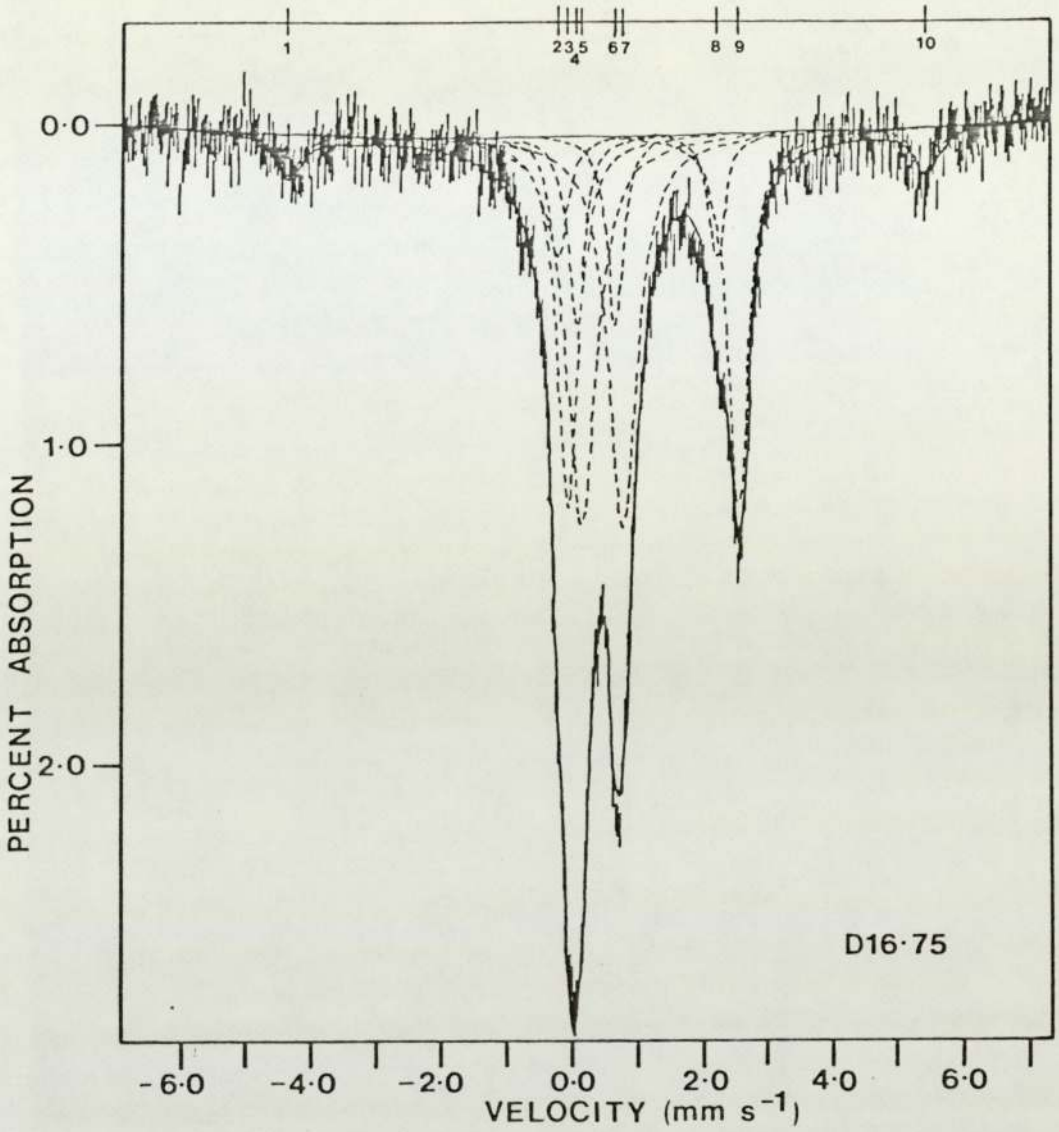


Figure 4-6. Final ten peak computer fit to the Mössbauer spectrum from specimen D16.75. The assignment of peaks is as follows; peaks (1,10) are assigned to iron in greigite, $Fe_3S_4$, peaks (2,9) and peaks (3,8) are assigned to high-spin ferrous iron in chlorite, peaks (4,7) are assigned to low-spin ferrous iron in pyrite, and peaks (4,5) are assigned to all ferric contributions.

(see Table 4-2). The new high-spin ferrous doublet has a smaller quadrupole splitting than the first one and is also lower in intensity.

Not shown in figures 4-5a.b. and c, which are plots of the central part of the spectrum for sample D16.75, are an outer pair of peaks shown in figure 4-5d. The peaks occur at very low and very high velocity and are of approximately equal intensity. These peaks must constitute part of a magnetic hyperfine split spectrum. After fitting a pair of peaks to these data (figure 4-5d) together with a simple two doublet fit to the central part of the spectrum, the next stage was to incorporate all of the peaks fitted in the earlier stages into a composite fit.

In order to fit the composite spectrum, which invoved the fitting of a total of ten peaks, it was necessary to apply a large number of constraints to prevent the program from diverging. Initially, twenty constraints were applied. Positions of all the peaks were constrained to the parameters obtained in the earlier stages (a total of 9 constraints), this was necessary in order to prevent switching of peak positions occuring, particularly in the central part of the spectrum. Area constraints were used so that peaks belonging to a doublet, and the pair of peaks forming the magnetically split part of the spectrum, were constrained to be equal to each other in intensity (a total of 5 constraints). The width constraints were used in a similar manner to the area constraints, that is, the peak widths of the pairs of peaks were constrained to be equal to one-another (a total of 5 constraints). The final constraint was applied to the base line. The resulting spectrum is illustrated in figure 4-6.

The Mössbauer parameters obtained for this stage with twenty

constraints are shown in table 4-3. Releasing of the constraints was attempted by first releasing the area constraints on the outer high-spin ferrous doublet. The effect of this on the Mössbauer parameters is only apparent in changes in the half widths of the component peaks. The statistical fit obtained with the 19 remaining constraints is not as good as that obtained with 20 constraints. With 20 constraints the chi-squared is 494.04 with 497 degrees of freedom which reduces to a chi-squared of 474.55 with 496 degrees of freedom when 19 constraints are applied. Further release of constraints was attempted and a fit with 17 constraints, made by releasing the position constraints on peaks 1 and 2 and peaks 9 and 10, resulted in a large change in the quadrupole splitting of the outer high-spin ferrous doublet from 2.60$\pm$ 0.00 to 2.64$\pm$ 0.00 mm $s^{-1}$. The inner, less intense, high-spin ferrous doublet also shows a change in the quadrupole splitting from 2.41 $\pm$0.00 to 2.45 $\pm$0.00 mm $s^{-1}$ as a result of the release of the position constraints. Again there is a decrease in the goodness of fit so that a chi-squared of 460.89 with 494 degrees of freedom is obtained (table 4-3).

It can thus be concluded that further release of constraints would result in fits of increasingly poor quality and that the first of these fits, made with 20 constraints, is the best computer fit of the data for sample D16.75.

Assignment of the peaks to particular mineral species and to particular crystallographic sites was now attempted using knowledge already obtained about the iron-bearing mineralogy of the samples from optical microscopy, the scanning electron microscope and from X-ray diffraction studies, and also by comparing the Mössbauer parameters obtained by computer fitting with those

Specimen D16.75.

| 20 CONSTRAINTS | | | | | |
|---|---|---|---|---|---|
| Doublet | Quadrupole splitting (mm $s^{-1}$) | Isomer shift (mm $s^{-1}$) | Half width (mm $s^{-1}$) | Goodness of fit | |
| | | | | $\chi^2$ | degrees of freedom |
| (1,10) | peaks of magnetic split spectrum | | | | |
| (2,9) | 2.60±0.00 | 1.18±0.00 | 0.39±0.01 | | |
| (3,8) | 2.41±0.00 | 0.94±0.00 | 0.31±0.03 | | |
| (4,7) | 0.59±0.00 | 0.31±0.00 | 0.29±0.03 | | |
| (5,6) | 0.62±0.00 | 0.40±0.00 | 0.53±0.02 | 494.0 | 497 |
| 19 CONSTRAINTS | | | | | |
| Doublet | Quadrupole splitting (mm $s^{-1}$) | Isomer shift (mm $s^{-1}$) | Half width (mm $s^{-1}$) | Goodness of fit | |
| | | | | $\chi^2$ | degrees of freedom |
| (1,10) | peaks of magnetic split spectrum | | | | |
| (2,9) | 2.60±0.00 | 1.18±0.00 | 0.37±0.01 | | |
| (3,8) | 2.41±0.00 | 0.94±0.00 | 0.32±0.03 | | |
| (4,7) | 0.59±0.00 | 0.31±0.00 | 0.34±0.03 | | |
| (5,6) | 0.62±0.00 | 0.40±0.00 | 0.53±0.02 | 474.6 | 496 |
| 17 CONSTRAINTS | | | | | |
| Doublet | Quadrupole splitting (mm $s^{-1}$) | Isomer shift (mm $s^{-1}$) | Half width (mm $s^{-1}$) | Goodness of fit | |
| | | | | $\chi^2$ | degrees of freedom |
| (1,10) | peaks of magnetic split spectrum | | | | |
| (2,9) | 2.64±0.00 | 1.19±0.00 | 0.38±0.01 | | |
| (3,8) | 2.45±0.00 | 0.95±0.00 | 0.32±0.03 | | |
| (4,7) | 0.59±0.00 | 0.31±0.00 | 0.34±0.03 | | |
| (5,6) | 0.63±0.00 | 0.40±0.00 | 0.54±0.02 | 460.9 | 494 |

TABLE 4-3. Mössbauer parameters for the five doublet fit to the spectrum for specimen D16.75 showing the effect of releasing the constraints on the goodness of fit and on the quadrupole splitting and isomer shifts. Note the general decrease in the goodness of fit as constraints are released.

available in the literature. Sources of Mössbauer data are listed in Stevens and Stevens (1958 to 1975). Bancroft (1973) also lists Mössbauer data for a variety of minerals. The first stage in the assignment of iron, represented by particular peaks or pairs of peaks, to a particular mineral species is to determine the oxidation state and electronic configuration of the iron. For this purpose Bancroft et al. (1967) studied a variety of geological materials and were able to define a series of ranges of both the quadrupole splittings and isomer shifts for iron with particular oxidation states and coordination numbers. A modified version of these data are given in Bancroft (1973) and illustrated in figure 4-4.

The only pair of peaks assigned to a particular mineral species before fitting were those for pyrite. As mentioned earlier, because of the mineralogical complexity of the sample, it was decided to constrain peaks for pyrite (which is known to be present from studies of the specimens in glycerine mounts and in studies of the specimens under the scanning electron microscope). The Mössbauer parameters for pyrite were obtained from the published data of Vaughan (1971) and Vaughan and Craig (1978) and were constrained into the program (peaks 4 and 7 of the final fit). Peaks 2 and 9 form a quadrupole doublet with a quadrupole splitting of 2.60 $\pm$0.00 mm $s^{-1}$; and an isomer shift of 1.18 $\pm$0.00 mm $s^{-1}$. The Mössbauer parameters for this doublet using the data of Bancroft (1973) and figure 4-4, correspond to ferrous iron with a coordination number of six (octahedral site) and suggest that the iron is most likely situated in a silicate framework. The most important iron-bearing silicates in these sediments are the clay minerals. A search of the literature for published Mössbauer data

of iron in clay minerals was made; the data for a variety of clay minerals analysed by Mössbauer spectroscopy are listed in appendix 4.

X-ray diffraction of the sediments has shown that the major iron-bearing clay mineral present in the sediments is an iron-rich chlorite. Comparison of the quadrupole splitting and isomer shift values for peaks 2 and 9 of the spectrum D16.75 shows good comparison with the published data of Taylor et al. (1968) and that of Goodman and Bain (1978) for high-spin ferrous iron in octahedral coordination (Appendix 4 ). The data of Taylor et al. (1968) for the isomer shift (1.20 and 1.25 mm $s^{-1}$) is greater than that measured from specimen D16.75, which may be a result of fitting only one ferrous doublet. However, comparisons with the high quality data of Goodman and Bain (1978) shows better agreement for the isomer shift. In the work by Goodman and Bain (1978), analysis of pure samples enabled the resolution of a second ferrous site in chlorite with a similar isomer shift to the main ferrous doublet, but with a smaller quadrupole splitting in the range 2.30 - 2.51 mm $s^{-1}$. Comparison of the data for peaks 3 and 8, which have a quadrupole splitting of 2.41 mm $s^{-1}$ and an isomer shift of 0.94 mm $s^{-1}$, with that for the inner ferrous doublet of the samples studied by Goodman and Bain (1978) shows good agreement for the quadrupole splitting. However, the measured isomer shift is slightly smaller (0.94 mm $s^{-1}$) than their published data (1.12 - 1.15 mm $s^{-1}$). The only other layer silicates which have similar Mössbauer parameters to chlorite are the mica group of minerals including muscovite and biotite. Bowen et al. (1969) have recorded Mössbauer parameters for muscovite which shows a similar quadrupole splitting and isomer shift to those of chlorite.

Ferrous iron in muscovite is unlikely to be forming a significant component to the spectrum of specimen D16.75 since it forms only a relatively minor component of the sediments as shown by optical microscopy and also because muscovite contains only minor amounts of iron (Deer et al., 1966). More recent data by Hogg and Meads (1970) have established, that ferrous iron occurs in both the A and B octahedral sites in muscovite. The data from this work differs markedly from those obtained for sample D16.75 in that the outer (higher velocity) ferrous doublet has a much greater quadrupole splitting with a range of 3.02 - 3.04 mm $s^{-1}$ and, conversely, the inner ferrous doublet has a relatively small quadrupole splitting of 2.14 - 2.25 mm $s^{-1}$.

Biotite also contains high-spin ferrous iron in octahedral coordination. Taylor et al. (1968) have described Mössbauer parameters for ferrous iron in a variety of biotites, one of which has a quadrupole splitting of 2.60 mm $s^{-1}$ and an isomer shift of 1.25 mm $s^{-1}$. Similar values for the quadrupole splittings and isomer shifts obtained for biotite by Taylor et al. (1968) were obtained by Bowen et al. (1969). Hogg and Meads (1970) identified two octahedral ferrous sites in biotite, niether of which compares favourably with the data obtained from specimen D16.75.

It is thus concluded, that the two high-spin octahedral ferrous sites which give rise to peaks 2,3,8 and 9 in the spectrum of specimen D16.75 are best assigned to the high-spin ferrous iron which occurs in chlorite. The more intense doublet probably arises from ferrous iron in octahedral sites in the "talc-like" layers in chlorite and the values of isomer shift and quadrupole splitting (table 4-3) shows reasonably good agreement with the published data for this mineral (eg. Coey et al., 1974; Goodman and Bain,

1978) and specifically for ferrous iron in an octahedral site, suggested by Goodman and Bain (1978) to be analogous to the site with cis OH groups in biotite. It is possible that this major component arises from ferrous iron in the octahedral sites of the 2:1 layer (talc layer) of chlorite and that the second ferrous doublet arises from ferrous iron in the hydroxide sheet (brucite layer).

The final component of the central part of the spectrum is a ferric doublet with a quadrupole splitting of 0.62 mm $s^{-1}$ and an isomer shift of 0.40 mm $s^{-1}$ corresponding to peaks 5 and 6 of the computer fitted spectrum (figure 4-6). These peaks correspond to ferric iron in tetrahedral coordination, however, the large half widths of these peaks suggests that iron in more than one site is contributing to these peaks, probably including some ferric iron in octahedral coordination. Goodman and Bain (1978) have reported that chlorites may contain ferric iron in both tetrahedral and octahedral coordination. Hence a total of four iron sites are possible in the chlorite structure, two ferrous and two ferric sites.

In the study by Goodman and Bain (1978), chlorites with a range of compositions were studied. Table 4-4 shows the relative amounts of iron in each of the four sites. Although the data are only a representative sample of the many chlorites that are known to exist, and hence are not a statistically representative sample, the data do show that in all cases the ferrous component is the largest with ferrous iron constituting 50 - 92% of the total iron in the samples analysed. If the magnesium-rich chlorite is excluded from the list (since the chlorite examined in the Wash sediments has been shown to be an iron-rich chlorite from X-ray stud-

| Specimen | Ferrous iron | | | Ferric iron | | |
|---|---|---|---|---|---|---|
| | Site 1 | Site 2 | Total | Site 1 | Site 2 | Total |
| 1. Clinochlore | 40% | 21% | 61% | 15% | 24% | 39% |
| 2. Clinochlore | 39% | 11% | 50% | 50% | - | 50% |
| 3. Penninite | 36% | 17% | 53% | 42% | 5% | 47% |
| 4. Penninite | 36% | 20% | 56% | 44% | - | 44% |
| 5. Magnesium chlorite | 41% | 51% | 92% | 8% | - | 8% |
| 6. Clinochlore | 43% | 19% | 62% | 39% | - | 39% |
| 7. Thuringite | 44% | 33% | 77% | - | 23% | 23% |
| 8. Chamosite | 57% | 28% | 85% | 9% | 7% | 16% |
| 9. Daphnite | 63% | 17% | 80% | 11% | 9% | 20% |

TABLE 4-4. The distribution of ferrous and ferric iron in each of the four sites found in chlorites (based on the data of Goodman and Bain, 1978).

ies) the range of ferrous iron becomes 50 - 85% of the total iron. With the exception of the magnesium-chlorite, all the samples shown in table 4-4 have the ferrous iron in the high velocity doublet in excess of that in the low velocity ferrous doublet. This relationship shows good comparison with the data from specimen D16.75 (table 4-6) in which the high velocity ferrous doublet to low velocity ferrous doublet intensity ratio is 3.75 : 1. The best comparison using the data of Goodman and Bain (1978) occurs with samples 2(Clinochlore) and 9(Daphnite) where ratios of the high velocity to low velocity ferrous doublets are 3.54 : 1 and 3.71 : 1 respectively.

It is not known how much of the ferric iron, which accounts for 43% of the total iron present in sample D16.75, can be accounted for in the chlorite structure. As mentioned above, the data of Goodman and Bain (1978) suggest that a range of 50 - 85% of the total iron in chlorite can be expected to be ferrous iron, thus leaving 15 - 50% as ferric iron. So, of the 43% ferric iron in sample D16.75, 11 - 38% can be accounted for in chlorite. This therefore leaves between 5 and 32% of the total iron which must be accounted for in other ferric sites.

Some of the remaining ferric iron may be accounted for in the other clay minerals identified previously by X-ray diffraction. These minerals are illite, montmorillonite and kaolinite. The chemical composition of kaolinite usually shows little variation from stoichiometric $Al_4(Si_4O_{10})(OH)_8$ and only minor substitution of iron in the ferric state into the octahedral sites has been reported (Malden and Meads, 1967). This iron has the following Mössbauer parameters; isomer shift 0.39 mm $s^{-1}$, quadrupole splitting 0.50 mm $s^{-1}$. It is unlikely that the small amount of iron in the

relatively low concentrations of kaolinite (mean 20.0% total clay) in the Wash sediments makes a significant contribution to the Mössbauer spectra obtained.

The substitution of iron into the lattice of montmorillonite however is more usual and results in octahedrally coordinated ferric iron entering the ferric M(1) and M(2) (trans and cis) sites and also some ferrous iron in the M(1) and M(2) sites (Rozenson and Heller-Kallai, 1977). Mössbauer data for the montmorillonite group of minerals are given in appendix 4 ; the most recent and comprehensive study being that of Rozenson and Heller-Kallai (1977), other data from Weaver et al. (1967) and Raclavsky et al. (1975) are also given. In the poor quality data analysed by Weaver et al. (1967), only one ferric site was identified. The data for the two ferric sites quoted in Raclavsky et al. (1975) shows good agreement with the data obtained by Rozenson and Heller-Kallai (1977); however, there is quite large variation in all the parameters quoted for different montmorillonites. The Mössbauer spectrum of specimen D16.75 shows no evidence for the occurence of the ferrous iron in montmorillonite, or for the ferric doublet with the larger quadrupole splitting (0.85 - 1.32 mm $s^{-1}$). However, it is feasible that some of the ferric iron in specimen D16.75 can be attributed to the inner ferric doublet of montmorillonite which has the Mössbauer parameters; isomer shift 0.27 - 0.36 mm $s^{-1}$ and quadrupole splitting in the range 0.45 - 0.61 mm $s^{-1}$.

The final clay mineral which is present in the Wash sediments is illite and this comprises 48.0% of the total clay in the $< 2\mu m$ fraction and forms a significant component of the sediments. Weaver et al., (1967) were able to identify an octahedral site in

illite which was capable of being occupied by either ferrous or ferric iron. In the illite analysed by Raclavsky et al. (1975) two ferric sites were identified (appendix 4 ). These ferric sites give rise to two doublets. The inner doublet has an isomer shift of 0.376 mm $s^{-1}$ and a quadrupole splitting of 0.185 mm $s^{-1}$, whilst the outer ferric doublet has an isomer shift of 0.376 mm $s^{-1}$ and a quadrupole splitting of 0.505 mm $s^{-1}$. The isomer shifts of these doublets compare well with the isomer shift obtained for the ferric doublet in specimen D16.75. However, the quadrupole splitting of the ferric doublet in specimen D16.75 is much greater than those reported for illite. The peaks forming the ferric doublet obtained for specimen D16.75 have large half widths of 0.53 mm $s^{-1}$, much greater than that normally obtained for a single mineral (a value of 0.30 mm $s^{-1}$ is quoted by Bancroft, 1967 as the optimum value for the half width of a peak representing one site of a single mineral species). It is thus plausable that some of the counts forming this peak are from ferric iron in illite.

Finally, the only other major contribution to this ferric doublet is likely to arise from ferric iron in iron oxyhydroxides such as goethite or from the central part of the spectrum of greigite. The iron oxyhydroxide, goethite normally gives a magnetically ordered six-peak spectrum as shown in the data of Forsyth et al. (1968) and Murad (1979), but if the goethite is very fine-grained then the spectrum "collapses" because the mineral is in a super-paramagnetic state so that the resulting spectrum consists of a single doublet. Because of the nature of the "collapse" the values of the isomer shift and quadrupole splitting vary depending on its extent. Weaver et al. (1967) measured a sample of super-paramagnetic goethite with the following Mössbauer parameters;

isomer shift 0.37 mm $s^{-1}$ and quadrupole splitting 0.27 mm $s^{-1}$. Greigite also exhibits a six-line magnetically ordered spectrum but at temperatures above 4.2°K the greigite spectrum "collapses" to a single quadrupole split doublet (Vaughan and Ridout, 1971). This is also a superparamagnetic effect due to the rapid relaxation of atomic spins. The contribution to the spectrum by greigite is discussed in more detail below. Mackinawite, which is also suggested to be present in the sediments (Love, 1967) gives only a single peak at 4.2°K with a small isomer shift (0.2 mm $s^{-1}$) which has been attributed to low-spin ferrous iron by Vaughan and Ridout (1971). Because of the complexity of the spectrum of sample D16.75 it was not possible to resolve the single peak for mackinawite. However, the presence of pyrite and greigite together with the black colouration of the sediment would suggest that it is present.

So far only the central part of the spectrum obtained for sample D16.75 has been discussed. Examination of figure 4-6 shows that at very low and very high velocity are a further pair of peaks (at -4.357 mm $s^{-1}$ and 5.300 mm $s^{-1}$ repectively). These peaks must constitute part of a magnetic hyperfine split spectrum. Initially it was suspected that these peaks were peaks 2 and 5 of the spectrum for magnetite, since detrital magnetite is the major remanence carrier in these sediments (see section 7-1). Comparison of the peak positions obtained does not give good agreement with those in the literature for magnetite (see for example Evans and Hafner, 1969), or with the corresponding peak positions obtained for a sample of magnetite extracted from the sediment (sample D13, chapter 7). The peaks of the magnetite spectrum (for specimen D13) which are closest to those of the peaks in specimen D16.75 occur

| Source of data | Type of iron | Temp of spectrum | I.S. ($mm\ s^{-1}$) | Q.S. ($mm\ s^{-1}$) | Hyperfine magnetic field (kG) |
|---|---|---|---|---|---|
| 2 | High-spin octahedral $Fe^{2+}$ | 4.2°K | 0.70 | 0.30 | 322 |
| 2 | High-spin octahedral $Fe^{3+}$ | 4.2°K | 0.45 | 0.40 | 465 |
| 2 | High-spin tetrahedral $Fe^{3+}$ | 4.2°K | 0.40 | 0.00 | 485 |
| 1 | High-spin tetrahedral $Fe^{3+}$ | 300°K | 0.26 | - | 311 |
| 1 | High-spin octahedral ($Fe^{2+}$ and $Fe^{3+}$) | 300°K | 0.55 | - | 310 |
| 3 | ? | 300°K | 0.39 | 0.00 | 297 |
| 3 | ? | 300°K | 0.28 | 0.48 | - |
| 3 | ? | 300°K | 0.31 | 0.55 | - |

TABLE 4-5 Published Mössbauer data for iron in greigite.

Sources of data are; (1) Coey et al. (1970), (2) Vaughan (1971), and (3) Morice et al. (1969).

at -4.327 mm $s^{-1}$ and 4.881 mm $s^{-1}$. The first of these at -4.327 mm $s^{-1}$ representing the A site in magnetite gives good agreement with peak 1 in specimen D16.75 which occurs at 4.357 mm $s^{-1}$ however, the peak for the high velocity A and B sites at 4.881 mm $s^{-1}$ differs greatly from the peak in specimen D16.75 which as shown in table 4-6 and figure 4-6 occurs at 5.300 mm $s^{-1}$. It is concluded, therefore, that these peaks cannot be attributed to magnetite. These peaks also cannot be attributed to the hematite spectrum, the nearest corresponding peaks being at -4.46 mm $s^{-1}$ and at 4.85 mm $s^{-1}$ which are peaks 2 and 5 of the hematite spectrum (Greenwood and Gibb, 1971).

Comparison of the magnetically ordered peaks of the spectrum for sample D16.75 with the published data for the Mössbauer parameters of the iron sulphide, greigite (cubic $Fe_3S_4$) was next attempted. The Mössbauer effect as observed in greigite has been studied by Morice et al. (1969); Coey et al. (1970); and Vaughan and Ridout (1971) (see table 4-5).

The greigite spectra have only been obtained for fine particle synthetic materials in which magnetic reversals due to thermal motion take place in a shorter time than the Mössbauer transition at room-temperature (i.e. they are superparamagnetic); therefore spectra have to be recorded at very low temperatures to overcome this effect. Vaughan and Ridout (1971) have recorded spectra from greigite at temperatures down to 1.4°K in which they observed ferrous and ferric iron, magnetically ordered in both tetrahedral and in octahedral sites. Greigite is strongly ferrimagnetic and may be considered as the sulphur analogue of magnetite.

Calculation of the hyperfine magnetic fields for peaks 1 and

10 of spectrum D16.75 (assuming they are peaks 1 and 6 of a six line magnetic split spectrum) gave a field of 299 kG. This compares favourably with the hyperfine magnetic fields of all the available data on synthetic greigite for room temperature ($300^{o}K$) spectra for which the range of magnetic hyperfine fields is 297-310 kG (see table 4-5). Calculation of the isomer shift and quadrupole splittings could not be determined accurately for the magnetically ordered part of the spectrum of specimen D16.75 because the inner peaks to this spectrum had not been fitted. It was possible to estimate the positions of peaks 2 and 5 of the six line spectrum however, and so approximate values for the isomer shift and quadrupole splitting could be calculated. The approximate positions of peaks 2 and 5 of the six line spectrum are at -2.343 mm $s^{-1}$ and at 3.590 mm $s^{-1}$. The estimated value of the isomer shift is -0.304 mm $s^{-1}$ and that for the quadrupole splitting is 0.548 mm $s^{-1}$. The isomer shift doesnot compare very well with the reported values for greigite (table 4-5) but this may be largely due to the estimation of the peak positions of lines 2 and 5. The calculated value for the quadrupole splitting does however compare well with the published data and particularly with that of Coey et al. (1970). It is thus concluded that the magnetically split part of the spectrum for sample D16.75 can be assigned to the iron sulphide, greigite.

Having assigned all the peaks to minerals or mineral groups, it was next possible to calculate the relative amounts of iron in each of these minerals from the intensities of the absorption peaks. The results of these calculations are shown in table 4-6 together with the mineral assignments.

It is important to realise that these calculations are appro-

| Specimen D16.75 | | | |
|---|---|---|---|
| Peak Number | Peak Positions ($mm\ s^{-1}$) | %Contribution to total Fe | Mineral Assignment |
| (1,10) | -4.36<br>+5.30 | ~8% | Greigite |
| (2,9) | -0.12<br>+2.48 | ~30% | Chlorite $Fe^{2+}$ |
| (3,8) | -0.27<br>+2.15 | ~8% | Chlorite $Fe^{2+}$ |
| (4,7) | +0.02<br>+0.61 | ~11% | Pyrite $Fe^{2+}$ |
| (5,6) | +0.09<br>+0.71 | ~43% | all $Fe^{3+}$ contributions |

TABLE 4-6. Mössbauer data for the ten-peak computer fit to the spectrum from specimen D16.75 showing the assignment of the peaks to specific minerals or mineral groups. The approximate percentage contribution of the iron in each of these groups to the total iron iron in the sample is also shown.

ximate as they do not take into account the possible variations in the recoil-free fractions for different mineral species. Also, in calculating the percentage contribution of iron in greigite it is assumed that the peak areas of the greigite spectrum follow a 3:2:1:1:2:3 ratio relationship. Examination of the spectra from synthetic greigite samples shows a considerable tendency for the samples to exhibit superparamagnetism which has been attributed to the small particle size of the samples. If the greigite in specimen D16.75 is of similar particle size then it can be concluded that the estimate of 8% of the total iron being in the form of greigite is too low. It is thus best to regard the figure of 8% of the total iron in greigite as a minimum. The contribution of chlorite to the total iron budget is 38% with 30% being in the high velocity, high-spin octahedral ferrous site and the remaining 8% being in the low velocity, high-spin octahedral ferrous site. Eleven percent of the total iron occurs in the form of pyrite and the remaining 43% of the total iron is attributed to all ferric contributions.

4-2-3. Results and Interpretation of the Series of Freeze-dried Specimens.

The freeze-dried samples from core D1 were measured at room-temperature and all the spectra with the exception of one (specimen D18.50) have been fitted with two doublets. The spectrum of sample D18.50 was of poor quality due to its low iron content and, although showing similar shape to that of the other spectra, a satisfactory fit could not be achieved and the data were discarded from this study. The data for the other spectra fitted with two doublets are shown in table 4-7. Six of these spectra (from

specimens D12.50, D13.50, D14.50, D17.50, D19.50 and D110.50) are shown in figure 4-7. As these examples show, there is a systematic increase with depth in the relative intensity of the doublet with low isomer shift and small quadrupole splitting (inner doublet) compared to the doublet arising from ferrous iron in clay minerals, mainly chlorite (outer doublet). Although the inner doublet arises both from ferric and from ferrous iron in pyrite and could be evidence of an increase in ferric iron concentration with depth, the more likely interpretation is that it represents an increase in the relative amount of iron in pyrite with depth in the core. This observation would agree with the colour zonation within the core which, with depth, goes from brown to dark grey or black and then to grey. Love (1967) has shown that this is due to increased concentrations of, firstly, iron monosulphide and greigite, and then pyrite. Two of the specimens (numbers D16.50 and D19.50) do not fit into this overall trend, both of these specimens are from the fine sands of the Arenicola sand flat subenvironment where it has already been shown that great variations in the clay mineral compositions, geochemistry and grain size of the sediment occurs.

No further pairs of peaks were fitted by computer to the whole set of spectra for the freeze-dried specimens because of the high noise level of the data, but a number of other observations can be made about the data. Firstly, examination of the low velocity side of the high velocity peak of the outer doublet reveals a shoulder which is apparent in all of the spectra. This shoulder can be attributed to a second ferrous doublet analogous to the doublet fitted to the spectrum for specimen D16.75 which was assigned to iron in the hydroxide sheet, or brucite layer,

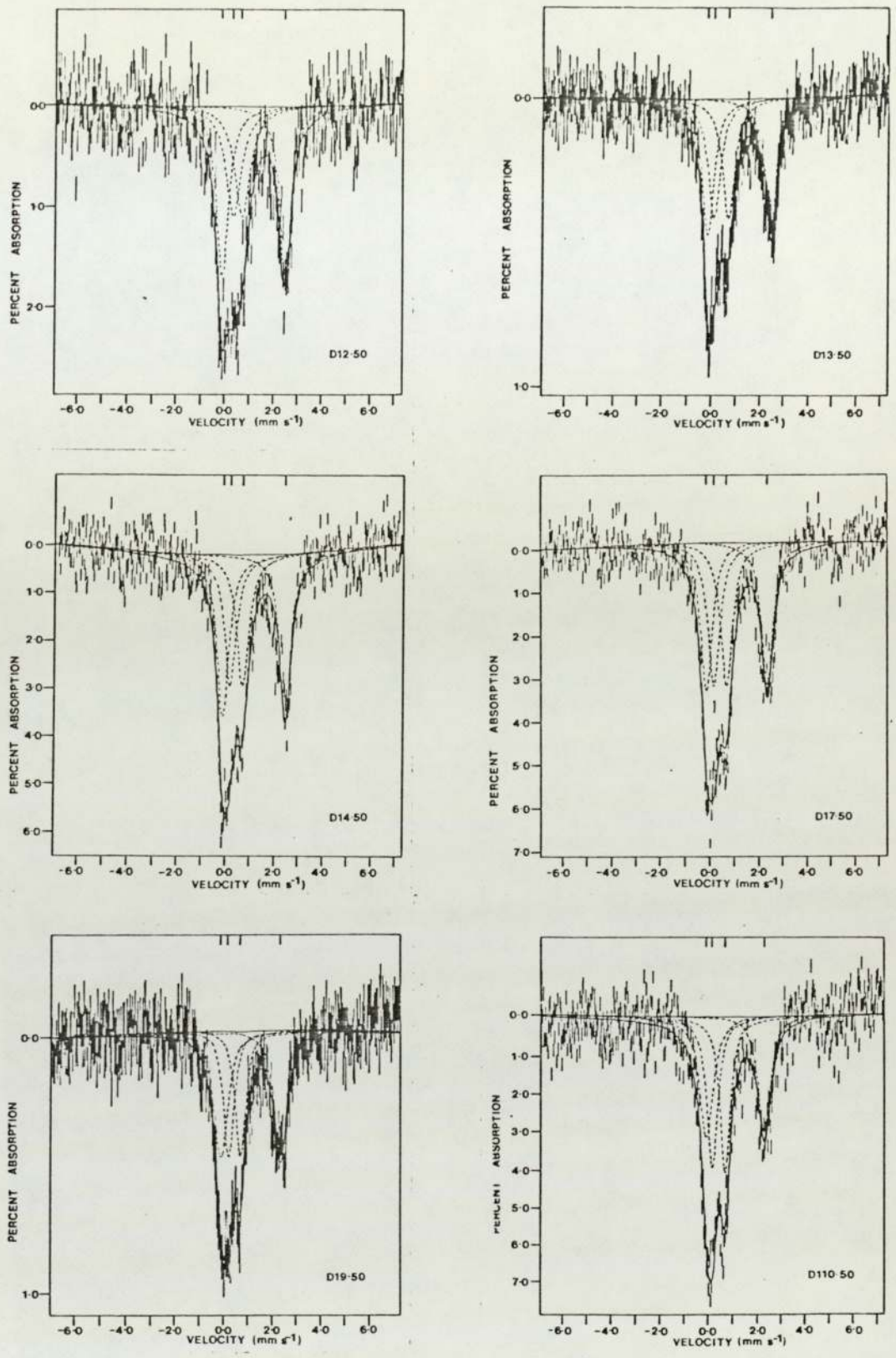


Figure 4-7. Representative Mössbauer spectra from the series of samples from core D1. Computer fitting of two doublets has been applied to all of the spectra and shows an overall increase in the intensity of the inner doublet (representing in part pyrite) with increased depth in the core.

of chlorite. In all of the samples studied this ferrous doublet is of lower intensity than the ferrous doublet representing iron in the talc layer of chlorite.

One of the samples (sample D14.50) gave a sufficiently good spectrum that it was possible to fit a further ferrous doublet to the data, the resulting Mössbauer parameters are shown in table 4-8 together with the corresponding computer fit for specimen D16.75. The three doublet fit to the spectrum of specimen D14.50 compares well with the data of specimen D16.75 and, in particular, to the two ferrous doublets which have been identified as being due to octahedrally coordinated ferrous iron in chlorite.

Analysis of the quadrupole splitting values of the outer doublets in the two doublet fits shows a variation which is dependant on the lithological type from which the samples were taken. The variation occurs in the size of the quadrupole splitting, which in the samples from the fine grained sediments, samples D12.50, D13.50, D14.50 and D16.75, show larger quadrupole splittings in the range 2.38 - 2.44 mm $s^{-1}$. This variation is also reflected in the values of isomer shift which again can be divided into two groups, one with values in the range 1.11 - 1.14 mm $s^{-1}$ and another group with isomer shifts in the range 1.08 - 1.12 mm $s^{-1}$. Examination of the spectra (figure 4-7) reveals that this variation in isomer shift and quadrupole splitting can be interpreted as being due to an increase in the intensity of the inner ferrous doublet (attributed to the brucite layer in chlorite). This increase in the intensity of the inner ferrous doublet gives rise to the decrease in the quadrupole splitting and isomer shift observed in the ferrous doublets fitted in the two doublet fits of table 4-7.

| Sample | Outer doublet | | | Inner doublet | | | Goodness of fit | | $I_o/I_i$ |
|---|---|---|---|---|---|---|---|---|---|
| | Q.S. (mm $s^{-1}$) | I.S. (mm $s^{-1}$) | H.W. (mm $s^{-1}$) | Q.S. (mm $s^{-1}$) | I.S. (mm $s^{-1}$) | H.W. (mm $s^{-1}$) | $\chi^2$ | degrees of freedom | |
| D12.50 | 2.55±0.01 | 1.11±0.01 | 0.58±0.02 | 0.36±0.02 | 0.46±0.02 | 0.77±0.06 | 784.9 | 499 | 1.16 |
| D13.50 | 2.54±0.02 | 1.11±0.02 | 0.58±0.03 | 0.57±0.02 | 0.38±0.02 | 0.61±0.04 | 523.4 | 500 | 1.08 |
| D14.50 | 2.53±0.01 | 1.13±0.01 | 0.57±0.01 | 0.50±0.01 | 0.41±0.01 | 0.60±0.02 | 394.4 | 496 | 1.17 |
| D15.50 | 2.41±0.05 | 1.12±0.05 | 0.64±0.10 | 0.51±0.06 | 0.41±0.06 | 0.68±0.17 | 474.1 | 500 | 1.20 |
| D16.50 | 2.44±0.03 | 1.08±0.03 | 0.70±0.04 | 0.42±0.04 | 0.47±0.04 | 0.60±0.09 | 446.1 | 500 | 1.41 |
| D17.50 | 2.45±0.01 | 1.08±0.01 | 0.59±0.01 | 0.51±0.01 | 0.42±0.01 | 0.60±0.01 | 418.8 | 500 | 1.01 |
| D18.50 | (low iron content fitting not possible) | | | | | | | | |
| D19.50 | 2.41±0.02 | 1.08±0.02 | 0.70±0.04 | 0.48±0.02 | 0.42±0.02 | 0.53±0.04 | 558.7 | 500 | 1.33 |
| D110.50 | 2.38±0.01 | 1.08±0.01 | 0.66±0.02 | 0.52±0.01 | 0.42±0.01 | 0.52±0.01 | 405.5 | 500 | 0.99 |
| *D16.75 | 2.60±0.01 | 1.14±0.01 | 0.46±0.01 | 0.61±0.01 | 0.35±0.01 | 0.47±0.01 | 769.3 | 500 | 0.70 |

TABLE 4-7 Mössbauer parameters for the two-doublet computer fits to the spectra from the series of samples from core D1.

* Specimen D16.75 was an iron-rich clayey sediment, the spectrum from this sample was used in more detailed computer fitting as is discussed in section 4-2-2.

$I_o/I_i$ is the ratio of the intensities of the outer to inner doublets.

| Sample | Doublet (1,6) | | | Doublet (2,5) | | | Doublet (3,4) | | |
|---|---|---|---|---|---|---|---|---|---|
| | Q.S. ($\pm$1) (mm s$^{-1}$) | I.S ($\pm$1) (mm s$^{-1}$) | H.W. ($\pm$1) (mm s$^{-1}$) | Q.S. ($\pm$1) (mm s$^{-1}$) | I.S. ($\pm$1) (mm s$^{-1}$) | H.W. ($\pm$1) (mm s$^{-1}$) | Q.S. ($\pm$1) (mm s$^{-1}$) | I.S. ($\pm$1) (mm s$^{-1}$) | H.W. ($\pm$1) (mm s$^{-1}$) |
| D14.50 | 2.58$\pm$0.00 | 1.19$\pm$0.00 | 0.38$\pm$0.01 | 2.42$\pm$0.01 | 0.92$\pm$0.01 | 0.43$\pm$0.03 | 0.50$\pm$0.00 | 0.43$\pm$0.00 | 0.54$\pm$0.01 |
| D16.75 | 2.60$\pm$0.00 | 1.18$\pm$0.00 | 0.39$\pm$0.01 | 2.41$\pm$0.01 | 0.94$\pm$0.01 | 0.27$\pm$0.03 | 0.62$\pm$0.00 | 0.36$\pm$0.00 | 0.47$\pm$0.01 |

TABLE 4-8 Mössbauer parameters for the three doublet computer fits applied to the spectra of specimens D14.50 and D16.75.

Another feature of these spectra is the large half widths obtained for the inner doublet. These arise because no distinction has been made between the ferric sites and the low-spin ferrous iron in pyrite which are both present in the samples. The fitting of the further high-spin ferrous doublet for chlorite would also have helped to reduce these half widths.

Finally, many of the spectra show an indication that a magnetically ordered pair of peaks occur at very high and at very low velocity. The positions of these peaks coincides with those which were identified as being due to the presence of greigite in the spectrum of sample D16.75 and can therefore be assigned to the presence of greigite.

## 4-3 Low-temperature studies of samples from core D2.

### 4-3-1. Sampling and Experimental Methods.

From the second Delft core (core D2) a series of nine samples were taken for Mössbauer analysis at low-temperatures. Sampling of the core was not made at regular intervals as in the room-temperature study of the freeze-dried samples from core D1 but, samples were selected to represent the range of lithologies and oxidation states found in the core, that is; oxidized brown clay, reduced black silty clay, reduced black clay and the grey fine sand of the pyritic zone.

The observation of the Mössbauer effect at low-temperatures is advantageous because firstly, it overcomes the problem of the very low recoil-free fraction of many $\gamma$-ray transitions at ambient temperatures and secondly, it permits the study of the temperature dependance of hyperfine effects. However, in this study, the major reason for carrying out low-temperature studies was that it allowed analysis of samples taken "fresh" from the core, the low temperatures freezing the sample and inhibiting dehydration and oxidation of the sample.

Sample preparation was achieved in the same way as described for the room-temperature study except that the samples were taken "fresh" from the newly-opened core and were not subjected to the process of freeze-drying. The Mössbauer apparatus was modified to allow cooling of the sample (absorber) to 77°K (the boiling point of liquid nitrogen) as shown in figure 4-8. The sample was mounted onto the blade of a copper cold finger in which an aperture had been cut to allow transmission of the $\gamma$ -rays. The absorber and upper part of the cold finger were then mounted in the

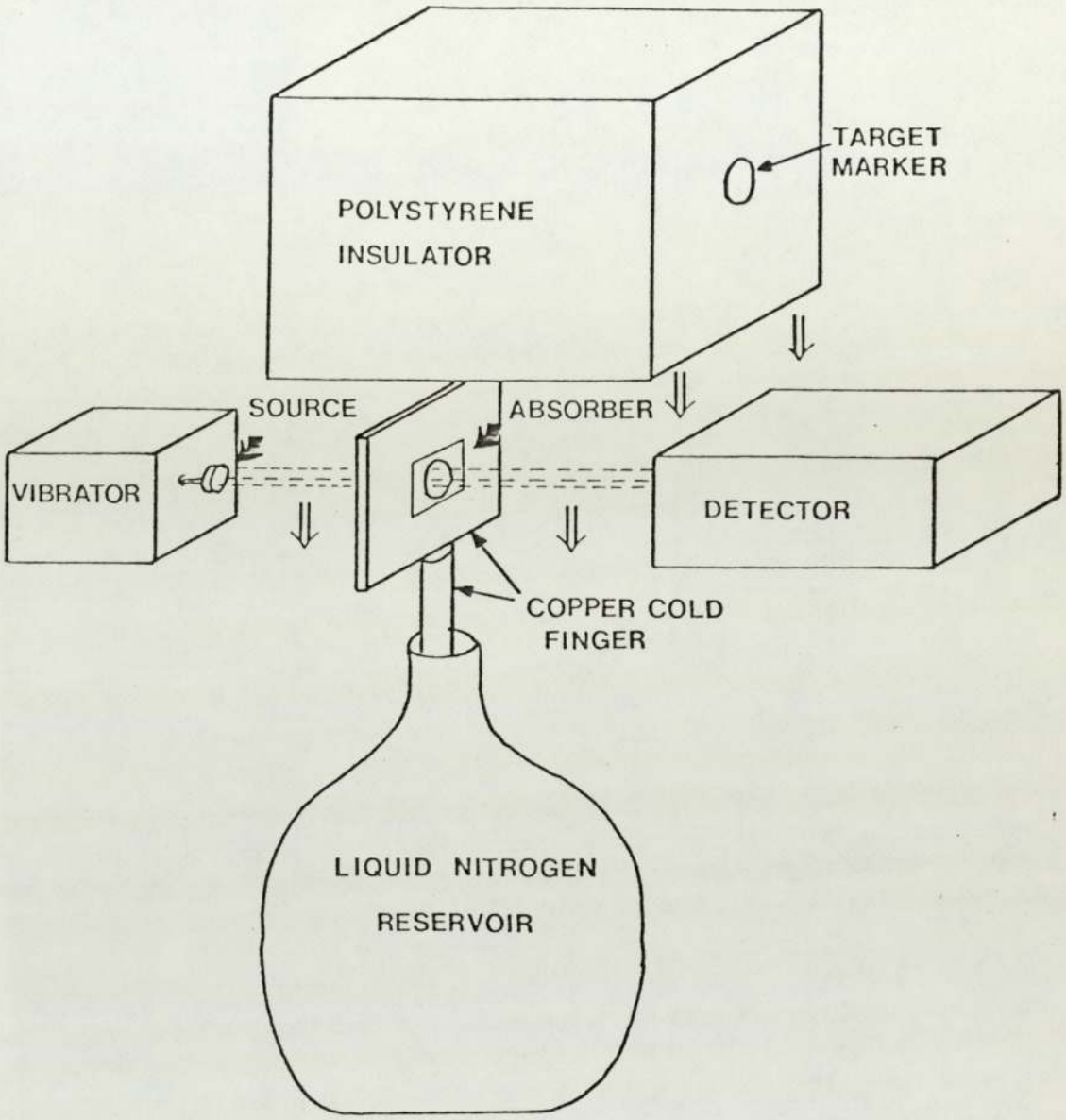


Figure 4-8. Low-temperature liquid nitrogen Mössbauer apparatus showing the positions of the various components used in this study. The block of polystyrene, which is used as an insulator, is shown raised from its normal position so that the location of the absorber on the copper cold-finger can be seen.

centre of a thick (20cm sided) cube of polystyrene. The remaining part of the copper tube forming the cold figer was then lowered into a large reservoir of liquid nitrogen contained in a cryogenic dewar taking care to align the absorber with the source and detector. Collection of the spectra, once the sample was completely cooled, then proceeded in the usual way. Calibration of the spectra was again made with an iron foil absorber at room-temperature. Computer fitting of the spectra was undertaken using the methods already described for the room-temperature spectra.

4-3-2. Results and Interpretation of the Low-temperature Spectra.

Since one of the objectives of this study was to determine if any major differences in the Mössbauer parameters, and hence iron-bearing mineralogy, occured between the different oxidation states and lithologies represented in the core, the results are shown together with details of the oxidation states and lithologies of the samples. Initially two doublets were fitted to all of the spectra and the results from these fits are shown in table 4-9 with examples of the spectra obtained in figure 4-10.

As in the room-temperature spectra the outer doublet represents high-spin ferrous iron in octahedral coordination in chlorite. The inner doublet is assigned to all ferric contributions as well as to the low-spin ferrous iron which occurs in pyrite. Inspection of the data for the quadrupole splittings of the outer doublets again shows a trend of decreasing quadrupole splittings as we go down the core. This trend is enhanced if the data are plotted so that the lithology and oxidation states of the sediments are taken into account (figure 4-9 ).

The ranges of quadrupole splitting and isomer shift values

| Sample | Outer doublet | | | Inner doublet | | | Goodness of fit | | $I_o/I_i$ | Lithology |
|---|---|---|---|---|---|---|---|---|---|---|
| | Q.S. ($mm\ s^{-1}$) | I.S. ($mm\ s^{-1}$) | H.W. ($mm\ s^{-1}$) | Q.S. ($mm\ s^{-1}$) | I.S. ($mm\ s^{-1}$) | H.W. ($mm\ s^{-1}$) | $\chi^2$ | degrees of freedom | | |
| D22.52 | 2.80±0.01 | 1.21±0.01 | 0.35±0.02 | 0.65±0.02 | 0.41±0.02 | 0.72±0.05 | 557.9 | 500 | 0.65 | 1 |
| D23.15 | 2.72±0.01 | 1.20±0.01 | 0.48±0.02 | 0.51±0.02 | 0.41±0.02 | 0.46±0.03 | 618.1 | 500 | 1.67 | 2 |
| D23.46 | 2.75±0.01 | 1.19±0.01 | 0.48±0.02 | 0.48±0.02 | 0.44±0.02 | 0.51±0.04 | 670.1 | 500 | 1.71 | 2 |
| D23.47 | 2.73±0.01 | 1.19±0.01 | 0.46±0.02 | 0.55±0.02 | 0.40±0.02 | 0.62±0.04 | 557.5 | 500 | 1.26 | 2 |
| D23.55 | 2.73±0.01 | 1.19±0.01 | 0.43±0.01 | 0.54±0.01 | 0.41±0.01 | 0.45±0.02 | 693.9 | 499 | 1.31 | 3 |
| D24.80 | 2.69±0.01 | 1.18±0.01 | 0.56±0.02 | 0.46±0.02 | 0.44±0.02 | 0.53±0.04 | 668.2 | 500 | 1.89 | 4 |
| D24.100 | 2.67±0.02 | 1.19±0.02 | 0.71±0.04 | 0.36±0.03 | 0.53±0.03 | 0.44±0.07 | 600.6 | 500 | 3.38 | 4 |
| D25.30 | 2.73±0.01 | 1.20±0.01 | 0.49±0.02 | 0.51±0.02 | 0.43±0.02 | 0.53±0.04 | 604.4 | 500 | 1.61 | 3 |
| D26.32 | 2.74±0.02 | 1.18±0.02 | 0.57±0.05 | 0.44±0.04 | 0.45±0.04 | 0.58±0.09 | 647.7 | 499 | 1.64 | 3 |

TABLE 4-9 Mössbauer parameters for the two-doublet computer fits for the spectra from the series of samples from core D2. All of the spectra were run with the absorber at 77°K. The lithologies are as follows; (1) Brown clay, (2) Black silty clay, (3) Black clay, and (4) Grey fine sand.

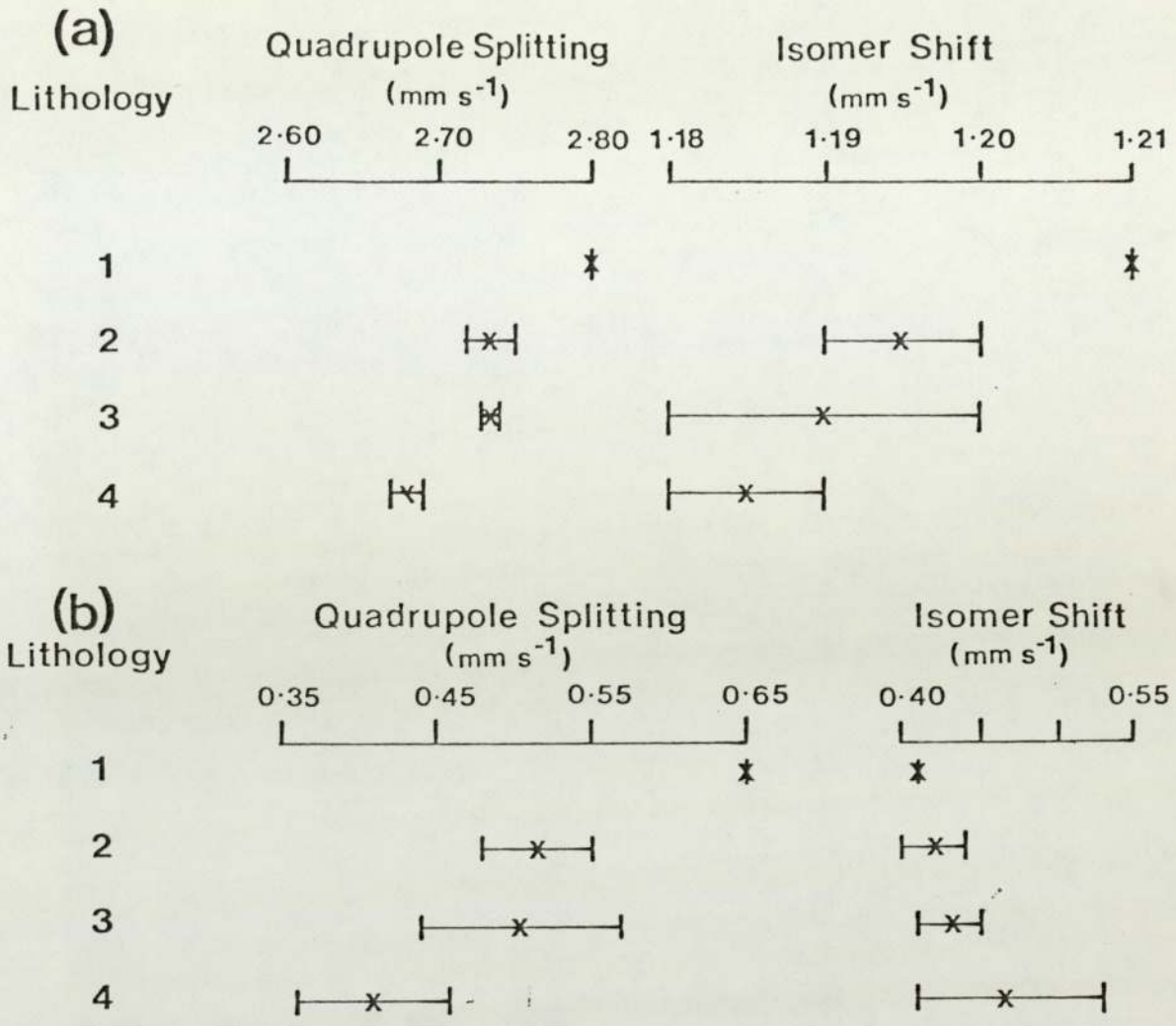


Figure 4-9. The range of quadrupole splitting and isomer shift values obtained from the outer (a) and inner (b) doublets of the series of spectra obtained from core D2 are shown plotted for each of the lithological types encountered. The lithology numbers are the same as those used in Table 4-9.

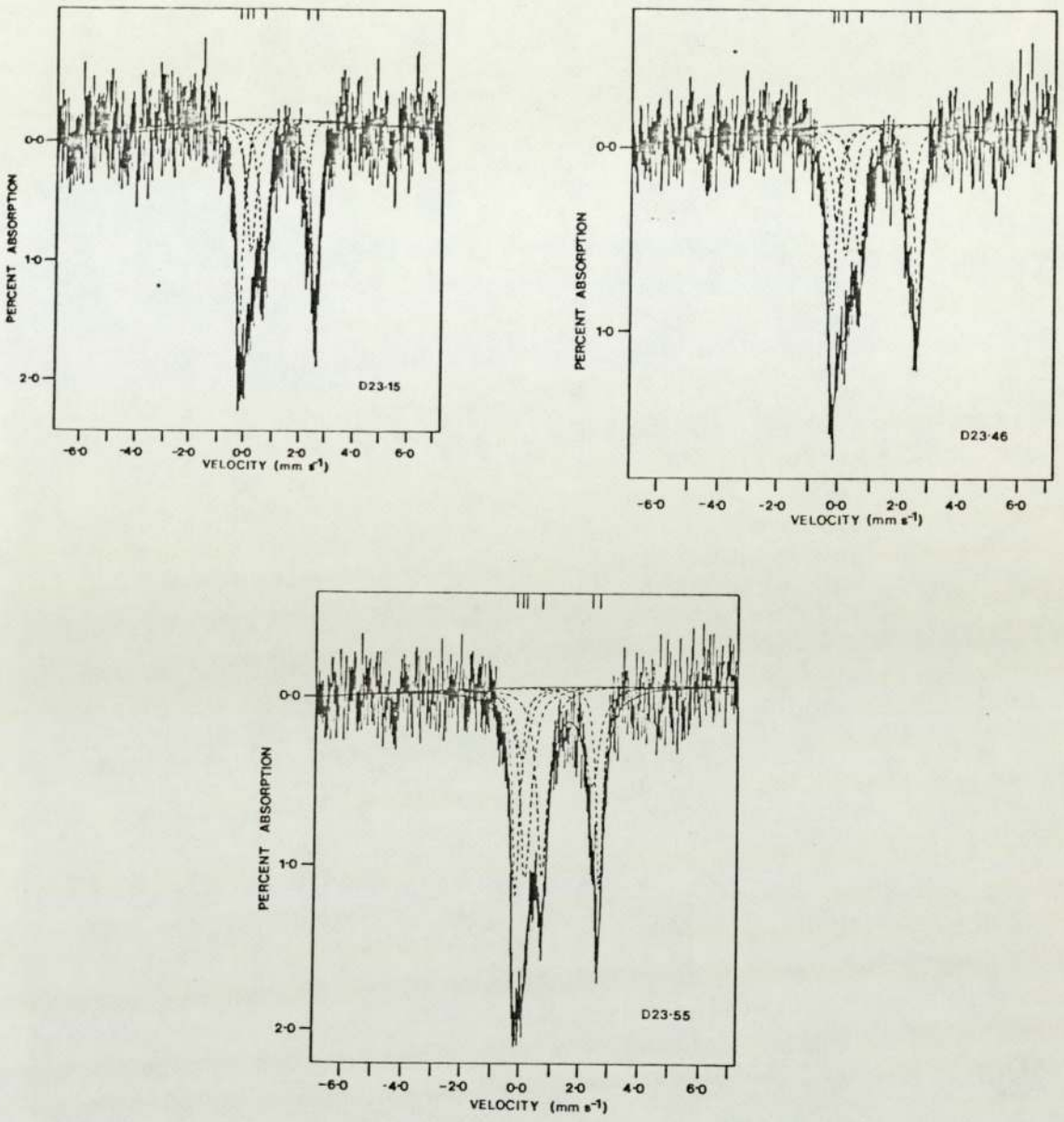


Figure 4-10 Representative Mössbauer spectra for specimens run at low-temperature (77°K). The three spectra shown here, from specimens D23.15, D23.46 and D23.55, have been fitted by computer with three doublets. The outer two doublets (peaks (1,6) and peaks (2,5)) are assigned to high-spin ferrous iron situated in chlorite. The inner doublet (peaks (3,4)) is assigned to both ferric iron and to the low-spin ferrous iron which occurs in pyrite.

encountered in the different lithologies represented in the core plotted in figure 4-9 show that at the top of the core the brown clay of the oxidized zone gives an outer doublet quadrupole splitting for ferrous iron of 2.80 mm $s^{-1}$ but with increased depth within the monosulphidic zone (black colouration) the outer doublet quadrupole splitting reduces to lie in the range 2.72 - 2.75 mm $s^{-1}$ in lithology 2, and 2.73 - 2.74 mm $s^{-1}$ in lithology 3. Finally in the bisulphidic (grey coloured) sediment the quadrupole splitting has reduced to 2.67 - 2.69 mm $s^{-1}$. This trend was also encountered in the freeze-dried material from core D1 where it was attributed to a decrease in the relative intensity of the outer ferrous doublet of chlorite to that of the inner ferrous doublet of chlorite. Hence it is proposed that with depth, and increasing reducing conditions, the amount of iron in the brucite layer increases with respect to that in the talc-layer of chlorite. This could be interpreted as a net decrease in the iron from the talc layer as a result of increased reducing conditions and it could be that some of the iron is reacting with sulphide ions to form pyrite and its precursors greigite and mackinawite. In support of this observation is the diagenetic relationship between pyrite and chlorite observed in sediment from Lake Saint George, Toronto, Ontario (Manning and Ash, 1979) in which chlorite was proposed as the source of iron in the formation of diagenetic pyrite. The reaction observed by Manning and Ash (1979) differs from that observed in this study; firstly, no attempt was made in their work to differentiate between the two ferrous doublets found in chlorite and secondly, complete removal of chlorite from the sediment was observed in their study leaving only one pair of peaks assigned to the low-spin iron in pyrite.

A similar trend in the isomer shift is observed in the outer doublet results in which there is a decrease from 1.21 mm $s^{-1}$ in the oxidised brown clay (lithology 1) to 1.18 to 1.19 mm $s^{-1}$ in the reduced pyritic grey sand (lithology 4). This trend was also found in the two doublet fits of the room-temperature spectra and is due to the changes in the asymmetry of this ferrous doublet caused by changes in the relative intensities of the two component ferrous doublets which make up this pair of peaks.

Comparison of the quadrupole splittings of the low-temperature runs with those obtained from the room-temperature study shows that there is an expansion from 2.38 - 2.60 mm $s^{-1}$ in the room-temperature spectra to 2.67 - 2.80 mm $s^{-1}$ for the outer doublet of the low-temperature spectra. A similar effect is seen in the values of the isomer shift for this outer doublet which rise from 1.08 - 1.14 mm $s^{-1}$ for the room-temperature spectra to 1.18 - 1.21 mm $s^{-1}$ for the low-temperature spectra.

Inspection of the quadrupole splittings of the inner doublet also reveals a temperature dependance (although less marked than that in the outer doublet), in which the quadrupole splittings increase from 0.36 - 0.61 mm $s^{-1}$ in the room-temperature spectra to 0.36 - 0.65 mm $s^{-1}$ in the low-temperature spectra. A more noticeable increase is seen in the isomer shifts for the inner doublet which show an increase from 0.35 - 0.47 mm $s^{-1}$ in the room-temperature spectra to 0.40 - 0.53 mm $s^{-1}$ in the low-temperature spectra. As has been described previously, the inner doublet is in part formed by the peaks representing low-spin ferrous ions in pyrite. Studies of the behavoir of pyrite at low-temperatures have been made using the Mössbauer effect (Imbert et al., 1963; Temperley and Lefevre, 1966) which show increases in both

isomer shift and quadrupole splittings. Imbert et al. (1963) found an increase in the isomer shift from 0.30mm $s^{-1}$ (300°K) to 0.31 mm $s^{-1}$ (77°K) and in the quadrupole splitting from 0.60 mm $s^{-1}$ (300°K) to 0.61 mm $s^{-1}$ (77°K). The results of Temperley and Lefevre (1966) show a greater variation, in the isomer shift an increase from 0.31 mm $s^{-1}$ (300°K) to 0.40 mm $s^{-1}$ (81°K) in the isomer shift and from 0.61 mm $s^{-1}$ (300°K) to 0.62 mm $s^{-1}$ (81°K) in the quadrupole splitting. This increase in the quadrupole splitting and isomer shift observed in the low-spin ferrous iron in pyrite could, in part, explain the similar effect observed at low-temperature (77°K) in the inner doublets of the samples from core D2. Similar effects to this affecting the quadrupole splitting and isomer shift of the ferric iron, which also form this inner doublet, have been observed in the parameters for ferric iron in clay minerals.

Examination of the ratios of the areas of the peaks representing the outer to inner doublets again shows a dependance on lithology and on oxidation state. The lowest ratio for the intensity of the outer to inner doublet peak areas occurs in the spectrum for specimen D22.52 (Brown clay) where a ratio of 0.65 is obtained. This ratio is especially low because the chlorite in this specimen appears to have iron mainly in the talc-layer since no shoulder occurs on the low velocity side of the peak (figure 4-19)this is also shown by the small half-widths (0.35 mm $s^{-1}$) of the peaks comprising this doublet (table 4-9).

The specimens which come from the black silty clay, and the black clay from the reduced zone (monosulphidic zone) of sediment (specimens D23.15, D23.46, D23.37, D23.55, D25.30 and D26.32) show similar ranges of quadrupole splitting and isomer shift

values and also similar outer to inner doublet intensity ratios. The black silty clay shows outer to inner doublet intensity ratios of 1.26 - 1.71 and for the black clays the ratios fall in the range 1.31 - 1.64. The specimens which are derived from the bi-sulphidic zone or pyritic zone represented by the grey fine sands (D24.80; D24.100) show a further increase in their outer to inner doublet intensity ratios (1.89 - 3.38). This trend of increasing inner to outer doublet ratios is the converse of what was observed in the room-temperature study where the ratio decreased with repect to increasing depth and reduction of the sediment. This anomaly probably arises because the peaks which have been fitted to the low-temperature spectra are firstly really composite peaks formed from the contribution of several peaks with slightly different Mössbauer parameters. Secondly, because of the expansion in quadrupole splittings and the changes in the isomer shifts which occur at low-temperatures, peak positions change and hence the areas of the composite doublets fitted in this series of two doublet fits cannot be compared with those fitted to the room-temperature spectra.

One feature of the spectra obtained from the low-temperature runs is the increased resolution and general higher quality of the spectra which has meant that three of the spectra (D23.15, D23.46 and D23.55) could be further resolved by performing a three-doublet fit. The additional doublet fitted to these spectra was the inner ferrous doublet, the high velocity peaks of which form a shoulder to the high velocity peak of the ferrous doublet already fitted, the shoulder forming on the low velocity side. This ferrous doublet has already been attributed to the high-spin ferrous iron occuring in octahedral coordination within the bruc-

ite layer of chlorite. The results of these fits are shown in table 4-10 and figure 4-10.

All of the spectra fitted with three doublets show an improvement in the statistical fit (compare the data in table 4-9 with that in table 4-10) indicating a better prediction of the component peaks represented in the spectra. The main feature which results when a further ferrous doublet is fitted is that the larger (high velocity) intensity ferrous doublet fitted to the two doublet spectra shows an increase in its quadrupole splitting from values in the range 2.72 - 2.75 mm $s^{-1}$ for the two doublet fits and 2.82 - 2.86 mm $s^{-1}$ in the three doublet fits. As was explained earlier, specimen D22.52 shows only one ferrous doublet, the outer doublet, which has a quadrupole splitting of 2.80 mm $s^{-1}$ (table 4-9) compares favourably with the equivalent doublet of the three doublet fits in table 4-10. A small increase also occurs in the isomer shift of the outer ferrous doublet so that the range of isomer shifts rises from 1.19 - 1.20 mm $s^{-1}$ for the two doublet fits to 1.20 - 1.21 mm $s^{-1}$ for the three doublet fits. Thus, at the low-temperature used in this study (77°K) the outer ferrous doublet in the chlorite structure has shown an increase in its quadrupole splitting from 2.58 - 2.60 mm $s^{-1}$ (table 4-8) at room temperature (298°K) to 2.82 - 2.86 mm $s^{-1}$ at liquid nitrogen temperatures (77°K). The isomer shifts of this doublet also have a dependance on temperature, at room-temperature (298°K) the isomer shifts fall in the range 1.18 - 1.19 mm $s^{-1}$ which expand to 1.20 - 1.21 mm $s^{-1}$ at 77°K.

The new ferrous doublet fitted in these three doublet fits of the spectra from the specimens run at low-temperature show a range of quadrupole splittings from 2.25 - 2.41 mm $s^{-1}$, and a

| Sample | Doublet (1,6) | | | Doublet (2,5) | | | Goodness of fit | | %Total Fe Contribution | | |
|---|---|---|---|---|---|---|---|---|---|---|---|
| | Q.S. ($mm\ s^{-1}$) | I.S. ($mm\ s^{-1}$) | H.W. ($mm\ s^{-1}$) | Q.S. ($mm\ s^{-1}$) | I.S. ($mm\ s^{-1}$) | H.W. ($mm\ s^{-1}$) | $\chi^2$ | degrees of freedom | Doublet (1,6) | Doublet (2,5) | Doublet (3,4) |
| D23.15 | 2.82±0.01 | 1.20±0.01 | 0.36±0.02 | 2.25±0.02 | 1.13±0.02 | 0.20±0.04 | 562.2 | 496 | 49.0 | 12.2 | 38.8 |
| D23.46 | 2.86±0.01 | 1.21±0.01 | 0.33±0.03 | 2.41±0.03 | 1.13±0.03 | 0.44±0.07 | 608.1 | 496 | 37.7 | 25.6 | 36.7 |
| D23.55 | 2.83±0.01 | 1.20±0.01 | 0.28±0.03 | 2.41±0.04 | 1.16±0.04 | 0.54±0.08 | 617.3 | 496 | 29.2 | 28.5 | 42.3 |

TABLE 4-10 Mössbauer parameters for the three doublet computer fits to the spectra of samples D23.15, D23.46 and D23.55. The percentage contribution to the total iron in the samples by each doublet is also shown.

range of isomer shifts from 1.13 - 1.16 mm $s^{-1}$. The first of the spectra, from specimen D23.15, shows the largest differences in the quadrupole splitting, isomer shift and the half widths of the peaks forming the inner ferrous doublet (table 4-10). The half widths are much smaller than those for the other two spectra (0.20 mm $s^{-1}$ as opposed to 0.44 - 0.54 mm $s^{-1}$). For these three doublet computer fits the percentage contribution of each doublet to the total iron concentration has been calculated (table 4-10). In this respect, specimen D23.15 also differs significantly from the two other spectra. The difference occurs in the intensity of the inner ferrous doublet (peaks 2 and 5) the contribution of which to the total iron concentration is only 12.2% as opposed to 25.6 - 28.5% total iron in the other two spectra. Specimen D23.15 lies below specimen D22.62 in the core, and hence it appears that in the upper part of the core, the chlorite firstly contains iron in just the talc-layer and then with depth the iron in the brucite layer increases from 12.2% in specimen D23.15, to 25.6% in specimen D23.46 and to 28.5% in specimen D23.55.

No systemmatic variations occur in the ferric, low-spin ferrous doublet (peaks 3 and 4) as a result of performing a three doublet fit. This doublet contributes 36.7 - 42.3% of the total iron and as mentioned earlier can be assigned to all ferric contributions (from both clays and ferric hydroxides) and to low-spin ferrous iron in pyrite. No further attempt was made to resolve these spectra.

Analysis of the raw data plotted on the spectra in figure 4-10 shown as bars representing the standard deviation of the data points shows that in all of the spectra there is at least an indication of a pair of magnetically ordered peaks occuring

at very high and at very low velocity, best seen in the spectrum of specimen D24.80. These peaks correspond to those identified as peaks 1 and 6 of the spectrum of greigite identified in the room-temperature study of freeze-dried specimens.

## 4-4. Conclusions.

The use of the Mössbauer effect in studying the iron-bearing mineralogy of the Wash sediments has been shown both to be a feasible method for identifying the minerals and also in determining their relative contributions to the total iron content of the sediment. Changes in the concentrations, site distributions and oxidation states of iron in different minerals can thus be monitored.

The iron-bearing minerals have been identified by fitting a series of doublets to one of the spectra (from specimen D16.75) which was of exceptionally good quality. Identification of the iron-bearing minerals and interpretation of the spectra was achieved using a "finger-print" technique in which existing knowledge about the specimens, obtained from optical and scanning electron microscopy together with X-ray diffraction data, was used. Where particular minerals were known to be present, their Mössbauer parameters obtained from the literature were incorporated into the computer fitting program. Comparison of the Mössbauer parameters obtained with the data of Bancroft (1973) was used to interpret the oxidation state, and coordination numbers of the iron species and then these parameters were compared with the published data for probable minerals.

Having followed this system of interpretation for spectrum D16.75 the following minerals were identified as the major iron-bearing minerals; chlorite, pyrite, illite, montmorillonite, iron hydoxides and greigite. This is the first time Mössbauer data for a naturally occuring greigite has been recorded in the room-temperature spectra of a whole sediment sample. There is good agreement for the Mössbauer parameters of this greigite with

those published in the literature for synthetic samples of greigite.

From the intensities of the peaks it was possible to determine the percentage contribution to the total iron by each mineral. Most of the iron, 43%, is to be found occuring as ferric iron in the form of clay minerals and in iron hydroxides. The next major contributor to the iron-bearing mineralogy is chlorite which contributes up to 38% of the total iron, this iron is in the ferrous state and has been found occuring in two octahedral sites which can be best attributed to the two component layers of chlorite, the talc-layer and the brucite-layer. The talc-layer contributes the largest proportion, 30%, of this iron, leaving 8% of the total iron in the sample occuring in the brucite -layer in common with the iron-bearing chlorites described by Goodman and Bain (1978). The remaining 19% of the total iron is in the form of iron sulphides, 8% in the form of greigite and 11% in the form of low-spin ferrous iron in pyrite. As has been described earlier, the estimate of 8% total iron in greigite must be the minimum figure, since calculation was made from peaks 1 and 6 of the six-line spectrum of greigite which are assumed to form together a half of the total iron in greigite. This assumption is not strictly true if the particle size of the greigite is small and there is a resulting superparamagnetic effect.

Analysis of the series of samples from core D1 was made by fitting just two doublets to the spectra. From these fits it was possible to identify an increasing growth of pyrite in the core represented by an increase in the intensity of the inner doublet. From the magnitude of the quadrupole splittings of the outer doublet it was possible to show how the intensity of the inner

ferrous doublet of chlorite, representing the brucite-layer, increased with depth with respect to the ferrous iron in the talc-layer. Not fitted to these spectra but represented in most of the spectra were a pair of magnetically ordered peaks, these correspond to the peaks assigned to greigite in sample D16.75.

The study of samples taken "fresh" from the core and run at low-temperature ($77^{o}K$) confirmed the variation in the location of iron within the chlorite structure, one specimen from the oxidised zone of brown clay at the top of the core showed no iron at all in the inner brucite-layer but with increased depth and reduction of the sediment more ferrous iron is found in the brucite-layer of the chlorite. All Mössbauer parameters calculated for the low-temperature spectra show increases in magnitude due to reduced thermal motion of their electrons.

Because of the better resolution of the spectra run at liquid nitrogen temperatures it was possible to fit the inner ferrous doublet of chlorite to three of the spectra. The resulting minor changes in the Mössbauer parameters of the outer ferrous doublet give consistent new quadrupole splittings and isomer shifts in good agreement to each other and to the parameters obtained for sample D22.62 in which this outer ferrous doublet was the only high-spin ferrous doublet present. Because of the variations in peak positions which occur at low-temperature compared to those obtained at room-temperature and also because of the polymineralic nature of the doublets fitted in these simple fits it is not possible to compare the intensity ratios of the two sets of data. Indeed the observed trends in the ratios, although both showing a dependance on the lithology and oxidation state of the sediment, show opposite trends. This however is

attributed to the differences in temperature dependence between the Mössbauer parameters for different sites. With higher quality data, and more comprehensive computer fitting, or with simpler spectra this problem would be overcome.

The importance of the identification of greigite in the samples, is that it forms a significant proportion of the sediment, 8% of the total iron, and since greigite is strongly ferrimagnetic it may form an important secondary magnetic component to the natural remanence of the sediments. The importance of greigite in carrying a secondary componetent of magnetization in recent sediments has been described by Hedley and Vandievoet (1980). In the Wash sediments studied here, there is no evidence that would suggest that the contribution of a secondary magnetic remanence (a chemical magnetic remanence, CRM) by greigite leads to the modification of the natural magnetic remanence of the sediments (see chapter 7).

## Chapter 5. The Sulphide Mineralogy of the Tidal Flat sediments.

### Introduction.

Superimposed on the depositional variables are diagenetic effects which further modify the chemistry and mineralogy of the sediments and their constituent pore waters. In chapter 4, it is shown how the formation of pyrite in the Wash sediments proceeds with depth, agreeing with the earlier observations of Love (1967).

In this study further observations on the occurence of the sulphide phases, through observations of the colour variations in the cores, petrographic studies and studies using the scanning electron microscope will be presented.

Firstly, however, a review of the current literature on low-temperature sulphide formation will be made. The sulphide minerals considered here are those of low-temperaure authigenic origin and not any high-temperature sulphide minerals which may be present in very minor proportions of the detrital component of the sediments. The study is also restricted to low-temperature iron-sulphide minerals. Initially, it is necessary to discuss the source of both the sulphide and iron ions needed for iron sulphide formation.

Kaplan et al. (1963) showed that biological sulphate reduction is the most important process in the sulphur cycle and that sulphur released from decaying organic matter plays only a small role in the sulphur economy. In the marine environment the sea-water provides an almost infinite source of sulphate for biological reduction to sulphide ions. Elsewhere in some lakes and swamps dissolved sulphate is very low and thus the main source of sulphide ions is from the reduction of decaying organic matter (Berner,

1971). Hutchinson (1957) points out, however, that in fresh-water sediments where there are sulphide minerals forming, the waters are generally high in dissolved sulphate. In the tidal flat sediments of the Wash therefore, the sea-water is the major source of sulphate ions for reduction to sulphide ions.

The bacteria responsible for the biological reduction of the sulphate belong to the genera, Desulphovibrio and Desulphotomaculum (Trudinger, 1976). The species Desulphovibrio desulphuricans is particularly adept at coping with variations in salinity between 0 and 12 per cent (Littlewood and Postgate, 1967), and is primarily responsible for the reduction of sulphate in marine waters (Trudinger, 1976). Rarer species such as Clostridium nigrificans and Desulphovibrio rubentshickii also reduce sulphate (Postgate, 1958).

Iron is transported mainly as ferric oxides in the form of stabilized colloids or adsorbed coatings on detrital particles. Ferric oxides may be stabillized by organic matter (Shapiro, 1964) or by clay minerals (Carroll, 1958). Sand grains also transport adsorbed iron oxide as shown by their rusty colour (Wedepohl, 1969). Since the clay minerals have a greater surface area, they are capable of carrying more iron and thus the finer-grained beds or laminae are often richer in iron, agreeing with the results of the geochemical analysis (chapter 2) and also with the rock magnetic observations (chapter 7). Evans (1965) also observed that the finer-grained sediments in the Wash contained the highest iron concentrations. The adsorbed ferric oxide occurs in the form of goethite and hydrogoethite, in various degrees of hydration.

Formation of the iron sulphides proceeds by reduction of the ferric oxides by hydrogen sulphide produced by bacteria to ferrous iron, which then combines with further hydrogen sulphide. Berner (1964a) has shown experimentally that the initial product of the reaction of hydrogen sulphide with ferric minerals and dissolved ferrous ion under typical sedimentary conditions (20°C, pH 7-9) is an acid soluble poorly crystallised black iron monosulphide, the mineral mackinawite. This initial precipitate is often X-ray amorphous with an approximate formula of FeS (Berner, 1964b). Mössbauer analysis (chapter 4) and X-ray diffraction (chapter 3) have failed to identify conclusively the presence of this phase in the tidal flat sediments studied here. When sufficiently well crystallised to enable X-ray identification, the black sulphides consist of mackinawite (FeS) and/or greigite ($Fe_3S_4$). Both of these phases are thermodynamically unstable with respect to pyrrhotite or pyrite in marine sediments (Berner, 1967).

With increasing depth of burial the black colour caused by the mackinawite and/or greigite often gives way to grey coloured sediment in which the stable sulphide mineral is pyrite. However, the black iron monosulphides may persist, probably due to an original deficiency in the amount of elemental sulphur available to convert them to pyrite (Berner, 1974). This is the case in the Pliestocene deep basin sediments of the Black Sea (Berner, 1974).

Black and grey coloured sediments may alternate as shown also in the sediments of the Black Sea (Berner, 1970). The cause of this Berner (1974) believes, is due to varying rates of deposition, not as he earlier suggested (Berner, 1970) due to

fluctuations in the salinity of the Black Sea. Reversed sequences in which the black reduced material occurs at the top have also been recorded, such as in a long core of sediment from the Black Sea (Shishkinia, 1961), in sediment from Lake Mendota (Murray, 1956), and in the deep part of Lindsley Pond, Connecticut (Doyle, 1968).

In order to understand the mechanism of formation of sedimentary sulphides it is necessary to study their phase equilibria. In marine sediments, Berner (1971) has shown that as the pH is relatively constant (pH 7.0 - 8.0) a disadvantage arises in the use of Eh - pH diagrams. Thus Berner (1971) has made use of equilibrium diagrams in terms of the Eh and the $pS^{2-}$ (where $pS^{2-}$ is the negative logarithm of the activity of the sulphide ion).

Berner (1967) uses a metastable equilibrium diagram using Eh and $pS^{2-}$ to illustrate the stability fields for greigite and mackinawite (figure 5-1). This diagram applies to Recent sediments in which pyrite and pyrrhotite have not yet formed from mackinawite and greigite. A close proximity in the range of naturally measured Eh-$pS^{2-}$ conditions with those of the greigite-mackinawite boundary supports observations that the black iron sulphide of many Recent sediments is a mixture of mackinawite and greigite.

Rickard (1969) has summarised the reactions of ferrous ions, in aqueous solution, with sulphur, sulphide and polysulphide ions in the form of the diagram shown in Figure 5-2. It is noted that almost all of the reactions are irreversible. In the presence of limited oxygen, Sweeney and Kaplan (1973) have shown that macki-

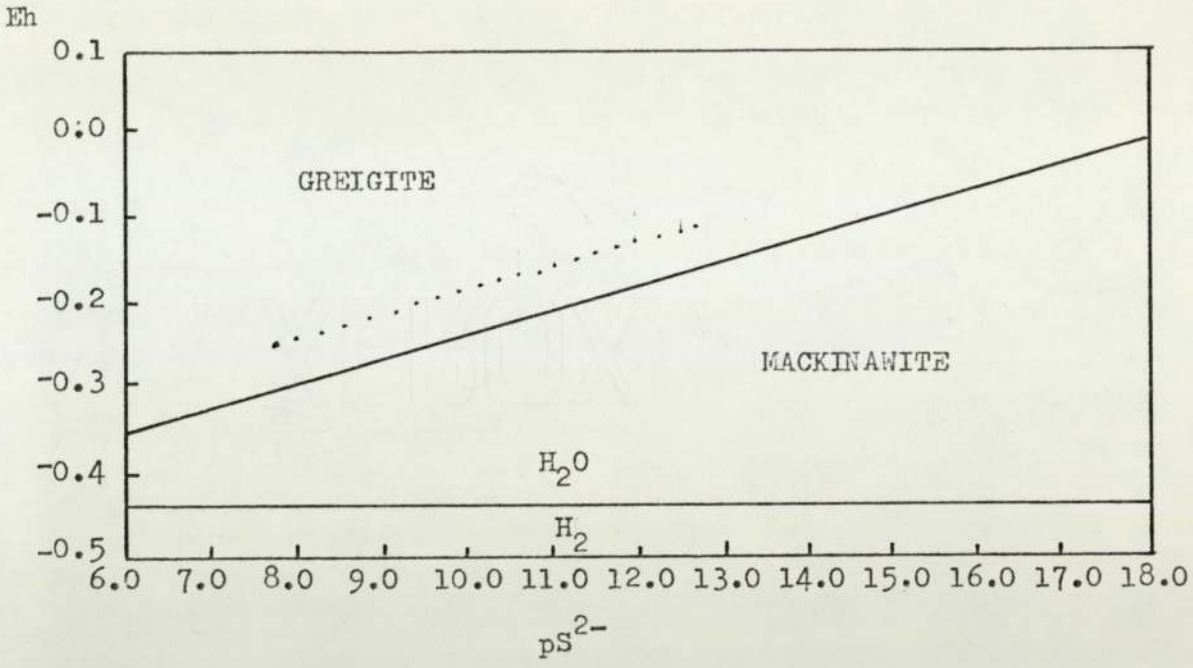


Figure 5-1. Eh - $pS^{2-}$ diagram for mackinawite and greigite at 25°C and 1 atm. total pressure. pH = 7.5 (after Berner, 1967).
(..... range of values for natural marine sediments).

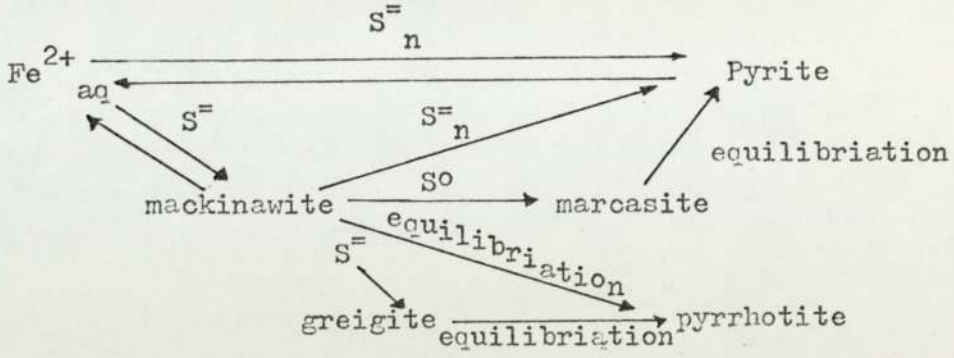


$S^{o}$ = Sulphur

$S^{=}$ = Sulphide

$S^{=}_{n}$ = Polysulphide

Figure 5-2. Reaction relationships of iron sulphides in aqueous solution showing the relationships involving $Fe^{2+}$ and sulphur species (after Rickard, 1969). Note that most of the reactions are irreversible.

nawite can form hexagonal pyrrhotite and that further reaction will produce greigite and finally pyrite. Pyrite may also be formed by the reaction of mackinawite and sulphur (Rickard, 1969 and 1975). Elemental sulphur is not generally abundant in sulphide-rich Recent sediments (Kaplan et al., 1963; Berner, 1964c) and so in order for it to be important as an oxidising agent it must consantly be formed and used up. The formation of elemental sulphur in sulphidic sediments is best accomplished by the oxidation of hydrogen sulphide and mackinawite by dissolved oxygen at the sediment-water interface. This may be aided by the occasional oxidation produced by storm erosion and bioturbation (Wedepohl, 1969).

Berner (1969) has discussed the problem of the transport of iron and sulphur within anaerobic sediments during early diagenesis, and concludes that such migration may result from a variation in the organic content of an otherwise homogeneous sediment. Thus bands of pyrite may then form by interdiffusion of dissolved iron and sulphide or by an upward diffusion of ferrous ions into an oxygenated sediment-water interface.

The sulphide mineralogy of the tidal flat sediments of the Wash have been subject to only one other study (known to the author), that of Love (1967) In the Wash, the pale brown or brownish-red oxidised zone was found to vary from a few centimetres to one metre in thickness, below this a reduced zone of intense black colouration altering at a depth of two metres to a grey bisulphidic or pyritic zone was encountered (Love, 1967). Love (1967) also discovered that the thickness of the upper oxidised zone was closely related to the depth of fluctuation of the tidal water table.

5-1. Colour zonation of the sediments.

The three zones of sulphide formation, represented by three differently coloured zones of sediment, recognised by Love (1967) have also been encountered in this study. The colour zonation is best illustrated by reference to plate 25 ( see also plate 1, chapter 2), which shows the trench from which core W1 was taken. The three zones shown (plate 25) comprise, the upper oxidized zone consisting of 15 cms of reddish-brown fine-grained sand, below this the sediment is black or dark-grey in colour, representing the monosulphidic zone. Finally, at the base below a depth of 40 cms the sediments grade into a medium-grey coloured sequence of fine sands representing the the bisulphidic zone.

Two features which suggest that the formation of pyrite from the iron monosulphides is a progressive process are; the gradual gradation from black to medium-grey coloured sediment, and secondly, the occurence of patches of bisulphidic sediment (black) in the monosulphidic zone and vice versa. In contrast the boundary between the oxidized zone and the monosulphidic zone has a sharp contact which often picks out a particular bedding plane, and follows compactional and bioturbational structures in the sediments (plate 25).

Not all of the sequences analysed in this study show the simple three colour zonation. In the cores from Freiston Shore it was found that several thin (1-2 cm ) laminations of oxidized sediment occured within the upper 20cm of the mono-sulphidic zone. These are probably caused by oxygenated waters moving along, coarser grained, more porous sediments during tidal movements. Similarly, oxygenated waters are often introduced

Plate 25. Wrangle Flats, showing the location of the trench from which core W1 was recovered. Note the small current ripples on the sediment surface. The colour zonation of the sediment is also illustrated. Zone 1, is the reddish-brown fine-grained sand belonging to the oxidized zone. Zone 2, is the black or dark-grey sediment of the monsulphidic zone. Zone 3, consists of a sequence of grey-coloured sediments belonging to the bisulphidic zone.

along fractures in the sediment, caused by slumping, which again leads to oxidation of the sediments along the margins of the fracture. In this situation, a thin crust (upto 2mm) of iron oxides is formed (plate 26 and plate 27). Plate 26 shows the occurence of the iron oxides at the margin of a fracture in core 2 from Freiston Shore. The oxidized zone, which is about 1000um thick, is made up of an iron oxide cemented sediment (plate 27) in which the iron oxide has stained all the matrix material a yellowish-brown colour. The iron oxide has poor crystallinity and appears amorphous in transmitted light, no successful X-ray diffraction pattern was achieved from the sample, so further identification is not possible here. A similar occurence of this oxide phase is found as a cement to the sediment around worm burrows. The iron oxide clearly results from the oxidation of the unstable iron sulphide phases in the sediment.

Plate 26. Iron oxide (brown) cement resulting from oxidation of sulphide phases in the monosulphidic zone, along the side of a shear plane in the sediment. Plane polarized light.

Plate 27. Close-up of the iron oxide cement showing its amorphous-poorly crystalline nature. Plane polarized light.

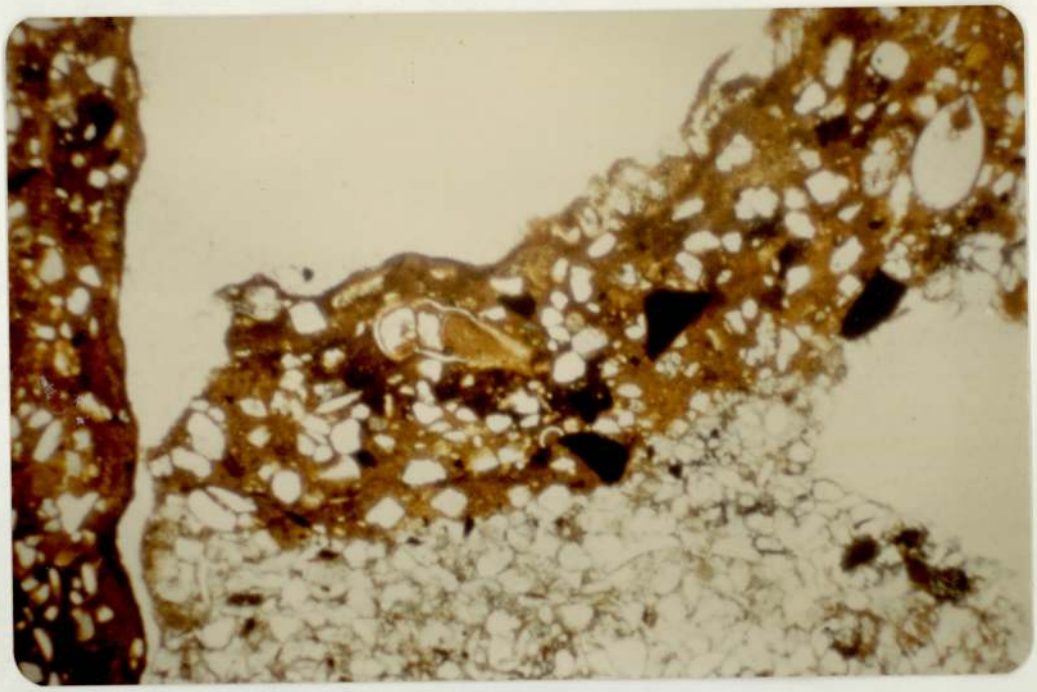

Plate 26.

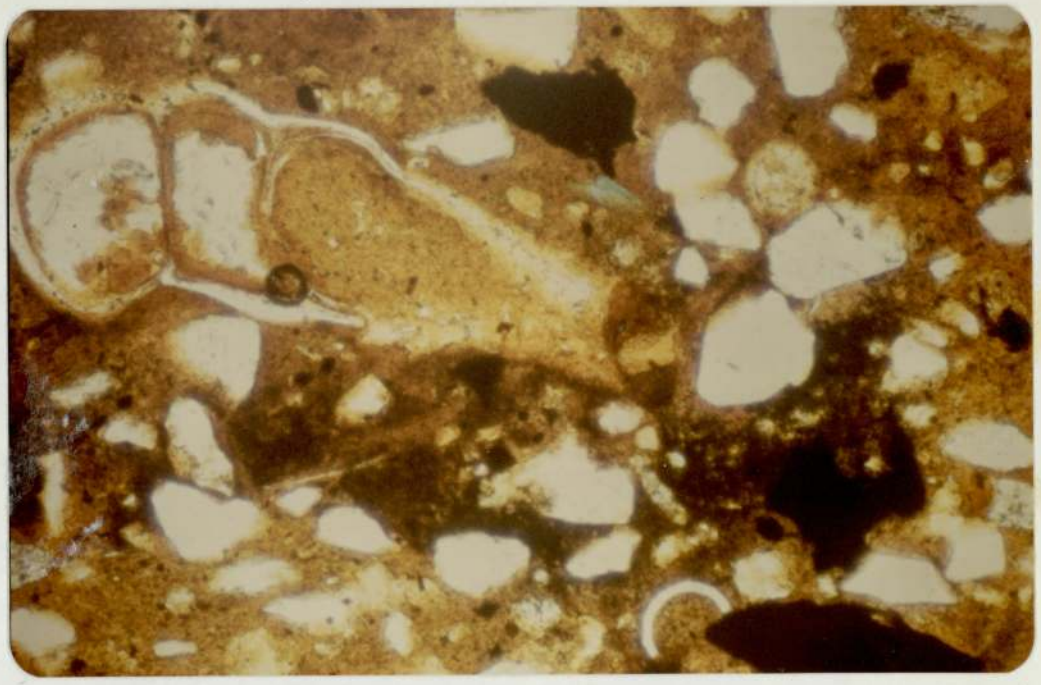

Plate 27.

## 5-2. Occurence of the Sulphide Minerals.

Mention has already been made of the occurence of the iron sulphide minerals in two previous chapters (chapter 2 and chapter 4) using observations from transmitted light microscopy and Mössbauer spectroscopy. To recap on the conclusions of those studies, it was found that pyrite occured primarily in the form of circular grains, inferred to be pyrite framboids, and that these were commonly dispersed throughout the sediment or concentrated in organic-rich areas of the sediment. Typically the pyrite framboids are found infilling foraminiferal tests, they may also be found in association with ferroan calcite.

The Mössbauer study of samples from the Delft cores permitted the identification of the low-spin ferrous iron in pyrite and also was able to show the gradual increase in pyrite abundance with increased depth in the cores. A lithological control on the formation of pyrite in the Mössbauer study was also identified. Greigite also was identified in most of the samples analysed using Mössbauer spectroscopy.

In this study further evidence on the occurence of the iron-sulphides will be presented. Initially, samples from the monosulphidic and bisulphidic zones were analysed using both transmitted light and reflected light microscopy using oil immersion.

Analysis of the samples from the monosulphidic zone revealed that the samples contain a large amount of disseminated black pigment, with low reflectivity, which only rarely shows sufficient crystallinity to form very small (less than 1μm) black specks of indeterminite morphology. It is probable that the amorphous material is the iron monosulphide, mackinawite and the "black specks" may be the iron sulphide, greigite.

Pyrite framboids are identified throughout the bisulphidic zone and are also present within the monosulphidic zone (black coloured sediment). The size distribution of the pyrite framboids has been studied using specimens of air-dried sediment, from the bisulphidic zone, mounted in glycerine. No significant variations between samples were found and the framboids were found to range in size from 4-75 μm with a mean grain-size of 20 um (figure 5-3).Their distribution shows an approximately lognormal unimodal size distribution which is positively skewed. The mean grain-size is larger than that quoted by Love (1967), although the grain-size range is similar. The data of Love (1967) suggests a mean grain-size of only 5 or 6 μm. This may be caused by an instrumental error, and/or a failure to recognise specimens of a particular size range, however, the data of Love (1967) is lacking in records of pyrite framboids over 10 μm in diameter of which many are found in the samples studied in this work.

Another iron-bearing phase present in the samples is a red ferric hydroxide, this mineral is also formed when samples of the monosulphidic zone are allowed to oxidize, in air.

Further analysis of the pyrite framboids has been made using the scanning eletron microscope (SEM) (with edax, energy dispersive X-ray analysis). The samples used in this study are from a heavy mineral concentrate of the sediment from core-section D13. Most of the pyrite framboids encountered are freely dispersed in the sediment (Plate 28) and consist of spherical grains with a mean diameter of approximately 10 μm. The individual pyrite framboids are made up of microcrysts which are small ( 0.75 μm) cubic crystals of pyrite packed in a close packed hexagonal arrangement (Plates 29 and 30). However, some of the microcrysts occur loose

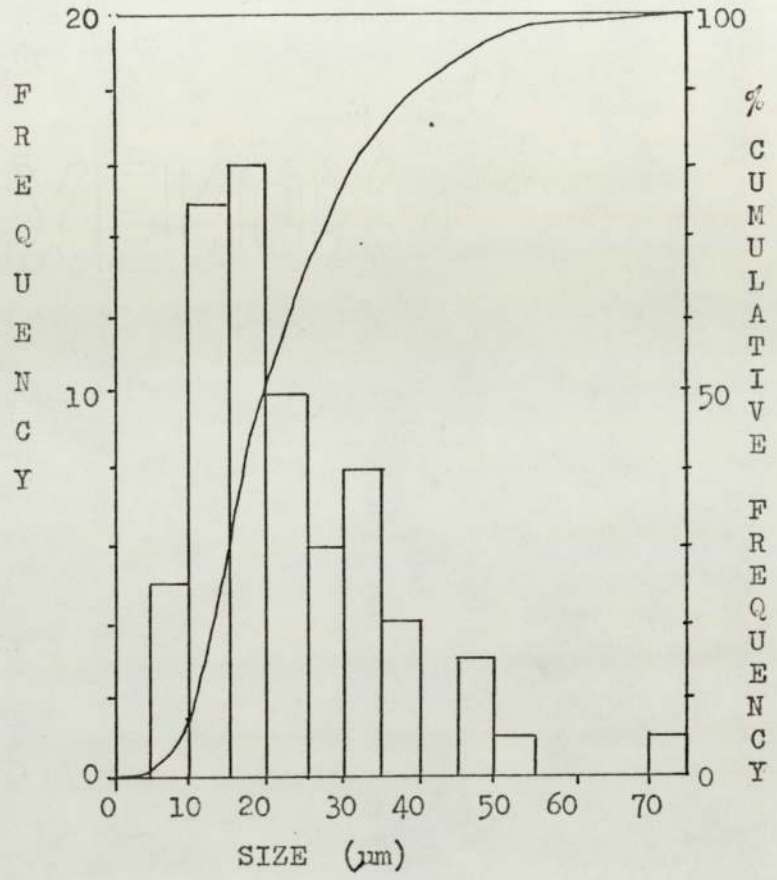


Figure 5-3. Grain-size distribution of a sample of pyrite framboids, concentrated using a heavy mineral concetration. The graph also shows the cumulative frequency (percentage) distribution of the sample.

Plate 28. SEM photomicrograph showing the occurence of scattered pyrite framboids between quartz and clay mineral grains.

Plate 29. SEM photomicrograph showing the morphology of one of the pyrite framboids. Note the close packed hexagonal arrangement of the microcrysts.

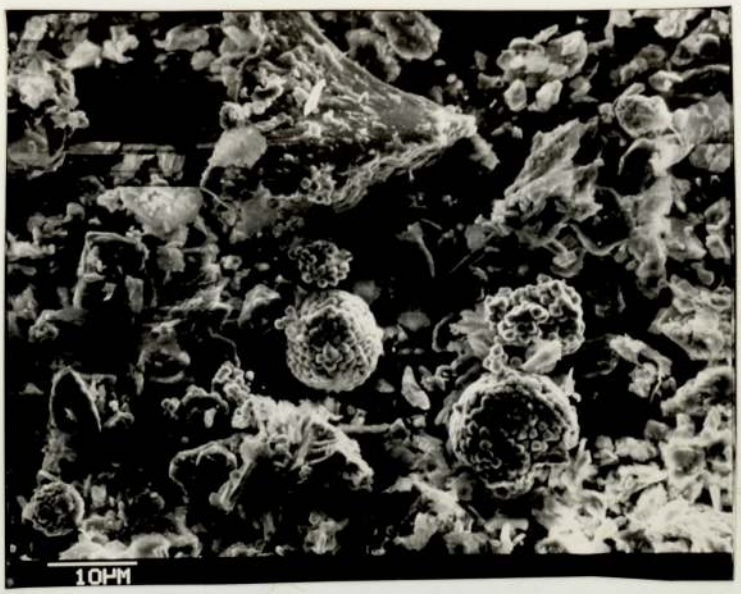


Plate 28.


Plate 29.

Plate 30. SEM photomicrograph showing two pyrite framboids. The larger framboid shows typical close packing of the microcrysts whilst the small framboid above it shows an irregular arrangement of its microcrysts. At the lower left of the photomicrograph loose pyrite microcrysts can be seen.

Plate 31. SEM photomicrograph showing a non-spherical pyrite framboid. Note also that the individual microcrysts are not cubic and have flattened faces on the external surface of the framboid.

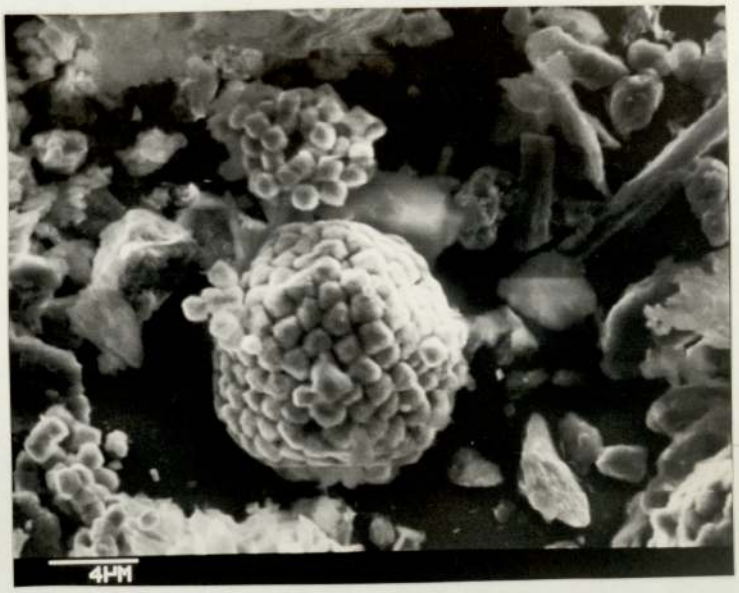


Plate 30.

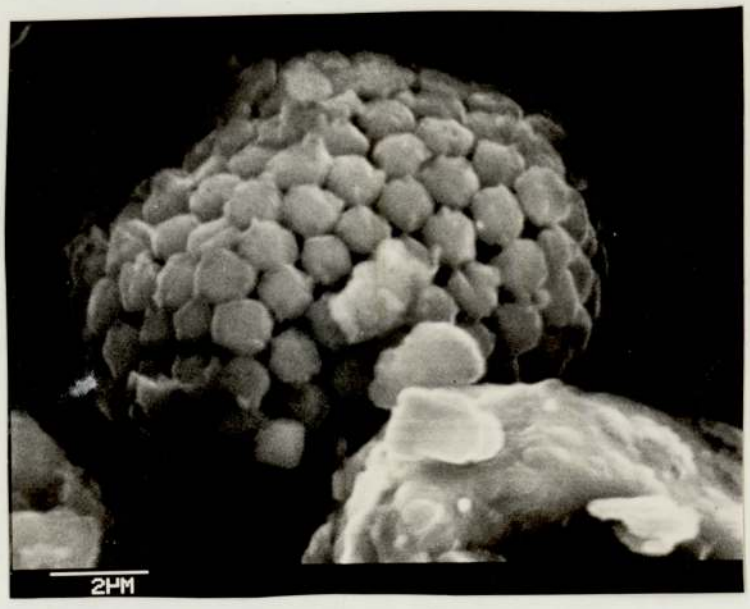


Plate 31.

or in irregular clusters (Plate 30). It is possible that the free of pyrite are caused in part by by the fragmentation of original pyrite framboids during preparation of the samples. Some of the pyrite framboids exibit features which suggest that they were formed by pseudomorphing some pre-existing body (Plate 31). Such framboids are not completely spherical, and also show flattening of the outer microcrysts, also suggesting that they are formed against some physical boundary. In the example shown in Plate 31, the microcrysts, although still exhibiting close hexagonal packing, are no longer cubic, possibly indicating the final stages of the infilling of whatever the pyrite is pseudomorphing. One rare example of a fairly amorphous, but perfectly spherical, pyrite framboid was found. The framboid with a diameter of 18 μm (Plate 32) contains an irregular arrangement of very fine microcrysts (<0.25μm) which exhibit no regular packing arrangement. It is probable that such grains represent the earliest stages in the precipitation of pyrite framboids.

Finally, many of the shell fragments analysed using the SEM were found to either have pyrite framboids attached to their outer surfaces (Plate 33) or were found to contain small framboids (upto 6 μm) within pores at the edges of the shell material (Plate 34). Analysis of all the pyrite framboids using the Edax facility fitted to the SEM shows that they are composed of pure $FeS_2$ with no other cations identified in their structure (figure 5-4).

Plate 32. SEM photomicrograph showing a completely spherical pyrite framboid which contains an irregular arrangement of very fine microcrysts (<0.25um)

Plate 33. SEM photomicrograph showing two pyrite framboids on the surface of a calcite grain.

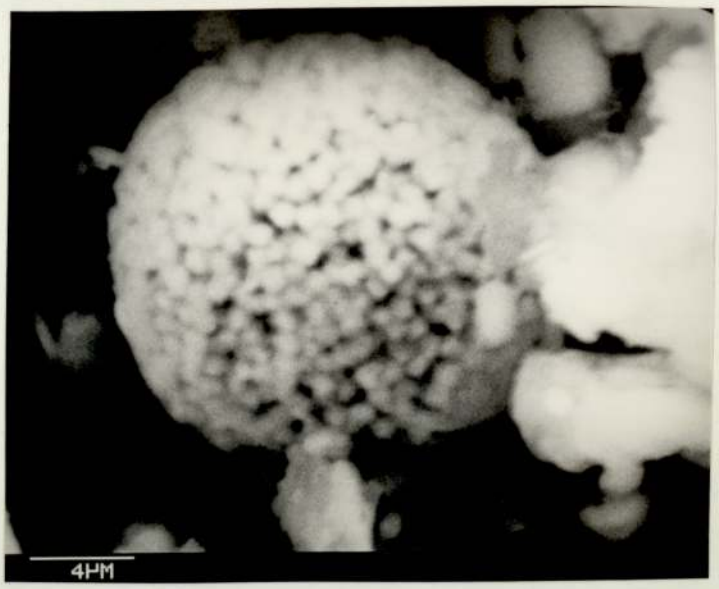


Plate 32.


Plate 33

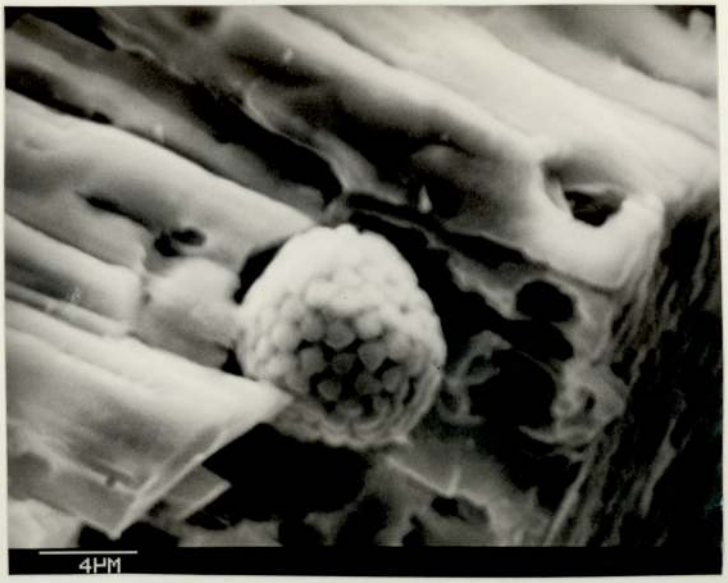


Plate 34. SEM photomicrograph showing the occurence of a pyrite framboid which has formed in the pore near to the surface of a shell fragment.

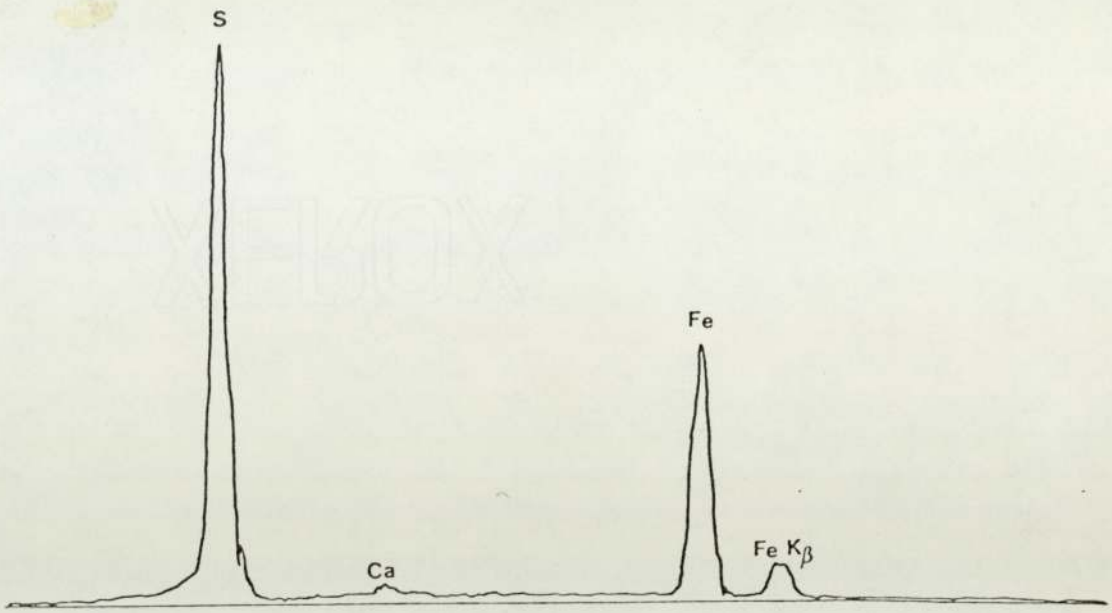


Figure 5-4. Edax spectrum of a pyrite framboid, showing it to be composed entirely of iron and sulphur. The minor calcium peak is from an underlying shell fragment.

Chapter 6.

Palaeomagnetism.

Introduction.

As explained earlier, the objective of this study is principally to ascertain the feasibility of using tidal flat sediments in palaeomagnetic studies and to gain an idea of their suitability for studying the secular variation of the Earth's magnetic field. Only one previous study of the palaeomagnetic properties of Recent tidal flat sediments is known to the the author, which is a study of the palaeomagnetism of the Recent tidal flat sediments of San Francisco Bay, California by Graham (1974). In that study Graham (1974) shows that the tidal flat sediments do record a stable natural magnetic remanence (NRM), which Graham (1974) identifies as being of post-depositional origin. This post-depositional magnetic remanence (PDRM), Graham (1974) suggests is acquired through the churning activity of the wet sediment by organisms. The collection of the samples used in Grahams work is in the form of oriented blocks of sediment cut from the sediment surface and from which sub-samples are taken in plastic boxes with a volume of 6 $cm^3$. No cores of sediment were obtained in the study by Graham (1974) and it was therefore not possible to obtain secular variation records from the data gathered. However, the possibility of using reversal stratigraphy in studies of ancient esturine deposits and perhaps more importantly the possibility of studying the secular variations of the Earth's magnetic field as recorded in modern times by tidal flat sediments are mentioned by Graham (1974). Graham (1974) also points out that such studies will need to consider the "lag", if any, between the time of deposition and

the time when the post-depositional remanent magnetization is "frozen" in. Graham (1974) speculates that this fixation of the PDRM takes place only beneath the bioturbated layer of sediment near to the sediment surface. If this is the case then the depth of this layer would be dependant on sedimentation rates and also on the types of organisms living within it. Using known sedimentation rates of roughly 0.3 - 1.3 metres per 1,000 years, and knowing that the bioturbated layer is only 1 metre thick, Graham (1974) calculates that the lag time between deposition and permanent fixation of the NRM in the tidal flat sediments of San Francisco Bay, is of the order of several thousand years.

## 6-1. Palaeomagnetic Results from the One-Metre Cores.

### 6-1-1. Collection and sampling.

Collection of the cores used in this study was made at two locations using one-metre long PVC tubes. The location of the coring sites, at Freiston Shore (Grid reference TF 408421) and at Wrangle Flats (Grid reference TF 452487) are shown in figure 6-1. A total of five cores were collected with four from the higher mud flat sub-environment at Freiston Shore and the final one from the higher mud flat at Wrangle Flats. The cores from Freiston Shore were collected close to a creek so that it was possible to obtain a vertical sequence through the higher mud flat sub-environment depicted by the diagrammatic representation of the cores in figure 6-2. Because the collection of the cores was made close to a creek, precautions were taken to sample in areas which were free from slump structures associated with the proximity of the creek, and also to avoid areas which had been subjected to reworking by the migrating creek. The local ity of the cores coincides closely with the area studied by Evans (1965) and where the sediments of the higher mud flat are found to be relatively free of bioturbation, as evidenced by the uniformly laminated clays and silts from which the sediments are formed. The lack of major bioturbation is also seen in thin sections of the sediments (chapter 2).

The core taken from Wrangle Flats was used because the sediments at Wrangle are generally coarser grain-sized than those at Freiston Shore and it was thus hoped to show if variations in grain-size would be critical in determining the quality of the palaeomagnetic results obtained.

The one-metre PVC core tubes, which were used to sample the

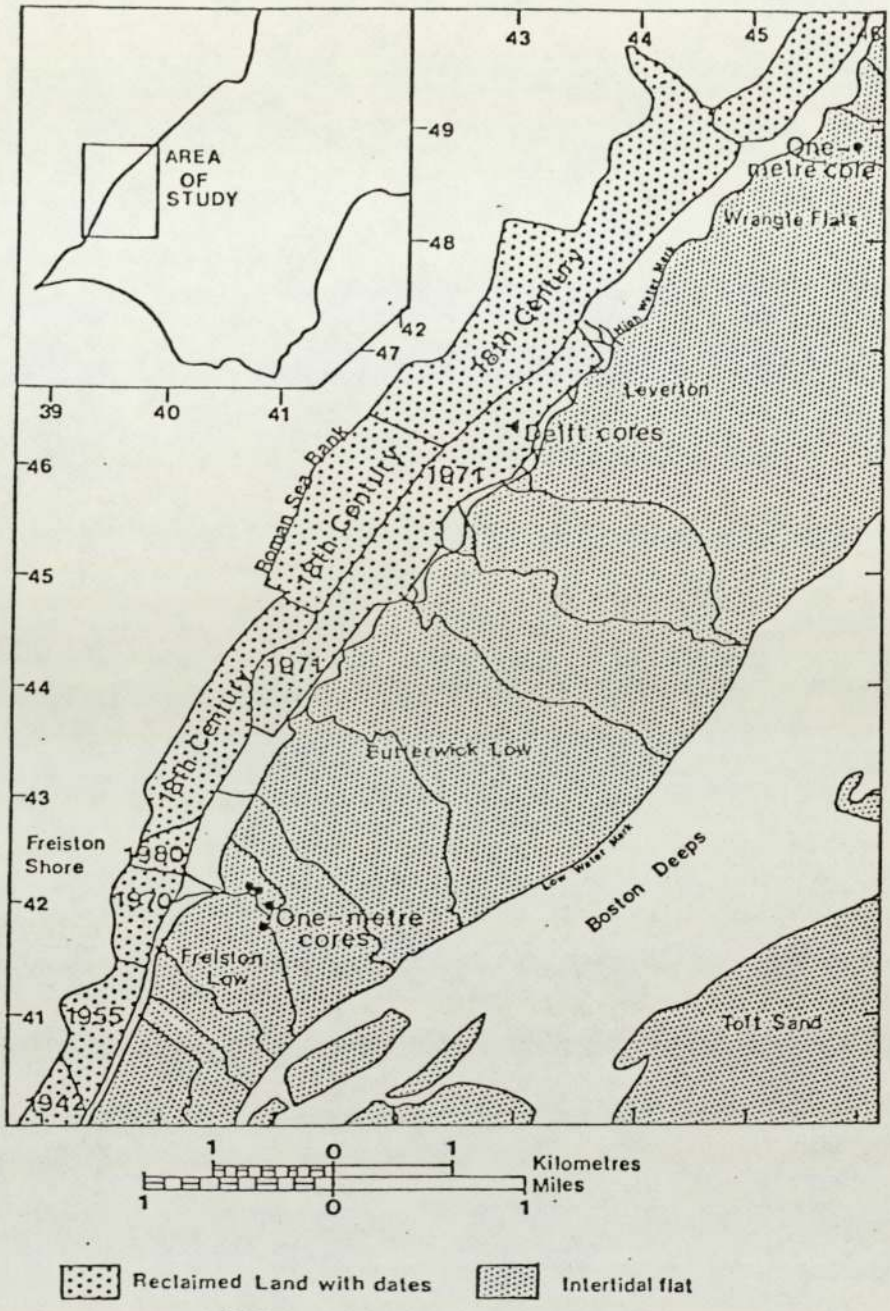


Figure 6-1. Location map showing the position of the one-metre and Delft cores.

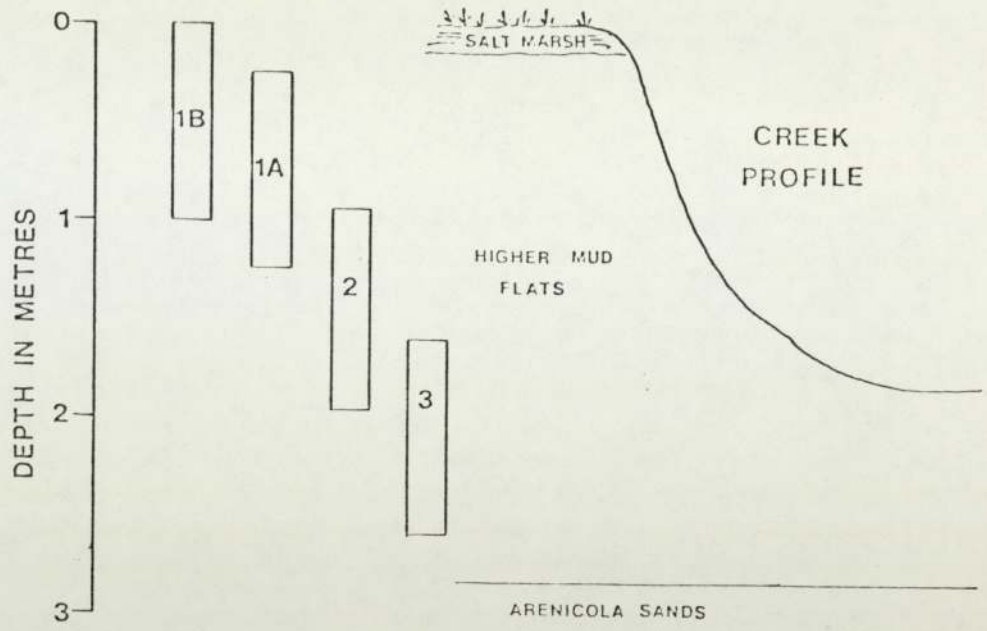


Figure 6-2. Diagrammatic representation of the positions of the one-metre cores in relation to the sub-environments of deposition at Freiston Shore.

sediments, were hammered into the sediments, then oriented with respect to true north and then removed, by digging a trench, and sealed with rubber bungs. The resulting cores which have a diameter of 100 mm were found on opening and slicing to be free from disturbance caused by the method of sampling except for a very minor 2mm thick film around the edge of the core (see chapter 2). This feature is particularly well dislayed by the preservation of the fine laminations common to many of the sediments. From these observations and the cohesive nature of the sediments it is thought unlikely that any remagnetization of the sediments can have taken place as a result of the coring process, or as a result of the subsequent transportation of the cores to the laboratory.

Palaeomagnetic measurements were made as soon as possible after recovery of the cores, in order to minimize physical and chemical changes in the cores, such as dehydration and oxidation which might have lead to a laboratory induced modification to the remanent magnetization. Sub-sampling of the one-metre cores from Freiston Shore was made using plastic cylinders (internal dimensions; 22 mm diameter, and 23 mm in length) which meant that between 22 and 38 samples could be collected from each one-metre core. This was achieved by pushing the plastic cylinders into the freshly extruded core, after first cutting a flat surface at right angles to the fiducial line (true north), so that the specimens could be accurately oriented. After removal from the core the top and bottom of each sample was sealed using plastic discs. Because of the relatively small number of samples obtained using the plastic cylinders, the core from Wrangle Flats, core W1 was therefore, subsamples using plastic boxes (internal dimensions 19 x 19 x 14 mm). With the plastic boxes it was possible

to obtain a total of 47 sub-samples per metre. It was also found that the plastic boxes are easier to orient with respect to the fiducial line. Thus in the studies of the palaeomagnetism of the sediment samples from the Delft cores, the plastic boxes were used for sampling.

6-1-2. Measurement of the Natural Remanent Magnetization (NRM).

The natural remanent magnetization of the samples was measured immediately after their removal from the cores using a Digico Balanced Fluxgate Rock Magnetometer (Digico Computers Limited). The first results obtained from core 1A were made using the magnetometer at the University of Newcastle upon Tyne, all the other measurements of NRM were made with the newly acquired magnetometer at the University of Aston.

The measurement of the NRM is undertaken by spinning the specimens in each of six orientations for a given number of revolutions, dictated by the intensity of magnetization of the sample. In this study the range of observed magnetic intensities allowed the use of $2^5$ spins (32 spins in each orientation).

The magnetization observed in a specimen after collection is defined as its natural remanent magnetization (NRM). This NRM may be composed of the primary magnetization together with any later secondary magnetizations. In detrital sediments, such as the tidal flat sediments studied here, the dominant primary magnetization process is detrital remanent magnetization (DRM). A DRM originates when magnetic grains become oriented with repect to the Earth's magnetic field as they are deposited through a column of water. Secondary magnetizations which may modify this primary magnetization include chemical remanent magnetization (CRM), a process which usually involves the formation of iron oxides at

low-temperatures, but may also involve the formation of magnetic iron sulphide minerals such as pyrrhotite and greigite. Re-alignment of magnetic grains after deposition in responce to a changing magnetic field, or improved alignment to a contemporary magnetic field leads to the formation of another form of secondary magnetization, a post-depositional remanent magnetization (PDRM). Thus the acquisition of secondary magnetizations to the primary magnetization leads to the modification of the observed remanent magnetization and it is the resultant of these processes which is termed the natural remanent magnetization (NRM).

The rock magnetometer permits the measurement of both the intensity of this NRM and also its direction. The intensity of magnetization is measured in microgauss (μG) units which are equivalent to emu/cc x $10^{-6}$. Since the intensity of magnetization of the sample as measured by the magnetometer is dependant on the volume of the sample corrections must be applied if the specimen differs from the ideal sample size, which for the instruments used here is a cylinder with a diameter of 2.54 cm and a long axis of 2.54 cm. Since the plastic cylinders used here are of the ideal size no corrections were required. However, in the study using the plastic microboxes a correction for volume had to be applied. Since the plastic microboxes are used more fully in the study of the Delft core, the method of correcting for the changed volume is described in detail in section 6-2-2.

The direction of magnetization obtained from the samples is expressed as a resultant vector, in terms of a horizontal component, the declination, angle and a vertical component, the inclination, angle. These terms are expressed in degrees, and are computed directly from the measured X, Y, and Z components of magnet-

ization using the standard Digico program, and no corrections are applied for changes in the volume of the sample.

6-1-3. Results and Interpretation of the Natural Remanence.

The measurements of the directions of the NRM for the cores from Freiston Shore are illustrated in figure 6-3. The tie lines indicate the approximate vertical relationship between the cores. In figure 6-3 both the raw NRM directions (obtained directly from the magnetometer) and a smoothed direction along the core are shown. The smoothed line represents a three-term running mean of the raw data. The first feature to notice about the declination measurements is the strong discrepancy between the present Earth's field and that recorded by the sediments at the top of the core sequence, in cores 1A and 1B. Since the cores were oriented with respect to true north in the field this apparent error in the declination must be real. Discounting the measurements at the very top of the cores (1A and 1B) as being possibly modified by the activity of burrowing organisms and plant roots, it can be seen that the maximum discrepancy in the declination is of the order of $60^{\circ}$ to the east.

At the base of core 1B and at a depth of approximately 65 cm in core 1A there is a feature where the declination shows a swing to a declination of approximately $10^{\circ}$ east which provides a good tie-line or marker horizon between the two cores. Since this feature occurs so early in the record and since it only occurs over the interval represented by three or four samples it is unlikely to represent a real excursion of the Earth's magnetic field. The most likely cause of this initial discrepancy in the declination values is that they represent a bedding error related to alignment of magnetic particles in response to a current flow

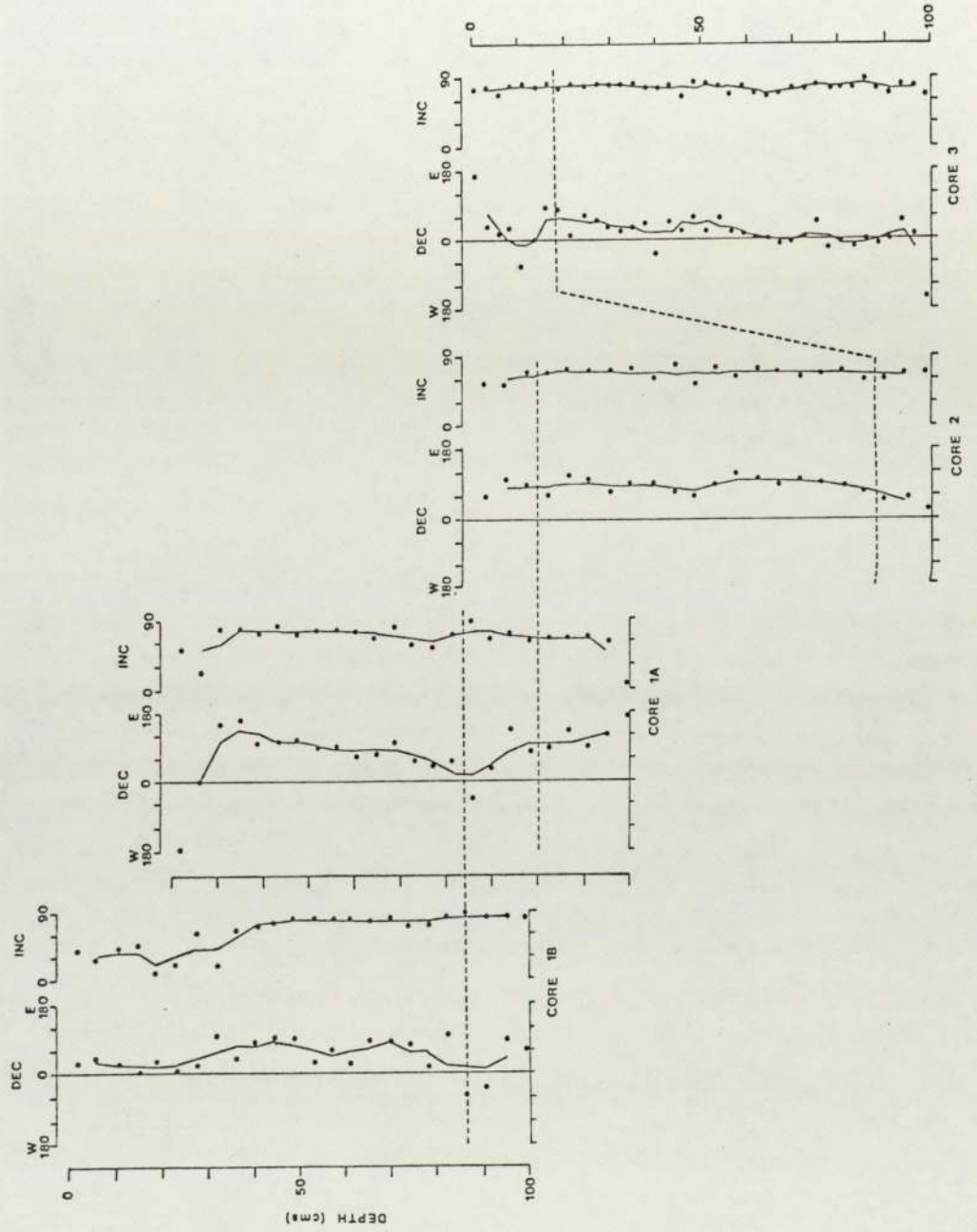


Figure 6-3. Declination and inclination measurements for the one-metre cores from Freiston Shore. The results have been smoothed using a three-term running mean (solid line). Tie lines indicate correlation between the cores.

direction during deposition. This would imply that at least in the upper part of the sequence at Freiston Shore the dominant contribution to the NRM is a detrital remanent magnetization (DRM).

With increasing depth within the sequence, in cores 2 and 3, the initial large declination error is progressively corrected, until at the base of core 3 the declination has reached values typical of the Earth's present magnetic field. There is an indication that this is the maximum of this gradual westward swing in the declination, Since it was not possible to continue sampling and to obtain a more complete sequence using this method, it cannot therefore be definitely identified as the apex of a westward trend in the declination.

If it is assumed that the base of core 3 lies at least near to the maxima of this westward drift, and that the initial bedding error of the detrital remenent magnetization is a feature common throughout the sequence then it is likely that this feature coincides with the most recent of the westward drifts recorded by the Earth's magnetic field. This most recent feature has been reported in the records made of the geomagnetic field in London which are summarized in the data of Bauer (1897) and has been dated as occuring at 1820 AD (160BP). Figure 6-4 shows an illustration of this data. Another explanation is that the eastward declination error is carried by an unstable DRM and the correction we see with increased depth is due to a progressive correction brought about by the acquisition of a PDRM. If this is the true interpretation then it is apparent that the fixation of PDRM does not take place until at least the base of core 3. In order to help resolve this problem it is necessary to look at the

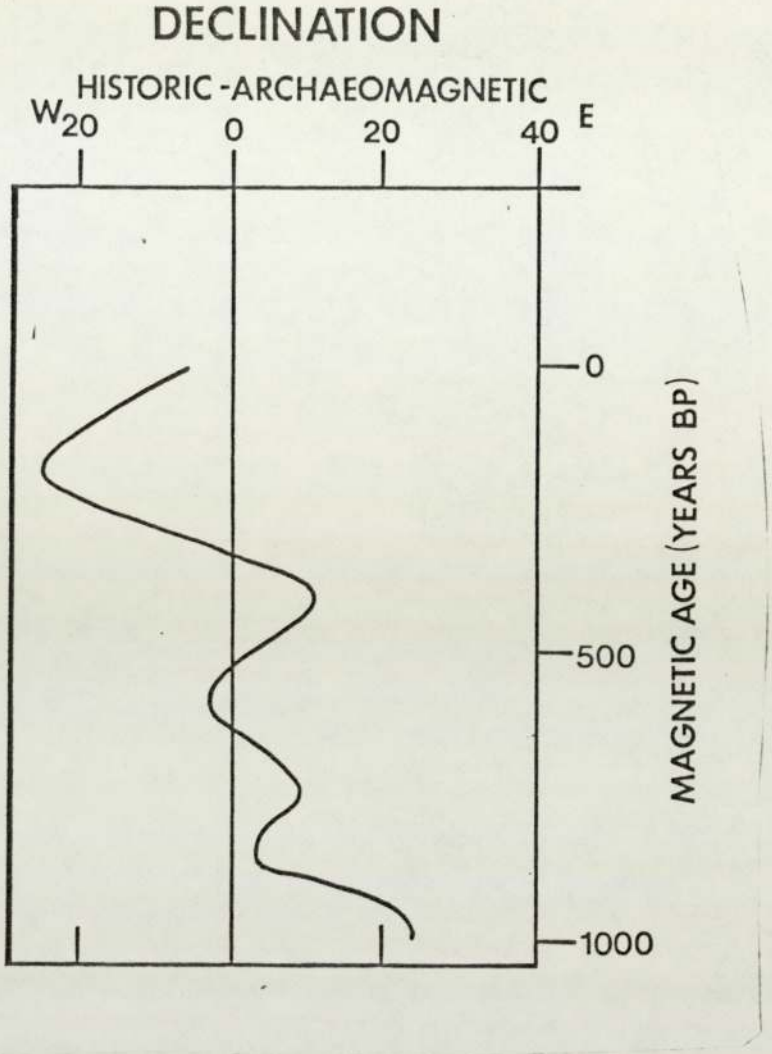


Figure 6-4. The historic - archaeomagnetic secular variation curve for London, (after Bauer, 1897 and Aitken, 1970).

behaviour of the vertical component of magnetization, the inclination.

Measurements of the inclination of the magnetic vector, recorded by the NRM of the samples are shown in figure 6-3. Again at the tops of cores 1B and 1A the values of inclination show large errors which are not corrected until depths of approximately 40 cm in core 1B and 15 cm in core 1A are reached. It is useful to note here that the present-day inclination of the Earth's magnetic field at Freiston Shore may be calculated using the following relationship:

$$I_c = \arctan(2 \tan L)$$

where $I_c$ is the inclination of the present Earth's field.

and L is the geographic latitude at the site.

This model assumes that the Earth's field conforms to an axial dipole field. The resulting value therefore, for the inclination at Freiston Shore (lattitude 52° 57') is 69.3°. After achieving values typical of the present Earth's field in cores 1A and 1B the inclination values remain relatively constant throughout the length of the sequence represented in cores 2 and 3. It thus appears that the inclination, at least, is fixed early in the sequence after a fairly rapid fixation of a PDRM. This fixation of PDRM occurs after an initial depositional error is progressively corrected, as shown by the steepening inclination with increased depth. Initially, this inclination error is up to 55°.

Measurements of the intensity of magnetization are shown in figure 6-5, also plotted against depth. Again a simple three-point running mean has been used to smooth the data. The values

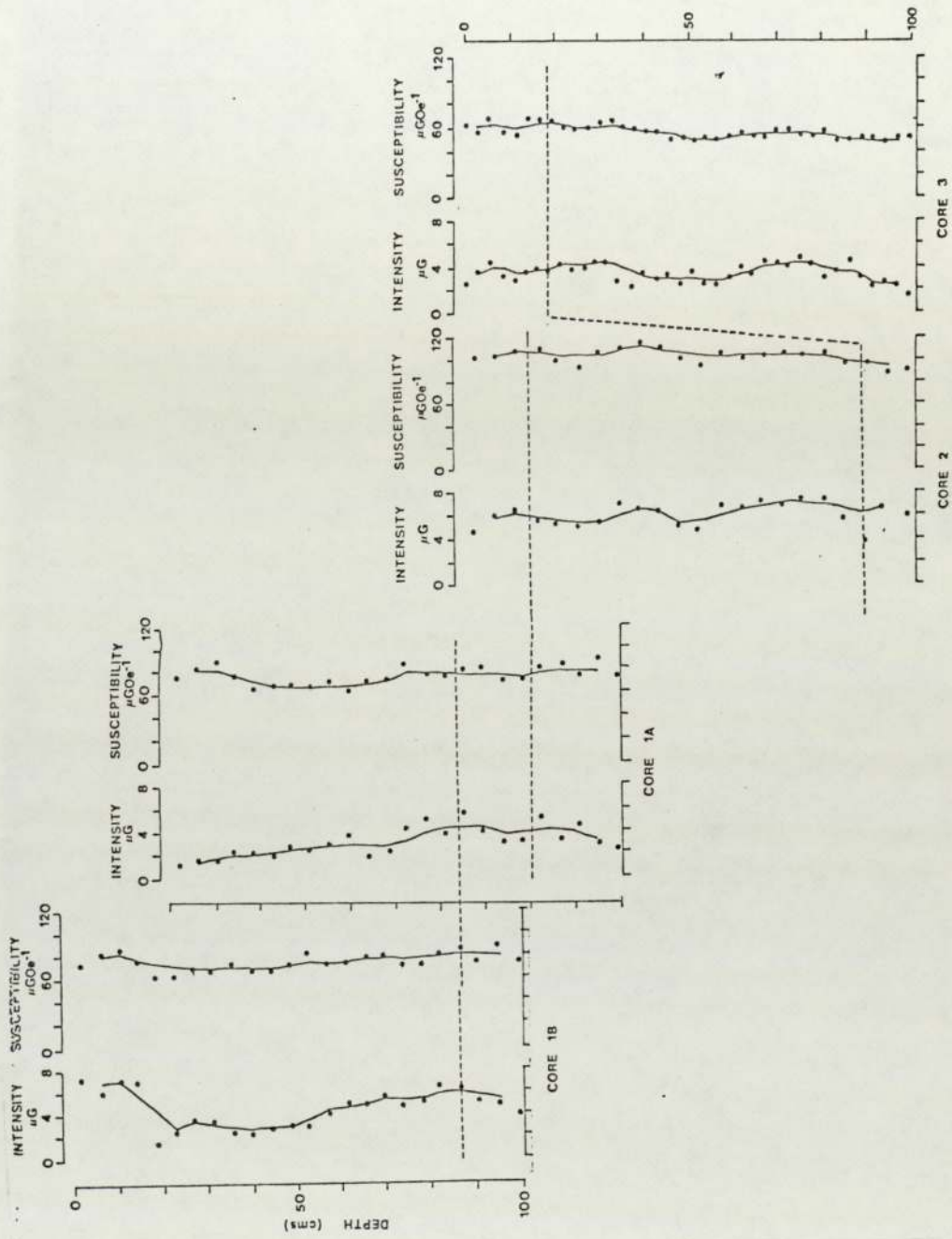


Figure 6-5. Intensity of magnetization and magnetic susceptibility logs for the one-metre cores from Freiston Shore. The results have been smoothed using a three-term running mean (solid line). Tie lines indicate correlation between the cores.

of intensity range from 1.2 to 7.6 μG. At the top of the sequence in Core 1B, initially high values of intensity are found in the upper 15 cms of sediment, these are associated with clay-rich sediments which mark the transition between the salt marsh and higher mud flat sub-environments. However, the overall trend below this level in cores 1B and 1A is for an initial increase in magnetic intensity from about 2μG to about 4μG. This progressive increase can be interpreted as being due to improved alignment of magnetic grains with depth. Such an improvement is a good indication that a post-depositional remanence is being acquired. Below cores 1B and 1A, in core 2, the intensity measurements show no further improvement indicating that no further alignment of magnetic grains is taking place. In core 3, the intensity of magnetization is generally lower than in core 2. The reason for this is not clear, but it may be due to the slightly increased grain-size with depth, or due to the higher water saturations at this depth. Such higher water saturations could allow some release of magnetic particles into new alignments. However, as will be shown later, susceptibility measurements indicate a lower concentration of magnetic minerals indicating that the former alternative is the most likely.

Also shown in figure 6-5 are the measurements of magnetic susceptibility made on each specimen after measurement of its NRM. Measurements of the magnetic susceptibility are an indication of the amount of "magnetic" material present in the samples. The measurements are recorded in units of microgauss per Oersted ($\mu G Oe^{-1}$). The measurements of magnetic susceptibility have been made using a Highmoor Variable Temperature Magnetic Susceptibility Bridge (Highmoor Electronics Limited) at room-temperature. The measure-

ments were calibrated using two ferrous sulphate ($Fe_3SO_4 \cdot 7H_2O$) standards of the same dimensions as the samples (one contained in a plastic box and one in a plastic cylinder). The standard susceptibilities are 83.66 $\mu GOe^{-1}$ for the plastic box and 125.67 $\mu GOe^{-1}$ for the cylindrical standard.

The results show, firstly, that there is little overall variation in the magnetic susceptibility throughout the sequence except for very low values in core 3. The low values in core 3 mentioned earlier are thought to be due to the changing sedimentation regime associated with the proximity of the Arenicola sands. Another minor feature of the magnetic susceptibility measurements is the slight increase in susceptibility at the top of core 1B corresponding to high intensity measurements recorded earlier, supporting the theory that the nearby salt marsh sediments contain more "magnetic" material.

To conclude, it can be shown that the higher mud flat sediments of the tidal flats at Freiston Shore do record a NRM. From studies of the behaviour of these measurements with depth it is apparent that initially the sediments are deposited with a large declination and inclination error. This bedding error is progressively corrected until the remenance becomes fixed, through the acquisition of a PDRM. Whilst the inclination error is completely corrected, declination values retain an easterly error. These conclusions are supported by the initial rise in the intensity of magnetization throughout cores 1B and 1A, which since the magnetic susceptibility shows no corresponding change, must provide further evidence of the improved alignment of magnetic grains. It is therefore concluded that the NRM in the recent higher mud flat sediments is of post-depositional origin, and that in this

case at least, high errors in declination can be attributed to prefered alignment at deposition, possibily due to a current induced error.

For a possible cause of this error, reference is made to the study of sediment transport directions made by Amos (1974) along this section of the Wash shoreline. Amos (1974) shows that the sediment transport paths along this north-western coast of the Wash are made up of two components. At right-angles to the shore sediment is transported seawards during the ebb-tide and landwards during the flood-tide (figure 6-6). However, during the ebb-tide material is carried along shore to the north-east. Thus whilst the sediment transport at right angles to the coast will tend to cancel out, there will be a net movement of sediment northeastwards parallel to the coast. The orientation of this current is approximately 045° (with respect to true north), which closely coincides with the measured declination recorded in the upper sediments at Freiston Shore. This is therefore put forward as the most likely cause for the bedding error observed in these sediments.

Finally, one other one-metre core of sediment was collected, core W1, at Wrangle Falts. Because of the slower sedimentation rate at Wrangle Flats it was anticipated that a more condensed sequence would be obtained and hence a more condensed palaeomagnetic record. The results of declination and inclination measurements for this core are shown in figure 6-7. The first feature to note is that the declination values do not show the large bedding errors recorded by the sediments at Freiston Shore, thus implying that there is no current effect on the magnetic particles as they are deposited. This implies that any prefer-

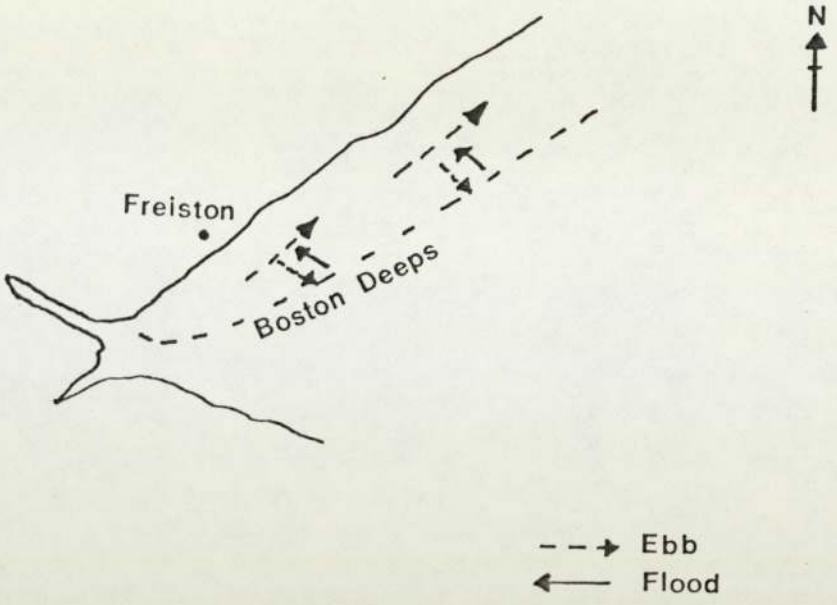


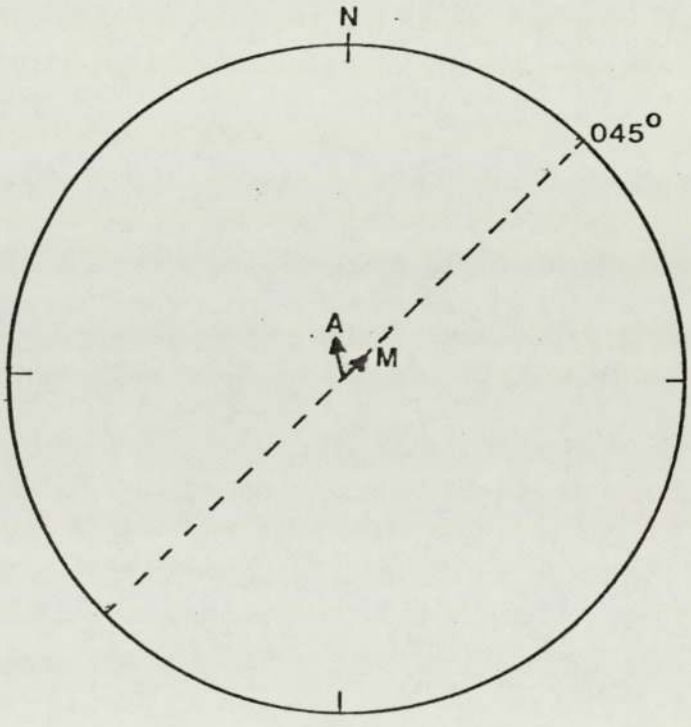


Figure 6-6. Diagram showing the flow directions at the flood and ebb tides over the tidal flats near Freiston (upper). The lower diagram shows the direction of the earths field (A) the direction of the magnetic vectore from core 1A (M) and the line of the shoreline (at 045°) plotted as a dashed line.

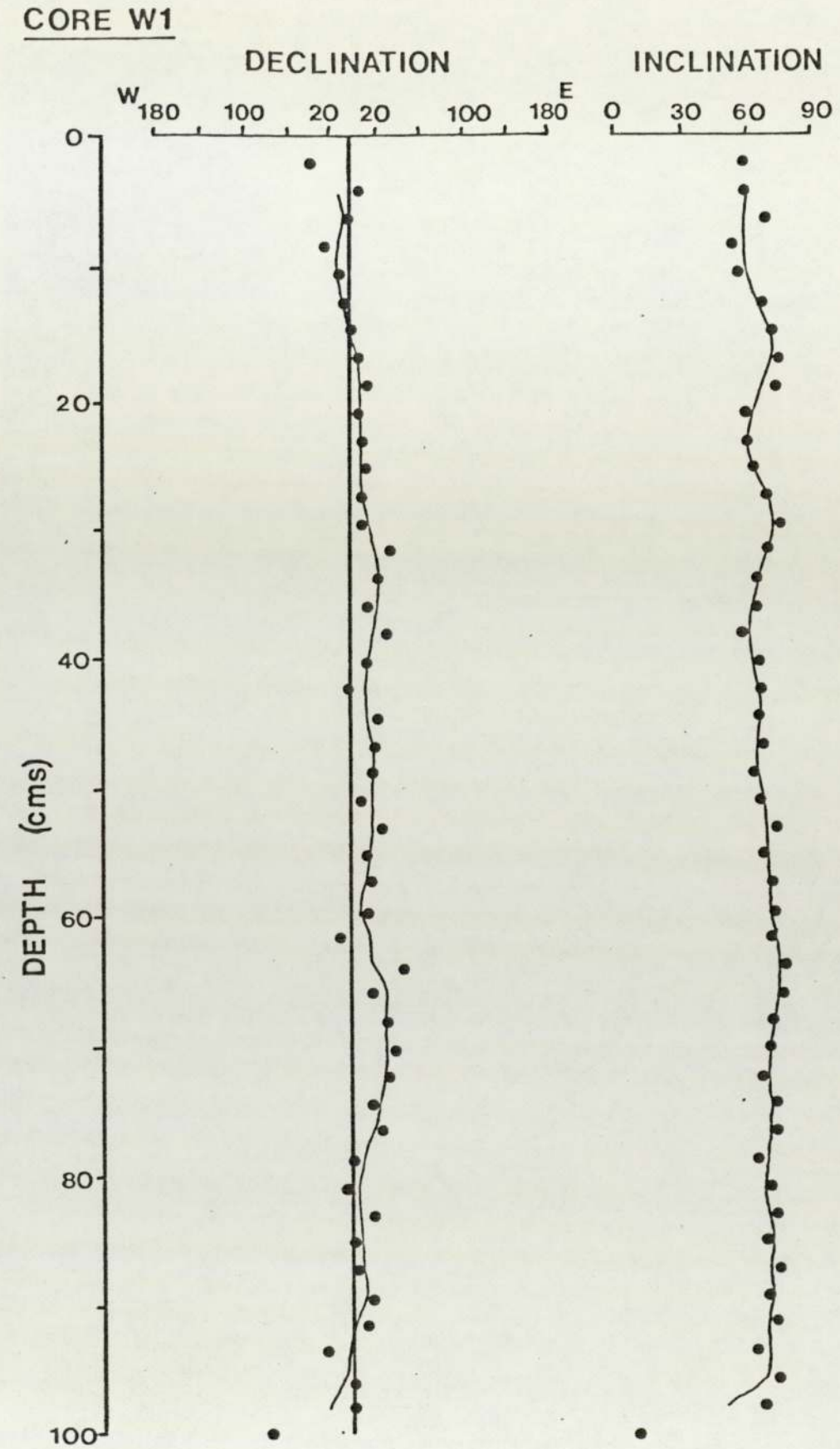


Figure 6-7. Declination and inclination measurements for Core W1. The solid line represents a 3-term running mean of the raw data.

red current direction has insufficient energy to overcome the torque applied to the magnetic grains by the Earth's magnetic field. The results do however show a gradual shift from easterly declinations in the lower part of the core to westerly ones near the top. The record however, is too incomplete to allow its use as a dating tool.

Measurements of the intensity of magnetization and the magnetic susceptibility for the samples from core W1 are shown in figure 6-8. The results of the intensity measurements show no initial increase with depth, as is observed in the upper cores form Freiston Shore, but just a general variation in the range of 2-4 $\mu$G. This therefore, further supports the concept of an early acquisition of a stable magnetic remanence and agrees with the conclusions based on observations of declination and inclination. It thus appears that in this core the sediment has acquired a stable DRM or that a PDRM is acquired very soon after deposition. A decline in the intensity of magnetization, to values of approximately 2 $\mu$G, below a depth of 70 cm is observed and this can partly be assigned to release of magnetic grains into new alignments associated with higher water saturations found in these sediments. Another possible cause is the reduction in the amount of magnetic material present in the sediments for which evidence is presented below.

Measurements of the magnetic susceptibility show initially high values in the top 10 cms of core (between 110 and 70 $\mu GOe^{-1}$). The susceptibility then shows a progressive decline from a depth of 10 cms, where a magnetic susceptibility of 70 $\mu GOe^{-1}$ is recorded, to the base of the core where magnetic susceptibilities average only 40 $\mu GOe^{-1}$. The initial high values in the upper 10 cms

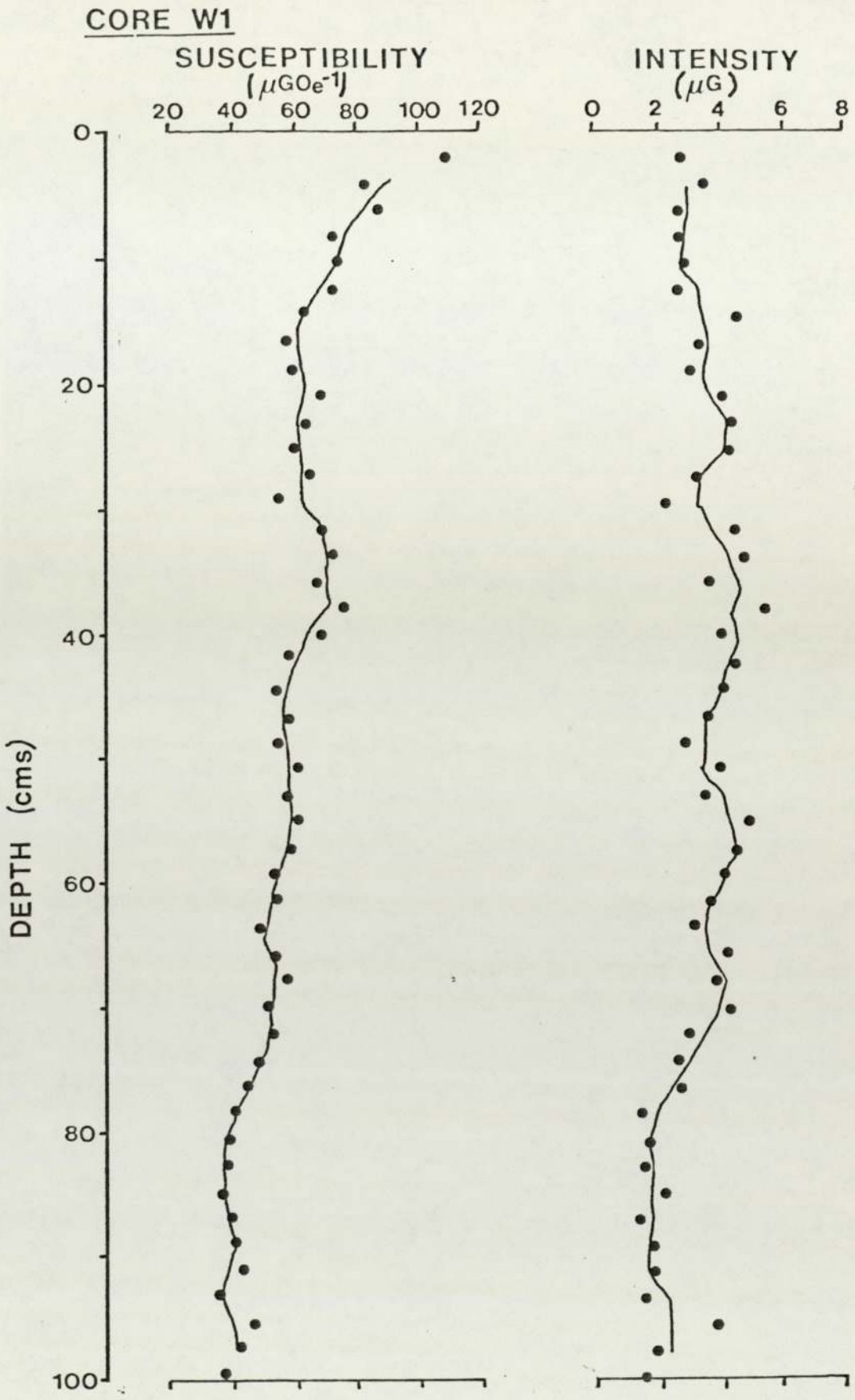


Figure 6-8. Magnetic susceptibility and magnetic intensity logs for core W1, Wrangle Flats. The solid line represents a 3-term smoothing of the raw data.

of the core may be correlated with the oxidized zone of sediment (see figure 2-7, plate 1) at this level. The results imply that the iron oxides and iron hydroxides present in this zone, responsible for its reddish-brown colouration, are progressively removed in the upper 10 cms of core. The more general decline in the susceptibility observed with increased depth, throughout the core, is probably due to a decline in the amount of "magnetic" grains present in the sediments as they become slightly coarser-grained. This is a similar situation to that observed in core 3 from Freiston Shore.

To conclude, it can be seen that the sediments at Wrangle Flats do record a NRM which is probably acquired at or very soon after deposition, in contrast to the sediments at Freiston Shore. The reason for this may be due to the lower sedimentation rate at Wrangle Flats and also to the slightly increased grain-size of these sediments, compared to those at Freiston Shore. Also, it is concluded that, with repect to coring there is a need for a method which will allow larger sequences of sediment to be collected and analysed.

6-1-4. Stability of the Natural Remanent Magnetization.

A measure of the stability of the NRM of the sediments is to repeatedly measure their remanence at intervals of time, after their collection and whilst they are subjected to some other magnetic field to that in which they were deposited.

The method used here, was applied to all of the samples from core 1B. Between measurements the samples were stored in an orientation of 270° (Magnetic North) in the ambient laboratory field. That is in a field with a declination approximately at right-angles to that in which they had been deposited. Repeat measurements

were performed after; one week, two weeks, three weeks, and after ten weeks. During this period of time the sediments were observed to dry-out somewhat resulting in some specimens being discarded at later stages of the experiment.

The results of the measurements of intensity of magnetization, declination and inclination are shown in figure 6-9. Measurements of the magnetic susceptibility were made at the conclusion of the experiment so that the small field applied did not have an effect on the results of the stability experiment. It is assumed that no changes in the magnetic susceptibility occured during the course of the experiment, such changes would only occur as a result of significant chemical changes in the sediments mineralogy.

After one week, it is apparent that the sediments show some changes in declination with a general tendancy for the declination to swing to the west. It is important to note at this stage that the clay-rich sediments at the top of the core show the least swing, indicating that they are more stable than the coarser-grained sediments below. The measurements of inclination show minor changes with about half of the samples showing a steepening in inclination, and about a half showing a shallowing in their inclination.

The measurements of magnetic intensity show minor changes also. In the clay-rich sediments, at the top of the core, the largest changes occur with initially quite large decreases in the intensity of two of the samples. These changes are not evidenced by changes in the declination and inclination measurements. In the remaining part of the upper half of this core the changes in intensity are positive indicating a net increase in the alignment of the magnetic grains as they swing back towards magnetic north.

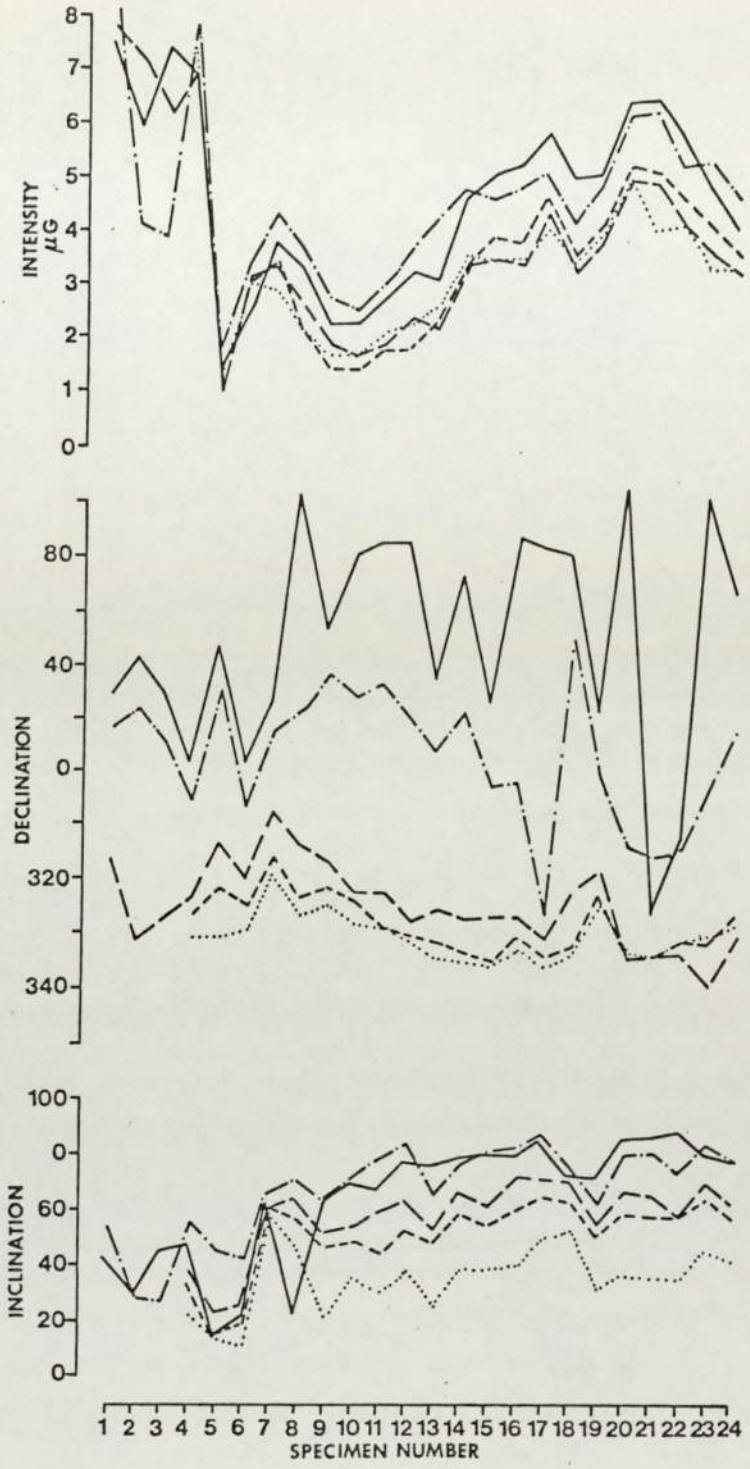


Figure 6-9. Repeat measurements of samples from core 1B. Samples were stored in the ambient laboratory field.

_____= initial measurement: _·_·_·_·_ =after one week:

__ __ __ = after 2 weeks: - - - - - = after 3 weeks

.....= after 3 weeks.

Below this level, in the lower half of the core, only a small amount of the intensity of magnetization is lost.

After a period of two weeks, a more dramatic swing in the declination values is observed with the declination swing being of the order of $70^{\circ}$, thus giving declinations with a mean of approximately $310^{\circ}$. The changes have affected all samples, and it is noted that the original trends and variations are no longer reflected in the new declination record.

The measurements of the inclination now all show a decline, but still "mirror" the original variations in the inclination record.

Measurements of the intensity of magnetization show further changes also. Beneath a depth of about 10 cms, all of the samples show a decrease in their magnetic intensities, indicating that whilst the new remanence is being acquired, there is still a proportion of misaligned grains in this portion of the core. However, in the upper 10 cms of the core, it is interesting to note that the change in the lithology is marked by a change in the behavoir of the intensity of magnetization results, which in this instance have increased in intensity. It is concluded that in this part of the core the new remanence has already become dominant, as evidenced by the dip in intensity after the first week and then the increase in intensity after week two as the new remanence is acquired. Unfortunately, complete drying of these sediment samples at this stage meant that no further measurements of these samples from the top 10 cms of the core could be made.

After three weeks, the declination values in the remaining samples show a consistant, but much reduced, swing to the west as the new remanence becomes fixed. Inclination values also show

a minor shallowing throughout the core. The intensity of magnetization also shows changes. In the upper half of the core the intensity of magnetization shows a net, though minor, decrease with respect to the results from week two. In the lower half of the core the intensity shows a minor increase in magnetic intensity over the results from week two.

The final set of measurements were made after a total of 10 weeks had elapsed. From the declination measurements, which only show minor changes since week three, it is apparent that the declination has become fixed. The mean declination of approximately 330° is approximately 60° from the measured field in which the samples were stored, indicating that a significant component of the original NRM has been preserved.

The measurements of the inclination after 10 weeks however, continue to show a decline. Whilst this is difficult to explain in terms of the ambient laboratory field, it may be explained as being due to the compaction of the samples resulting from their dehydration during the period of the experiment. Measurements of the intensity of magnetization at this stage show only minor changes with respect to the results obtained after 3 weeks.

It can thus be concluded, from this study, that the NRM of the tidal flat sediments at Freiston Shore is fairly soft, but that even after storage of periods of upto 10 weeks in another magnetic field direction of similar intensity to that in which they were deposited, they still retain a component of their original NRM. This is indicated by the fact that the new field direction is not completely acquired. It has also been shown that the finer-grained sediments show a slower tendency for these changes to occur in the first week, but after two weeks no

significant differences in the behaviour of the two similar lithologies can be detected.

6-1-5. Conclusions.

Palaeomagnetic measurements of one-metre cores of Recent tidal flat sediments have confirmed that they do record a soft but stable NRM. At Freiston Shore it has been shown that this NRM is a PDRM. Since, the sediments of the higher mud flat at Freiston Shore show relatively minor evidence of bioturbation (see chapter 2) it can be concluded that the acquisition of this PDRM is not related to the activity of burrowing organisms. This is in contrast to the conclusions of Graham (1974) whose studies were made on the tidal flat sediments of San Francisco Bay, California.

It can also be shown that the sediments at Freiston Shore carry a large bedding error. This large bedding error is not completely corrected even by the acquisition of the PDRM, indicating that the NRM still carries a significant component of DRM. This bedding error can be attributed to a current flow direction along the coastline towards the northeast. This current flow direction, related to sediment transport paths (Amos, 1974), is found to occur during the ebb-tide.

A possible palaeomagnetic marker, or event in the secular variation record, is located in the record from the sediments at Freiston Shore. It is possible, though not proven, that this curve, peaking at a depth of 2.60 metres, can be dated as the peak of the westward drift in the magnetic field, which is known to have occured at 1820 AD (160BP). This would necessitate shifting all of the measurements of the declination to the west, and would assume that all the sediments had suffered a similar bedding error. If this is the correct interpretation, then it can be

concluded that an average sedimentation rate of approxiamately 1.63 mm $yr^{-1}$ could apply to this sequence of sediments (assuming a constant sedimentation rate).

In contrast the sediments at Wrangle Flats show a much condensed palaeomagnetic record due to their lower sedimentation rate. It is also apparent from the results that these sediments do not carry a large bedding error, in contrast to the sediments at Freiston Shore. Also it is apparent that the sediments at Wrangle Flats acquired their PDRM earlier than those at Freiston Shore. Several factors may account for this difference; firstly, the sediments are coarser-grained and were deposited more slowly than those at Freiston Shore, and secondly, the absence of a large bedding error may assist the early acquisition of a PDRM.

Finally, in the study of the stability of the NRM it is found that whilst the remanence is comparatively soft, a significant proportion of it is preserved, even after storage of the samples in the ambient laboratory field for 10 weeks.

With respect to further studies of the palaeomagnetism of Recent tidal flat sediments, the first conclusion is, that to obtain useful secular variation records of the geomagnetic field it is necessary to obtain more complete sequences of sediment. This would best be achieved using continuous cores of sediment in excess of 5 metres in length. Also, the water content, determined only visually in this study, has been identified as an important factor in the stability of the NRM and in determining the time at which the PDRM is fixed. It is thus concluded that the water content be determined quantitatively in future studies of the magnetism of tidal flat sediments. The effect of different lithologies has also been noted as an important factor in deter-

mining the history of the acquisition of the NRM in the tidal flat sediments.

Using these conclusions, the studies of the tidal flat sediments in the Delft cores, from Leverton, were undertaken. The results of these studies are discussed in the next section (section 6-2).

## 6-2. Delft Cores.

### 6-2-1. Collection and Sampling.

The palaeomagnetic results from the one-metre cores show that the tidal flat sediments of the Wash do carry a record of the Earth's magnetic field. However, the deposition rate of the higher mud flats at Freiston Shore is quite rapid due to a fairly fast build up of the sequence vertically. This is brought about as a result of recent reclamation works and by man-made straightening of the river Witham outfall. It was thus decided to, firstly, locate an area where sedimentation is not so rapid and, secondly, to obtain a more complete sequence preferably penetrating the entire tidal flat sequence. These requirements meant that a new coring technique capable of recovering several metres of the unconsolidated sediment was required. Hand sampling is clearly not capable of penetrating more than two or three metres at the maximum. A further requirement is to obtain undisturbed sediment and if possible to orient it with respect to magnetic north.

Previous palaeomagnetic studies of modern and Recent unconsolidated sediment have largely been restricted to material recovered from submarine or lacustrine sediments. Hence in these studies a variety of coring techniques have been tested, perhaps the most successful of these, the Mackereth corer (Mackereth, 1958) which has been used extensively in the study of lake sediments (Mackereth, 1971; Creer et al., 1972; Stober and Thompson, 1977; Thompson, 1978; Dickson et al., 1978; and, Creer et al., 1979). The Mackereth corer is pneumatically operated and is capable of sampling sediments in upto 80 metres of water. However, due to its method of operation it is not possible to use the Mackereth corer for land based sampling. Since the tidal flat is only covered by

shallow tidal water, it was not thought feasible to attempt to use the Mackereth corer. Other problems with the Mackereth corer are that sometimes entry into the sediment is not vertical, and also, Creer et al. (1979) have reported problems caused by twisting of the corer as it enters the sediment. It must be noted that precautions were taken to prevent the occurence of this twisting and to discard the cores which showed signs of twisting.

A variety of other corers have been used, and are almost entirely of the gravity-piston type. The following is a list of those corers which have proved successful in sampling sediments for palaeomagnetic studies; the "Cambridge" type gravity corer (Bishop, 1975), the Kullenberg piston corer (Thompson et al., 1974), the Benthos gravity corer, the Alpine piston corer and the Christensen sleeve corer all used in the study by Creer et al. (1976). All of these techniques require a depth of water above the sediment surface and hence, are unsuitable for sampling on modern tidal flats.

It was thus decided to assess the feasibility of a variety of coring devices, which could be used on land and still satisfy the previous requirements for sampling palaeomagnetic specimens. Deep sampling of modern sediments for palaeomagnetic purposes on land based sites with cores in excess of 3 metres has been attempted by few workers. Two quite different techniques have been developed. Firstly, the sampling of varved clays on emergent islands in southern Sweden by Noel (1975) was achieved using a foil corer (Kjellman et al.,1950). A foil corer was not available for use in this study. Secondly, Thompson et al. (1976) have reported the successful use of the Jowsey sampler (Jowsey, 1966). The Jowsey sampler differs from the other methods in that

the sample is recovered in one-metre lengths, and requires re-entry into the hole after each one-metre section. Also the sample recovered is semi-circular in cross section. Being specifically designed for sampling peat deposits, the sampler was not thought suitable for clays, silts and sands which are encountered in the tidal flat environment. Another disadvantage is that the sample is not easily sealed on collection making the prevention of dehydration and oxidation difficult. It is also doubtful that the depth required in this study can be reached by the Jowsey sampler, since the Jowsey sampler is a hand operated system.

A new technique of sampling the unconsolidated sediments for palaeomagnetic studies thus had to be found. An instrument which had previously been used on the Wash tidal flat sediments and which produced undisturbed sediment samples used in sedimentological studies by Amos (1974) is the Gifford corer (Gifford, 1969). This is a relatively simple instrument, but unfortunately is only able to sample to a depth of 2 metres, or if a trench is dug, perhaps upto 3 metres.

A sampling tool designed specifically for sampling cohesionless sands below the ground water level is the Bishop sampler (Bishop, 1948). Samples upto 1 metre in length are recovered one at a time, and hence it was considered that there could be problems in attaining a completely continuous sequence of sediments. Also the sampler is normally pushed into the sediment using a percusion drill, which it was felt could produce problems of remagnetization in the sediments.

The method which was finally chosen was the Delft corer (sole rights for the use in the United Kingdom are held by Soil

Mechanics Limited, of Bracknell). The Delft corer is capable of providing a continuous undisturbed sediment sample. The equipment which was developed by the Laboratorium Voor Grond Mechanica, Delft, Holland is available in two sizes; 29mm diameter and 66 mm diameter core samples used in conjuction with 2 ton and 10 ton Dutch sounding machines respectively. Since the larger diameter corer is able to penetrate to greater depths and since the 66 mm diameter core would provide adequate material for both sedimentological and palaeomagnetic studies, it was chosen in preference to the 29mm corer.

Operation of the corer preceeds by anchoring the sounding machine with four larger single bladed augers. A preliminary sounding is then taken, which indicates the expected depth of penetration of the corer, and also reduces the risk of damaging the sampler by trying to penetrate consolidated strata. The sampler consists essentially of two concentric tubes, each is about 1.5 metres long. The inner of these tubes is filled with a bentonite-based supporting fluid and has nylon stockinette tubing threaded onto its outer surface prior to sampling. As the sampler is advanced into the ground the inner tube recieves the sample, at the same time enclosing it in the stockinette. The sample and its nylon sleeve is supported over its entire length by the bentonite fluid. As the sampler is advanced, extension tubes are screwed into place until the desired depth has been reached, upto a maximum of 18 metres can be achieved. Sounding at Leverton indicated that the maximum depth of penetration would be 10 metres. After taking the sounding coring takes place by forcing the corer hydraulically into the sediment one metre at a time as new one-metre core sections are attached. After complete

penetration the sampler is withdrawn, and the one-metre core sections are cut as each metre is withdrawn. The samples are sealed with plastic caps in their stockinette and inner core liner tubes.

Sampling using the Delft corer could not be attempted on the present-day tidal flat sequence, however, sampling of recently reclaimed land was possible. The location selected for sampling was at Leverton (grid reference TF 429463) on a piece of land reclaimed from the salt marsh in the early 1970's (see figure 6-1). The site was chosen, firstly, because it represents one of the most recently reclaimed areas on the salt marsh, and also, because it is one of the areas with a slower vertical accretion rate. The site was also chosen because of its remoteness to the modifying effects of fluvial inputs to the Wash and their outfalls. In addition to the early 1970's sea bank to the seaward of the coring site, there are two other reclamation works to the landward which may have affected sedimentation at the site of the cores. The first of these is the Roman sea-bank (the 'Sea Bank' (in Gothic Script) of current Ordnance Survey maps. Some authorities believe that the Roman sea bank may be of more recent date (Bradshaw pers comm.) however, it is quite possible that it is of Roman age since the Romans were responsible for reclaiming large areas of the salt marshes for agriculture. The Roman sea bank now lies 1150 metres to the landward of the coring site. During the mid-eighteenth century further reclaimation of land to the seaward of the Roman sea bank took place with the building of a new sea bank some 700 metres from the Roman sea bank.

Coring took place about 100 metres inland from the present-

day sea bank. Two cores were taken separated laterally by 5 metres, these cores are refered to as cores D1 and D2 as explained in Chapter 2. Sounding, as mentioned earlier indicated that sampling to a depth of 10 metres would be possible, in actual fact sampling was only possible to a total depth of nine metres with both cores. An attempt was made to orient the core in the field by using a bent coring tooth, which it was hoped would score a fiducial line along the core during its recovery. The bent tooth was oriented with respect to the sounding rig and a sighting was then made along the axis of the rig. This attempt to orient the core was not successful in the lower parts of the cores, where non-cohesive sands were encountered. However, in the clays and very fine sands it was possible to discern the fiducial line and accurate orientation of these sections of core was possible. After recovery of the core in the one-metre core sections the core was sealed and taken to the laboratory for analysis.

6-2-2. Natural Remanent Magnetization.

On return to the laboratory the one-metre core sections from core D1 were opened one at a time to prevent dehydration and oxidation whilst the palaeomagnetic specimens were being prepared. The cores were easily extruded from their polyvinyl chloride (PVC) core liners, as the supporting bentonite fluid acted as a lubricant between the core and the core tube. Extrusion of the cores proceeded in lengths of approximately 200 mm and specimens were prepared from each exposed section prior to extruding a further 200 mm. In each core section two parallel sequences of specimens were prepared as illustrated in figure 6-10. From each core section it was possible to prepare two sequences of between 39 and 49 specimens, the variation in total number being

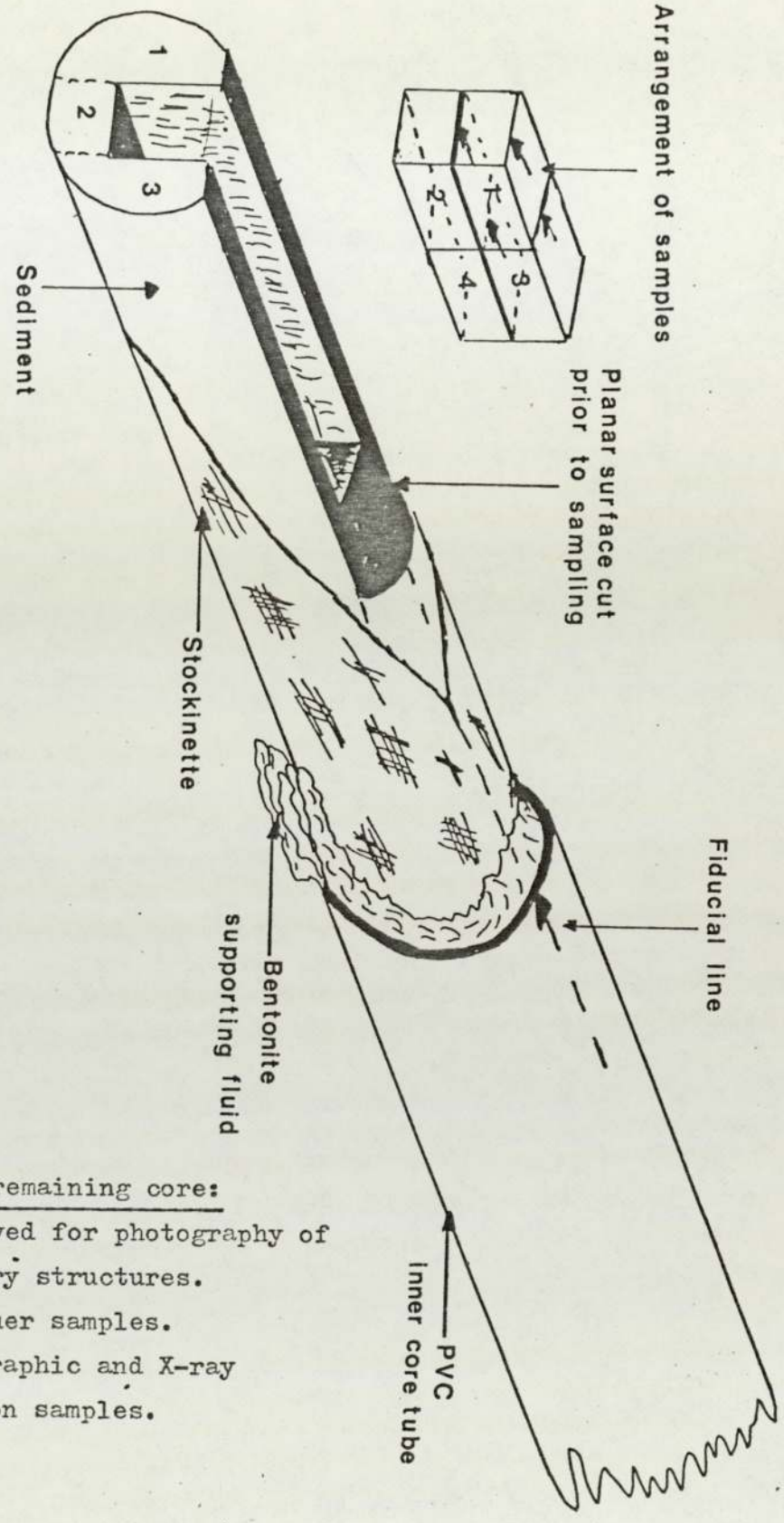


Figure 6-10. Diagram showing the location and numbering method of the palaeomagnetic samples, and the usage of the remaining core material.

due to the difficulty of cutting the fine sands, which tend to crumble more easily than the silts and clays. A total of 836 specimens were prepared, by firstly, cutting a flat surface at right-angles to the fiducial line and parallel to the axis of the core (figure 6-10). A pillar of sediment was then cut to the dimensions of the sample holder and this was then slid onto the sediment sample which was then seperated from the core by cutting. Partial protection from oxidation and dehydration was provided by fitting a lid to the sample holder. The sample holders used throughout the sampling of the Delft core consisted of plastic microboxes with tight fitting plastic lids. The internal dimensions of the microboxes (19 x 19 x 14 mm) meant that all measurements of the intensity of magnetization had to be corrected for volume using the following relationship:

$$INT_c = \sqrt{((X*R1)^2+(Y*R2)^2+(Z*R3)^2)}$$

where, $INT_c$ is the corrected intensity of magnetization in μG.

X,Y, and Z are the components of magnetization measured in the three orthogonal directions by the Digico magnetometer.

R1,R2, and R3 are the ratios of the assumed dimensions of the sample (2.54 mm in each orthogonal direction) to the actual dimensions of the sample in the X, Y, and Z directions respectively.

Since the standard program for the Digico magnetometer is only able to correct for sample size variations in the Z direction a simple seperate Fortran computer program was written to perform the intensity corrections. A listing, together with a brief explanation of this program is provided in appendix ( 5 ). No

corrections to the values for declination and inclination, made by the Digico program, are necessary. The magnetic susceptibility of the specimens was measured in the same way as described for the one-metre cores (sub-section 6-1-2).

The following system of labelling the samples was used; firstly, D1 refers to the core D1, secondly D12 refers to core D1 and core section D12. Each sample within a particular core section is then identified by a one or a two digit number. Since two sequences of samples were taken, odd numbers refer to one sequence and even numbers refer to the other sequence (figure 6-10). Otherwise the samples are simply numbered in multiples of two consecutively starting with one or two at the top of each core section. Thus sample number D18.42 would represent a sample from core D1, core section D18 and it would refer to the 21st sample in the even sequence of samples. By dividing 21 by the total number of samples in that core section, 48, and then multiplying the result by 1 metre, the approximate depth within that core section, 44 cms, is obtained.

As large quantities of data were to be gathered, the computer was used to store and to process most of the data. The first step was to orient the data from each one-metre core section with respect to the data from the other core sections. Initially, it had been planned that this could be achieved using a fiducial mark applied to the core by the head of the corer (section 6-2-1). However, in the majority of the cores this proved unsatisfactory. As a result it was decided to take the mean declination of each suite of samples (odd or even) from a particular core section, and use that mean declination as the fiducial line to join the data to that of adjacent cores. Whilst this method has obvious

disadvantages, for example, if large swings to the east or west are encountered within one core section the method will tend to reduce the magnitude of these swings, it is considered the best method available. Table 6-1 shows the mean declination for both suites of samples for each one-metre core section. The mean declination was next applied as a correction factor to bring all the samples relative to magnetic north. Joining of the core sections for the other data, inclination, intensity of magnetization and magnetic susceptibility, does not require these adjustments.

The results of the standard deviations about the mean declination (Table 6-1) are worthy of mention here. These results show that the largest standard deviations, of greater than $50^{\circ}$ occur in the lower three core sections (D18, D19, and D110). The best quality data, that showing the least variance occurs in core section D13, which represents sediments belonging to the higher mud flat sub-environment. Samples from core section D12 have a larger variance as indicated by standard deviations of $28-35^{\circ}$. This indicates that these sediments are less well magnetized than the underlying sediments of core section D13, a possible indication of the existence of a PDRM in the lower sediments. Further evidence of this PDRM will be presented below.

Plots of the raw data for the NRM obtained from the Digico magnetometer also show the larger amount of scatter found in the lower parts of core D1 (figures 6-11, 6-12, 6-13 and 6-14). Because of this scatter it was decided to apply a smoothing technique to the raw data in order to identify more clearly the variations in the declination and inclination so that these could be related to variations in the known geomagnetic field in Great

ODD DATA SET

| Core Section | D12 | D13 | D14 | D15 | D16 | D17 | D18 | D19 | D110 |
|---|---|---|---|---|---|---|---|---|---|
| No. Samples | 48 | 45 | 39 | 48 | 48 | 46 | 48 | 49 | 40 |
| Mean Dec. | 10° | 46° | 267° | 271° | 23° | 26° | 170° | 270° | 31° |
| Std. Dev. | 35 | 9 | 40 | 22 | 17 | 19 | 57 | 40 | 69 |

EVEN DATA SET

| Core Section | D12 | D13 | D14 | D15 | D16 | D17 | D18 | D19 | D110 |
|---|---|---|---|---|---|---|---|---|---|
| No. Samples | 48 | 45 | 39 | 48 | 48 | 46 | 48 | 49 | 40 |
| Mean Dec. | 3° | 44° | 283° | 275° | 21° | 22° | 184° | 269° | 43° |
| Std. Dev. | 28 | 12 | 15 | 23 | 15 | 29 | 55 | 64 | 63 |

TABLE 6-1. Statistical data for the odd and even data sets of declination used to join the data from each core section. The table shows the total number of samples in each core section, the mean declination and also the standard deviation about that mean.

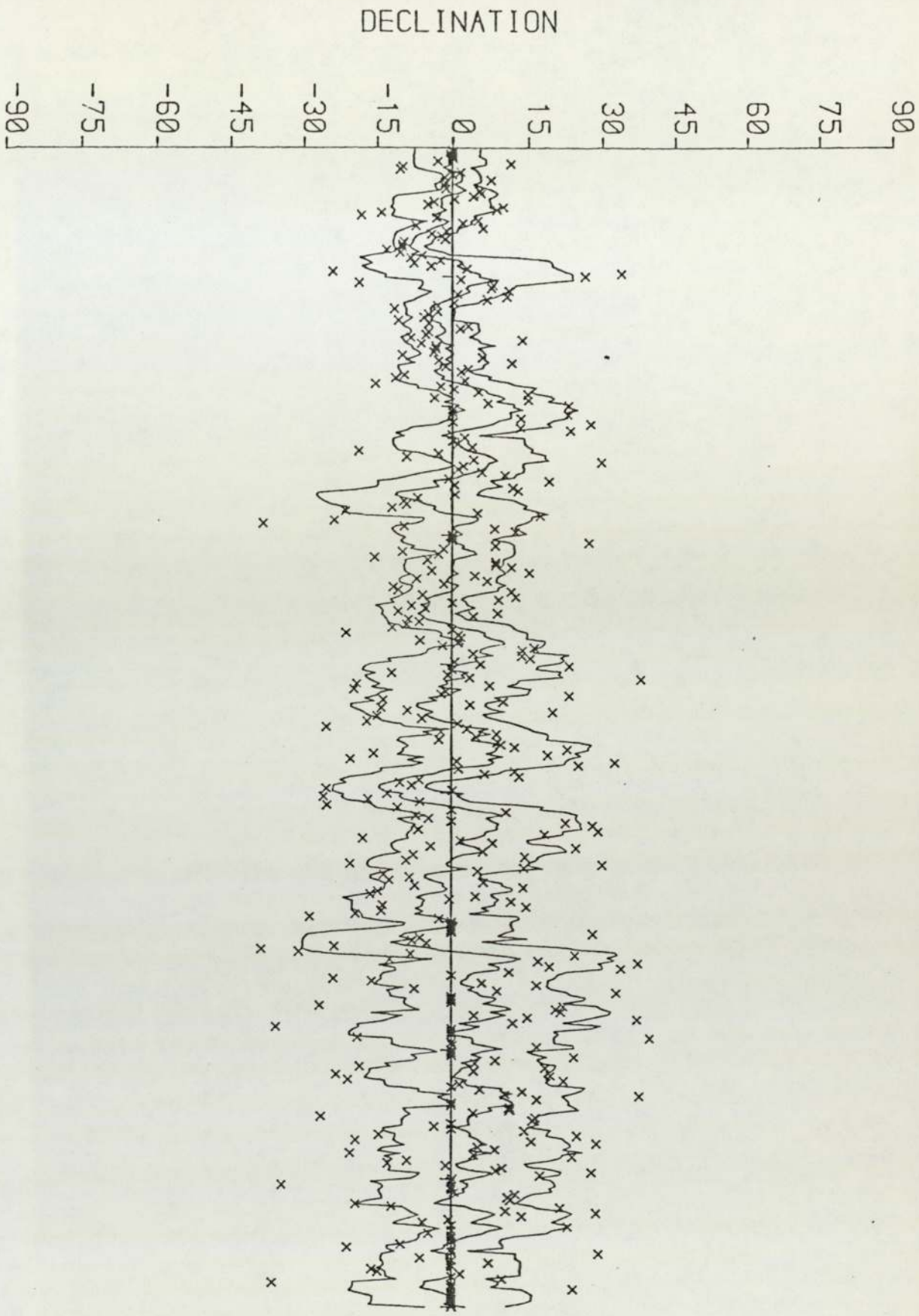


Figure 6-11. Nine-term smoothing with a 40° filter of the raw data (x) for core D1 (odd data set). The "tram lines" show the standard deviation for each smoothed point. (see inclination logs for depth scale).

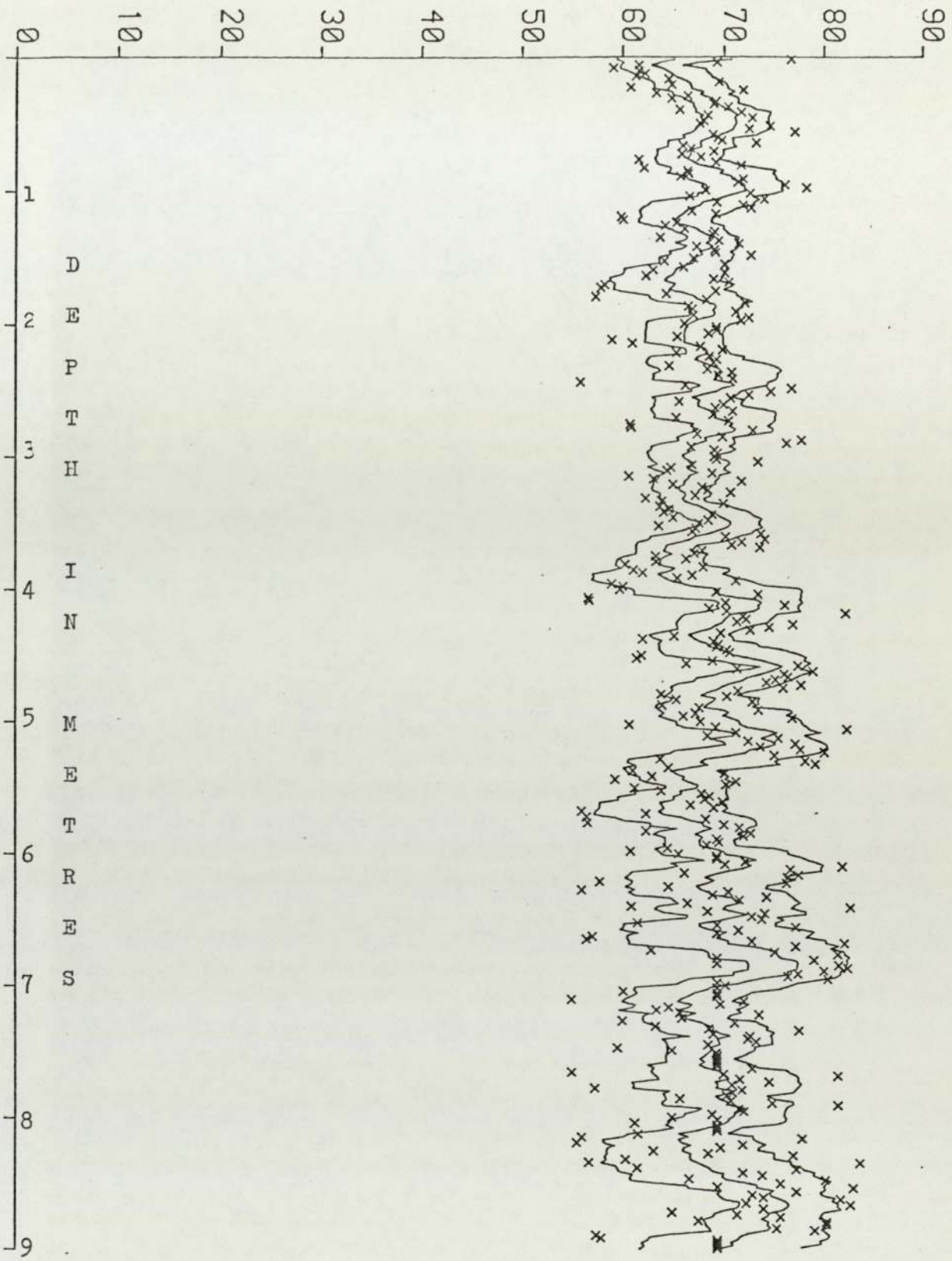


Figure 6-12. Nine-term smoothing with a 15° filter of the raw data (x) for core D1 (odd data set). The "tram lines" represent the standard deviation about each smoothed data point.

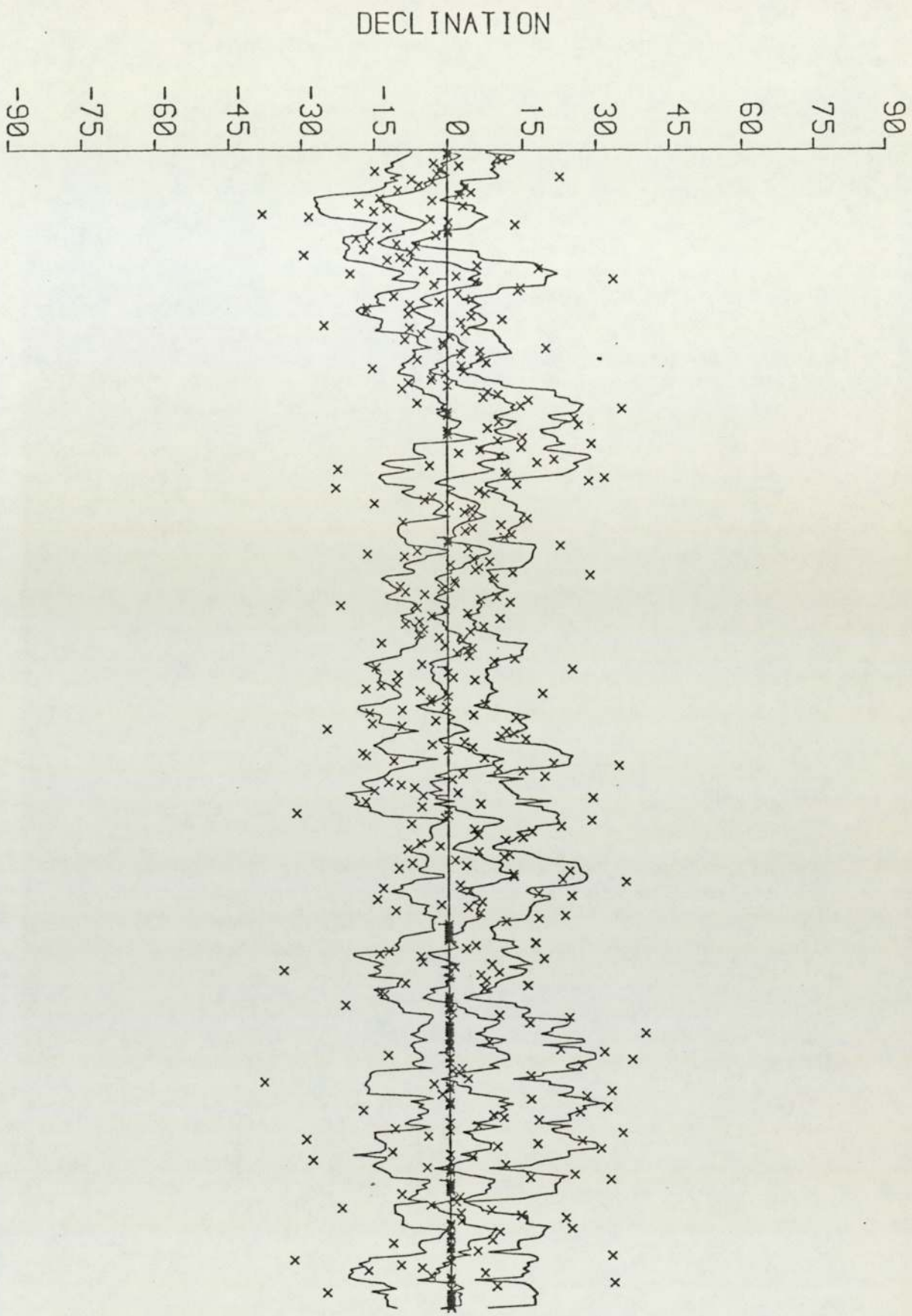


Figure 6-13. Nine-term smoothing with a 40° filter of the raw data (x) for core D1 (even data set). The "tram lines" represent the standard deviation about each smoothed data point.

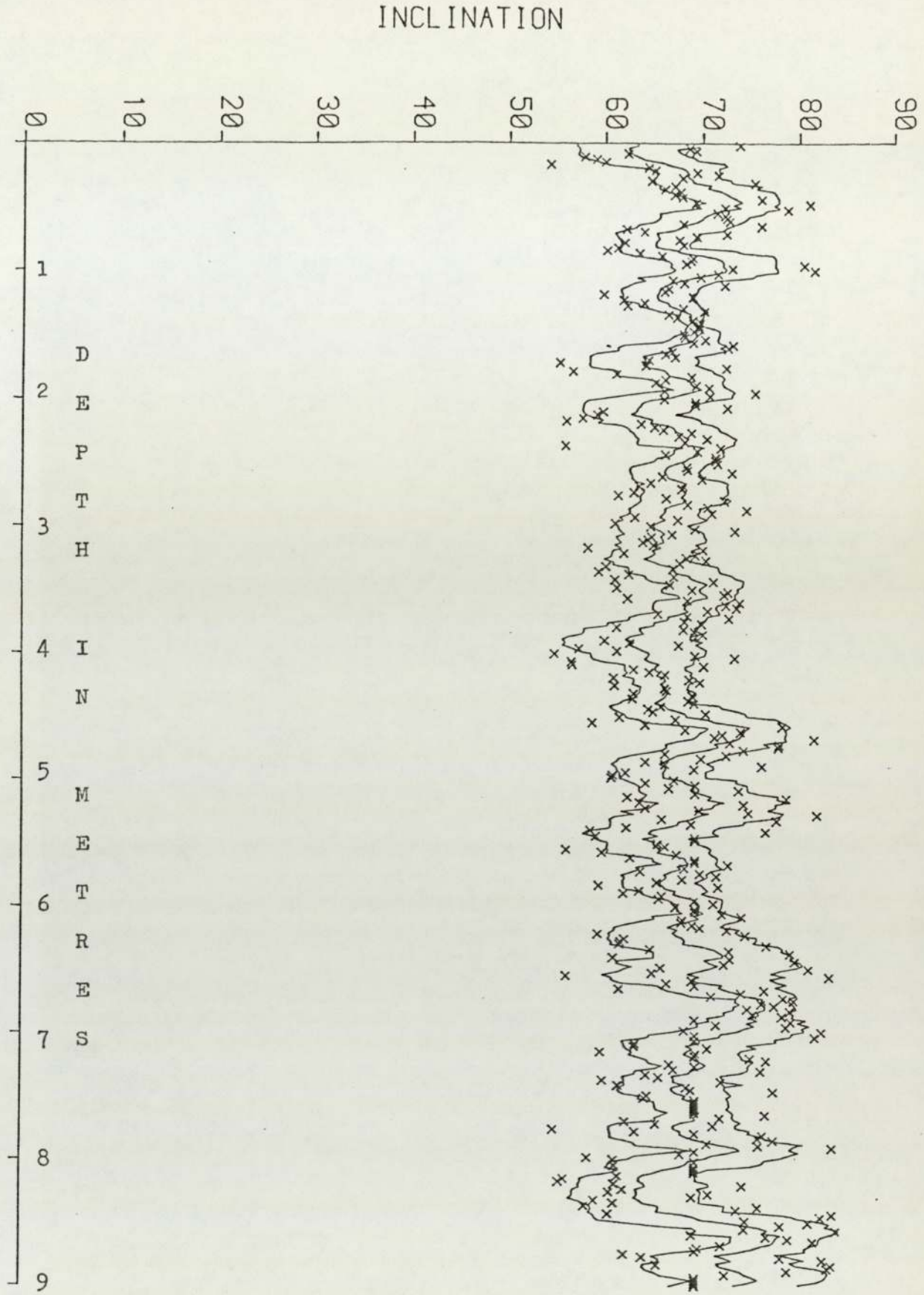


Figure 6-14. Nine-term smoothing with a 15° filter of the raw data (x) for core D1 (even data set). The "tram lines" show the standard deviation about each smoothed data point.

Britain. Further analysis of the NRM will be discussed in the section dealing with the secular variation recorded by the sediments (section 6-2-6).

6-2-3. Smoothing of the Natural Remanent Magnetization.

A variety of smoothing techniques have been developed to smooth palaeomagnetic data in other studies of secular variation, (a brief review of some of these methods is given by Thompson, 1977). The chief methods used are; running means, polynomial fitting and fourier smoothing. More elaborate techniques have been developed, the most successful of which is a method of cross-validation using a cubic spline (Clarke, 1975). This method, however, is not used here where preference has been given to using a simple technique, the running mean (or moving average). The only addition to the simple running mean smoothing is the application of a filtering mechanism for removing spurious data points.

A simple Fortran program has been written (developed from the subroutines of Davis, 1973) to perform this task. A listing of this program together with a brief explanation appears in appendix ( 6). Two versions of the program were used in processing the data, the first, DECSEC, was used to smooth the declination data, and the second, INCSEC, to process the inclination data. DECSEC in addition to smoothing and filtering the data also is able to orient the core sections with respect to one another using the method described in section 6-2-2. Graphical subroutines were used to provide plots of the raw and smoothed data. Also plotted by the programs DECSEC and INCSEC are "tramlines" which represent the standard deviation about the smoothed data points. The standard deviation relates to the

number of samples used in the smoothing function, therefore, if smoothing is being carried out using a five-term running mean then the standard deviation represents that of the five data points used to obtain the smoothed data point.

The program INCSEC is similar to the program but does not apply an orientation correction to the data, since this is not necessary.

In order to find the optimum smoothing function for the running mean (ie. the number of samples over which a mean is taken for each data point) and also the optimum filter for the elimination of spurious data, a number of plots were made for the two data sets (appendix7 ). The results of these different plots were then assessed visually, by comparing the effects of using various filters and smoothing functions. The combinations of these plots used for the declination measurements were; smoothing factors of 5, 9, and 15 each with filters of $20^{\circ}$, $40^{\circ}$ and $60^{\circ}$, giving a total of nine combinations of smoothing for each of the two data sets.

After assessing the results of these smoothing processes, it was decided that a nine-term smoothing function and a filter removing any data points differing from the mean declination for the core by more than $40^{\circ}$ gave the best results (Table 6-2). Smoothing of the inclination data using the same 9-term smoothing function used for the declination measurements was next undertaken using filters of $10^{\circ}$, $15^{\circ}$, and $20^{\circ}$. This gave a total of three different plots for the two sets of inclination data. The results of these plots were again assessed visually, and it was decided that the best results were obtained using a filter of $15^{\circ}$.

| | FILTER | | | | | |
|---|---|---|---|---|---|---|
| | Declination | | | Inclination | | |
| Smoothing factor | 20 | 40 | 60 | 10 | 15 | 20 |
| ODD 5 | FX | X | HX | | | |
| ODD 9 | FY | Y | HY | FY | Y | HY |
| ODD 15 | FY | Y | HX | | | |
| EVEN 5 | FX | X | HX | | | |
| EVEN 9 | FY | Y | HY | FY | Y | HY |
| EVEN 15 | FY | Y | HY | | | |

TABLE 6-2. The table shows the combinations of smoothing factors and filters used in the computer plots of the smoothed palaeomagnetic data. The symbols indicate: F = flattening of the curves; H = high amplitude variations not removed; X = high frequency variations present; Y = high frequency variations subdued.

The results of these fits are shown in appendix (7), and the best fits are shown in figures 6-11, 6-12, 6-13, and 6-14. From the results of using the running mean as a smoothing method, it was decided that this provides a satisfactory method for smoothing the palaeomagnetic data obtained in this study.

6-2-4. Cleaning of the NRM.

A common source of the noise seen in palaeomagnetic measurements is the presence of secondary magnetizations carried by the sediments. These can be introduced after deposition or by the processes of coring and removal of the sediments to the laboratory. Magnetic cleaning of specimens is a standard palaeomagnetic practise used to determine the magnitude and direction of these secondary magnetizations.

Two main techniques of cleaning are employed in palaeomagnetic studies, these are, thermal demagnetization, and alternating field demagnetization (see for example, Tarling, 1971; and McElhiney, 1973). Thermal demagnetization requires that the specimens are heated to successively higher temperatures in field free space, and that measurements of the magnetic remanence be made after each heating stage. Heating of the specimens used in this study could not be made without destroying them, because of their unconsolidated nature and because of the modifying effect heating would have on the unstable iron sulphide minerals present in them.

Therefore, alternating field (A.F.) demagnetization was used to clean the samples in this study. The method involves passing an alternating current through a coil which produces an alternating field along its axis. The specimen is placed on the axis of the coil and the Earth's magnetic field is cancelled

using a Helmholtz coil system to help prevent the addition of anhysteritic magnetization. A second precaution against the acquisition of an anhysteritic magnetization is to rotate the sample in a tumbling device about three mutually perpendicular axes whilst the alternating field is applied. Thus the specimen is presented to as many different orientations of the demagnetizing field and the anhysteritic field as possible.

The equipment used in this study was the alternating field demagnetization equipment at the University of Birmingham. A total of 13 pilot samples were subjected to alternating field demagnetization. The pilot samples were subjected to progressively increasing alternating fields in the range 50-700 Oe. Examples of the results of the AF demagnetization experiments are shown in figure 6-15, which shows demagnetization curves for a sample from each of the three main lithological groups represented in core D1.

Specimen D12.15 (figure 6-15) represents the sediments belonging to the salt-marsh, unit 1, specimen D12.75 represents the higher mud flat sediments, unit 2, whilst specimen D18.25 represents the specimens from the Arenicola sands of unit 3. The results show that there is no apparent grouping of magnetic vectors other than at the original NRM direction. This indicates that no spurious or secondary magnetizations are carried by the sediments.

Measurements of the mean destructive field for each sample, taken from the results of the AF demagnetization experiments, are shown in figure 6-16 plotted against depth. The range of the mean destructive field values clearly shows a dependance on the lithology of the samples. The samples exhibiting the highest

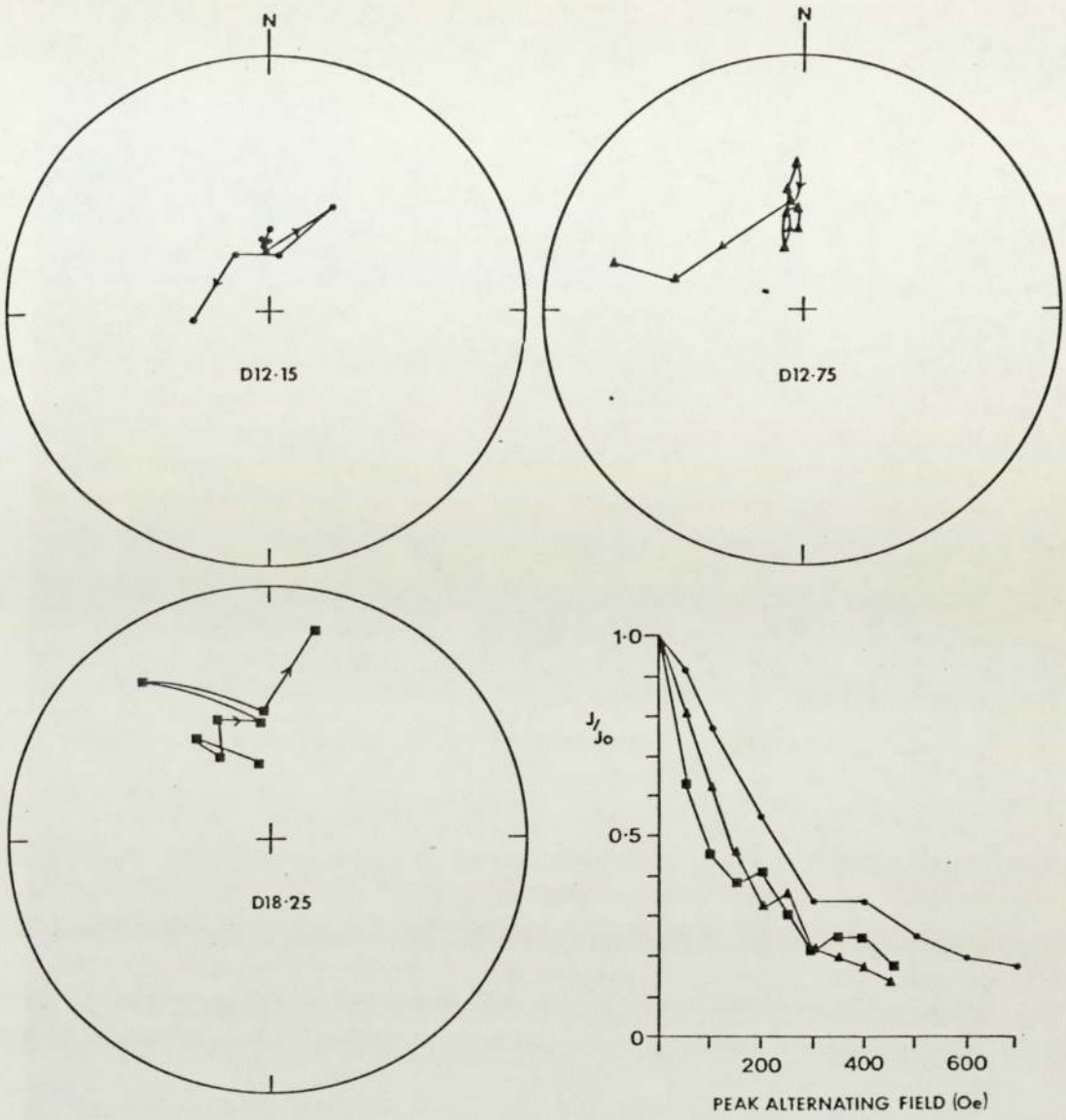


Figure 6-15. Examples of the results of alternating field demagnetization of samples from the three major lithological types in the Delft core. Specimen D12.15 is derived from the salt marsh sediments, specimen D12.75 from the higher mud flats and specimen D18.25 from the Arenicola sands.

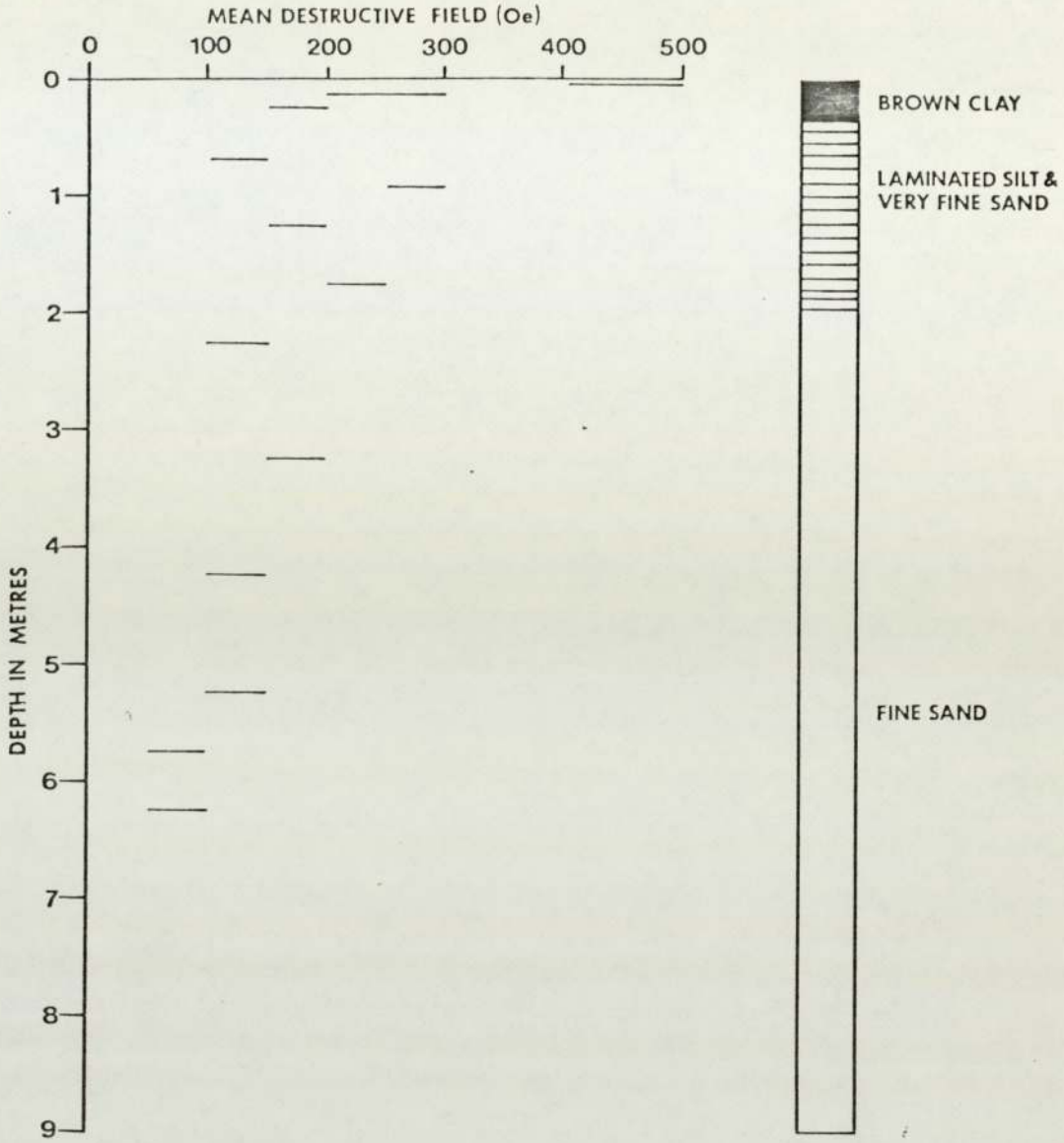


Figure 6-16. Variations of the mean destructive field with depth and lithology in the Delft core D1.

coercivities are the clays found at the top of the core which have mean destructive fields in the range of 150 - 500 Oe. The sediments of the higher mud flats, consisting of laminated silt and very fine sand show intermediate coercivities with values for their mean destructive fields in the range 100 - 300 Oe. As the sediment grain-size and water content of the samples increases the coercivity of the samples continues to decline within the sediments of unit 3, the Arenicola sands, where mean destructive fields of 50 - 200 Oe are found.

Since the mean destructive field for the sediment samples seems to be dependant on the grain-size of the sediments, it may be that in the fine sands, the remanence is carried by multidomain particles with a relatively low coercive force, whereas in the clays, the remanence is carried by finer-grained particles with higher coercive force and possibly including single domain or pseudo-single-domain particles. However, another possibility is that the sands, during the tumbling proceedure suffer physical disorientation giving the impression that the remanence is of anom lously low coercive force.

The results of this pilot study of the behav r of samples of tidal flat sediments from core D1, therefore suggest that no systematic cleaning of the samples in an optimum alternating magnetic field is necessary. Therefore the measurements of the raw and uncleaned NRM directions have been used in all attempts to determine secular variation trends from the sediments.

6-2-5. Bedding errors and the processes of fixation of the NRM.

The palaeomagnetic studies of the one-metre cores showed that

in some instances, as at Freiston Shore, large errors in the declination from that of the Earth's present field are recorded by the sediments. These errors in declination have been attributed to a current induced bedding error. In contrast, the sediments from Wrangle Flats show no evidence of such an error in their declination record.

Analysis of the palaeomagnetic results from the Delft core (figure 6-11), from Leverton, shows a similar situation to that at Wrangle Flats with little evidence of a bedding error in the recorded values of declination. This is especially well demonstrated by the results form core section D12, which was successfully oriented in the field. The mean declination for core section D12 is $10^{\circ}$ for the odd data set and $3^{\circ}$ for the even data set, thus if a bedding error is present it is very small. Assessment of the role of the bedding error in the lower parts of the core cannot be made since attempts to orient the lower core sections proved unsatisfactory. However, it is possible to conclude that for the upper section of core representing the higher mud flat sediments and salt marsh sediments, no bedding error occurs. This is in agreement with the location of the coring site, which is closer to the location of core W1 from Wrangle Flats where a bedding error was also absent.

It was found in the study of the one-metre cores of sediment that qualitative studies of the water content of the samples yeilded important evidence with regard to the fixation of the remanence in those sediments (section 6-1). In this study of the Delft core quantitative measurements of the water content of the sediments have been made to try to gain an insight into the role of water content in the magnetization of these sediments (Suttill,

1980b)

Measurements of the water content of the sediment samples were made by weighing the samples immediately after the first palaeomagnetic measurements, of NRM, were made. After allowing the samples to dry out completely, by storing them for approximately three months in the laboratory, the samples were reweighed and the water content was determined by subtraction as a percentage weight loss.

The results from the core sections below the upper two core sections (D12 and D13) have been deleted from the study since, they showed anomolously low water contents as a result of partial dewatering of the cores during sample preparation and after recovery from the field. However, the results from core sections D12 and D13 do show meaningful variations, probably because the finer grained sediments from these core sections ar more able to retain water.

The measurements obtained of the water content for core sections D12 and D13 are shown in figure 6-17. Also illustrated in this figure are the Koenigsberger Ratios (Q-ratios) and the iron content of some of the samples, from the geochemical study of the core (chapter 2). These unsmoothed data show distinctive trends. From the plot of the Koenigsberger ratios it is apparent that there is little variation in the upper 40 cms of the core, but beneath that depth the Koenigsberger ratio shows a progressive increase with depth. In the plot of the percentage water content there is an initial rapid decline from 30% water to about 20% in the upper part of the core, representing the zone occupied by the brown clay of the salt marsh. Beneath this level the sediments of the higher mud flats show a reversal in this trend with

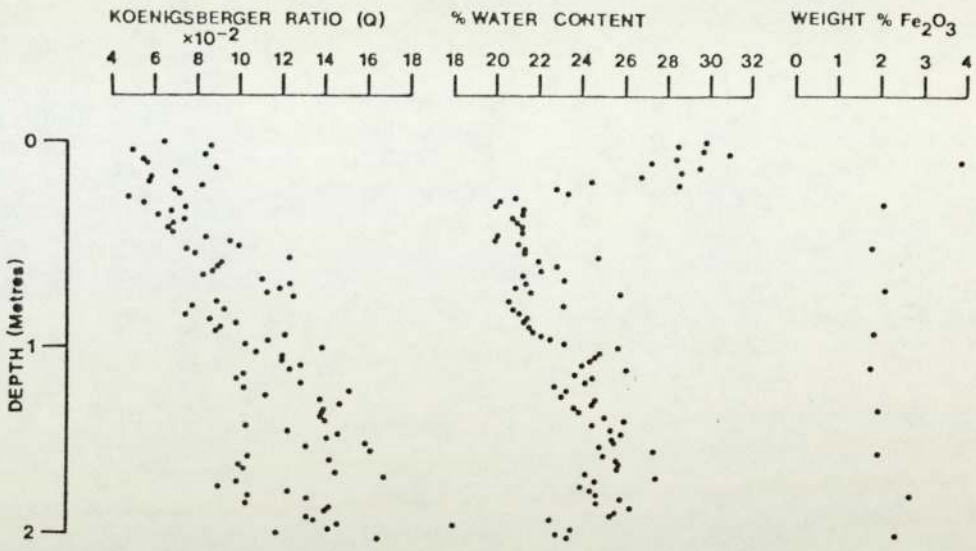


Figure 6-17. Logs of core sections D12 and D13 showing the raw data for the Koenigsberger ratio, the percentage water content and the iron content of the sediments.

a gradual increase in the water content from 20% to 25%. The iron distribution, refered to in chapter 2, shows the initial high iron content (4%) in the salt marsh sediments, and the more or less constant values (2%) in the sediments from the higher mud flats.

Smoothing of these data using the same nine-term smoothing method applied to the NRM data makes identification of these trends clearer. The results of smoothing the Koenigsberger ratios and the percentage water contents are shown in figure 6-18. The Koenigsberger ratio (or Q-ratio) is the ratio of the intensity of magnetization to the magnetic susceptibility, and can be thought of as an indication of the amount of alignment of the magnetic grains in the sediments. Thus, at the top of the core in the sediments belonging to the salt marsh, poor grain alignment is shown by a low Q-ratio of $6\text{-}7 \times 10^{-2}$. No improvement in the Q-ratio is apparent within the salt marsh sediments depite a falling percentage water content (figure 6-18).In the underlying higher mud flat sediments the Q-ratio continues to show a constant value for a small depth interval and then shows a marked and progressive increase from a value of $6\text{-}7 \times 10^{-2}$ to almost $14 \times 10^{-2}$. This variation indicates that the magnetic grain alignment is improving with increasing depth within the higher mud flats. The water content in this interval shows a similar increase with depth with minor variations in the water content showing similar variations to those seen in the Q-ratio log (figure 6-18). This trend in water content is partly associated with the coarsening in grain-size of the higher mud flat sediments with increased depth and may also be due to water increasing as a result of the fluctuating water table in the tidal flat. Thus despite the

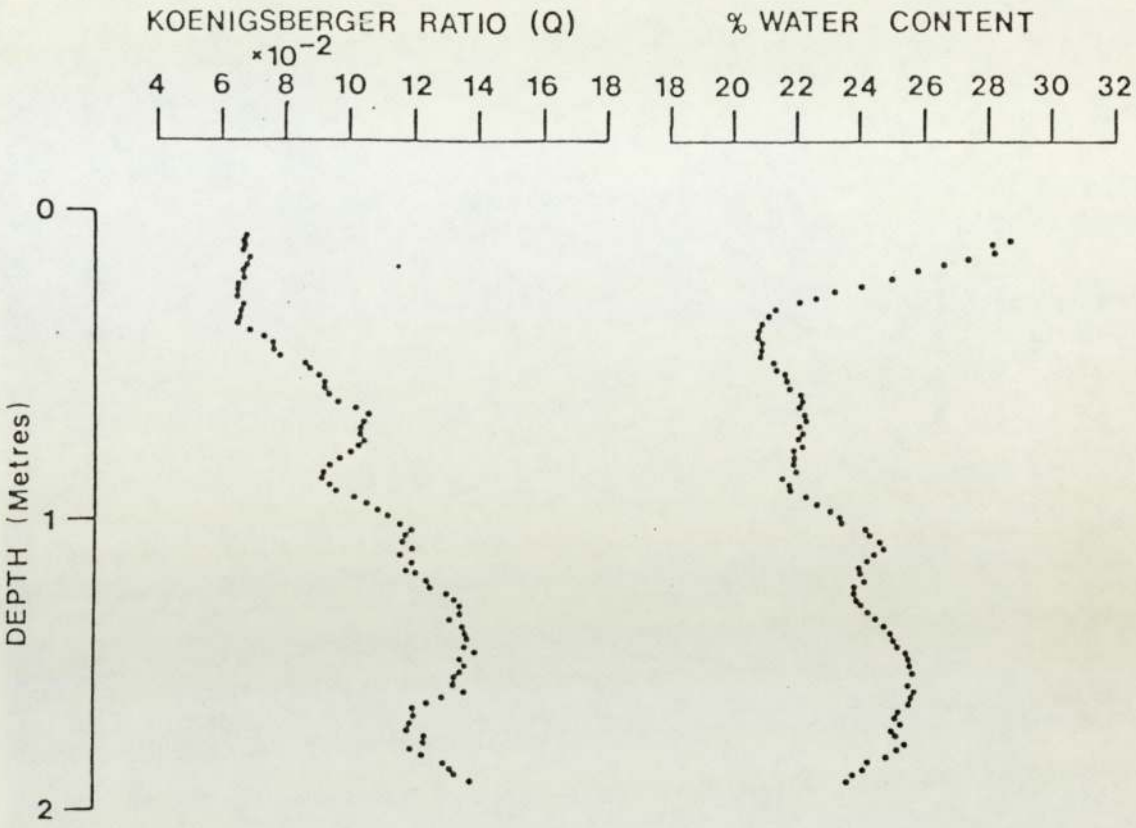


Figure 6-18. Logs showing the Koenigsberger ratio and percentage water content for the core sections D12 and D13. The data has been subjected to nine-term smoothing to resolve the variations.

increased water content the Koenigsberger ratio still shows an increase. One explanation for this, may be that the presence of water in the sediments gives them a certain amount of extra cohesion, possibly through surface tensional forces, and mechanical stability aiding the fixation of the magnetic remanence. Another possibility is that the increased alignment of magnetic grains with depth is due to increased fixation of these grains as a result of increased overburden.

A series of crossplots of various palaeomagnetic data were prepared to try to further resolve the problems in understanding these initial stages in the magnetisation of the tidal flat sediments. The plots for the data from core sections D12 and D13 have been plotted seperately to simplify reading of the diagrams. The first of these plots shows the smoothed (9-term) inclination record plotted against the smoothed (9-term) water content results (figure 6-19). It is apparent that the brown clay at the top of the core undergoes an increase in inclination together with the initial decrease in the water content. The water content continues to decrease past the salt-marsh - higher mud flat boundary (represented by the brown clay - laminated V. fine sand boundary) until the lowest water content of approximately 21% is reached. It thus appears that the relationship of decreasing water content and steepening inclination is independant of the lithology. As the sediments continue to coarsen in grain-size, with depth, their water content rises, and the variations in inclination remain dependant on the variations in the water content of the sediments. However, in the lower part of this core-section the inclination continues to increase despite an increase in the water content of the sediments. It is thus concluded, that

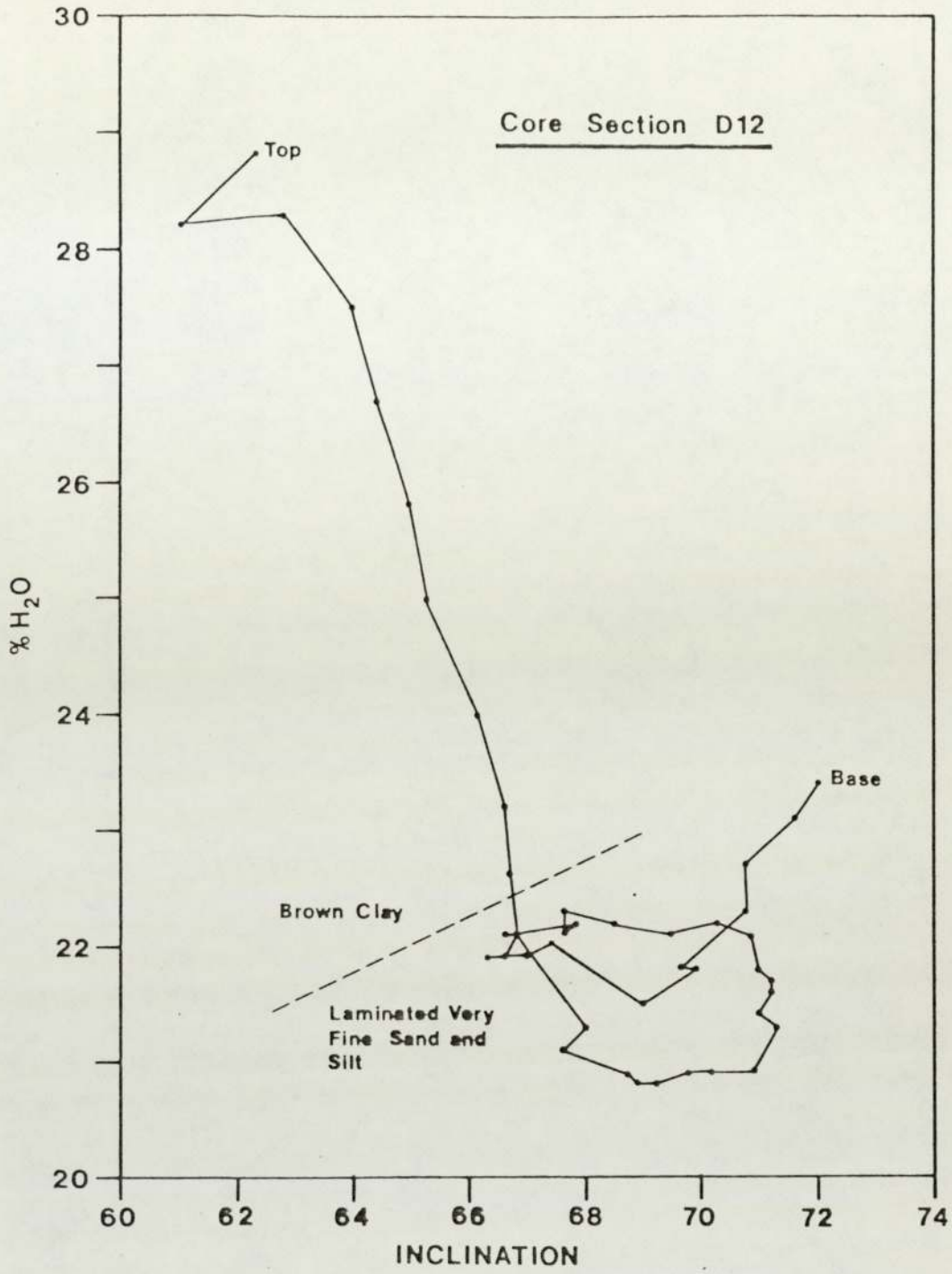


Figure 6-19. Percentage water content plotted against the inclination of the magnetic vector for core-section D12. The data have been subjected to a nine-term smoothing using a running mean.

variations in the water content are related to the fixation of the inclination component of the magnetic vector in these sediments. The inclination of the Earth's magnetic field at Leverton is 69.3° and from figure 6-19 it can be seen that the initial inclination error present in these sediments is progressively corrected as the water content decreases. At a point roughly corresponding to the inclination of the present Earth's field the water content has fallen to 21%. Below this depth variations in the inclination record are independant of variations in the water content.

Analysis of the results from the underlying sediments in core section D13 (figure 6-20) supports these conclusions, since the water content continues to rise, but the inclination record shows variations which are systemmatic yet independant of the variations in water content.

It is thus concluded that the sediments in core-section D12 show the process of fixation of a PDRM as illustrated by the correction of an initial inclination error.

Further crossplots were prepared, by plotting the percentage water content against the Koenigsberger ratio (Q-ratio) as shown in figures 6-21 and 6-22. In the plot for core-section D12 (figure 6-21) it is clear that despite a constantly decreasing water content, no increase in the Q-ratio is found until a critical water of less than 21% is reached. However, it is seen that a decrease in the water content after this point is marked by a decrease in the Q-ratio within core section D12. In core-section D13 (figure 6-22) the sediment shows variations in the Q-ratio which are now independant of the variations in the water content. It thus appears that the remanence has now become

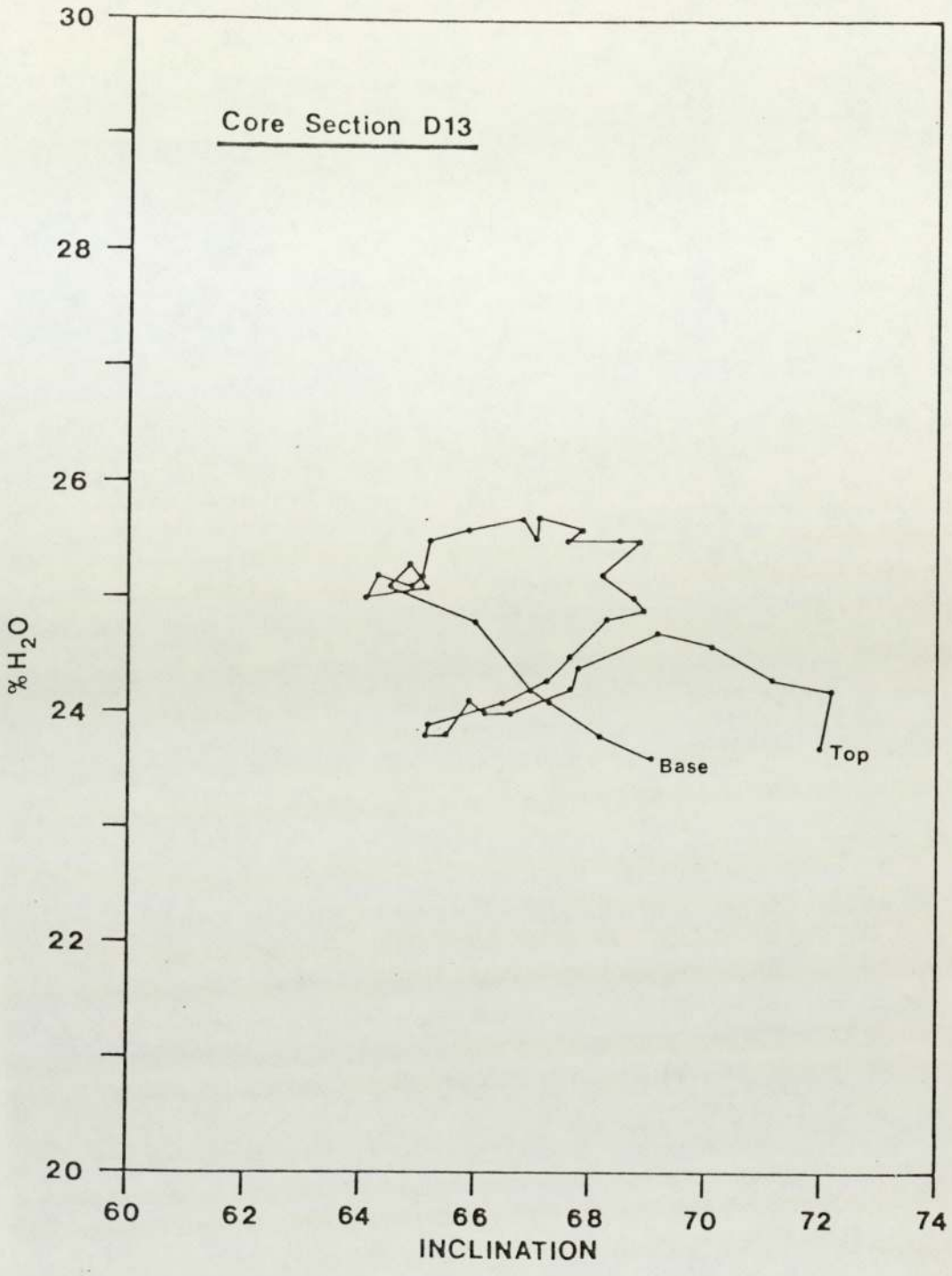


Figure 6-20. Percentage water content plotted against the inclination of the magnetic vector for core-section D13. The data have been subjected to a nine-term smoothing using a running mean.

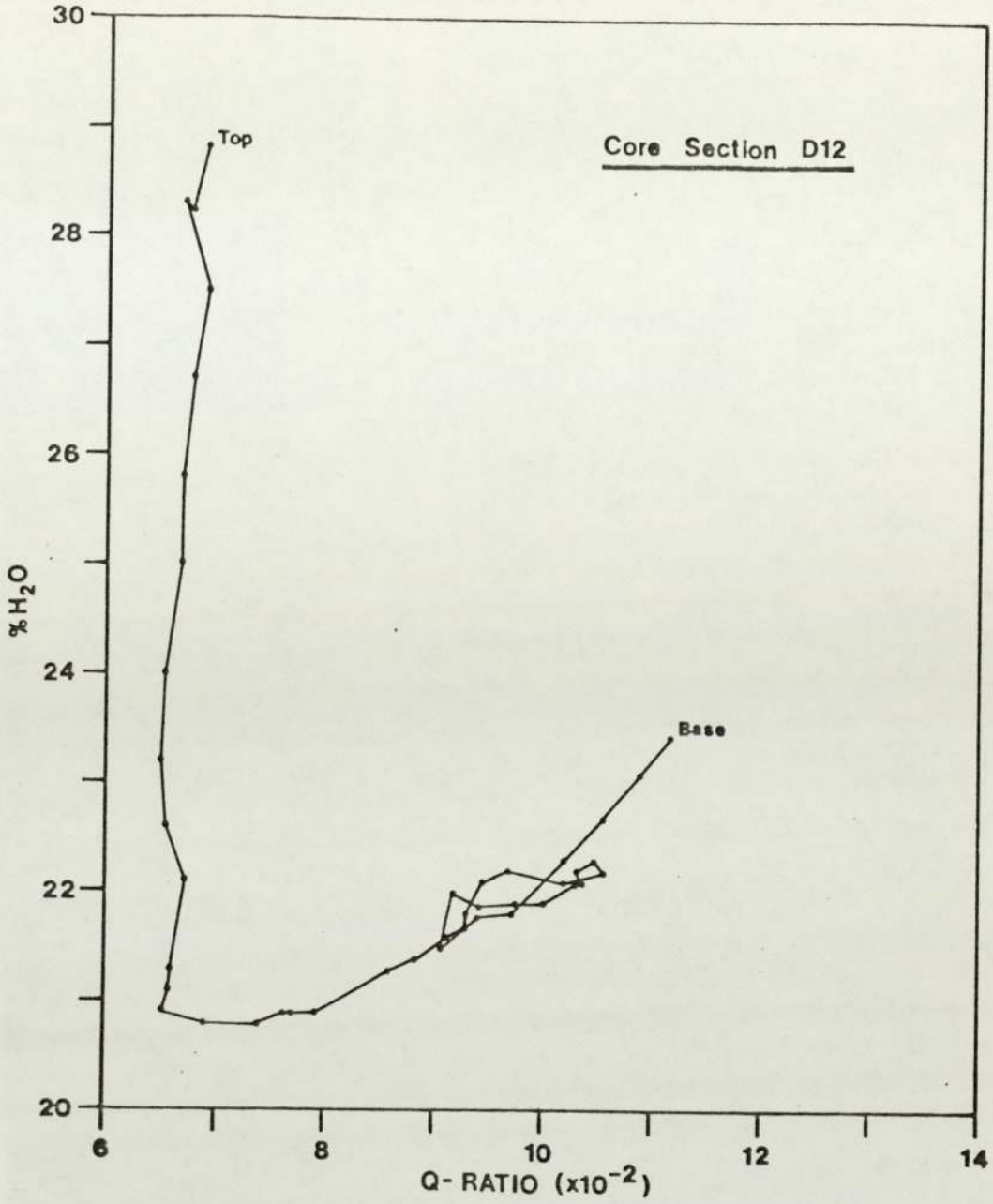


Figure 6-21. Percentage water content plotted against the Koenigsberger ratio (Q-ratio) for core-section D12. The data have been subjected to a nine-term running mean.

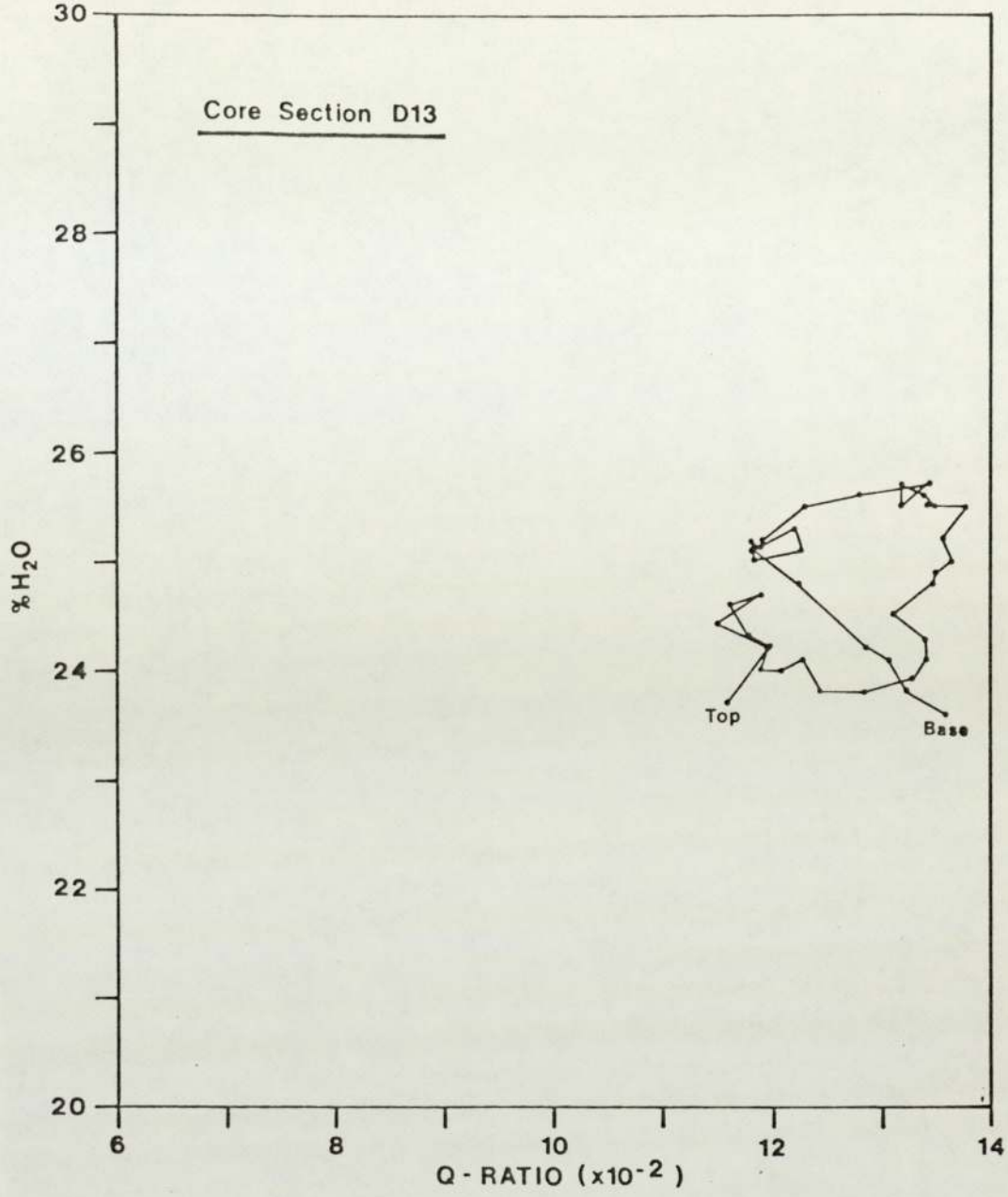


Figure 6-22. Percentage water content plotted against the Koenigsberger ratio for core-section D13. The data have been subjected to smoothing using a nine-term running mean.

fixed, and that no re-alignment of magnetic grains takes place as a result of further variations in the water content of the sediments.

The variations in the Q-ratio are also shown plotted against the measurements of inclination (figures 6-23 and 6-24). The interesting feature displayed by the results from the top of core-section D12 (figure 6-23) is that d spite a steadily steepening inclination, assumed to represent the period when the initial bedding error in inclination is corrected, there is no increase in the Q-ratio until the inclination has reached present-day values. Once a present-day value of inclination is reached, at $69.3^{\circ}$, the Q-ratio immediately starts to increase with depth. The Q-ratio then continues to increase from core-section D12 into core-section D13 (figures 6-23 and 6-24) where the highest Q-ratio of $13.8 \times 10^{-2}$ is reached. Variations in the inclination during this increase in Q-ratio do not appear to have a system atic relationship to variations in the Q-ratio.

Two final crossplots were prepared for the results from core-section D12. The first of these, shows the effect of plotting the ratio of inclination : water content against the Q-ratio (figure 6-25). Using the ratio of inclination (in degrees) and water content (as a percentage of the sediment) tends to smooth out variations caused by either of these variables and shows their joint relationship to variations in the Q-ratio. The major feature of this plot is the very sharp change from a steady Q-ratio to an increasing Q-ratio which occurs at the point at which it is thought that the magnetic remanence first begins to be 'fixed'. Prior to this point it seems that although the initial inclination error is being corrected there is no nett

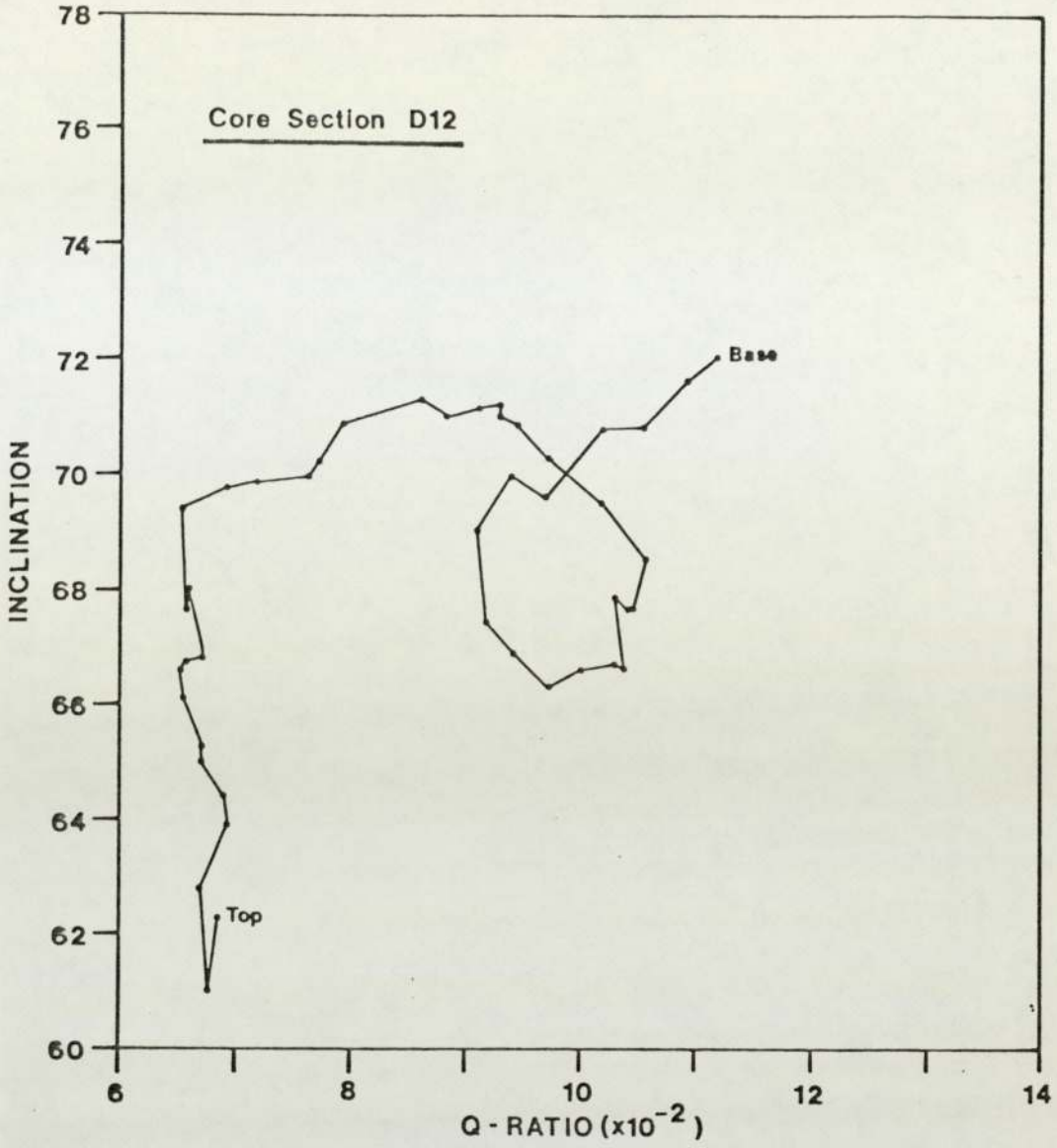


Figure 6-23. Inclination plotted against the Koenigsberger ratio for core-section D12. The data have been subjected to smoothing using a nine-term running mean.

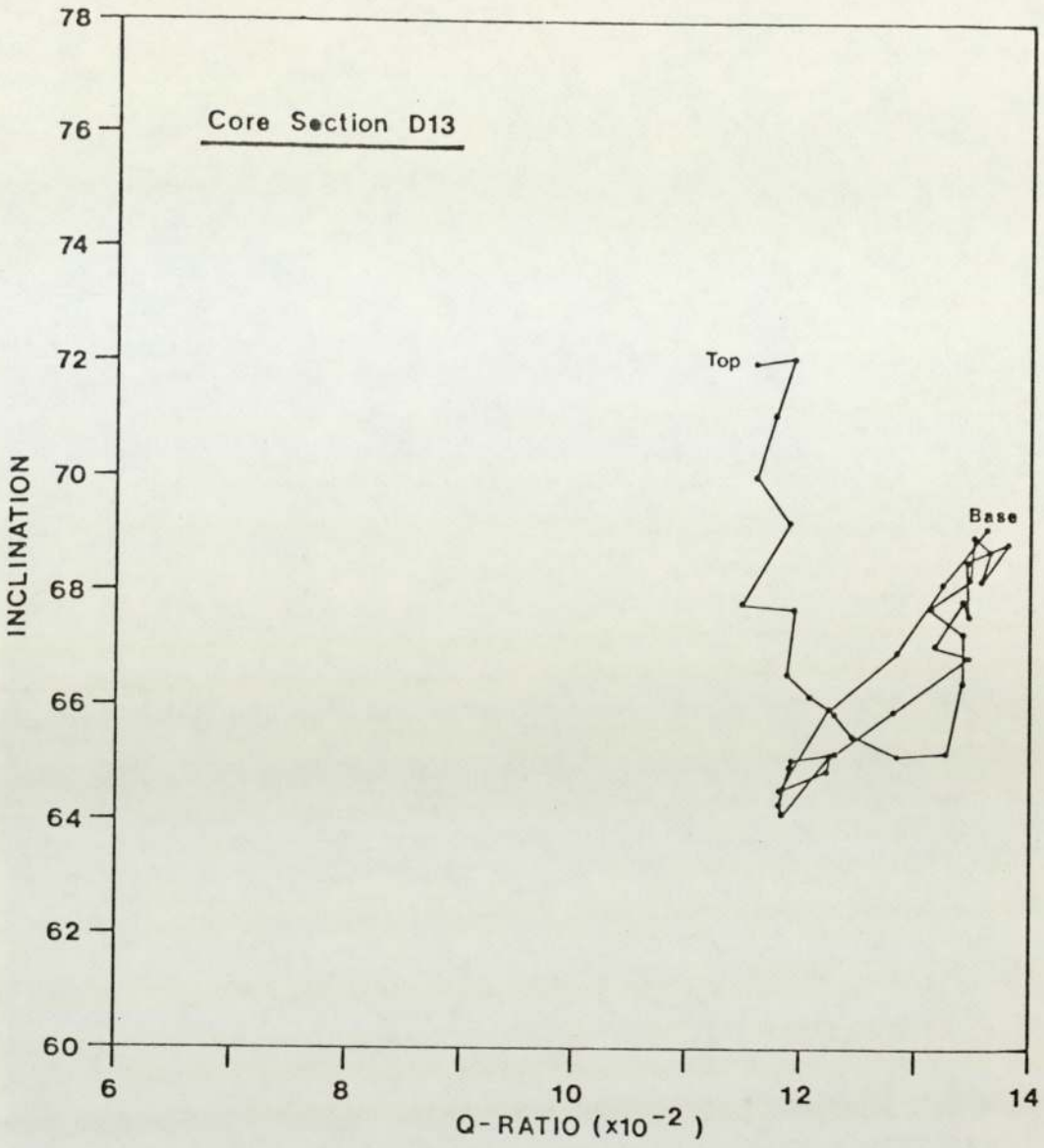


Figure 6-24. Inclination plotted against the Koenigsberger ratio for core-section D13. The data have been subjected to smoothing using a nine-term running mean.

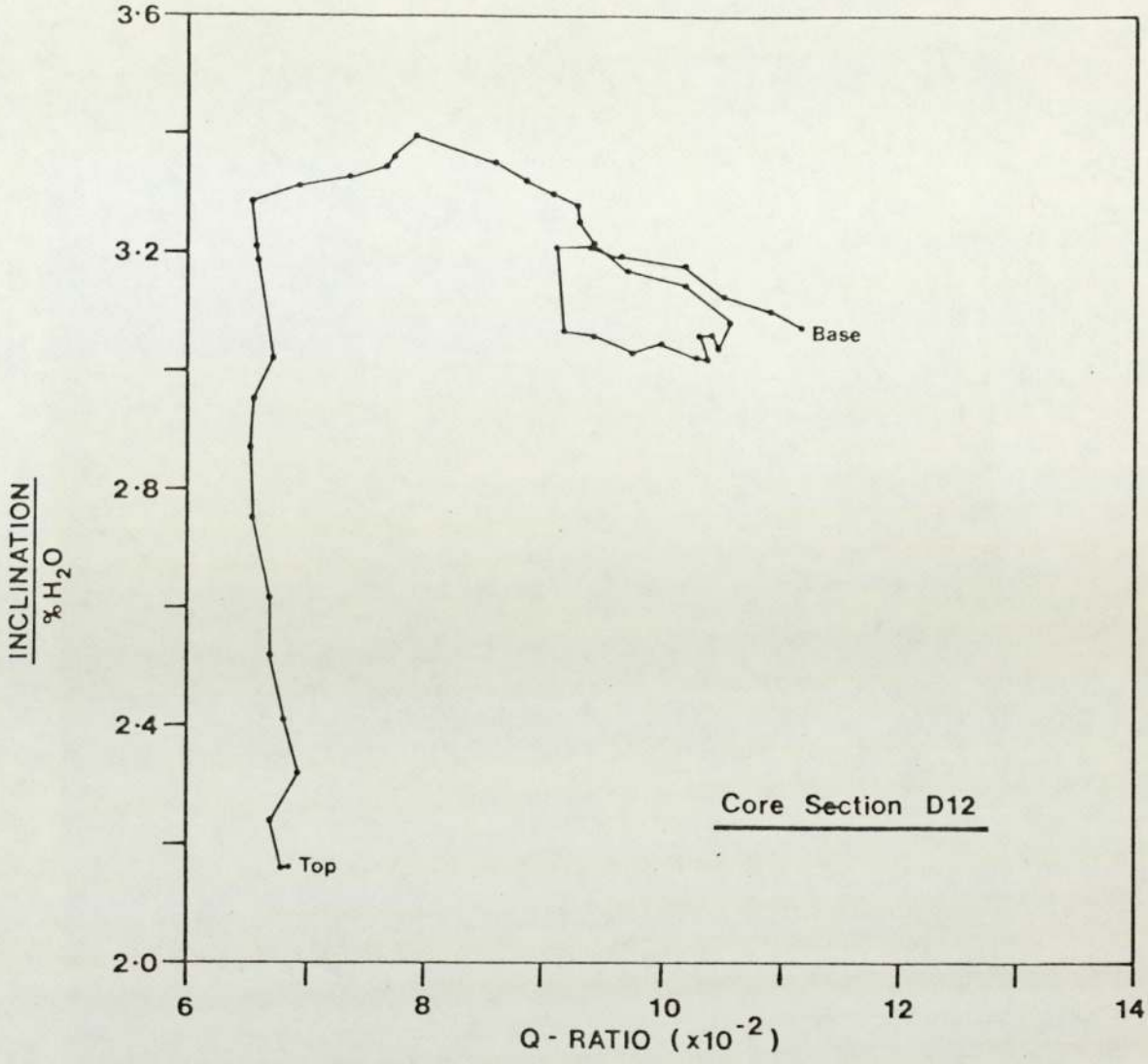


Figure 6-25. The ratio of inclination to percentage water content plotted against the Koenigsberger ratio for core-section D12. The data have been subjected to smoothing using a nine-term running mean.

increase in the degree of alignment of the magnetic grains. It thus appears that a significant proportion of the magnetic grains remain free to move in random directions prior to the point at which the Q-ratio begins to increase. These free grains may be smaller magnetic particles which are still free to rotate prior to some critical stage of compaction (represented here by sediments with an average water content of about 21%) which leads to their fixation. The fact that the process is a progressive one, supports this concept since with increased depth smaller and smaller magnetic grains would become fixed in position leading to a progressive increase in the Q-ratio.

Finally, a plot of the ratio of inclination to Q-ratio against the water content of the sediments (figure 6-26) is shown. This plot also shows the inflection point at about 21% water content where the remanence is interpreted to start becoming fixed.

In conclusion, measurements of the water content of the sediments from core D1 have been related to palaeomagnetic measurements. The results of these analyses show how measurements of the water content can be used to obtain an insight into the earliest stages of the acquisition of a stable post-depositional magnetic remanence.

From the accompanying crossplots, three stages of magnetization can be recognised (figure 6-27). The first stage occurs at the top of the sequence within the brown clay, where initial compaction and dewatering of the sediment leads to a steepening in the inclination, but no nett increase in the Q-ratio. In stage two, the Q-ratio increases as does the water content, however the inclination continues to show variations which appear to be

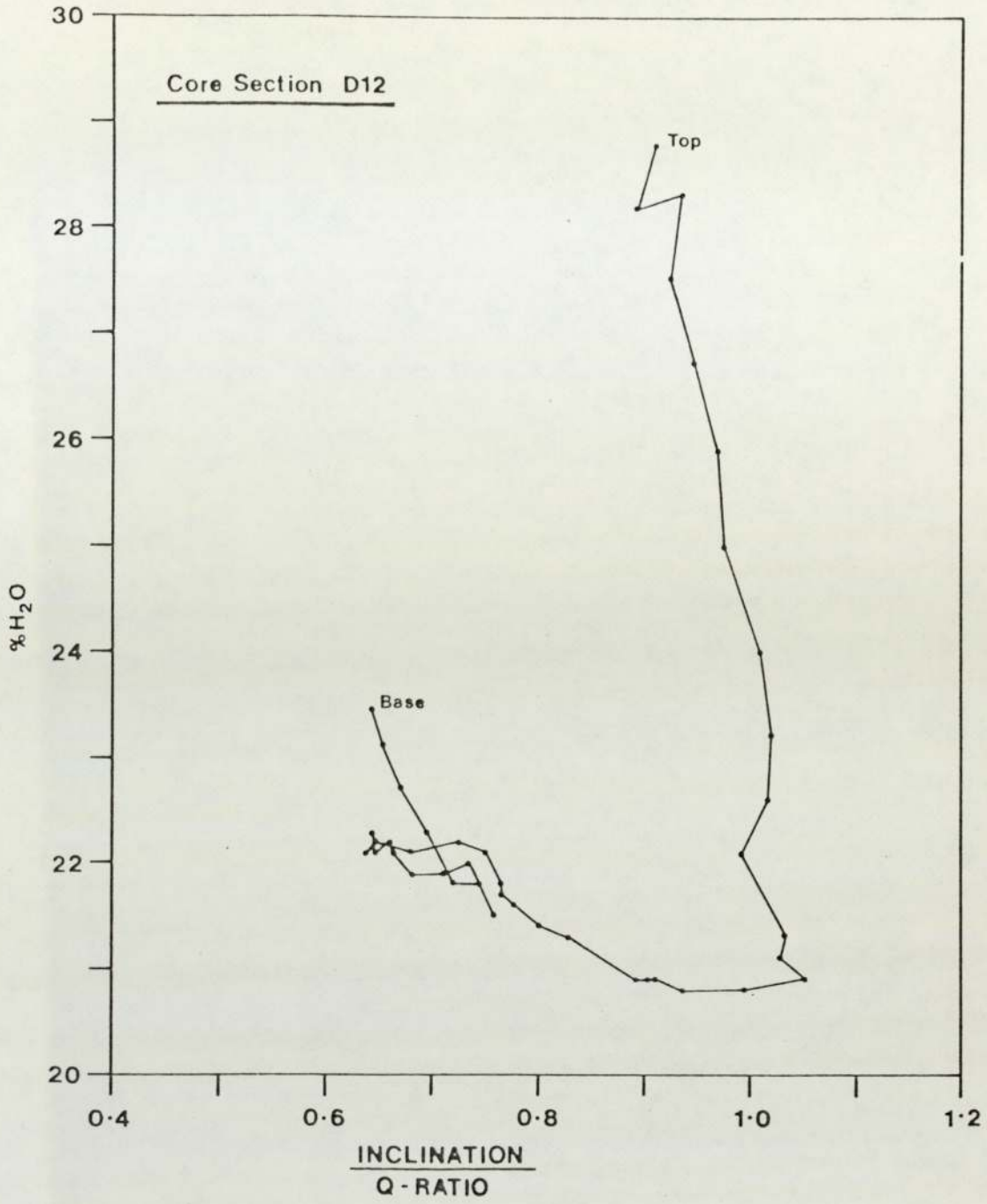


Figure 6-26. The percentage water content plotted against the ratio of the inclination to the Koenigsberger ratio for core-section D12. The data have been subjected to smoothing using a nine-term running mean.

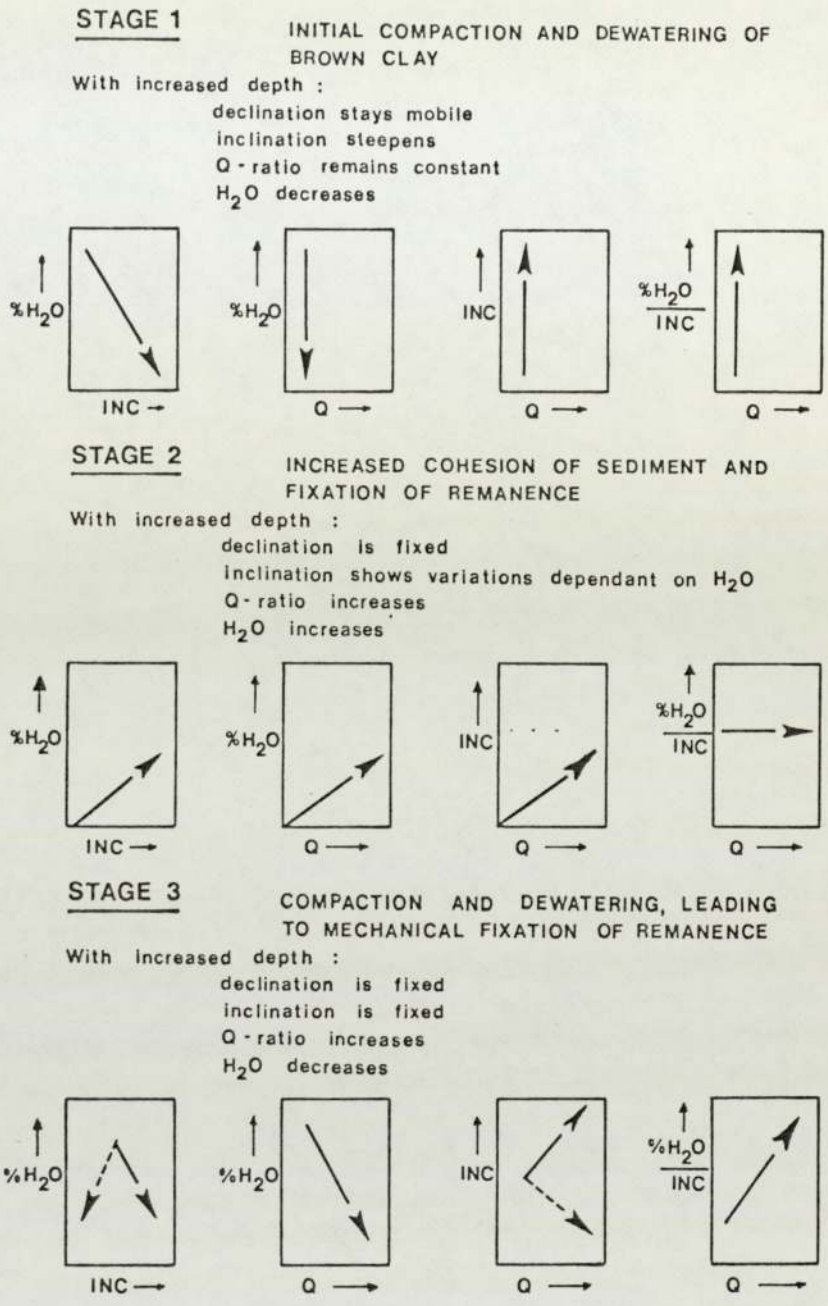


Figure 6-27. Diagram summarizing the major stages in the acquisition of PDRM in the recent tidal flat sediments from core D1.

dependant on the variations in water content. Declination values at this stage appear to have fully acquired the present-day magnetic field direction. Finally, in stage three, further compaction and dewatering, leads to a mechanical fixation of the remanence (both declination and inclination directions are being fixed in the sediment). The Q-ratio may still show an increase, but all magnetic variations are now independant of variations in the water content of the sediments.

As a result of this study, it is therefore recommended that in all further studies of the palaeomagnetism of unconsolidated sediments, the degree of compaction be measured directly, or indirectly by measuring the water content of the sediments, so as to be able to identify those sediments which are carrying a stable magnetic remanence. Such studies will also help to identify the processes involved in the acquisition of post-depositional magnetic remanence and also the point at which such magnetic remanence becomes fixed in the sediment.

6-2-6. Secular variation observed in Delft core D1.

The measurements of the declination and inclination of the magnetic vector in the samples from the Delft core have been subjected to smoothing using a nine-term running mean (sub section 6-2-3). Well defined oscillations in both declination and inclination occur (Figures 6-11, 6-12, 6-13 and 6-14). Measurements of the water content (Figure 6-21) show, when compared with palaeomagnetic data, that the remanence becomes fixed at a depth of about 30cms, giving a "lag", in the upper part of the core, between the palaeomagnetic age and true age of the sediments.

In order to date the sediments palaeomagnetically, the observed record must be compared with the known secular variation record for Great Britain. For the period 0-1000 years BP a well defined secular variation curve is available, derived from the data of Bauer (1897) and Aitken (1970). This record of the secular variation of the horizontal component of the geomagnetic field has proved useful in dating sediments by other workers (for example; Creer et al., 1976, Bishop, 1975, Mackereth, 1971). Such studies have mainly involved lacustrine deposits.

A more extensive master geomagnetic curve has recently been compiled for Great Britain (Thompson and Turner, 1979). The new geomagnetic curve (Thompson and Turner, 1979) covers the period 0-10000 years BP, and includes both declination and inclination curves. The curve has been established from a series of studies of lake sediments and shows 23 features which may be used for dating European sediments. The curve, in the upper section for the period 0-1000 years BP shows good agreement with the historic-archaeomagnetic curve of Aitken (1970).

Comparison of the results from Delft core D1 was first made with the curve of Aitken (1970) by drawing the secular variation curve of the declination at a variety of scales, to represent various time-depth ratios. Each curve was then compared with the two sets of data from the Delft core D1. Comparison here is made with only the odd data set, because of the similarity between the two data sets.

The best fit between the known secular variation record for the declination and the record for the odd data set from

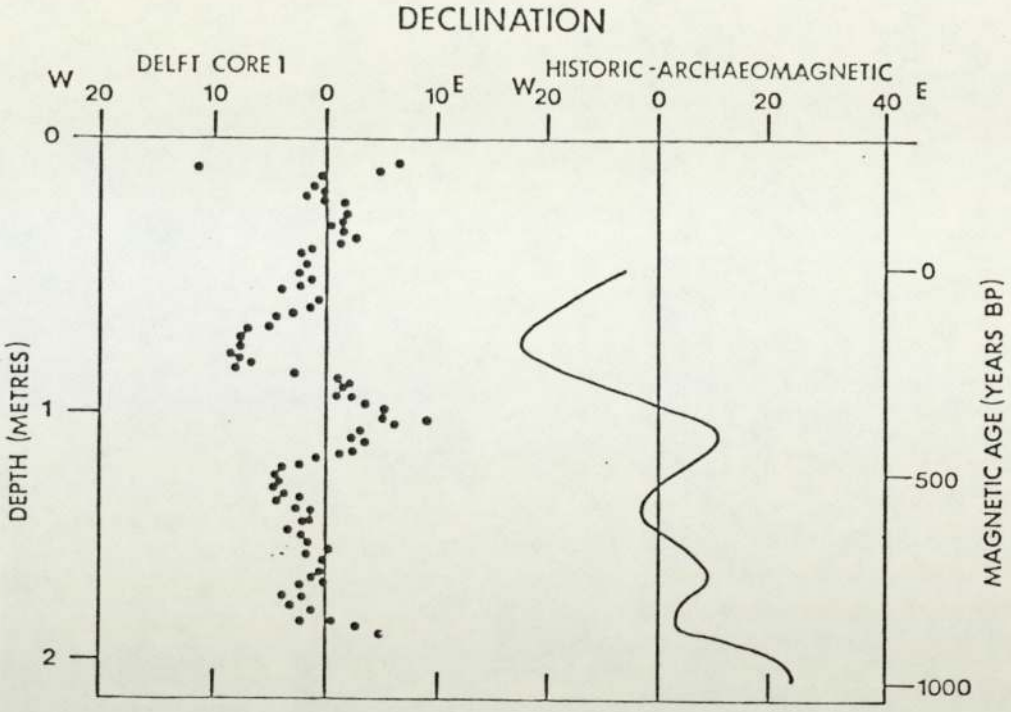


Figure 6-28. Comparison of the upper part of Delft core D1 with the historic-archaeomagnetic record of declination for the period 0 - 1000 years BP drawn for a sedimentation rate of 1.5mm/year. The data for the historic-archaeomagnetic curve are taken from Bauer (1897) and Aitken (1970).

core D1 for the period 0-1000 years BP is shown in figure 6-28. It can be seen from figure 6-28 that there is good agreement between the oscillations of the two sets of data. However, the amplitudes of the declination swings are approximately half of those observed in the historic - archaeomagnetic record. This may be a smoothing effect resulting from the long period during which a stable PDRM was being acquired. The decrease in the amplitude cannot be attributed to the processing of the data using the running mean smoothing program, since this results in only a 2-4% decrease in the amplitude of the swings.

The features represented in this section of core correspond to features a,b and c in the geomagnetic record of Thompson and Turner (1979). Attempts to fit the data from the lower seven metres of core D1 (figure 6-29) have proven unsuccessful because of the high noise level of the data below the higher mud flat sediments.

In addition, the record of inclination measurements for core D1 shows four well defined cycles in the upper two metres of core. The amplitude of these features is about $6^{\circ}$ and their wavelength is 0.45 metres, approximately equal to 300 years (using the dating achieved from declination measurements). There is no agreement with the inclination record shown in the geomagnetic record by Thompson and Turner (1979) and the data from core D1. The frequency of the features in the inclination record from the upper two metres of core suggests that these may be the high-frequency variations in inclination (Theillier, 1971) which have as yet eluded recognition in studies of recent sediments (Suttill, 1980a).

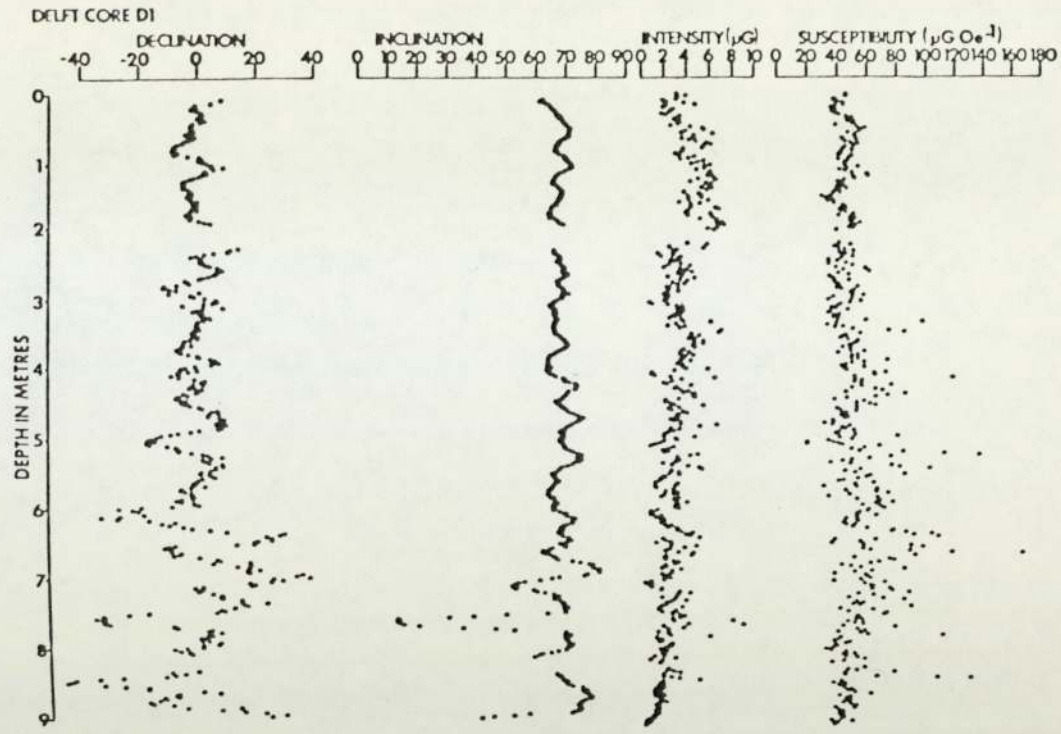


Figure 6-29. Complete declination, inclination, intensity of magnetization and magnetic susceptibility logs for the odd data set from core D1. The declination and inclination logs have been subjected to smoothing using a nine-term running mean. The intensity and susceptibility logs are unsmoothed.

Dating of the upper section of core gave a magnetic age of 1000 years BP at a depth of 2 metres in the core. The lag during which the PDRM was acquired is estimated at approximately 100 years (Suttill, 1980a) and therefore a true age for the base of the higher mud flat sediments is 1100 years BP. This date corresponds to the transition from deposition of the Arenicola sands to higher mud flat deposition. The present cycle of deposition in the Wash began after the Romano-British marine transgression dated at 2000 years BP (Godwin and Clifford, 1938). Therefore unit 3, the Arenicola sands, must have been deposited over a period of less than 900 years, as the base of the tidal flat sequence was not penetrated by the core.

6-2-7. Intensity of magnetization and magnetic susceptibility.

Measurements of the intensity of magnetization (corrected using the program INTCORRECT) and the magnetic susceptibility are shown in figure 6-29, together with the declination and inclination logs for the odd data set of core D1. The intensity and susceptibility logs have not been smoothed in this diagram. Variations of the intensity and susceptibility in the upper two metres of core have been discussed in relation to the studies of the acquisition of the NRM (subsection 6-2-5).

The intensity of magnetization shows a dependance on lithology. The clay at the top of the sequence, unit 1, shows intensities in the range 2-4 μG. Beneath the clays, the finely laminated silts and very fine sands, unit 2, have intensities in the range 3-7 μG. In the fine sands, unit 3, the Arenicola sands, there is a marked drop in the intensity of magnetization which is in the range 0.2 - 6μG, with minor measurements of upto 9μG.

These occasional high intensities correspond with the finely laminated black coloured laminations of clay in which it is suggested that ferrimagnetic greigite is contributing to the high intensities (section 7-9). The magnetic susceptibility shows little variation in the upper part of the core, but in the fine sands of unit 3, large variations are found. The highest values of susceptibility, in the range 90 - 168$\mu G Oe^{-1}$, correspond with the high intensity values and again it is suggested that authigenic greigite is contributing to the observed values.

6-2-8. Redeposition experiments.

Measurements of the variations in the magnetic properties of the one-metre cores as they dried showed important changes in their remanence as the water content decreased and the samples became friable. Studies of the water content in the samples from Delft core D1 also showed its effect on the early acquisition of the PDRM.

In addition to the above studies it was decided to further the understanding of these processes by conducting a series of redeposition experiments. The experiments were conducted in the ambient laboratory field, by depositing sediment into small plastic sample holders. The samples were deposited in beakers which allowed deposition through a column of water 150 mm deep. When deposition was complete the remaining water was siphoned away and the samples were left for 24 hours so that surface water would evaporate. Next the specimens were removed from the beakers and their remanence was measured immediately. The samples were next weighed (so that water content could be calculated). A series of eight redeposition experiments were conducted one

for each of eight grain-size fractions of the sediment. The sediment used was derived from core-section D13 of the Delft core D1.

The results of the experiments revealed a number of different conclusions. Firstly, measurement of the initial intensity of magnetization of each sediment sample was plotted (figure 6-30). The results show that the sediments in the range 0-38μm show the highest initial intensities, with a gradual decrease in the intensity as the grain-size increases.

Measurements of the magnetic susceptibility of the samples at the conclusion of the experiment shows a similar distribution, except that the sediments in the 38-53 μm grain size fraction are found to possess the highest values of $240\mu G0e^{-1}$. From this observation it can be concluded that the grain-size fraction 38 - 53 μm contains the largest concentration of "magnetic" material. Measurement of the grain-size- of the magnetite grains using the scanning electron microscope (Chapter 7) has shown that the mean grain-size of the magnetite is 53 μm, agreeing with the result obtained here.

After the ini tial measurements of the magnetic intensity half of the samples from each grain-size fraction were stored in the same field direction to that in which they had been deposited. The remaining samples were stored with their fiducial line (a horizontal axis pointing to magnetic north) pointing to the magnetic south pole, hence reversing the horizontal component of the field in which they were deposited.

Measurements of the natural remanence were then made over a period of approximately 20 days whilst the samples were allowed to dry out completely. Examples of the results of these experiments

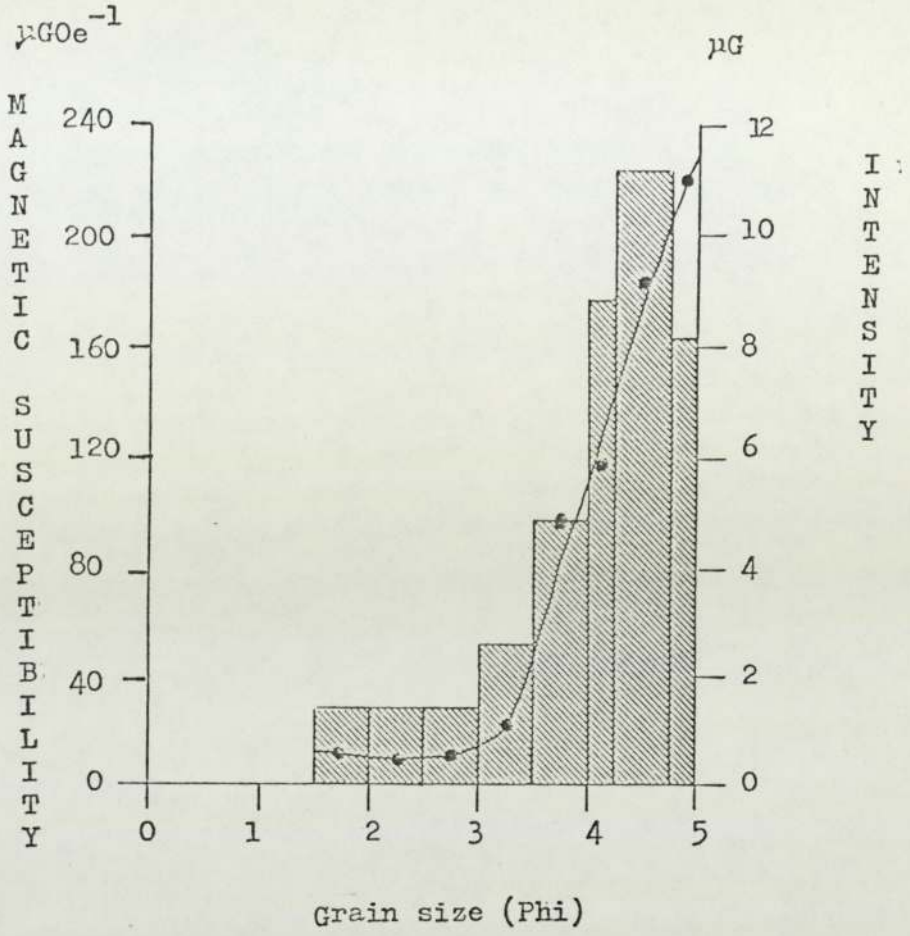


Figure 6-30. Magnetic intensity curve for the initial measurements of the samples of different grain sizes used in the redeposition experiments. The histogram shows the magnetic susceptibilities of the same samples.

are shown in figures 6-31, 6-32 and 6-33. Considering firstly, the results of the experiments in which the samples have been stored parallel to the field in which they were deposited, it is apparent that initially the samples show an increase in the intensity of magnetization. This stage is presumably caused by the addition of a PDRM to the existing depositional remanence. The magnitude of this increase is greatest in the coarser grained sediments which achieve $J/J_o$ values of up to 1.5 (figures 6-31, 6-32 and 6-33). In contrast the sediments of the finer fractions (below 90μm) show an initial decline in the intensity of magnetization followed by a more modest increase in intensity to a $J/J_o$ value of 1.2 (figure 6-31). The initial decline in intensity of these samples may be a function of minor randomisation of the NRM directions as a result of the spinning of the samples in the magnetometer.

Analysis of the directions of magnetization of the samples shows that there is no variation in the direction of the horizontal component of magnetization and only a minor increase in the vertical component, inclination.

Considering now the specimens which were stored with their field direction reversed. A different behaviour in the variations is shown by these specimens (figures 6-31, 6-32, and 6-33). Initially, all the samples show large declines in the intensity of magnetization which are often 50% of the intial intensities. Next a small amount of remanence is reacquired as the new field direction is taken up by the sample.

Directional changes in these specimens are quite small in the finer grained sediments, below 90μm, (figure 6-31), indicating the greater magnetic stability of the remanence in fine sediments.

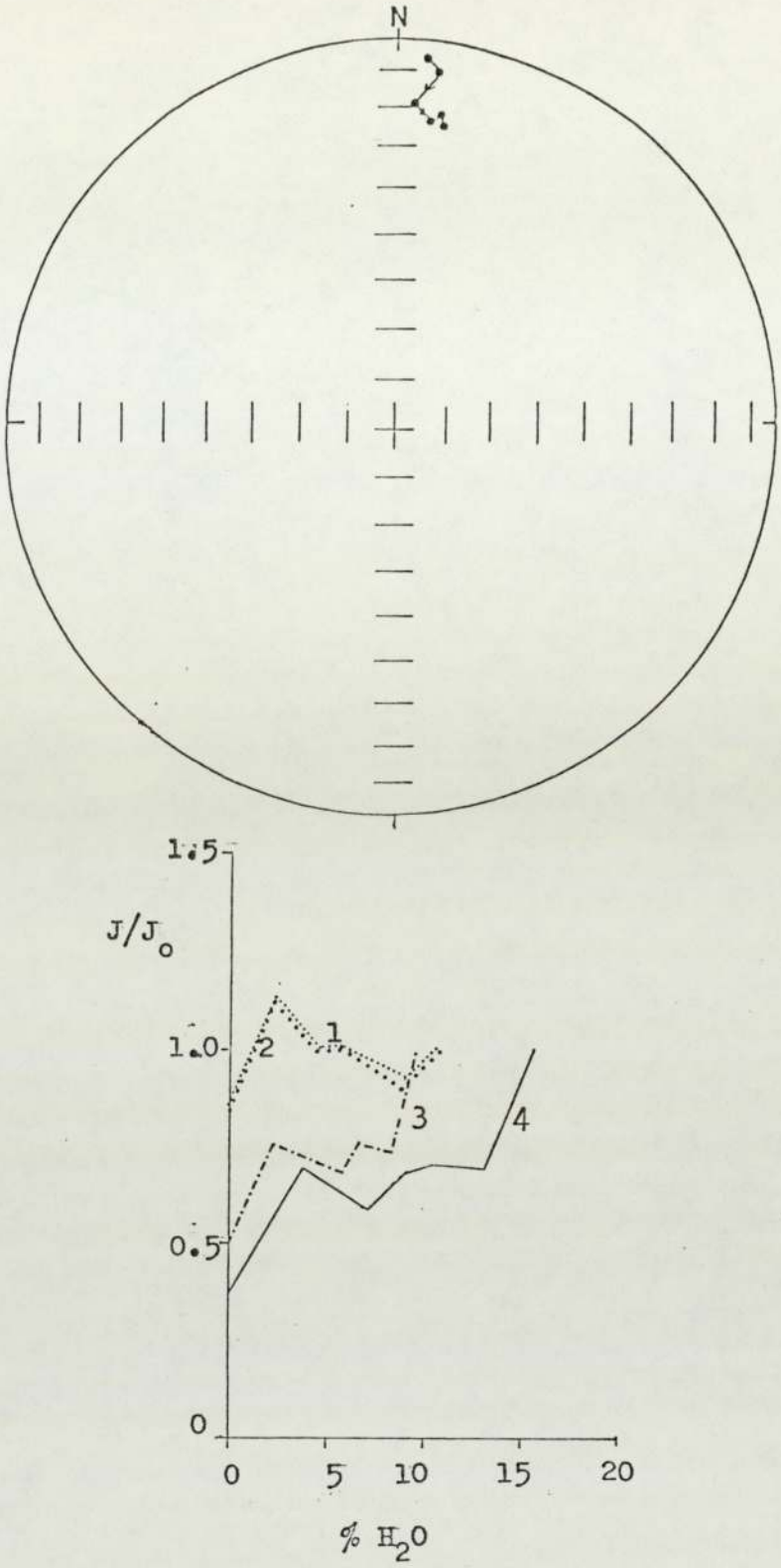


Figure 6-31. Results of the redeposition experiment with the 63-90 μm fraction of sediment. The stereonet shows the variations in direction of magnetization recorded by specimen 4. Specimens 1 and 2 were stored parallel to the field in which they were deposited. Specimens 3 and 4 were stored in a reversed field.

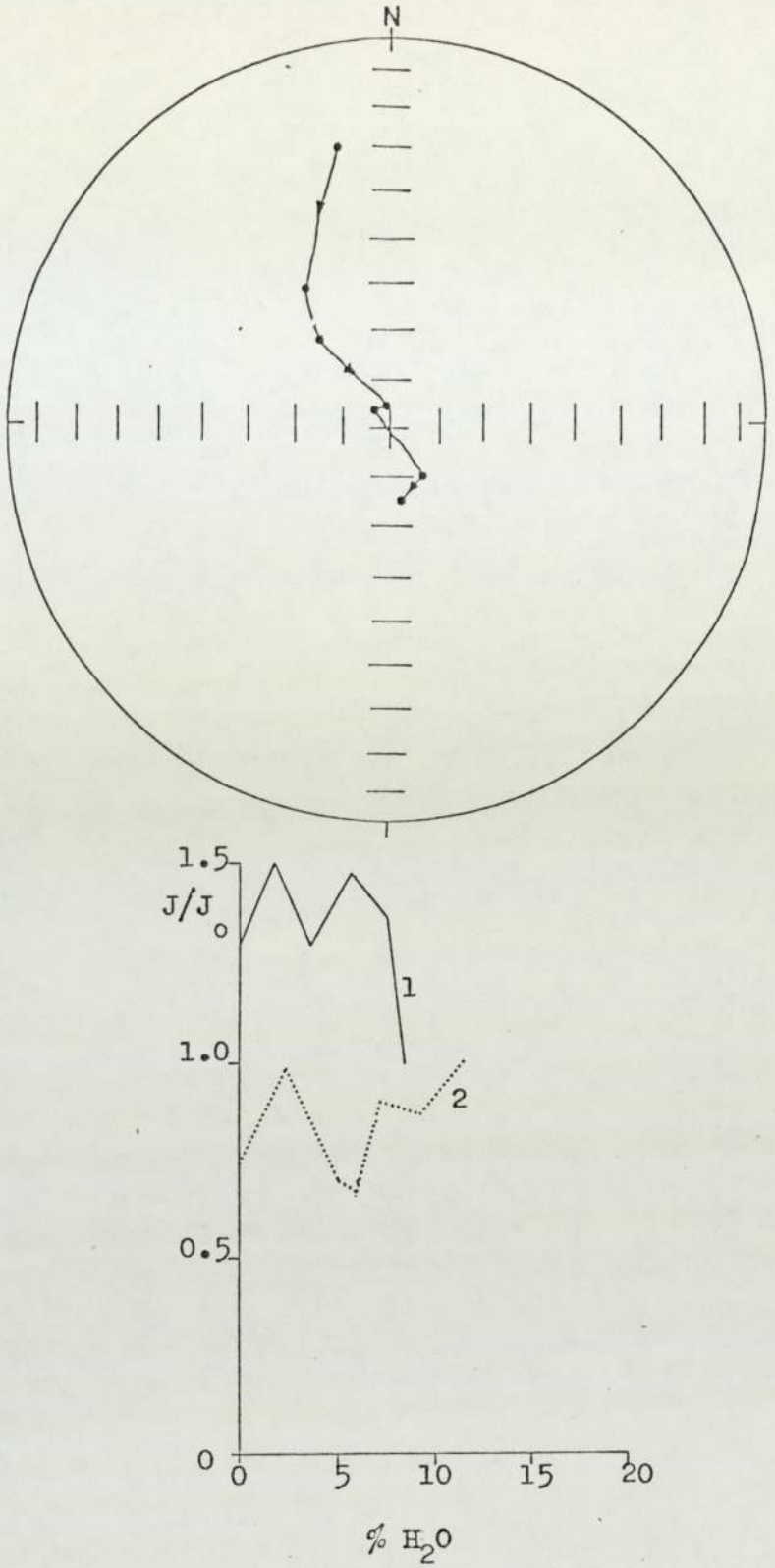


Figure 6-32. Results of the redeposition experiment with the 90-125 um fraction of sediment. The stereonet shows the variations in the direction of magnetization recorded by specimen 2. Specimen 1 was stored parallel to the field in which it was deposited. Specimen 2 was stored in a reversed field.

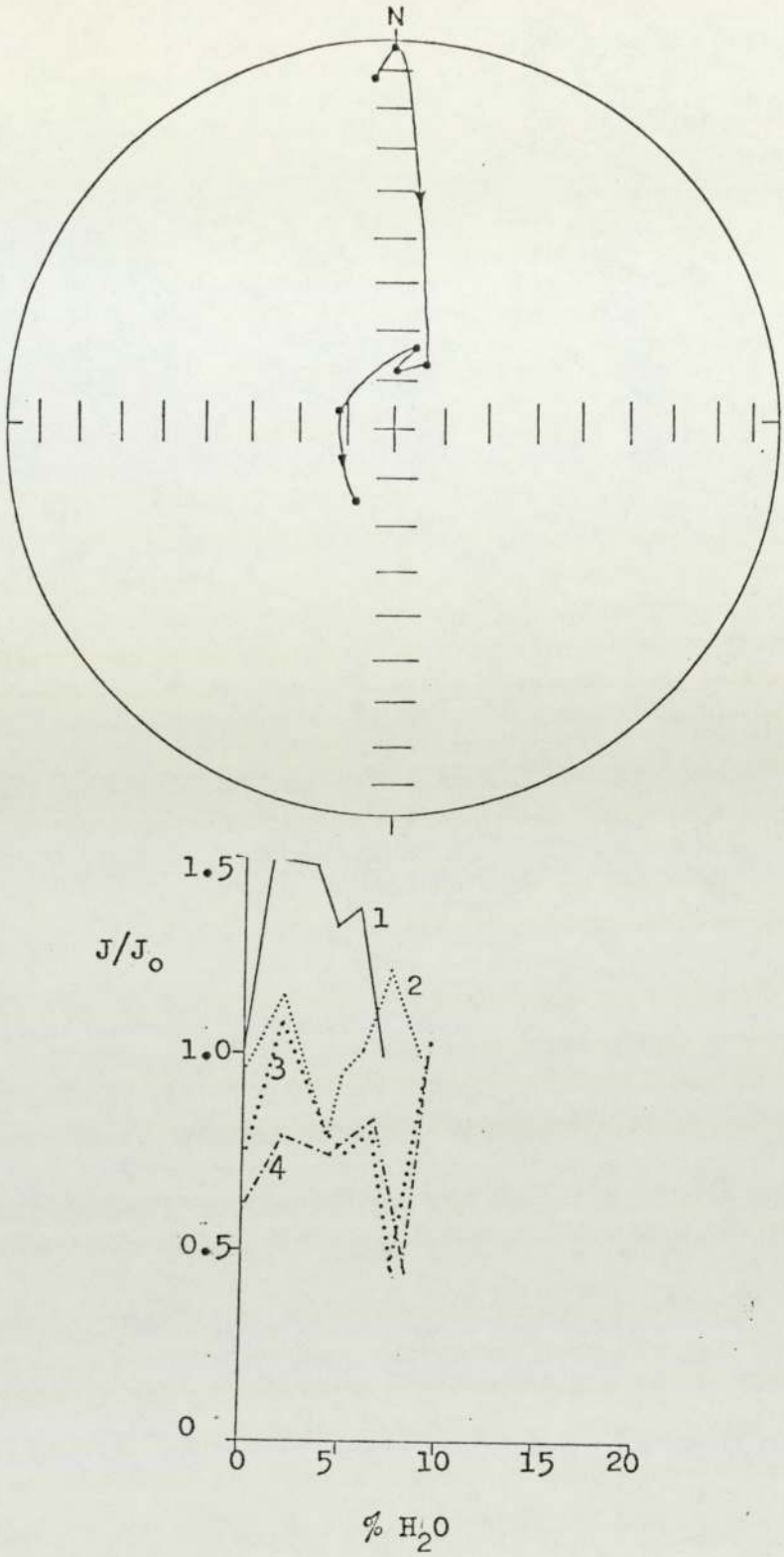


Figure 6–33. Results of the redeposition experiment with the 180–250 μm fraction of sediment. The stereonet shows the variations in the direction of magnetization recorded by specimen 3. Specimens 1 and 2 were stored parallel to the field in which they were deposited. Specimens 3 and 4 were stored in a reversed field.

In the coarser grained sediments the declinations are completely reversed (figures 6-32 and 6-33). Similarly large changes in the inclination component take place as the new field direction is acquired.

Perhaps the most important feature however, is the fact that all of the samples show a decline in their intensity of magnetization once the water content of the samples falls below 2-3% by weight irrespective of the grain-size of the sediments. This corresponds to the stage at which the sediments loose their mechanical integrity and become loose and friable. It thus appears that at low concentrations water plays a role in maintaining the integr ty of the samples probably through surface tensional and capilliary forces, and that when these are released, randomisation of the magnetic grains is more easily achieved and a part of the remanence of the samples is lost. This shows the importance of measuring natural unconsolidated sediments as soon as they are recovered from the field, before drying of the sediments takes place.

## 6-2-9. Magnetic susceptibility anisotropy.

Palaeomagnetic measurements of the one-metre cores from Freiston Shore show that the NRM contains a large bedding error (section 6-1). Studies of the magnetic anisotropy of sediment samples from Delft core D1 were therefore made in order to determine if a bedding error was important in these sediments.

The magnetic fabric of clastic sediments, represented by susceptibility anisotropy, has two structural elements. These are a near-horizontal magnetic foliation produced by elongate and flattened grains coming to rest in response to gravitational

forces, with their major axes as low as possible, and a magnetic lineation within the foliation plane, due to the preferred orientation of elongate grains subjected to tangential forces such as those of depositional currents (Rees and Frederick, 1974).

It is the magnetic lineation component that is considered to be the primary cause of the large bedding errors in the NRM, such as occur at Freiston Shore.

Measurements of the magnetic anisotropy were made using the equipment at the University of Newcastle upon Tyne (by F. Addison). The results of the analyses are found to display a distinct maxima, with the major axis running horizontally, east - west (figure 6-34). The intermediate axis is found to be almost vertical and the minor axis runs north - south horizontally.

From analysis of the specimen dimensions the results suggest a strong modifying effect caused by shape anistropy, with the major and minor anisotropy ellipsoid axes coinciding with the major and minor axes of the samples. However, since the vertical and east-west axes of the samples are of equal dimensions, the fact that the vertical direction is consistantly the intermediate axis of the magnetic anisotropy ellipsoid, suggests that the true magnetic anisotropy of the sample is also contributing to the resultant directions.

In order to test these results a study of the magnetic anisotropy of a series of five surface sediment samples was conducted. The samples were collected from five different locations, six samples being collected at each location. The locations of the samples were chosen to represent a series of different environments of deposition. The locations of the samples, at Leverton, are as follows; sample 1A the Arenicola sands, sample 1B

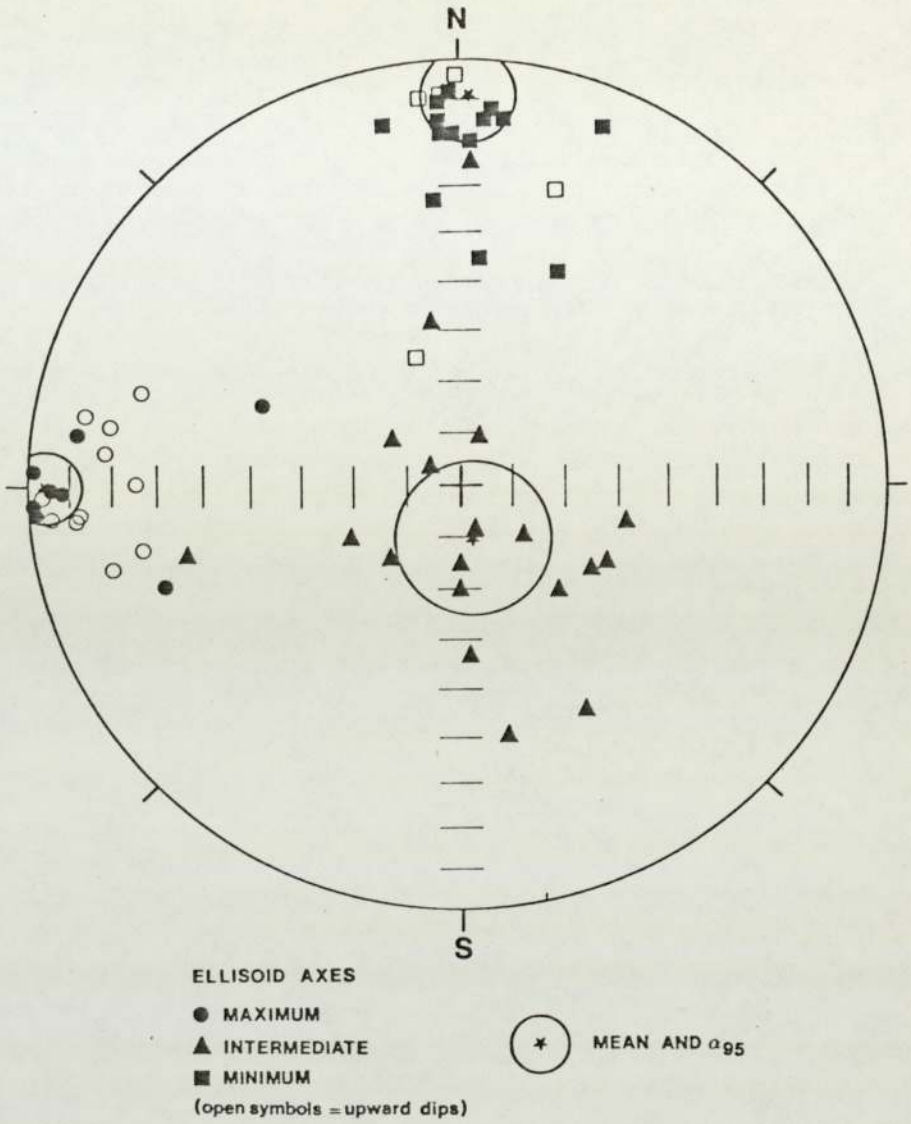


Figure 6-34. Stereographic projection showing the distribution of the magnetic anisotropy ellipsoid axes for samples from core D1.

20cm below the surface of the Arenicola sands, sample 2, surface of the strongly bioturbated Arenicola sands, sample 3, surface of the Arenicola sands near to its boundary with the higher mud flat and also near to a creek, and finally sample 4 was taken from the higher mud flat.

Sample orientations were changed from the orientation used in the cores, so that the minor axis of the sample was vertical and the major axes were horizontal. This was principally to facilitate sampling, but also served as a check, to compare with the results from core D1.

The results from location 1A (figure 6-35) show a vertical minor axis again suggesting a shape anisotropy effect. The maximum and intermediate axes lie in NE-SW and NW-SE orientations again suggesting correlation with the major axes of the sample. A strong shape effect is therefore still apparent in the results. A similar result to sample 1A was obtained from samples 1B, 2, and 4. However the results of the samples from locality 3 show major and intermediate axes lying horizontally N-S and E-W respectively (figure 6-38, compare with figures 6-35, 6-36, 6-37 and 6-39). It appears that the proximity of the creek to the sampling location has a modifying effect on the deposition and magnetic fabric of the sample which is sufficiently large to counter the shape anisotropy of the samples. The current direction of the creek is also indicated in figure 6-38.

Recalling the results of the declination measurements from the cores at Freiston Shore in which a large bedding error in the NRM was recorded, it is pertinent to note that at Freiston Shore the sampling locations were also in close proximity to a creek. It may therefore be concluded that the proximity of creeks has a

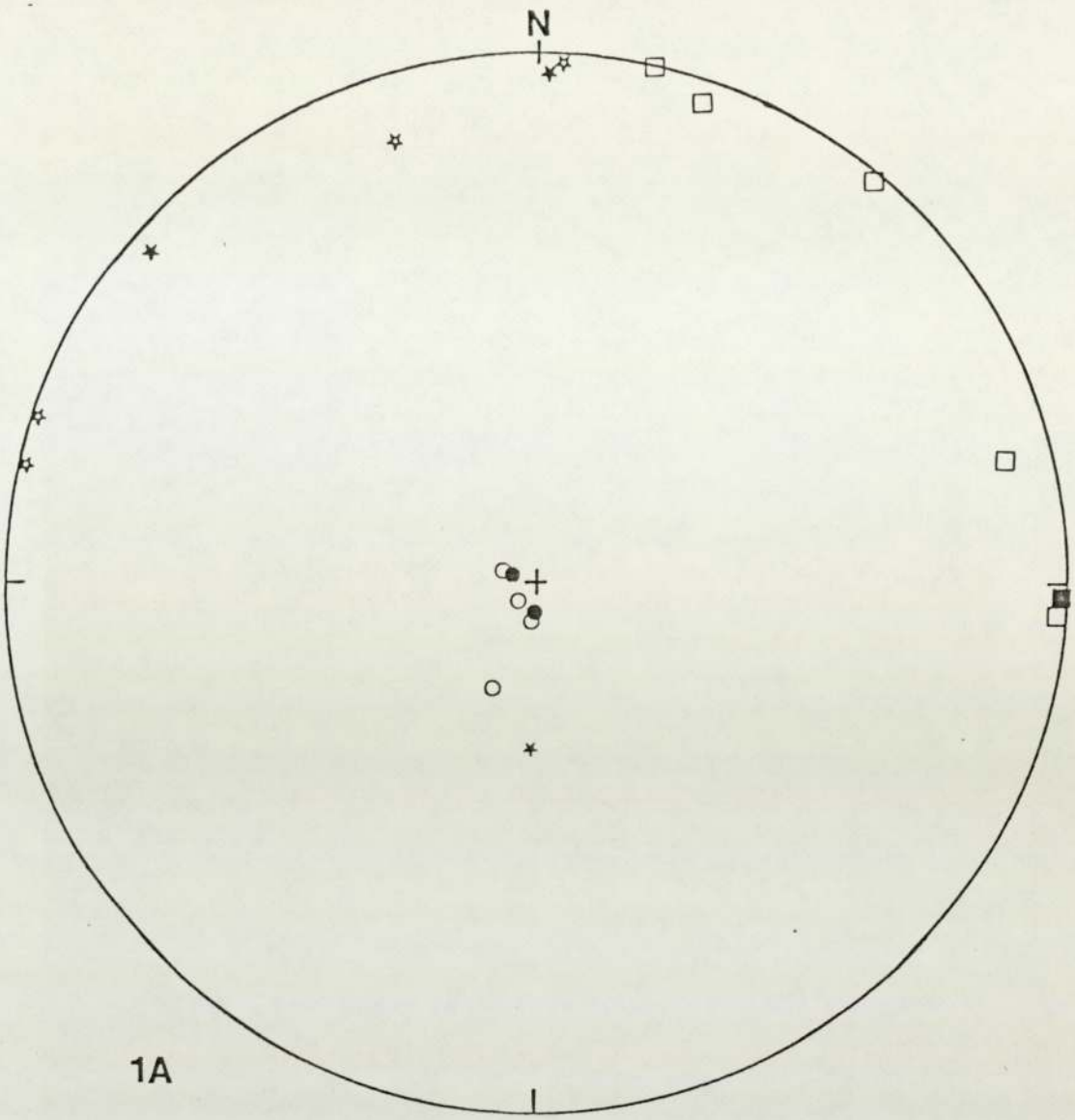


Figure 6-35. Stereographic projection showing the distribution of the magnetic anisotropy ellipsoid axes for samples from surface location 1A, at Leverton.

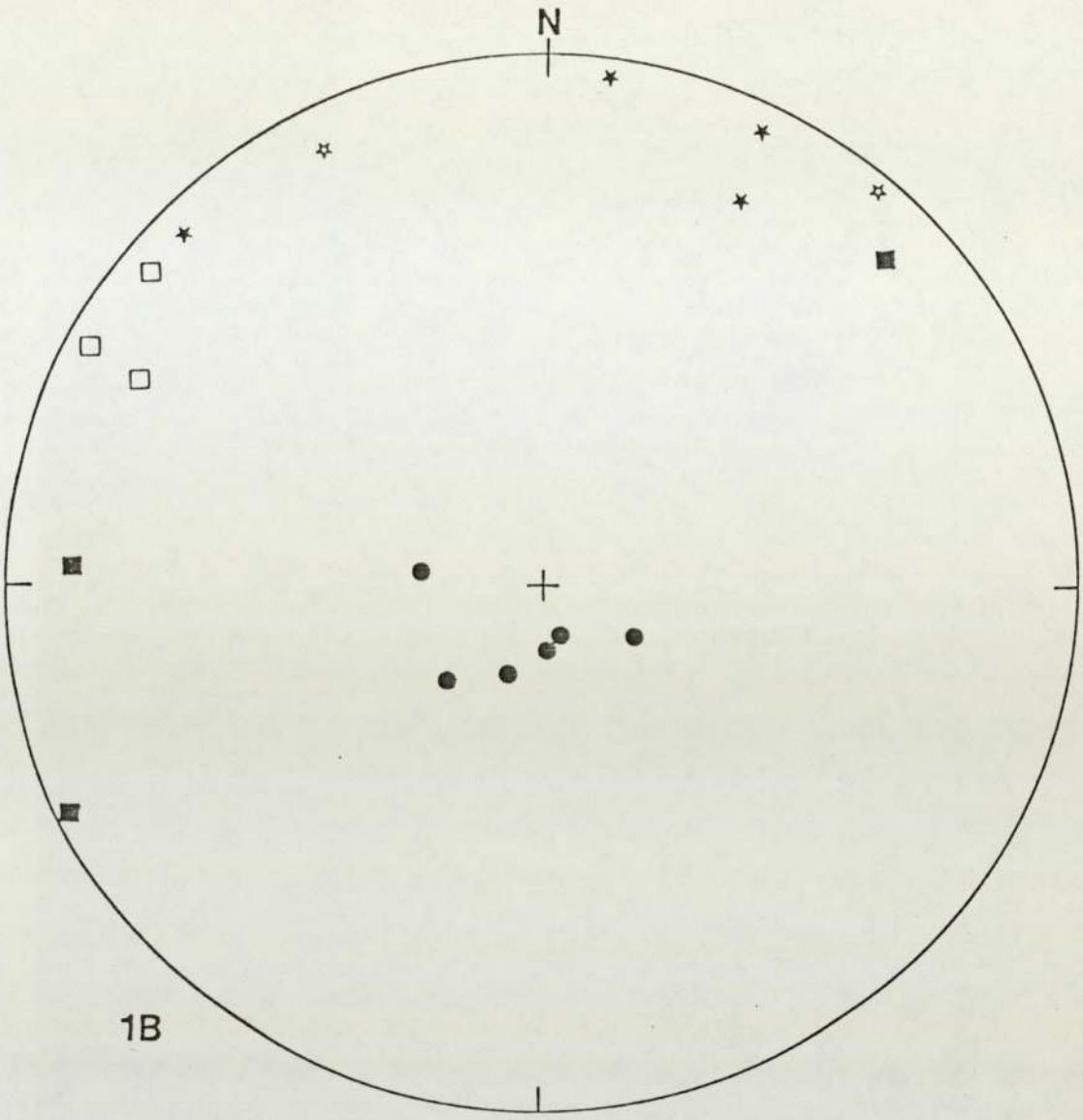


KEY AS FOR FIGURE 6-35.

Figure 6-36. Stereographic projection showing the distribution of the magnetic anisotropy ellipsoid axes for samples from location 1B, at Leverton.

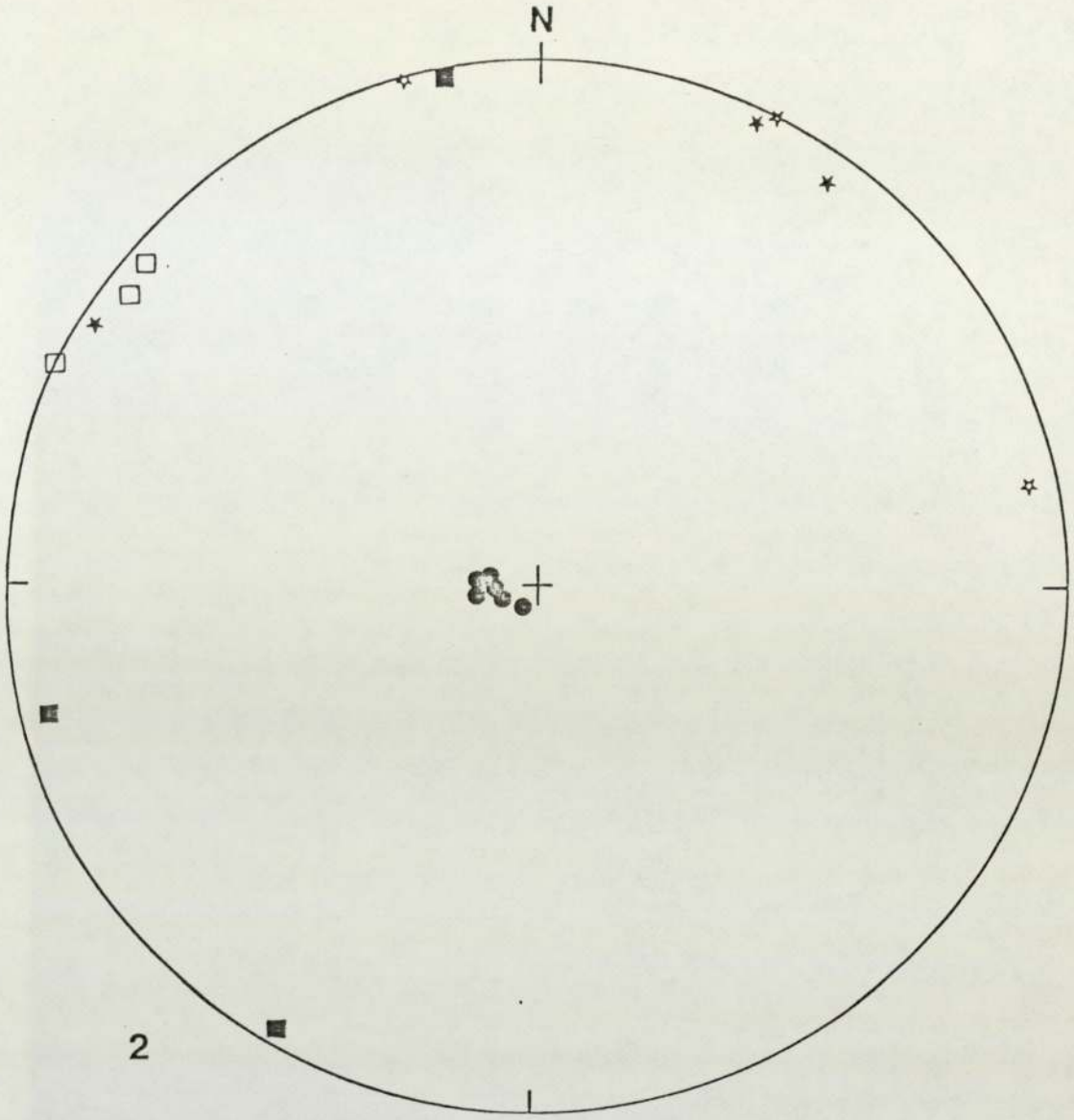


KEY AS FOR FIGURE 6-35.

Figure 6-37. Stereographic projection showing the distribution of the magnetic anisotropy ellipsoid axes for samples from location 2, at Leverton.

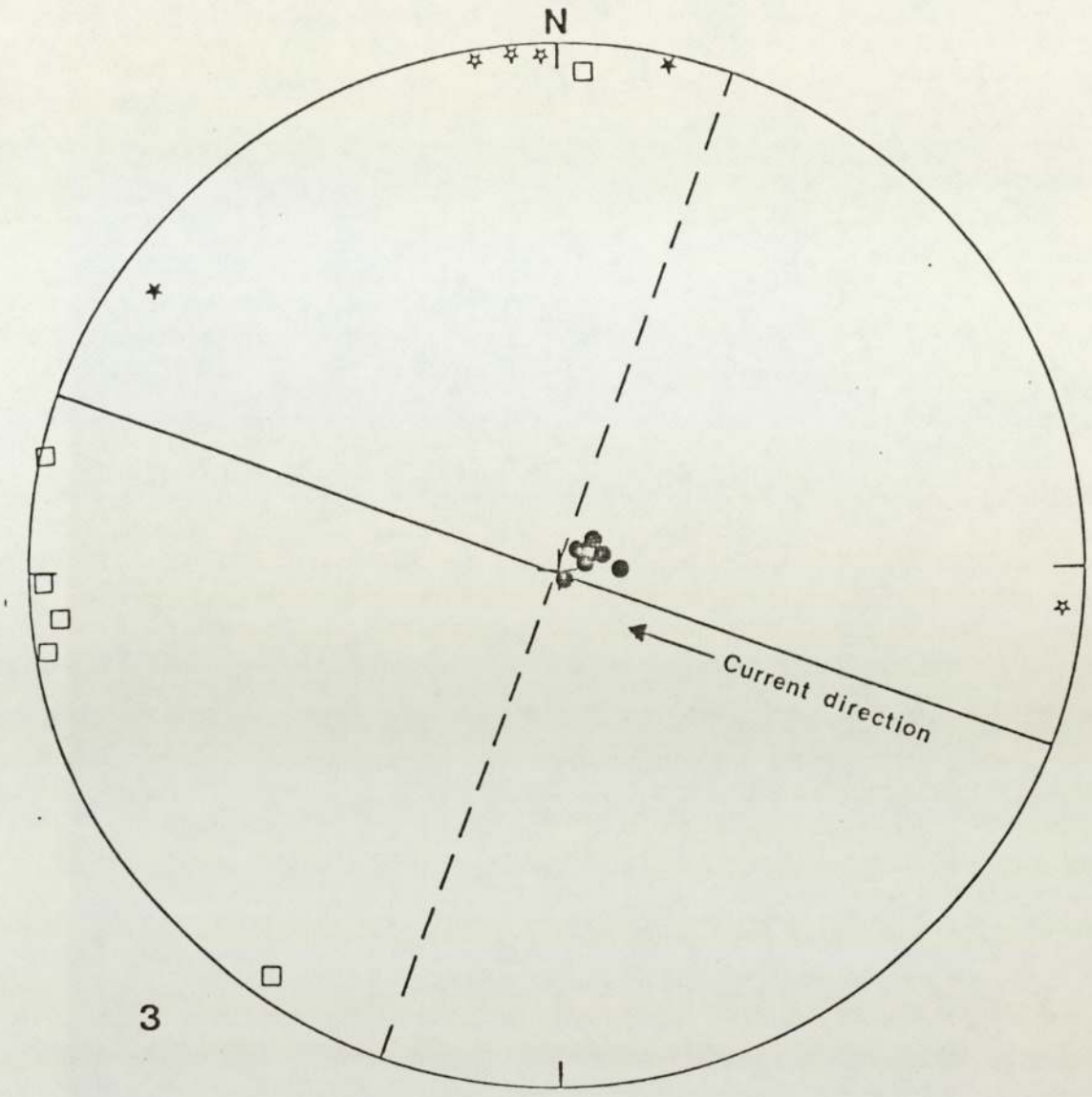


KEY AS FOR FIGURE 6-35.

Figure 6-38. Stereographic projection showing the distribution of the magnetic anisotropy ellipsoid axes for samples from location 3 at Leverton. The orientation of the current flow direction in a nearby creek is also shown.

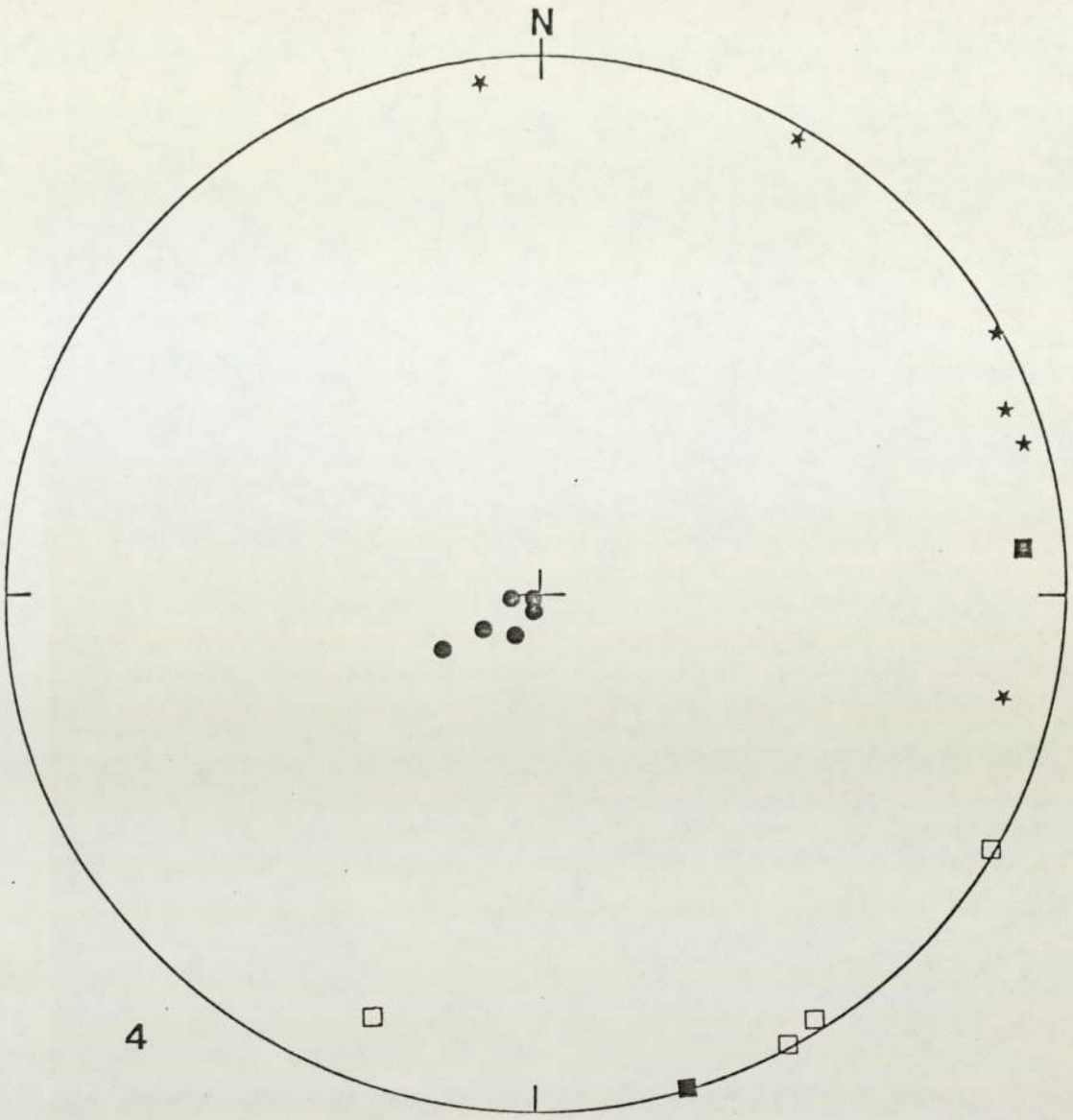


KEY AS FOR FIGURE 6-35.

Figure 6-39. Stereographic projection showing the distribution of the magnetic anisotropy ellipsoid axes for samples from location 4, at Leverton.

modifying effect on the surface sedimentation of the tidal flats which in turn can result in quite large bedding error in the NRM of the sediments and also large effects on the orientation of the magnetic anisotropy ellipsoid.

## 6-3. Applications of the Palaeomagnetic dating.

The study of the palaeomagnetic properties has shown that palaeomagnetic dating of recent tidal flat sediments is possible. The palaeomagnetic results from the various cores have shown that the most useful and successful results are obtained from studies of the salt-marsh and higher mud flat sediments.

Using the results of the dating from the Delft core D1 it is possible to show that the salt marsh and higher mud flat sediments have been deposited over a period of 1100 years. From the pairing of the historic-archaeomagnetic curve with the data from the core it is also apparent that sedimentation has occured at a fairly uniform rate throughout this period. Therefore it is possible to calculate an average rate for the salt marsh and higher mud flat sequence, the value obtained being 1.5 mm/yr, at Leverton.

The results for the Arenicola sand flats are of less use, but from the above discussion it is known that sedimentation of the Arenicola sands was complete by 1100 years BP. Tidal flat sedimentation in the Wash began after the Romano-British marine transgression, 2000 years BP (Godwin and Clifford, 1938). Therefore, since a complete tidal flat sequnce was not penetrated by the core, it can be concluded that the Arenicola sands must have been deposited over a period of less than 900 years. Hence, a much faster sedimentation rate must be implied for the period 2000 - 1100 years BP. An average rate greater than 7.7 mm/year is required in order to deposit the seven metres of sands (assuming a uniform sedimentation rate). The result of 7.7mm/year is in good agreement with the average sedimentation rate of the whole tidal flat, calculated by Amos (1974) to be 8mm/year.

The dating using palaeomagnetism may therefore be applied to calculating sedimentation rates, and also the dating of major sedimentological changes or events. For example in the Delft core it is possible to date the transition from Arenicola sand flat deposition to higher mud flat deposition, at 1100 years BP. The sharp break in sedimentation rates can be interpreted easily since deposition on the salt marsh and higher mud flat only takes place during high tides.

A feature of the palaeomagnetic results from below a depth of six metres in the Delft core worthy of note here is the greater scattering of the data, both for declination and inclination (figure 6-29). This lower part of the fine sands is also different from the sediments above in that it contains thin beds of broken shell fragments which indicate a higher energy depositional regime. It is possible that such a depositional regime could account for the greater variance in the magnetic results. Another possibility for the greater scatter is that the sediments at this depth are water saturated, probably also suffering diurnal water movements as a result of tidal movements. Such water movement would tend to randomise any remanence carried by the sediments.

The possibility of using the palaeomagnetic record to date diagenetic processes, such as the formation of pyrite may also be considered in the light of these results. By combining data from Mössbauer spectra, which illustrate increasing pyrite with depth, with the sedimentation rates obtained from magnetic dating, the rates of pyrite production may be estimated. It has been shown that the formation of pyrite is not purely dependant on the depth of burial, there is also a strong lithological control evidenced

by Mössbauer studies of freeze-dried samples and samples of differing lithology run at liquid nitrogen temperatures. However, there is a general trend for pyrite to increase with depth so that the outer to inner doublet ratios decrease from an approximate initial value of 1.17 to around 1.00 at a depth of around 5.00 metres, that is, in sediments deposited approximately 1500 years BP.

It can therefore be concluded, that palaeomagnetic dating of recent tidal flat sediments in addition to providing valuable data on the fluctuations in the geomagnetic field, may also be used in studies of the sedimentation rates of a large basin of deposition such as the Wash, and also may be used in determining the ages of diagenetic processes within them.

## 6-4. Conclusions.

Pilot studies of the palaeomagnetism of one-metre cores of sediment from Freiston Shore and Wrangle Flats show that successful palaeomagnetic results may be obtained from the tidal flat sediments of the Wash. This was found to be of post-depositional origin and therefore a lag-time must be added, representing the period of the acquisition of the PDRM, to the magnetic age in order to obtain the true age of the sediments.

A possible palaeomagnetic feature at a depth of 2.60 metres at Freiston Shore may be tentively identified as the swing in declination to the west which reached a peak value in 1820 AD (160 years BP). The date gives a sedimentation rate for the higher mud flats at Freiston Shore of 1.63 mm/year. From these studies it was decided to continue the study by obtaining greater sequences of sediments.

A study of coring techniques shows that the Delft corer is the best method available for the recovery of undisturbed cores on the tidal flat. Therefore the Delft corer was used to obtain two nine-metre cores from an area of recently reclaimed tidal flat at Leverton.

Palaeomagnetic results from one of these cores, core D1 confirms that good palaeomagnetic results can be obtained from the tidal flat sediments. Despite identifying the remanence to be of post-depositional origin, magnetic cleaning of the remanence was found not to be necessary. A strong lithological control on the magnetic properties of the sediments is also apparent. The most stable NRM is found in sediments belonging to the higher mud flats and to the salt marsh deposits.

Studies of the changes which occured in the magnetic direct-

ions of samples from one of the one-metre cores shows the importance of the water content of the samples in determining the stability of the natural remanence. It was therefore decided that in the study of the Delft core, all samples would have their water content determined. A series of plots were prepared to show the effect of compaction (as shown by decreasing water content) on the acquisition of a stable PDRM.

Palaeomagnetic dating of the Delft core D1 was successful in the upper two metres of core, representing the higher mud flat and salt marsh sediments. The base of the higher mud flat sediments can be dated with a magnetic age of 1000 years BP and a true age of 1100 years Bp. This gives a sedimentation rate for the higher mud flats and salt marsh deposits of 1.5 mm/year, at Leverton. This value is in close agreement with the value of 1.6 mm/year obtained for sediments from the same environment at Freiston Shore. Calculation of the sedimentation rate of the Arenicola sands in the lower seven metres of the core, shows a large increase in the sedimentation rate to greater than 7.7 mm/year. This figure shows good agreement with the average sedimentation rate for the tidal flats obtained using conventional methods (Amos, 1974) of 8 mm/year.

An important conclusion regarding the choice of sampling localities, in future palaeomagnetic studies of tidal flat sediments, is to avoid areas close to creeks. This is because sediments close to creeks have been found to possess large bedding errors in their declination records, as shown by the study of one-metre cores from Freiston Shore. These errors are not completely removed by the acquisition of PDRM. Further evidence of the effect the proximity of creeks has on the magnetic fabric

of the sediments has been achieved using studies of the magnetic anisotropy of samples of sediment recovered from the sediment surface close to a creek at Leverton.

Finally, it has been shown how the palaeomagnetic dating is of use in dating major sedimentological changes in the history of the sediments and also how the dating may be used to date diagenetic events in the sediments.

## Chapter 7. Rock Magnetism.

### Introduction.

In all palaeomagnetic studies of sediments and sedimentary rocks it is important to identify the magnetic minerals so that correct interpretations of the behaviour of the sediments when subjected to various palaeomagnetic experiments can be made. In the sediments from the tidal flats of the Wash it was assumed that the magnetic minerals would be derived from both detrital origins and also some authigenic minerals, associated with the early diagenesis of iron sulphides, would be present. Hence, experiments were designed to attempt to identify both of these contributions.

There have been numerous detailed studies of other Recent sediments, such as deep sea, lacustrine or glacial deposits (Creer et al., 1972; Creer et al., 1979; Thompson, 1977; Verosub, 1977; Kent and Lowrie, 1974) which have shown that "magnetite" (more correctly the various titanomagnetites and their oxidized equivalents, the titanomaghemites) of detrital origin, is the principal magnetic phase present. Some of the observations presented here have been discussed in Suttill et al., (1982) which is thought to be the first detailed study of the magnetic mineralogy of tidal flat sediments.

### 7-1. Techniques and experiments used in mineral identification.

Two methods of analysis were used in order to attempt to identify the magnetic minerals of the sediments. The first set of experiments, were palaeomagnetic experiments which collectively have the advantage of being relatively quick to perform and also preserve the specimens for the later, second series of analyses.

This second group of analyses were based on more conventional mineralogical observations of the specimens.

The first group of palaeomagnetic experiments included the use of IRM (isothermal remanent magnetization) acquisition curves to differentiate between heamatite and magnetite. The Lowrie - Fuller test was also used to determine if the magnetic grains were single, pseudo-single or multidomain. Low temperature magnetic transitions, observed by recording the variations in magnetic susceptibility which occur as a sample is heated from very low temperatures, w ere used to support the evidence of IRM acquisition curves. Also observation of the variations in the bulk susceptibility have been used to indicate variations in the total ferromagnetic mineral component.

The second group of observations consist of mineralogical data. The methods used include the following; Mössbauer spectroscopy, to identify the magnetic minerals in both magnetic concentrates and in samples of the natural (unconcentrated) sediment; X-ray diffraction of the mineral concentrates to confirm identification by Mössbauer spectroscopy; Reflected light microscopy to give evidence regarding grain shape, alteration, and compositional variation; and finally, the scanning electron microscope (SEM) was used to determine the morphology of the magnetic grains and also their size. A further advantage of using the SEM was that the availability of an edax (energy dispersive X-ray analysis) attachment meant that the chemical composition of the various magnetic grains could be determined semi-quantitatively.

7-2. Isothermal remanent magnetization (IRM)acquisition curves.

A simple rock magnetic experiment frequently used for the identification of remanence carriers and which may be applied to unconsolidated sediments involves the application of an isothermal remanent magnetization (IRM). The method used here (conducted at the University of Newcastle upon Tyne) involves the application of a DC field to the specimen in a stepwise manner involving an increase in the field from 0 - 7.6 KOe. The remanence of the specimen is measured immediately after subjecting it to the DC field.

Four specimens from core-section D12 were used. Three of these samples (D12.09,D12.77, and D12.79) show a large increase in the IRM intensity (figure 7-1) upto 1 x $10^{-3}$G, but do not saturate completely in fields upto 7.6 KOe. This large increase and near saturation suggests the presence of magnetite (Dunlop, 1972) and the failure of the specimens to saturate suggests the presence of a small amount of "hard" magnetic material (haematite or goethite) which may have formed in situ during sample oxidation (eg. from pyrite). These results do not preclude the presence of greigite, since, its magnetization characteristics are expected to be similar to those of magnetite.

The fourth specimen (D12.07) shows a slower initial rise in intensity and also does not saturate completely in fields upto 7.6 KOe, probably indicating the presence of a higher proportion of the "hard" magnetic material (haematite or goethite).

7-3. The Lowrie - Fuller Test.

Various methods have been used in this study to determine the grain-size of the magnetite in the tidal flat sediments, since

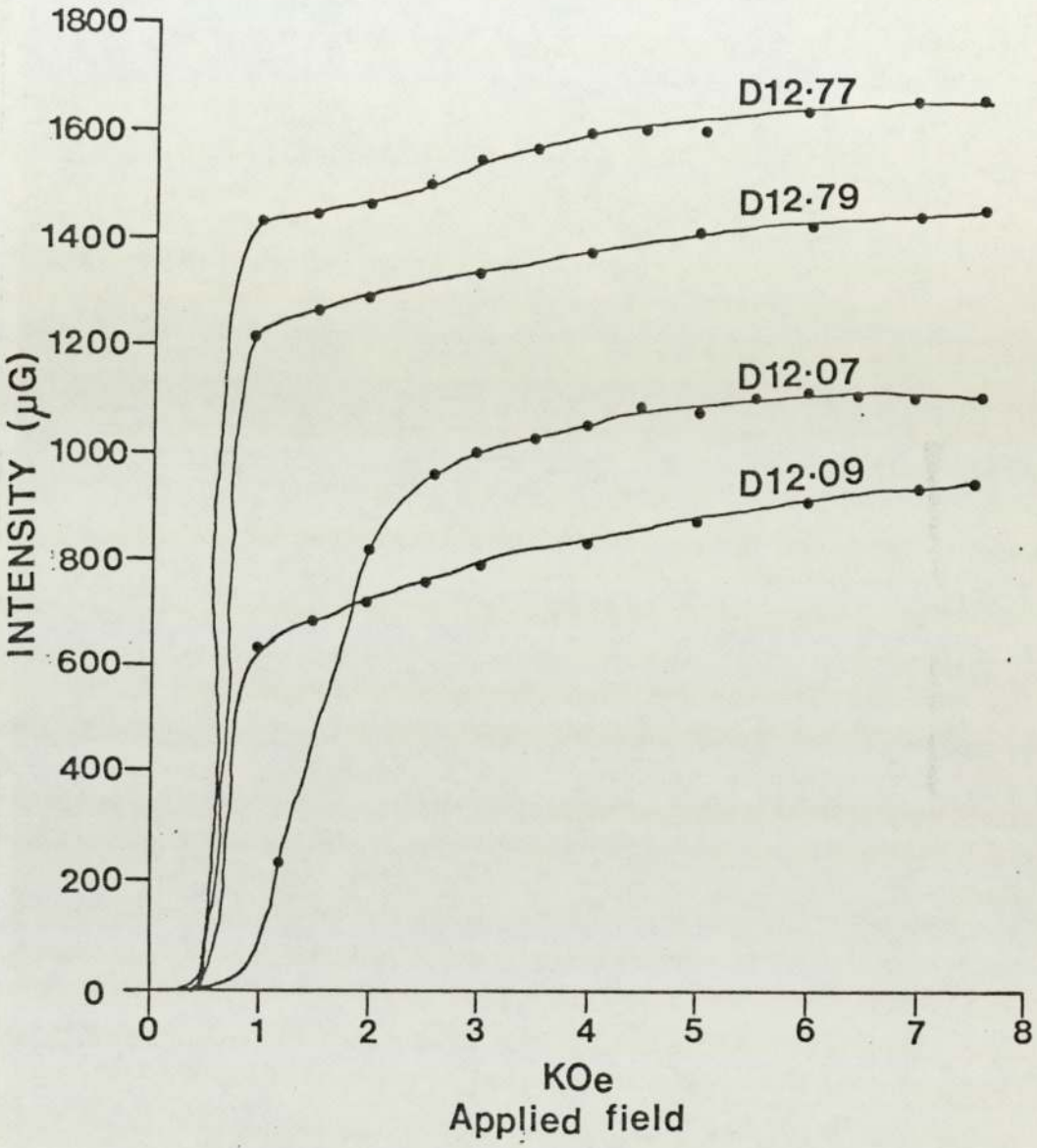


Figure 7-1. Isothermal remanent magnetization curves for specimens D12.07, D12.09, D12.77 and D12.79.

this is a crucial variable in the acquisition of PDRM by unconsolidated sediments. A rock magnetic method which enables the distinction of single or pseudo-single domain (PSD) from multidomain magnetite is the Lowrie - Fuller test (Lowrie and Fuller, 1967) which compares the alternating field (AF) demagnetization curves of the thermoremanent magnetization (TRM) and IRM of a particular sample. This test has been modified by McElhinney and Opdyke (1973) who used an anhysteretic remanent magnetization (ARM) (which is approximately equivalent to TRM, Stephenson and Collinson, 1974) in order to avoid the problem of chemical changes during heating.

In multidomain magnetite, the IRM is softer than the ARM and, typically both show concave upwards AF demagnetization curves. The result of the modified Lowrie - Fuller test on specimen D12.77 (conducted at the University of Newcastle upon Tyne) strongly suggests the presence of multidomain magnetite (figure 7-2). The intersection of the NRM and IRM demagnetization curves at 240 Oe could be due to a small amount of PSD magnetite (Johnson et al., 1975) but in view of the IRM acquisition curve for this specimen, it is more likely to be due to a small amount of "hard" ferric oxide (haematite or goethite).

Since the multidomain size-range of magnetite is very large (above c. 0.3μm) the modified Lowrie - Fuller test gives little information on the actual magnetite particle-size. Measurements of the actual particle size were therefore made using the SEM (see section 7-8).

7-4. Low-temperature magnetic transitions.

By monitoring changes in the intensity of magnetization or magnetic susceptibility over a temperature range from

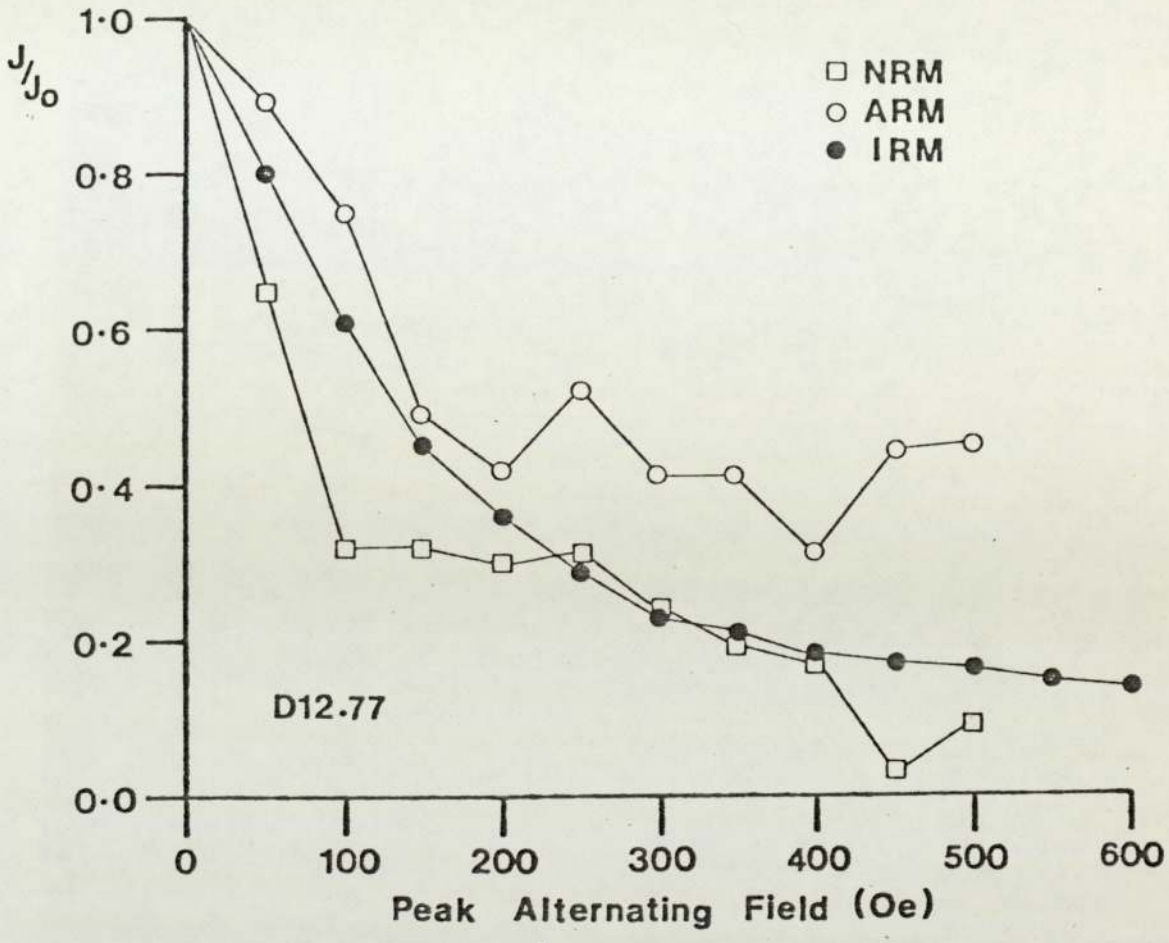


Figure 7-2. Diagram showing the result of the Lowrie-Fuller experiment on specimen D12.77.

-196°C to 10°C it is possible to observe structural transitions in both magnetite (at about -150°C) and in haematite (at about -10°C). In this study, heating curves showing the variation in magnetic susceptibility were used. The equipment used for the experiment was the same Highmoor Variable Temperature Magnetic Susceptibility Bridge used earlier to measure the bulk magnetic susceptibility of the sediment samples. However, the susceptibility bridge was now fitted with a water cooling jacket and was connected to a X,Y plotter so that a continuous measurement of the variations in the magnetic susceptibility could be made as the sample was allowed to heat to room-temperature (the sample having being initially cooled in liquid nitrogen).

The samples used in this study were concentrates of the "magnetic" fraction of the sediment from core-sections D13 and D14. The concentrates were prepared by separating the magnetic portion of the sediment using a strong electromagnet. The magnet used in this study was from a Frantz magnetic seperater. In addition to the two samples from the Delft core, a standard sample of magnetite was used to create a reference heating curve (figure 7-3). This standard consists of a magnetite sample of grain-size range 44-76 μm supplied by the National Coal Board.

The heating curves for the two samples show good agreement with the heating curve for the magnetite standard (figure 7-3). The wide temperature range over which the transition occurs can be explained by non-uniform heating of the sample. From this experiment magnetite, showing a transition at -150°C is thus identified as the principal remanence carrier in the tidal flat sediments of the Wash.

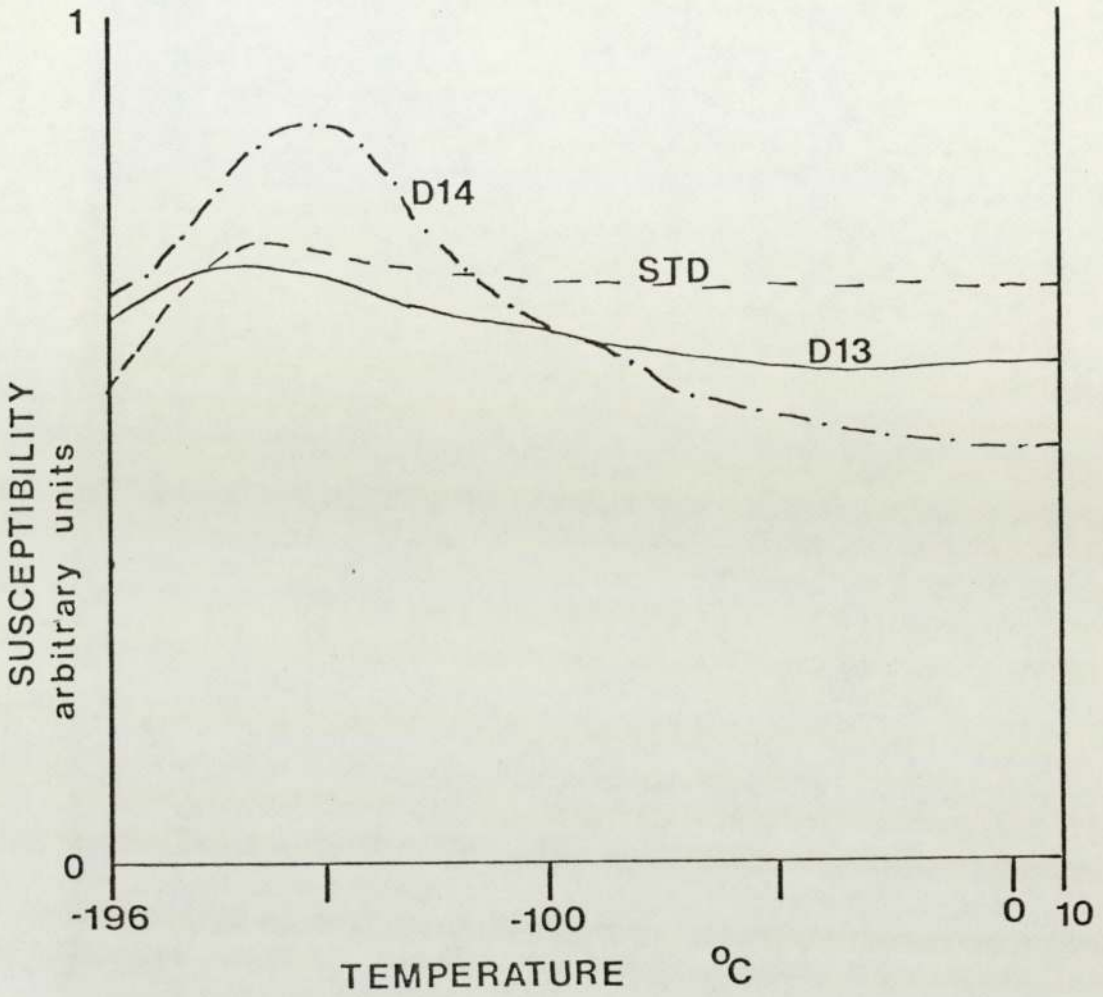


Figure 7-3. Low-temperature magnetic transitions for two magnetic concentrates from core-sections D13 and D14, compared with a standard magnetite sample (of grain-size 44-76μm) supplied by the National Coal Board.

## 7-5. Mössbauer Spectroscopy.

In addition to the studies of whole sediment samples from core D1 and D2, from which results have already been reported (Chapter 4), a magnetic concentrate was prepared for analysis by Mössbauer Spectroscopy. In the study of whole sediment samples greigite was identified as the principal ferromagnetic mineral in those spectra.

From core section D13, (the sequence of silt and very fine sand) a heavy mineral concentrate was prepared and from this a magnetic concentrate was extracted and used to produce the Mössbauer spectrum shown in Figure 7-4. The spectrum was produced at room-temperature. Parameters obtained for the two resolved magnetic hyperfine subspectra are given in Table 7-1. These data compare well with published data for magnetite and titanomagnetite, which are also shown in Table 7-1. The relatively small magnetic field at the Fe nucleus suggests that the sample is titanium-rich. The specimen D13 is therefore thought to consist of predominantly titanomagnetite grains.

## 7-6. X-ray diffraction of magnetic concentrate D13.

A further portion of the magnetic fraction of the heavy mineral concentrate used to obtain the Mössbauer spectra was used to obtain an X-ray diffraction trace. In table 7-2 the results of the X-ray diffraction trace are presented. The results show that the sample consists of magnetite (using the "loose" sense of the word) together with minor grains of quartz. Calculation of the cell parameters (a) was next made, since the cell parameter can be used to determine the titanium content of the magnetite (O'Reilly and Readman, 1971).

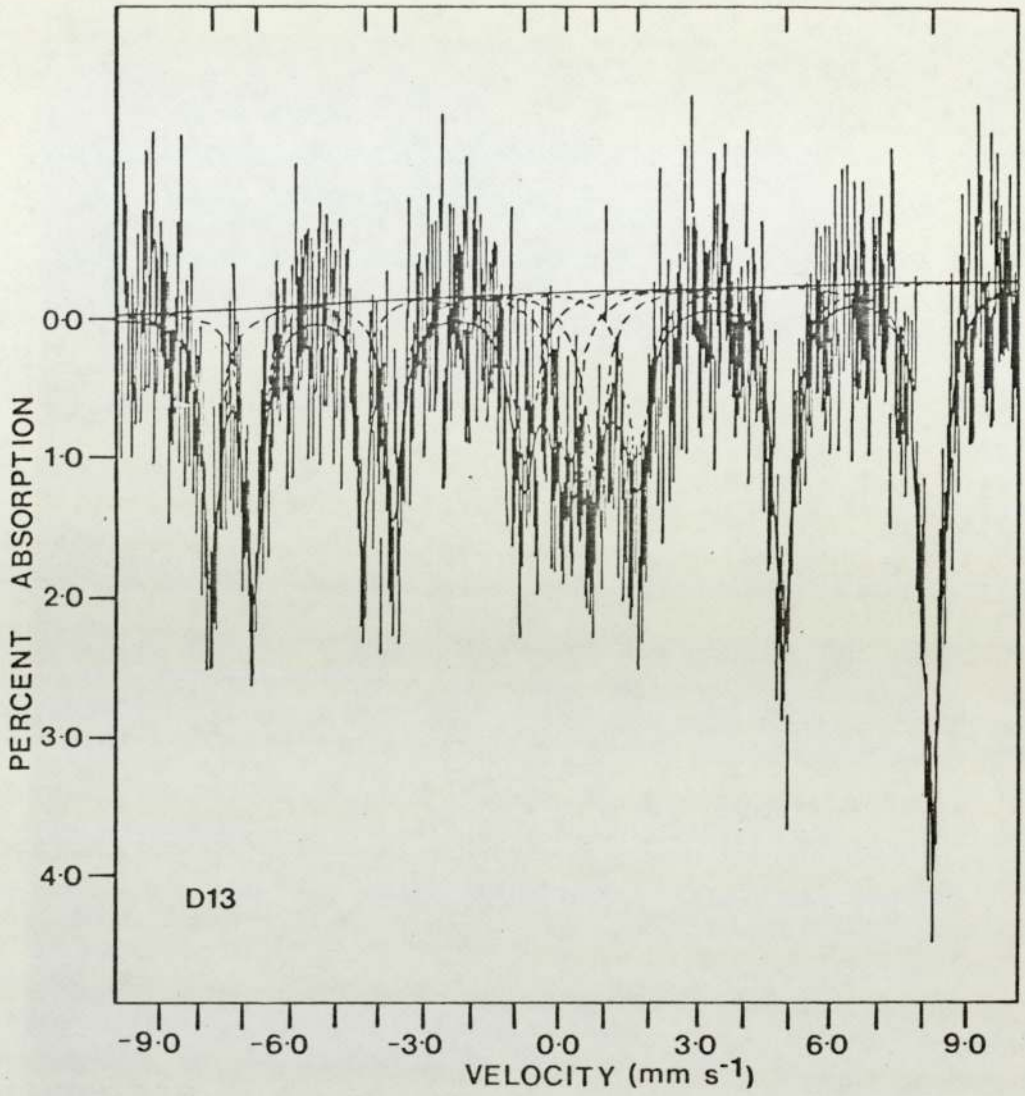


Figure 7-4. Mössbauer spectrum for the magnetic concentrate from core-section D13, showing the two resolved magnetic hyperfine subspectra.

| Source of Data | Temperature of Study ($^{o}$K) | | $H_{eff}$ (KOe) | I.S. mm/sec | $e^2qQ$ mm/sec |
|---|---|---|---|---|---|
| This work (D13) | 298 | (1) | 488±1 | +0.20±.02 | -0.15±.02 |
| | | (2) | 459±1 | +0.67±.02 | +0.10±.03 |
| Evans & Hafner (1969) | 298 (natural spec.) | (1) | 493±3 | +0.25±0.02 | 0±0.05 |
| | | (2) | 460±1 | +0.65±0.02 | 0±0.05 |
| | 298 (synthetic) | (1) | 491±1 | +0.27±0.03 | 0±0.02 |
| | | (2) | 460±1 | +0.67±0.03 | 0±0.03 |
| Kundig & Hargrove (1969) | 295 (synthetic $Fe_3O_4$) | (1) | 492±0 | +0.27±0.10 | (0.025) |
| | | (2) | 461±0 | +0.67±0.01 | |
| Banerjee et al. (1967) | 300 (syn. $Fe_3O_4$) | (1) | 491 | - | - |
| | | (2) | 453 | - | - |
| | 77 (syn. $Fe_3O_4$) | (1) | 503 | - | - |
| | | (2) | 480 | - | -2.0 |
| | 77 (syn. $Fe_{2.4}Ti_{0.6}O_4$) | (1) | 480 | - | - |

$H_{eff}$ = magnetic field at Fe nucleus.

I.S. = isomer shift (mm/sec) relative to iron foil.

$e^2qQ$ = quadrupole splitting (mm/sec).

Table 7-1. Mössbauer data for the magnetic concentrate from sample D13 together with published data for magnetite for comparison.

D13 Magnetic concentrate.

| | Sample D13 | | Magnetite | | | | Quartz |
|---|---|---|---|---|---|---|---|
| 2θCoK | d(Å) | I | d(Å) | I | hkl | $I_{obs}$ | d(Å) |
| 21.15 | 4.880 | 18 | 4.85 | 8 | 111 | 10 | |
| 24.20 | | 13 | 4.272 | | | | 4.26 |
| 31.00 | 3.350 | 37 | | | | | 3.343 |
| 35.10 | 2.969 | 54 | 2.967 | 30 | 220 | 30 | |
| 41.40 | 2.533 | 184 | 2.532 | 100 | 311 | 100 | |
| 49.65 | 2.133 | 12 | | | | | 2.128 |
| 50.60 | 2.095 | 33 | 2.099 | 20 | 400 | 19 | |
| 63.00 | 1.714 | 15 | 1.715 | 10 | 422 | 9 | |
| 67.35 | 1.615 | 39 | 1.616 | 30 | 511 | 21 | |
| 74.30 | 1.483 | 34 | 1.485 | 40 | 440 | 17 | |

Table 7-2. X-ray diffraction data for sample D13 (magnetic concentrate) with comparison data for magnetite and quartz (source: ASTM files).

The method of calculating the cell parameter is shown above Table 7-3. The resulting cell parameters calculated for the first six diffraction peaks are shown in Table 7-3. Using the mean cell parameter of the first six diffraction peaks, a value of 8.393Å ± 0.007Å is obtained. Thus using the data of O'Reilly and Readman (1971) the cell parameter indicates that the sample corresponds to a very iron-rich magnetite close to pure $Fe_3O_4$. A titanium content of only 0.02 mole fraction of $Fe_2TiO_4$ is indicated.

## 7-7. Petrographic studies of magnetic concentrate D13.

Initially, a sample of the magnetic concentrate from core-section D13 was mounted in araldite and polished so that it could be analysed using reflected light microscopy. By analysis of the sample under the microscope it was found that the sample is composed predominantly of magnetite (and its oxidized derivatives) with minor amounts of gangue minerals, chiefly quartz. These observations agree with the results of the X-ray diffraction study of the sample (section 7-6 and Plate 35). The magnetite grains occur in a variety grain shapes, from sub-rounded to angular, but are dominantly angular with a cubic habit. They range in size from 5 - 150μm and have a mean grain-size of approximately 75μm.

A variety of internal textures and alterations can be observed using the polished sections. Some of the magnetite grains show no internal features (plate 36) except for minor fractures and occassionally chemical dissolution, giving the external part of the grain a fluted, corroded surface. Such grains are often subhedral to euhedral in shape. A very common

Example showing the calculation of the cell parameter of the (111) diffraction peak in specimen D13:

$$\text{Using } Q = \frac{1}{d^2_{hkl}} = (h^2+k^2+l^2)A$$

$$\text{where } A = \frac{1}{a^2}$$

For (111) we have

$$\frac{1}{(4.880)^2} = (1+1+1)^1/a^2$$

$$\therefore \quad a^2 = 71.442$$

and

$$\underline{a = 8.452\text{Å}}$$

| Diffraction peak (hkl) | dÅ | cell parameter (Å) |
|---|---|---|
| 111 | 4.880 | 8.452 |
| 220 | 2.969 | 8.398 |
| 311 | 2.533 | 8.401 |
| 400 | 2.095 | 8.380 |
| 422 | 1.714 | 8.397 |
| 511 | 1.615 | 8.392 |

Mean cell parameter of first 6 peaks = 8.393Å

Table 7-3. Calculation of the cell parameters for the magnetite sample D13 with the table of cell parameters for each diffraction peak.

Plate 35. Polished section of magnetic concentrate D13 showing assemblege of magnetite grains.

Plate 36. Polished section showing euhedral magnetite grains. The absence of zoning in these grains suggests they probably pure iron-magnetites.

Plate 35. 100μm

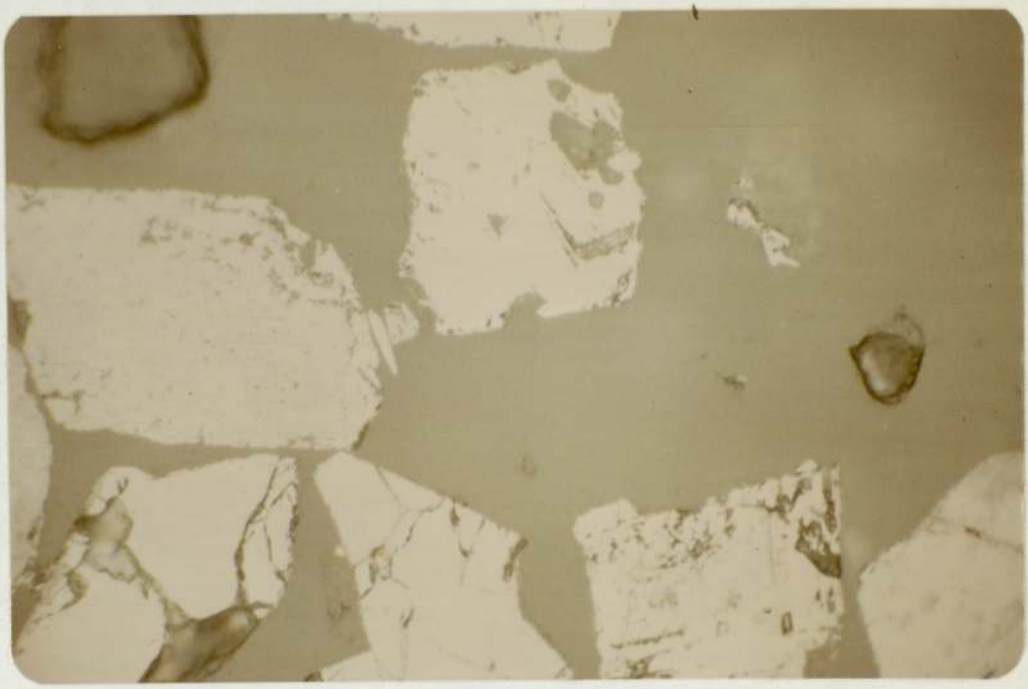

Plate 36. 100μm

feature is to find zoned magnetite grains, which dark and light coloured zones, possibly due to variations in their titanium content (Plate 37). Other grains show alteration along crystallographic directions (Plate 38) resulting from oxidation to maghemite and goethite. Oxidation to goethite may also take place along fractures in the magnetite grains (Plate 39).

Combinations of these features may occur within one grain (Plate 40). Finally, a rare feature is the occurence of grains which have a "cabbage-like" internal structure (Plate 41). The origin of such grains is uncertain. The general impression of all the magnetite grains, however, is that they have suffered little from the effects of decomposition and mechanical breakdown. It is thus concluded that the magnetite grains are probably derived from the erosion of igneous source rocks, and are not derived from the erosion of lithified sedimentary rocks. It thus seems likely that they share the same source as the rest of the sediment, that is they are derived from the boulder clay deposits of the North Sea floor, which themselves are derived from the erosion of igneous rocks in Scandanavia.

## 7-8. Studies of magnetic concentrate D13 using the Scanning Electron Microscope.

A further sample of the magnetic concentrate from core - section D13 was subjected to examination using the scanning electron microscope (SEM) with EDAX (energy dispersive analysis of X-ray radiation). This technique enabled accurate determination of the grain-size of the magnetite grains and also observation of their morphology, surface alteration and their chemical composition.

Plate 37. Polished section showing a heavily fractured and zoned detrital magnetite grain.

Plate 38. Polished section showing a magnetite grain with lteration preferentially along crystallographic directions.

50μm

Plate 37.

100μm

Plate 38.

Plate 39. Polished section of a magnetite grain showing alteration to goethite.

Plate 40. Polished section of titanomagnetite grain showing alteration along crystallographic directions and also the development of irregular zones.

Plate 39. 50μm

Plate 40. 100μm

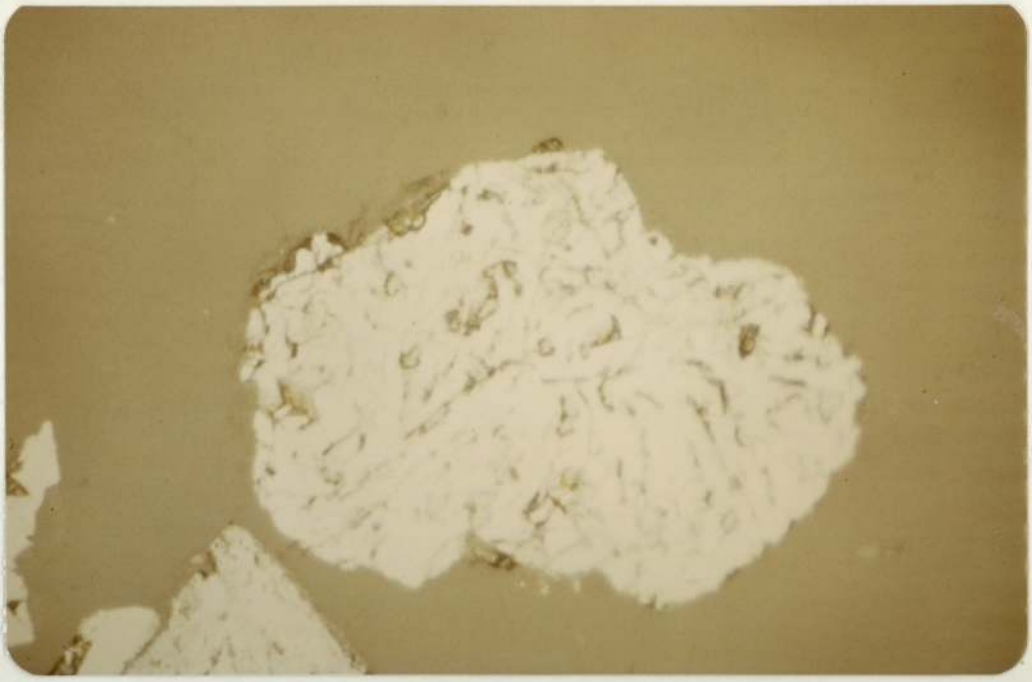

50µm

Plate 41. Polished section of a magnetite grain showing a complex "cabbage-like" internal structure.

The grain-size distribution of the magnetite grains was determined by measurement from a series of SEM photomicrographs. A total of 315 magnetite grains were measured, the largest visible dimension of each grain being measured in each case. The results of this analysis (Figure 7-5) show an essentially unimodal normal grain size distribution, except for a slight concentration of fine magnetite grains in the 5 - 10μm fraction. It is possible that the concentrate is somewhat depleted in the very finest magnetite grains because of problems in extracting this component from the whole sediment. However, the major trend is of a unimodal grain-size distribution in the range 1-124μm with a mean grain-size of 53μm. Although the estim estimate of the mean grain_size is smaller than that from optical studies using reflected light the range of grain-sizes is almost the same. Since the study using the SEM is a quantitative one the mean grain-size of 53μm is considered the most likely approximation. This places the magnetite grains well into the multidomain grain-size range and therefore, agrees with the result of the Lowrie-Fuller test (section 7-3).

A wide variety of grain shapes are observed using the SEM (Plate 42 and 43) and their morphologies can be divided into three groups; single crystal grains, polycrystalline grains, and spherical grains. The single crystal group are the most numerous. Within this group a variety of shapes can be identified. Most common are angular fragments of euhedral crystals (Plate 44) which show only minor evidence of roundening. Many of the grains are euhedral single crystals, often with perfect octahedral habit (Plate 45 and 46). Only a few grains are well rounded indicating that most of the grains are first-cycle magnetites

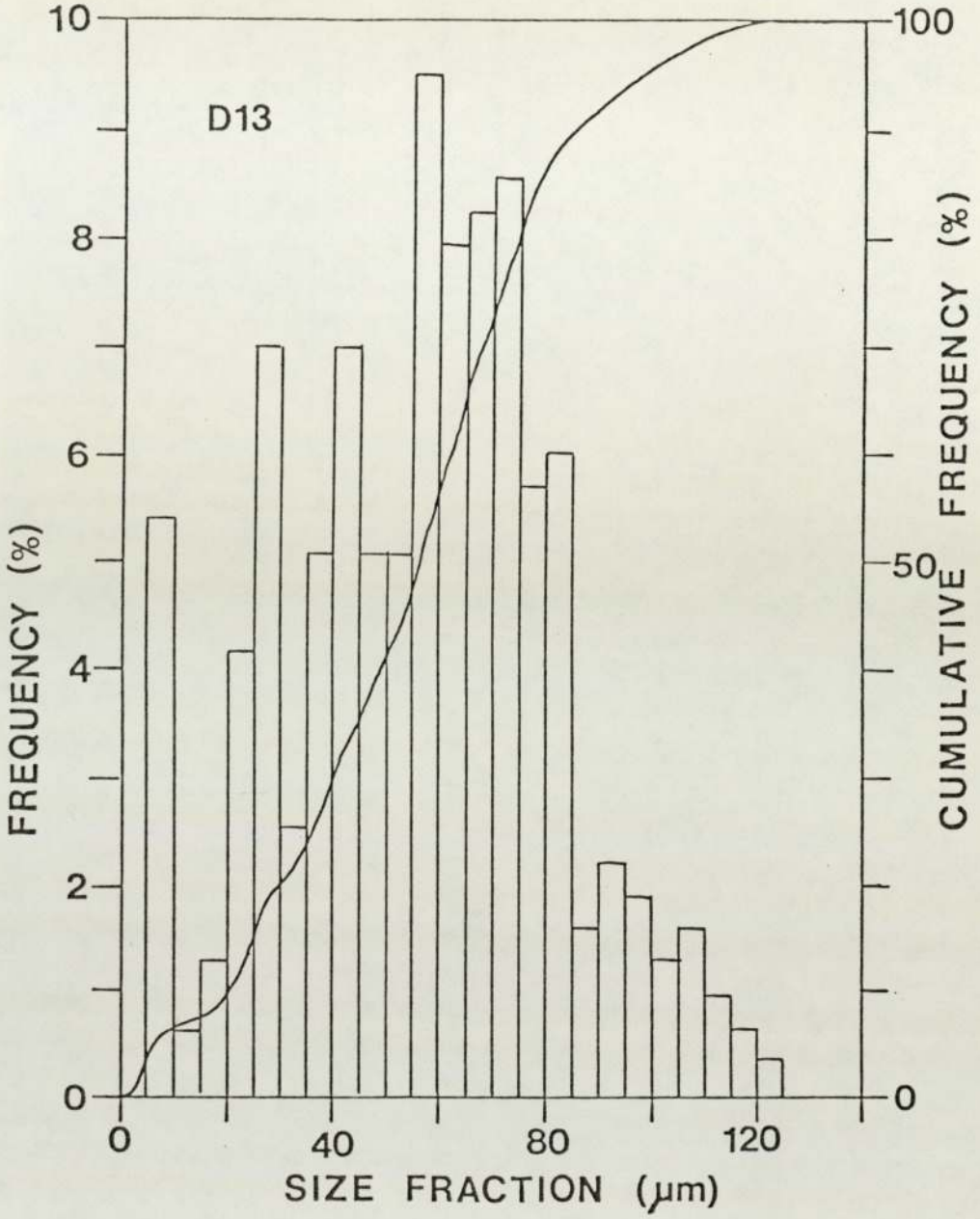


Figure 7-5. Histogram showing the grain-size distribution of magnetite grains in concentrate D13. A cumulative frequency curve is also indicated for the same data.

Plate 42. SEM photomicrograph showing an assemblege of magnetite grains from magnetic concentrate D13.

Plate 43. SEM photomicrograph showing an assemblege of magnetite grains from magnetic concentrate D13.

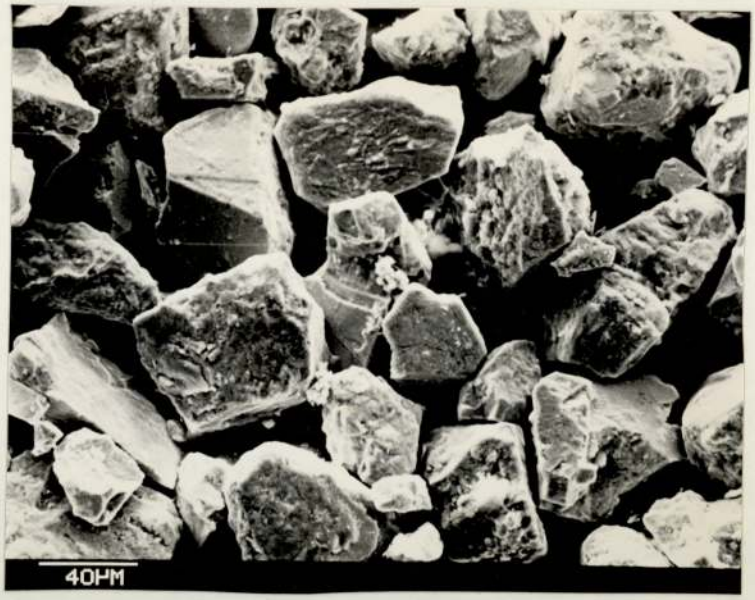


Plate 42.


Plate 43.

Plate 44. SEM photomicrograph showing a sub-angular fragment of a euhedral magnetite grain. Edax analysis shows this grain to be chromium-bearing.

Plate 45. SEM photomicrograph showing a euhedral, octahedral magnetite grain.

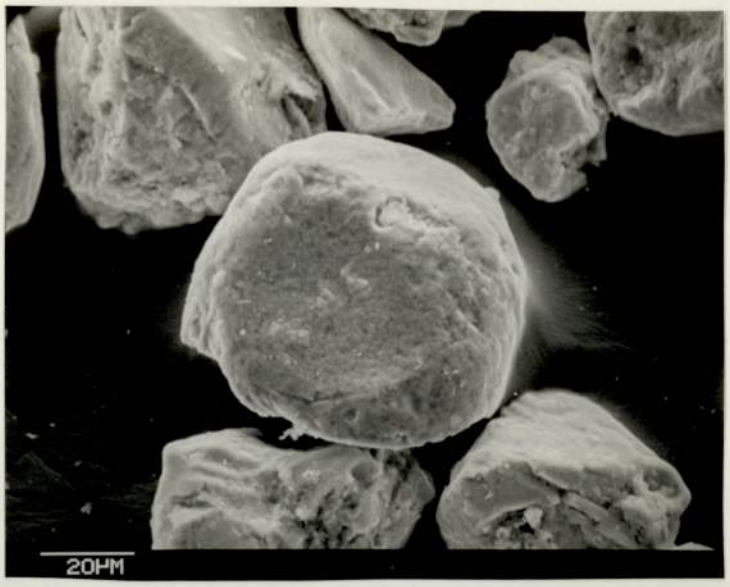


Plate 44.


Plate 45.


Plate 46. SEM photomicrograph showing a euhedral magnetite grain from magnetic concentrate D13.

derived from the erosion of igneous source rocks.

Polycrystalline magnetites form only a small proportion of the sample, approximately 10%. These polycrystalline grains also tend to have unabraided edges and are made up of euhedral grains. They, therefore, probably have a common source with the single crystal magnetite grains.

The final group is the rarest, forming less than 1-2% of the sample and consisting of almost perfectly spherical grains (plate 47 and 48). Edax analysis shows them to be composed of only iron (either metallic iron or an iron oxide). Sometimes ring-like pits are visible on their surfaces (Plate 48) which indicate crystallographic directions. These spherical grains have a diameter of 20-25μm. Similar black, magnetic spherules have been discovered in beach sediments by Parkin et al. (1970) and collected from the atmosphere in the eastern Gulf of Mexico by Doyle et al. (1976). Oldfield et al. (1978) discovered similar particles in ombrotropic peats and were able to provide evidence that they are derived from fly-ash coming from industrial areas.

The surface features and alteration of the magnetite grains are also of interest. Many of the grains show very little surface alteration with, at the most, only a slight "frosting" of surface oxidation (Plate 49). Other grains show a well developed oxidized crust (Plate 50 and 51), the composition of which includes, in addition to iron and sometimes titanium, silicon, aluminium and sometimes calcium (figure 7-6). It seems likely that this crust is composed of a ferric oxide coating which acts as a matrix in which fine clay particles become trapped (Plate 52). There is also evidence that this coating is, in some

Plate 47. SEM photomicrograph showing the rare occurence of a perfectly rounded magnetite grain (lower left of photograph). Such spherical grains are found to be only iron-bearing when examined using Edax.

Plate 48. SEM photomicrograph showing a similar magnetite spherule. In this grain ring-like pits can be observed on the surface of the grain, possibly related to crystallographic directions in the grain.


Plate 47.

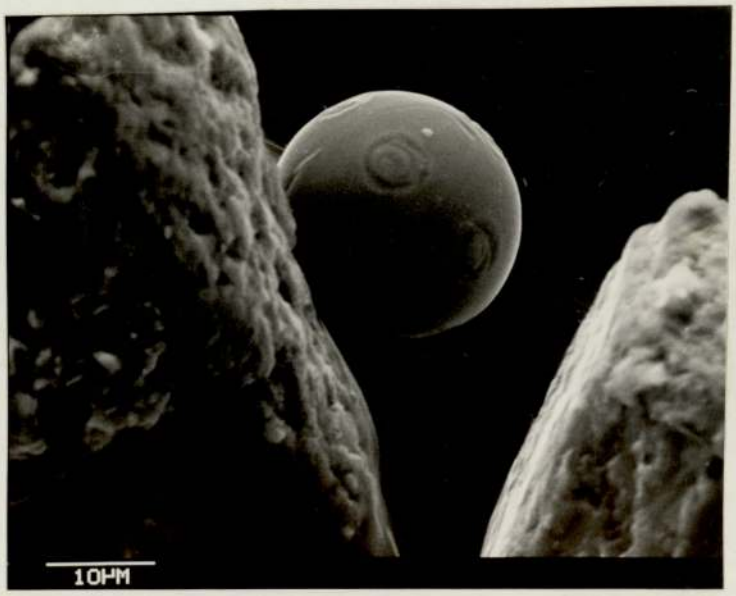


Plate 48.

Plate 49. SEM photomicrograph showing a euhedral magnetite grain with a slight "frosting" of surface oxidation.

Plate 50. SEM photomicrograph showing a euhedral magnetite grain with a well developed ferric oxide crust which includes clay particles.

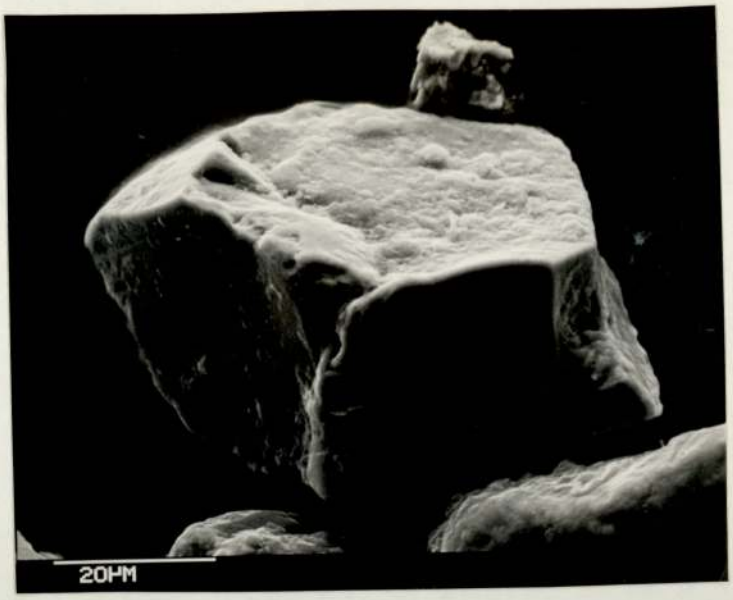


Plate 49.


Plate 50.

Plate 51. SEM photomicrograph showing detail of the ferric oxide-clay mineral crust on the grain shown in plate 50. The Edax trace for this coating is shown in figure 7-6 (B).

Plate 52. SEM photomicrograph showing evidence that the oxidised, clay-containing crust of some grains was formed prior to roundening of the grains.


Plate 51.


Plate 52.

instances, formed before roundening of the grains since plate 52, shows an originally coated euhedral, octahedral, magnetite grain which has since been rounded, breaking the surface ferric oxide/clay layer.

Other features include branching solution pits which cover the surfaces of some grains (Plate 53). Other grains show preferential solution along cleavages and may indicate preferential corrosion of zoned or altered magnetites (Plates 54,55, and 56) As observed in the study of polished sections many of the magnetite grains have large fractures (Plates 57, 58, 59, and 60). Many grains also show the early development of an oxidized coating, probably of goethite (Plate 61). Finally, a rare feature occuring on an elongate titano-magnetite grain (Plate 62) is the occurence of platey grains standing at right angles to the face of the host grain. Identification of these grains is not possible, but from their position it seems that they may be magnetically attracted to the host magnetite grain.

The composition of the magnetite grains has also been studied using energy dispersive analysis of the X-ray radiation with the SEM. A total of 38 magnetite grains were analysed using this method and a variety of compositions were observed. Twenty-seven of these grains were found to be composed of just iron or iron and titanium (Figure 7-7). The remainder also contained manganese and/or chromium (Figure 7-6). Although quantitative analysis is not possible using the Edax system, the ratio of iron to titanium was measured for all of the samples because this is a useful measure of the compositional variation of the magnetites and titano-magnetites.

Plate 53. SEM photomicrograph showing a heavily corroded magnetite grain with a series of branching solution pits on its surface.

Plate 54. SEM photomicrograph showing a concentricly zoned magnetite grain which has suffered preferential dissolution of the zones.

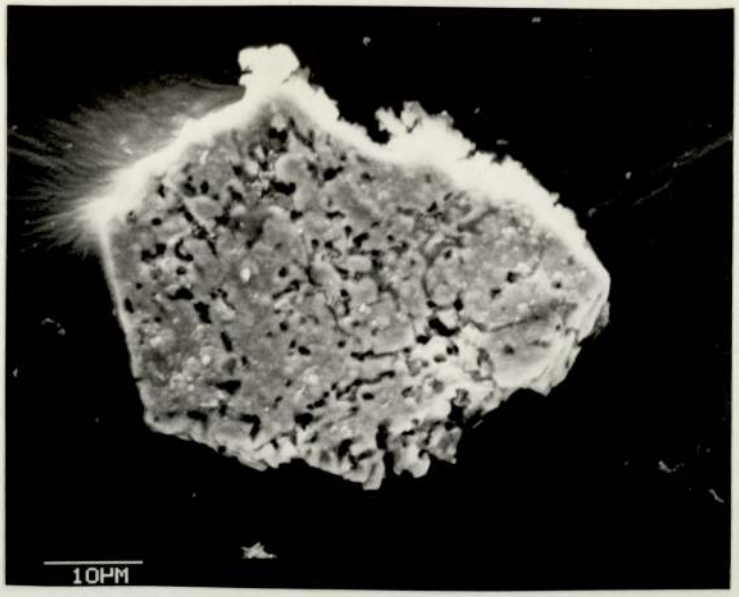


Plate 53.


Plate 54.

Plate 55. SEM photomicrograph showing a magnetite grain which has suffered oxidation along crystallographic directions and then dissolution of the intervening magnetite preferentially.

Plate 56. SEM photomicrograph showing a corroded magnetite which has been dissolved along linear features corresponding to crystallographic directions in the grain

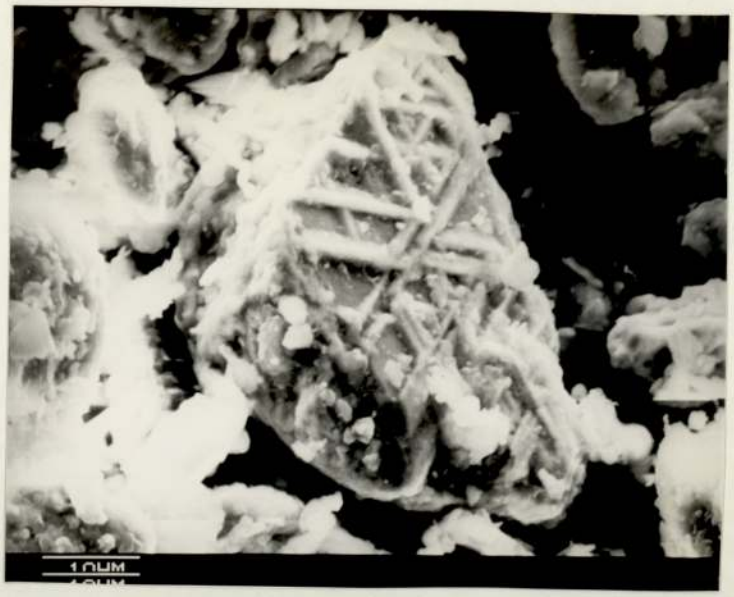


Plate 55.


Plate 56.

Plate 57. SEM photomicrograph showing a fracture developed at the apex of a euhedral magnetite grain

Plate 58. SEM photomicrograph showing the fractured surface of a magnetite grain (centre).

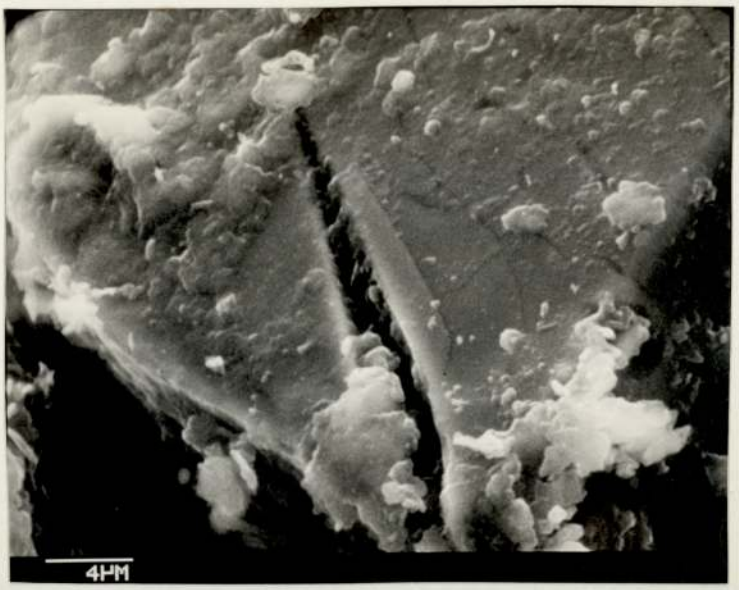


Plate 57.

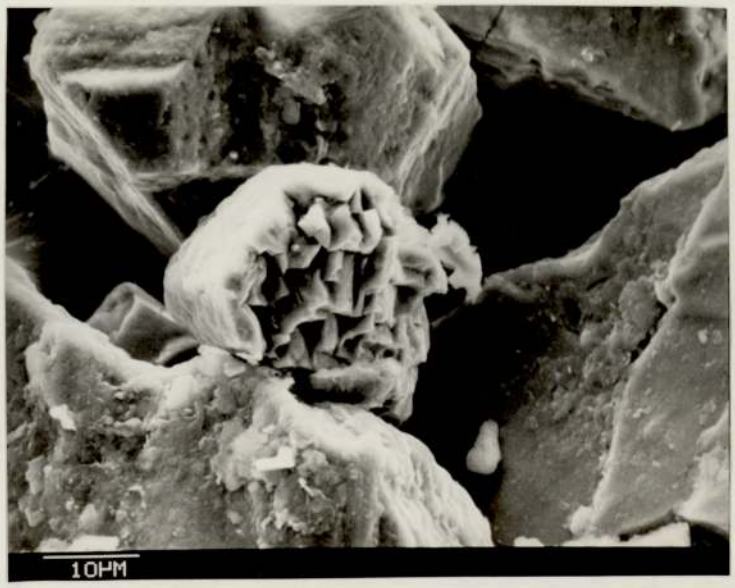


Plate 58.

Plate 59. SEM photomicrograph showing a heavily fractured magnetite grain, fracturing along cleavages.

Plate 60. SEM photomicrograph showing detail of the magnetite grain in Plate 59. Note the well developed cleavages.


Plate 59.


Plate 60.

Plate 61. SEM photomicrograph at high magnification showing the early development of an oxidized coating to a magnetite grain. Compare with the thicker coating seen in plate 51.

Plate 62. SEM photomicrograph at high magnification showing thin platy grains attached at right angles to the surface of a magnetite grain.


Plate 61.


Plate 62.

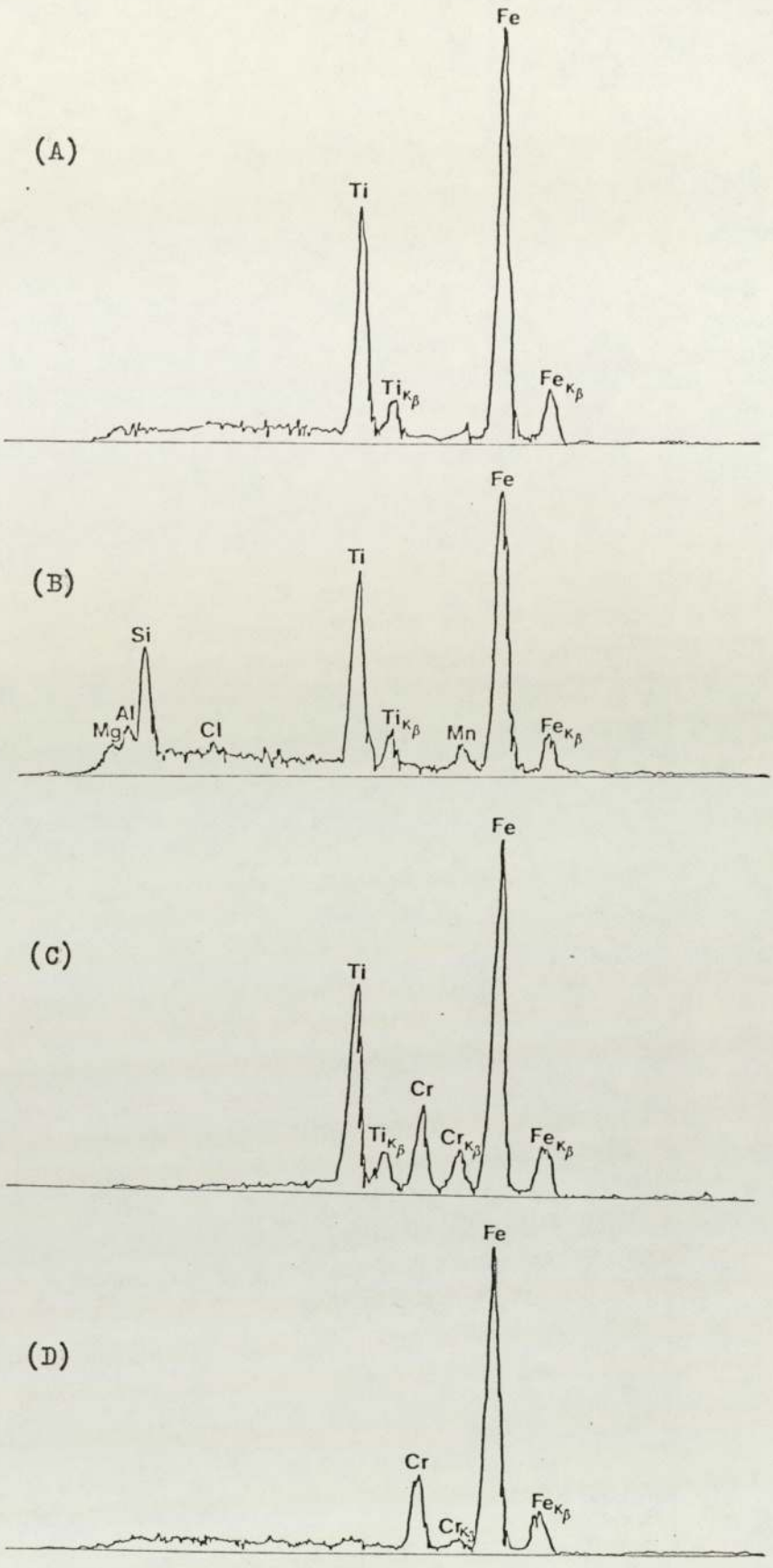


Figure 7-6. Edax traces for a variety of magnetites. A= Titanomagnetite, B= Titanomagnetite with minor manganese and clays. C= Chromium bearing titanomagnetite, D= Chromium bearing magnetite.

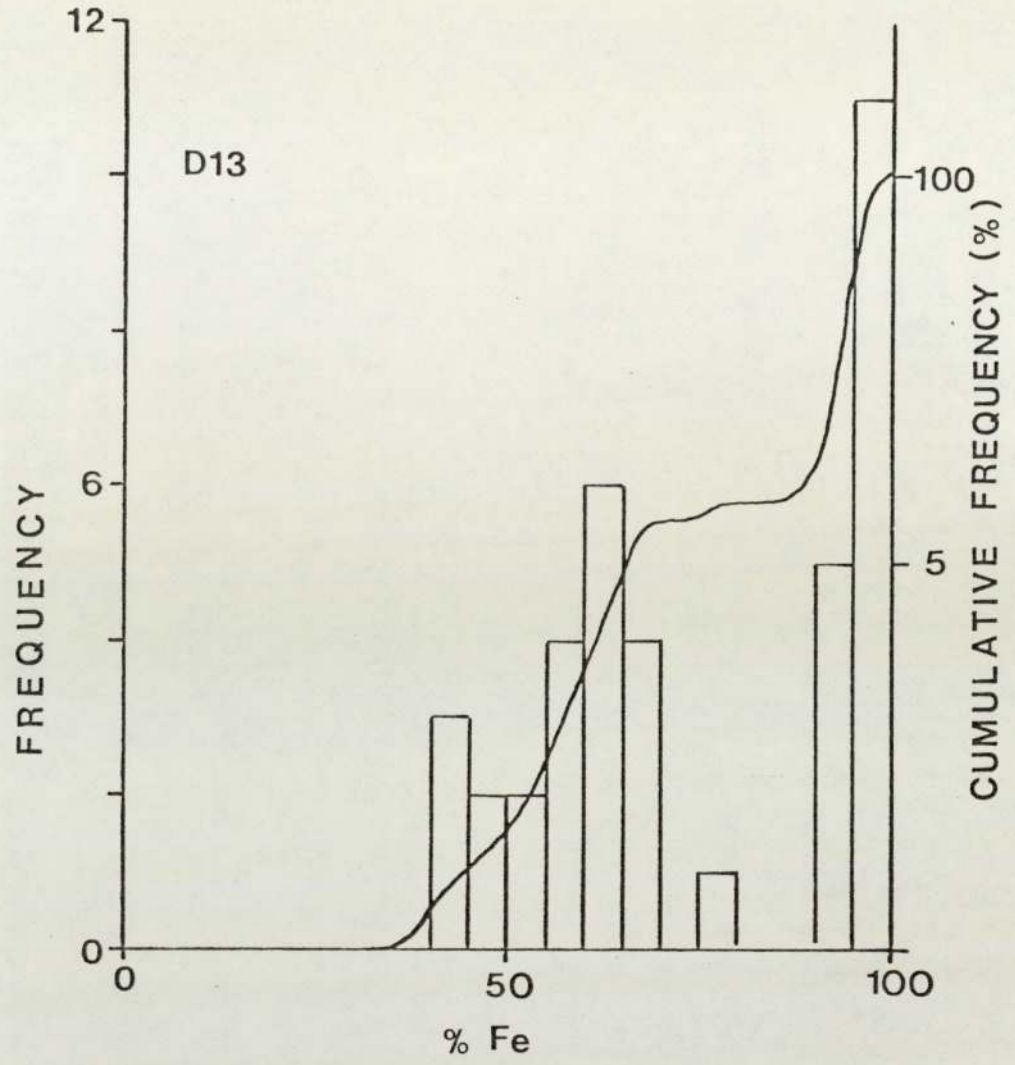


Figure 7-7. Histogram showing the distribution of the iron-titanium magnetite grains with respect to the percentage Fe estimated from the height of iron and titanium peaks in the Edax traces.

The variation in composition determined from measuring the relative peak heights of the titanium and iron peaks is shown in figure 7-7. This variation has a strongly bimodal distribution in which 58% of the samples is made up of titano-magnetites having a mean iron-titanium ratio of 54:46 and the remaining 42% is composed of almost pure magnetite with an iron-titanium ratio of greater than 90:10. The overall iron:titanium ratio of approximately 3:2 may be compared with data obtained from deep sea cores from the North Pacific by Kent and Lowrie (1974) in which a ratio of 4:2 was obtained. It is worth recalling here that X-ray diffraction studies of the same sample indicated that the sample contains only 0.02 mole fraction of $Fe_2TiO_4$. Therefore it can be concluded that the Edax traces can only used to identify the elements present in the magnetites and to qualitatively identify changes in their compositions.

Finally, many grains were found to contain minor amounts of manganese and/or chromium. Such grains included both magnetites and titano-magetites (Figure 7-6). A feature of many of the chromium bearing magnetites is that they usually occur as disc like grains due to quite good rounding (Plate 63).


Plate 63. SEM photomicrograph showing a sub-rounded to sub-angular magnetite grain. Edax analysis of the grain shows it to be chromium-bearing.

7-9. Bulk magnetic properties of the tidal flat sediments.

The bulk magnetic properties of samples from Delft core D1 provide an important measure of the total magnetic mineral composition, when considered with the other mineralogical and geochemical data. The initial susceptibility ($\chi_{vol}$) ranges from 30-168$\mu G Oe^{-1}$ and the NRM intensity ranges from 0.2-9.1$\mu G$ (figure 6-29). There is an indication that increases in the NRM intensity are, in places, accompanied by a rise in the initial susceptibility suggesting slight fluctuations in the ferrimagnetic mineral content. The principal paramagnetic constituent is chlorite, and clay mineral analysis (Chapter 3) suggests that this contributes very little to the observed variation. The increases in initial susceptibility and remanent intensity often correspond to obvious lithological changes, the highest values occuring in the black-sulphide-rich clay horizons. These are the zones in which greigite has been identified, and although they may also be enriched in detrital oxides, the implication is that greigite makes a contribution to the observed magnetic properties of these sediments.

7-10. Conclusions.

From the wide variety of methods used here a detailed knowledge of the ferrimagnetic mineralogy of the tidal flat sediments has been collected. Identification of the major remanence carrier as an iron oxide, magnetite containing varying amounts of titanium, manganese, and chromium has been made. In addition, some of the black clay-rich sediments, contain the authigenic iron sulphide mineral, greigite which is also ferrimagnetic and is capable of adding a chemical remanent magnetization (CRM) to the NRM of these sediments. Evidence for the occurence of greigite is provided by Mössbauer spectral studies, variations in the bulk magnetic properties of the sediments and by optical studies of samples in glycerine mounts. A third contributor to the NRM of the sediments is indicated in the IRM and Lowrie-Fuller experiments. This is the "hard" feric oxide which is probably haematite or goethite. Goethite alterations to magnetite grains have been observed in polished sections and under the scanning electron microscope.

The major remanence carriers of the tidal flat sediments are, however, the group of minerals referred to as magnetites. Petrographic and SEM studies show that they occur entirely as detrital grains, falling into three main morphological groups. These are; single crystals, polycrystalline grains and spherical grains. The magnetites generally, except for fracturing and superficial clay coatings and oxidation products, show little evidence of having suffered from the effects of transport over long distances.

Grain-size analysis, using the Lowrie-Fuller test shows that the magnetites are of multidomain grain-size, and measurement of

315 grains using the SEM shows them to have a mean-grain size of 53um. The grain-size distribution is essentially unimodal, but the presence of a significant quantity of grains below 10um suggests an abundance of small magnetite grains, possibly not recovered by the concentration technique used to prepare the sample examined here.

The magnetites show a bimodal compositional distribution, determined using Edax, which includes a series of very pure magnetites with only small concentrations of titanium, and also a series of magnetites or more correctly titanomagnetites possessing significant proportions of titanium. X-ray diffraction studies using the unit cell parameter as an indication of the titanium content of the sample suggests a mean titanium content of 0.02 mole fraction of $Fe_2TiO_4$. Edax analysis shows that minor concentrations of chromium and manganese are also present in the structure of many of the magnetite and titanomagnetite grains.

The spherical magnetites are found to be relatively rare in abundance and Edax analysis shows them to be composed of just iron oxide with no other major cation present. The spherical grains show strong similarities to particles described by Oldfield et al. (1978) which were described as being derived from fly-ash coming from industrial areas. Palaeomagnetic dating of the core for the interval from which these particles are taken gives an age of greater than 600 years Bp, which suggests that some other source is required.

The source of the remaining magnetite grains is less problematical. It is concluded, from their fresh appearance and lack of roundening, that these grains are derived from the erosion of igneous source rocks. The most likely origin is from the boulder

clay deposits of the North Sea, which are in turn derived from erosion of igneous complexes in Scandanavia.

# Chapter 8.

# Conclusions.

The objectives of this study, falling broadly into mineralogical and into palaeomagnetic fields, have been achieved using sediments recovered from the present-day, and the recently reclaimed, tidal flat areas. Three methods were used for the recovery of samples; including one-metre cores of sediment, Delft nine-metre cores, and surface sediment samples. The successful use of the Delft corer in obtaining an undisturbed continuous sediment sample, necessary for palaeomagnetic studies, enabled a much thicker sequence to be analysed than had previously been attempted.

Mineralogical studies of the sediments proce ded with a study of their whole sediment mineralogy, using optical microscopy, X-ray diffraction and geochemical studies. These studies enabled the identification of the major minerals in the sediments, which are; quartz, calcite, clay minerals, feldspars, and minor dolomite. Sedimentological studies have enabled the sediments recovered from the cores to be characterised using the sub-environments of Evans (1965) into the salt marsh, higher mud flat, and Arenicola sand flat sub-environments. Geochemical studies show the chemical differences between these lithologies. These differences are chiefly due to variations in the ratios of clay minerals to quartz. In addition, further areas of study were identified as being necessary from these whole sediment studies. Firstly, the distribution of iron, determined from the geochemical study suggests that much of it is in the form of clay minerals. Therefore, since one of the objectives of this study was to determine the source of iron

involved in the formation of the iron sulphides, a detailed examination of the clay mineralogy using X-ray diffraction of clay mineral concentrates was undertaken.

The clay minerals identified by X-ray diffraction were found to consist of illite, montmorillonite, kaolinite, chlorite and mixed layer illite-montmorillonite. In addition, the mixed-layer chlorite-montmorillonite clay mineral, corrensite has been identified in the sediments from the salt marsh. Analysis of the distribution of the clay minerals also shows a lithological control, which it is suggested might be used in the study of ancient sedimentary sequences of tidal flat origin. The palaeo-mean high-water level, occuring at the salt-marsh and higher mud flat boundary is particularly distinctive, being identified by a decrease in the abundance of kaolinite in the higher mud flat sediments. The major iron-bearing clay mineral present in the tidal flat sediments is chlorite which is present as 4-10% of the 2μm fraction of the sediment. Other clay minerals present in the tidal flat sediments which carry minor iron in their structures are illite, montmorillonite, mixed layer illite-montmorillonite and corrensite.

In order to gain a more detailed appraisal of the location of the iron in the sediments, the X-ray diffraction study has been followed with a study of the iron-bearing minerals using Mössbauer spectroscopy of whole sediment samples. The Mössbauer study enabled the identification of the major iron-bearing minerals and also their relative contributions to the total iron content of the sediments. Therefore, changes in the concentrations, site distributions and oxidation states of iron in different minerals could be measured. The following minerals were identified as the major

iron-bearing minerals; chlorite, pyrite, illite, montmorillonite, iron hydroxides and greigite. This is the first time Mössbauer data for naturally occuring greigite has been recorded in the room-temperature spectra of a whole sediment sample.

From the intensities of the peaks it was possible to determine the percentage contribution to the total iron by each mineral. Most of the iron, 43% is to be found occuring as ferric iron in the form of clay minerals and in ferric hydroxides. The next major contributor to the iron-bearing mineralogy is chlorite which contributes up to 38% of the total iron, this iron is in the ferrous state. The ferrous iron in chlorite has been found occuring in two octahedral sites which can best be attributed to the two component layers of chlorite, the talc-layer and the brucite-layer. The talc-layer contributes the largest proportion, 30% of the iron, leaving 8% of the total iron in the brucite-layer. The remaining 19% of the total iron is in the form of iron sulphides, 8% in the form of greigite and 11% in the form of low-spin ferrous iron in pyrite.

From a series of samples from core D1 it is possible to identify an increase in pyrite,diagenetically, with depth in the core. A second diagenetic feature identified in the Mössbauer study is the growth in the intensity of the ferrous doublet of chlorite, representing the brucite-layer, also with increased depth, with respect to the ferrous iron in the talc-layer.

The identification of this variation may suggest that some of the ferrous iron in the talc layer of chlorite is being removed and possibly used in the formation of diagenetic iron-sulphides.

An important feature of these results, with regard to the

palaeomagnetic studies, is the identification of greigite in some of the specimens. Greigite is strongly ferrimagnetic and may therefore form an important secondary magnetic component to the natural remanence of the sediments.

The occurence of the sulphide minerals has also been studied using glycerine mounts, thin sections and the scanning electron microscope. Conclusive evidence for the occurence of mackinawite (suugested by Love, 1967, to be present) has not been gained but from the presence of greigite, identified in the Mössbauer studies, its presence is inferred. However, examination of glycerine mounts have enabled the tentative identification of two black pigmentary phases, one amorphous and one consisting of small black reflective grains, as mackinawite and greigite respectively.

The identification of pyrite, in contrast provides no problems. The chief occurence is in the form of spherical and sub-spherical pyrite framboids, which can be seen in glycerine mounts, thin sections (as opaque phases) and under the scanning electron microscope.

Palaeomagnetic studies of the one-metre cores confirmed the presence of a soft but stable NRM. At Freiston Shore this NRM was found to be a PDRM. Dating of the sequence enabled an accretion rate of 1.63 mm/yr to be calculated for the sequence of salt-marsh and higher mud flat sediments at Freiston Shore. Studies of the stability of the NRM of the sediments whilst they dried out in the laboratory show the effect the water content of the sediments has on maintaining the NRM. Large changes in the remanence were recorded as the sediments dried.

Paleomagnetic results from the Delft core D1 from Leverton

were found to show good agreement with the known secular variation record for Great Britain for the period 0-1000 years BP. This part of the sequence represented by the salt marsh and higher mud flat sediments can therefore be dated accurately using palaeomagnetism. Firstly however, a lag-time, for the acquisition of the PDRM, must be added to the magnetic age to obtain a true age for the sediments. The lag time was found to be of the order of 100years, therefore the base of the higher mud flat sediments can be dated at 1100 years BP.

From this dating the sedimentation rate for the period 0-1100 years BP may be calculated. A rate of 1.5 mm/year is obtained which gives good agreement with the rate obtained at Freiston Shore. The lower sequence of fine sands, belonging to the Arenicola sand flats, cannot be matched easily with the known palaeomagnetic secular variation record for Great Britain, but we do know from studies by Godwin and Clifford (1938) that the sequence must be younger than 2000 years BP. Therefore, deposition must have occured within a period of 900 years giving a sedimentation rate of greater than 7.7 mm/year. This value is found to be in good agreement with the average sedimentation rate for the tidal flat of 8 mm/year measured by Amos (1974).

Again water content was found to be an important factor. The studies of the Delft core were oriented to determining the role of the water content of the sediments in the acquisiton of PDRM. The results have shown a good relationship between the water content of the sediments, itself a function of compaction, and the processes of acquisition of PDRM. It is therefore recommended that in further studies of the palaeomagnetism of unconsolidated sediments the water content, or some other measure of compaction

be determined.

An important conclusion regarding the choice of sampling locations, in future palaeomagnetic studies of tidal flat sediments, is to avoid areas close to creeks. This is because such sediments are found to possess large bedding errors, shown both by declination errors, and by rotation of the magnetic anisotropy ellipsoid axes.

It can therefore be concluded that with the correct choice of sampling locations, and with suitable sediments (such as those belonging to the higher mud flat and salt marsh sub-environments), detailed palaeomagnetic studies of tidal flat sediments are possible, and that the results can be used in sedimentological and diagenetic studies for dating the sediments and obtaining sedimentation rates of the sediments. Major breaks in sedimentation rates can also be identified. In addition, it is proposed that palaeomagnetic studies of tidal flats on a more extensive basis could provide valuable data on the variations in the geomagnetic field to augment data available from studies of lake sediments.

Finally, identification of the remanence carrying minerals has been made. The major mineral responsible for carrying the remanence is detrital magnetite, which occurs both as pure magnetite and as titaniferous magnetite. Both phases may contain minor concentrations of chromium and manganese. The grain-size of this magnetite has been found to be of multidomain grain size with a mean diameter of 53μm. The source of the magnetite appears to be from the same source area as the major part of the sediments, namely the boulder clay deposits of the North Sea floor, which were in turn derived from the erosion of igneous source rocks in

Scandanavia.

The conclusions derived from this research themselves suggest further areas of research which might be possible in the light of this work. Clearly the addition of palaeomagnetic studies of tidal flats to the data already available provides an important additional source of information in studies of the geomagnetic field. The addition of palaeomagnetic studies to sedimentological studies of recently infilled estuaries and embayments can provide valuable evidence regarding the rate at which these processes take place. Similarly palaeomagnetic dating may also be used to date diagenetic changes in the sediments which could be used to obtain the rates at which various diagenetic minerals are formed.

****

# APPENDIX 1.

Clay mineral calculations from X-ray diffraction data.

Example of the calculation of the percentages of the clay minerals from X-ray diffraction studies.

D12.70

| PEAK Å | GLYCOLATED (AREA) | HEATED (180°/1 hr.) (AREA) |
|---|---|---|
| 14 | 11 | 25 |
| 10 | 24 | 43 |
| 7 | 40 | 48 |
| 5 | 6 | 11 |
| 4.8 | 2 | 4 |
| 3.58 | 12 | 16 |
| 3.54 | 3 | 3 |

$$\%K+C = \frac{48/2.5}{(48/2.5)+43} \times 100 = \underline{30.9\%}$$

$$\%K = \frac{16}{16+3} \times 30.9 = \underline{26.0\%}$$

$$\%C = 30.9 - 26.0 = \underline{4.9\%}$$

$$\%I+M = \frac{43}{(48/2.5)+43} \times 100 = \underline{69.1\%}$$

$$\%I = \frac{24 \times (48/40)}{43} \times 69.1 = \underline{46.3\%}$$

$$\%M = 69.1-46.3 = \underline{22.8\%}$$

$$\text{TOTAL} = \underline{\underline{100.0\%}}$$

# APPENDIX 2

Results of the clay mineral analyses from core D1 and from surface sediment samples.

Tabulation of the results of the clay mineral analyses from core D1.

| Specimen | Kaolinite % | Chlorite % | Illite % | Expandables % | Total % |
|---|---|---|---|---|---|
| D12.10 | 13.0 | 8.2 | 34.7 | 44.1 | 100.0 |
| D12.30 | 20.3 | 5.6 | 45.0 | 29.1 | 100.0 |
| D12.50 | 24.3 | 6.5 | 41.4 | 27.9 | 100.0 |
| D12.70 | 26.0 | 4.9 | 46.3 | 22.8 | 100.0 |
| D12.90 | 23.2 | 7.0 | 44.0 | 25.8 | 100.0 |
| D13.10 | 19.5 | 5.7 | 44.1 | 30.7 | 100.0 |
| D13.30 | 18.6 | 8.2 | 47.7 | 25.5 | 100.0 |
| D13.50 | 18.1 | 6.1 | 35.5 | 40.3 | 100.0 |
| D13.70 | 19.1 | 9.5 | 68.3 | 3.1 | 100.0 |
| D13.90 | 16.2 | 8.7 | 41.1 | 34.0 | 100.0 |
| D14.50 | 16.8 | 6.7 | 41.2 | 35.3 | 100.0 |
| D15.50 | 15.5 | 10.3 | 53.6 | 20.6 | 100.0 |
| D16.50 | 19.4 | 6.5 | 62.5 | 11.6 | 100.0 |
| D17.50 | 20.9 | 4.2 | 51.4 | 23.5 | 100.0 |
| D18.50 | 22.3 | 4.5 | 51.2 | 22.1 | 100.0 |
| D19.50 | 20.8 | 6.9 | 52.4 | 19.9 | 100.0 |
| D110.50 | 26.6 | 8.0 | 55.2 | 10.2 | 100.0 |

Results of the clay mineral analyses for the surface sediment samples.

| Specimen | Kaolinite % | Chlorite % | Illite % | Expandables % | Total % |
|---|---|---|---|---|---|
| 1. | 18.3 | 4.6 | 42.0 | 35.1 | 100.0 |
| 2. | 19.1 | 7.8 | 48.1 | 25.0 | 100.0 |
| 3. | 19.0 | 6.1 | 44.1 | 30.8 | 100.0 |
| 4. | 20.4 | 7.7 | 47.1 | 24.8 | 100.0 |
| 5. | 22.3 | 7.7 | 41.7 | 28.3 | 100.0 |
| 6. | 22.0 | 7.3 | 45.5 | 25.2 | 100.0 |

Specimens are from the following locations:

1. Lower (seaward) Arenicola sands, Leverton.
2. strongly bioturbated Arenicola sands, Leverton.
3. upper (landward) Arenicola sands, Leverton.
4. the higher mudflat, Leverton.
5. the salt marsh, Freiston Shore.
6. reworked higher mudflat sediment in creek bottom, Freiston Shore.

# APPENDIX 3

X-ray diffraction results from the heating experiment on sample D12.50.

Peak area for the X-ray diffraction traces from specimen D12.50 after each stage of heating.

| Treatment | Peak (Å) areas | | | | | | |
|---|---|---|---|---|---|---|---|
| | 14 | 10 | 7 | 5 | 4.8 | 3.58 | 3.54 |
| Ethanediol | 8 | 28 | 52 | 6 | 4 | 11 | 4 |
| 180°C/1 hr. | 61 | 46 | 51 | 15 | 7 | 15 | 4 |
| 400°C/1 hr. | 35 | 97 | 47 | 11 | 4 | 12 | 3 |
| 500°C/1 hr. | 28 | 109 | 2 | 11 | 1 | abs | abs |
| 550°C/1 hr. | 23 | 93 | abs | 15 | abs | abs | abs |
| 600°C/1 hr. | 26 | 97 | abs | 15 | abs | abs | abs |
| 650°C/1 hr. | 21 | 100 | abs | 15 | abs | abs | abs |
| 700°C/1 hr. | 15 | 98 | abs | 11 | abs | abs | abs |
| 750°C/1 hr. | abs | 95 | abs | 11 | abs | abs | abs |

abs - indicates that a peak is absent

# APPENDIX 4

Mössbauer data for common clay minerals - from the literature.

Mössbauer data for common clay minerals - from the literature.

| Source | Mineral | Oxidation state | Lattice position | Isomer shift (mm/sec) | Quadrupole splitting (mm/sec) | Half Width (mm/sec) |
|---|---|---|---|---|---|---|
| Weaver et al. (1967) | 2:1 Dioctahedral Montronite | $Fe^{3+}$ | Oct | ~0.3 | ~0.3 | - |
| | Illite | $Fe^{2+}$ | Oct | ~1.1 | 1.0 | - |
| | | $Fe^{3+}$ | Oct | 0.35 | 0.32 | - |
| | Glauconite | $Fe^{2+}$ | Oct | ~1.1 | ~1.1 | - |
| | Montmorillonite | $Fe^{3+}$ | Oct | 0.4 | - | - |
| | 2-1 Chain Xylotile | $Fe^{2+}$ | Oct | ~1.2 | ~1.0 | - |
| | | $Fe^{3+}$ | Oct/Tet | 0.2 | ~0.4 | - |
| | Attapulgite | $Fe^{3+}$ | Oct | ~0.3 | ~0.2 | - |
| | 1.1 Trioctahedral Chamosite | $Fe^{2+}$ | Oct | 1.2 | 1.25 | - |
| | Cronstedtite | $Fe^{2+}$ | Oct | 1.3 | 1.2 | - |
| | | $Fe^{3+}$ | Oct | 0.4 | 0.3 | - |
| | | $Fe^{3+}$ | Tet | 0.05 | 0.4 | - |
| | 2.1 Trioctahedral. Biotite | $Fe^{2+}$ | Oct | 1.15 | 1.20 | - |
| | | $Fe^{3+}$ | Oct | - | ~0.2-0.6 | - |
| | Biotite | $Fe^{2+}$ | Oct | 1.15 | 1.20 | - |
| | Weathered Biotite | $Fe^{3+}$ | Oct | 0.35 | 0.30 | - |
| | Ferriannite | $Fe^{2+}$ | Oct | 1.15 | 1.20 | - |
| | | $Fe^{3+}$ | Tet | +0.5 | ≤0.40 | - |
| | Griffithite | $Fe^{2+}$ | Oct | ~1.2 | ~1.3 | - |
| | | $Fe^{3+}$ | Oct | ~0.4 | ~0.6 | - |
| | 1.1 Dioctahedral Iron Kaolinite | $Fe^{3+}$ | - | 0.37 | 0.27 | - |
| Taylor et al. (1968) | 2 sheet Trioctahedral Amesite | $Fe^{2+}$ | Oct | 1.28 | 2.55 | - |
| | | $Fe^{3+}$ | Tet | 0.45 | 0.90 | - |
| | | $Fe^{3+}$ | Oct | 0.45 | 0.90 | - |

| Source | Mineral | Oxidation state | Lattice position | Isomer shift (mm/sec) | Quadrupole splitting (mm/sec) | Half width (mm/sec) |
|---|---|---|---|---|---|---|
| | Cronstedite | $Fe^{2+}$ | Oct | 1.25 | 1.70 | - |
| | | $Fe^{3+}$ | Tet | 0.45 | 0.90 | - |
| | | $Fe^{3+}$ | Oct | 0.45 | 0.60 | - |
| | 3 sheet Dioctahedral | | | | | |
| | Nontronite | $Fe^{3+}$ | Oct | 0.50 | 0.40 | - |
| | Glauconite | $Fe^{2+}$ | Oct | 1.23 | 1.65 | - |
| | | $Fe^{3+}$ | Oct | 0.50 | 0.40 | - |
| | | $Fe^{3+}$ | Tet | - | - | - |
| | Glauconite | $Fe^{2+}$ | Oct | 1.25 | 1.70 | - |
| | | $Fe^{3+}$ | Oct | 0.50 | 0.40 | - |
| | | $Fe^{3+}$ | Tet | - | - | - |
| | 3 sheet Trioctahedral | | | | | |
| | Lepidomelane | $Fe^{2+}$ | Oct | 1.20 | 2.40 | - |
| | | $Fe^{3+}$ | Oct | 0.55 | 0.50 | - |
| | Biotite | $Fe^{2+}$ | Oct | 1.25 | 2.60 | - |
| | | $Fe^{3+}$ | Oct | 0.60 | 0.60 | - |
| | Biotite | $Fe^{2+}$ | Oct | 1.23 | 2.45 | - |
| | | $Fe^{3+}$ | Oct | 0.50 | 0.30 | - |
| | | $Fe^{3+}$ | Tet | 0.48 | 0.95 | - |
| | Biotite | $Fe^{2+}$ | Oct | 1.20 | 2.50 | - |
| | | $Fe^{3+}$ | Oct | 0.45 | 0.30 | - |
| | | $Fe^{3+}$ | Tet | 0.48 | 0.95 | - |
| | Chlorite | $Fe^{2+}$ | Oct | 1.25 | 2.60 | - |
| | | $Fe^{3+}$ | Oct | 0.60 | 0.40 | - |
| | | $Fe^{3+}$ | Tet | 0.55 | 1.10 | - |
| | Chlorite | $Fe^{2+}$ | Oct | 1.23 | 2.55 | - |
| | | $Fe^{3+}$ | Oct | 0.30 | 0.40 | - |
| | Minnesotaite | $Fe^{2+}$ | Oct | 1.25 | 2.60 | - |
| | | $Fe^{2+}$ | Siderite | 1.38 | 1.85 | - |
| | Vermiculite | $Fe^{3+}$ | Tet | 0.50 | 1.00 | - |
| | | $Fe^{3+}$ | Oct | 0.55 | 0.50 | - |
| | Vermiculite | $Fe^{3+}$ | Tet | 0.50 | 1.00 | - |
| | | $Fe^{3+}$ | Oct | 0.53 | 0.45 | - |
| | Stilpnomelane | $Fe^{2+}$ | Oct | 1.20 | 2.40 | - |
| | | $Fe^{3+}$ | Tet | 0.55 | 1.10 | - |
| | | $Fe^{3+}$ | Oct | 0.55 | 0.60 | - |
| | Chloritoid | $Fe^{2+}$ | Oct | 1.23 | 2.55 | - |
| | | $Fe^{2+}$ | Oct | 1.38 | 3.45 | - |
| | | $Fe^{3+}$ | Oct | 0.53 | 0.45 | - |

| Source | Mineral | Oxidation state | Lattice position | Isomer shift (mm/sec) | Quadrupole splitting (mm/sec) | Half width (mm/sec) |
|---|---|---|---|---|---|---|
| Raclavsky et al. (1975) | Montmoril-lonite | $Fe^{3+}$ | - | 0.344 | 0.456 | 0.485 |
| | | $Fe^{3+}$ | - | 0.438 | 1.076 | 0.528 |
| | Montronite | $Fe^{3+}$ | - | 0.416 | 0.396 | 0.414 |
| | | $Fe^{3+}$ | - | 0.258 | 0.834 | 0.433 |
| | Beidellite | $Fe^{3+}$ | - | 0.365 | 0.424 | 0.383 |
| | | $Fe^{3+}$ | - | 0.360 | 0.884 | 0.518 |
| | Glauconite | $Fe^{3+}$ | - | 0.370 | 0.346 | 0.369 |
| | | $Fe^{3+}$ | - | 0.390 | 0.942 | 0.518 |
| | | $Fe^{2+}$ | - | 1.056 | 2.050 | 0.728 |
| | Seladonite | $Fe^{3+}$ | - | 0.390 | 0.458 | 0.350 |
| | | $Fe^{3+}$ | - | 0.561 | 1.140 | 0.406 |
| | | $Fe^{2+}$ | - | 1.081 | 2.020 | 0.470 |
| | Illite | $Fe^{3+}$ | - | 0.376 | 0.185 | 0.380 |
| | | $Fe^{3+}$ | - | 0.375 | 0.505 | 0.530 |
| | Vermiculite | $Fe^{3+}$ | - | 0.386 | 0.870 | 0.590 |
| | | $Fe^{2+}$ | - | 0.941 | 2.180 | 0.350 |
| | | $Fe^{2+}$ | - | 1.101 | 2.740 | 0.350 |
| | Saponite | $Fe^{2+}$ | - | 1.200 | 2.401 | 0.401 |
| | | $Fe^{2+}$ | - | 1.176 | 2.710 | 0.260 |
| | Palygorskite | $Fe^{3+}$ | - | 0.336 | 0.430 | 0.350 |
| | | $Fe^{3+}$ | - | 0.330 | 0.998 | 0.469 |
| | | $Fe^{2+}$ | - | 0.316 | 1.015 | 0.290 |
| Rozenson et al. (1977) | Montmoril-lonite | $Fe^{3+}$ | - | 0.30 | 1.32 | 0.48 |
| | | $Fe^{3+}$ | - | 0.27 | 0.57 | 0.48 |
| | | $Fe^{2+}$ | - | 1.07 | 3.00 | 0.46 |
| | Montmoril-lonite | $Fe^{3+}$ | - | 0.30 | 1.29 | 0.49 |
| | | $Fe^{3+}$ | - | 0.27 | 0.61 | 0.49 |
| | | $Fe^{2+}$ | - | 1.06 | 2.95 | 0.46 |
| | Montmoril-lonite | $Fe^{3+}$ | - | 0.38 | 1.22 | 0.41 |
| | | $Fe^{3+}$ | - | 0.36 | 0.45 | 0.41 |
| | Montmoril-lonite | $Fe^{3+}$ | - | 0.34 | 1.07 | 0.44 |
| | | $Fe^{3+}$ | - | 0.29 | 0.57 | 0.44 |
| | Montmoril-lonite | $Fe^{3+}$ | - | 0.32 | 0.99 | 0.49 |
| | | $Fe^{3+}$ | - | 0.28 | 0.53 | 0.49 |
| | Montmoril-lonite | $Fe^{3+}$ | - | 0.41 | 1.16 | 0.48 |
| | | $Fe^{3+}$ | - | 0.29 | 0.54 | 0.48 |
| | Montmoril-lonite | $Fe^{3+}$ | - | 0.30 | 1.03 | 0.44 |
| | | $Fe^{3+}$ | - | 0.36 | 0.53 | 0.44 |
| | Montmoril-lonite | $Fe^{3+}$ | - | 0.31 | 0.85 | 0.51 |
| | | $Fe^{3+}$ | - | 0.29 | 0.49 | 0.51 |

| Source | Mineral | Oxidation state | Lattice position | Isomer shift (mm/sec) | Quadrupole splitting (mm/sec) | Half width (mm/sec) |
|---|---|---|---|---|---|---|
| | Montmoril-lonite | $Fe^{3+}$ | - | 0.42 | 1.09 | 0.50 |
| | | $Fe^{3+}$ | - | 0.30 | 0.56 | 0.50 |
| | | $Fe^{2+}$ | - | 1.07 | 2.80 | 0.39 |
| | Montmoril-lonite | $Fe^{3+}$ | - | 0.33 | 1.26 | 0.47 |
| | | $Fe^{3+}$ | - | 0.29 | 0.43 | 0.47 |
| | | $Fe^{2+}$ | - | 1.08 | 2.76 | 0.33 |
| | Beidellitic smectite | $Fe^{3+}$ | - | 0.48 | 1.35 | 0.56 |
| | | $Fe^{3+}$ | - | 0.30 | 0.59 | 0.56 |
| | | $Fe^{2+}$ | - | 1.10 | 2.74 | 0.34 |
| | Beidellitic smectite | $Fe^{3+}$ | - | 0.37 | 1.28 | 0.56 |
| | | $Fe^{3+}$ | - | 0.28 | 0.56 | 0.56 |
| | | $Fe^{2+}$ | - | 1.07 | 2.56 | 0.46 |
| | Nontronite | $Fe^{3+}$ | - | 0.27 | 0.70 | 0.39 |
| | | $Fe^{3+}$ | - | 0.26 | 0.28 | 0.39 |
| | Volkonskoite | $Fe^{3+}$ | - | 0.32 | 0.72 | 0.35 |
| | | $Fe^{3+}$ | - | 0.33 | 0.31 | 0.35 |
| | Metabentonite | $Fe^{3+}$ | - | 0.32 | 0.62 | 0.45 |
| Punakivi et al. (1975) | Mixture of dioctahedral chlorite & vermiculite | | | | | |
| | 1µm | $Fe^{2+}$ | - | 1.01 | 2.28 | - |
| | | $Fe^{3+}$ | - | 0.33 | 0.57 | - |
| | 2-20µm | $Fe^{2+}$ | - | 1.01 | 2.30 | - |
| | | $Fe^{3+}$ | - | 0.33 | 0.70 | - |
| | 20µm | $Fe^{2+}$ | - | 1.01 | 2.30 | - |
| | | $Fe^{3+}$ | - | 0.31 | 0.72 | - |
| | unseperated | $Fe^{2+}$ | - | 1.00 | 2.30 | - |
| | | $Fe^{3+}$ | - | 0.34 | 0.60 | - |
| Hogg et al. (1970). | Muscovite | $Fe^{2+}$ | A site,Oct | 1.15 | 3.02 | 0.16 |
| | | $Fe^{2+}$ | B site,Oct | 1.13 | 2.25 | 0.27 |
| | | $Fe^{3+}$ | Tet | 0.34 | 0.82 | 0.39 |
| | Muscovite | $Fe^{2+}$ | A site,Oct | 1.15 | 3.04 | 0.17 |
| | | $Fe^{2+}$ | B site,Oct | 1.10 | 2.14 | 0.26 |
| | | $Fe^{3+}$ | Tet | 0.37 | 0.74 | 0.33 |
| | Phlogopite | $Fe^{2+}$ | A site,Oct | 1.10 | 2.56 | 0.17 |
| | | $Fe^{2+}$ | B site,Oct | 1.08 | 2.24 | 0.21 |
| | | $Fe^{3+}$ | Tet | 0.47 | 0.80 | 0.22 |
| | Biotite | $Fe^{2+}$ | A site,Oct | 1.07 | 2.58 | 0.15 |
| | | $Fe^{2+}$ | B site,Oct | 1.06 | 2.14 | 0.20 |
| | | $Fe^{3+}$ | Tet | 0.39 | 0.72 | 0.23 |

| Source | Mineral | Oxidation state | Lattice position | Isomer shift (mm/sec) | Quadrupole splitting (mm/sec) | Half width (mm/sec) |
|---|---|---|---|---|---|---|
| | Biotite | $Fe^{2+}$ | A site,Oct | 1.13 | 2.74 | 0.12 |
| | | $Fe^{2+}$ | B site,Oct | 1.13 | 2.44 | 0.19 |
| | | $Fe^{3+}$ | Tet | 0.38 | 0.83 | 0.24 |
| Bowen et al. (1969) | Biotite | $Fe^{2+}$ | - | 1.11 | 2.47 | - |
| | | $Fe^{3+}$ | - | 0.50 | 0.60 | - |
| | Biotite | $Fe^{2+}$ | - | 1.12 | 2.51 | - |
| | | $Fe^{3+}$ | - | 0.50 | 0.80 | - |
| | Biotite | $Fe^{2+}$ | - | 1.11 | 2.42 | - |
| | | $Fe^{3+}$ | - | 0.30 | 0.60 | - |
| | Phlogopite | $Fe^{2+}$ | - | 1.11 | 2.44 | - |
| | | $Fe^{3+}$ | - | 0.4 | 0.9 | - |
| | Av. Trioctahedral mica. | $Fe^{2+}$ | - | 1.11 | 2.46 | - |
| | | $Fe^{3+}$ | - | 0.42 | 0.90 | - |
| | Muscovite | $Fe^{2+}$ | - | 1.09 | 2.89 | - |
| | | $Fe^{3+}$ | - | 0.38 | 0.69 | - |
| | Muscovite | $Fe^{2+}$ | - | 1.13 | 2.87 | - |
| | | $Fe^{3+}$ | - | 0.38 | 0.70 | - |
| | Av. Muscovite | $Fe^{2+}$ | - | 1.39 | 2.93 | - |
| | | $Fe^{3+}$ | - | 0.36 | 0.68 | - |
| | Glauconite | $Fe^{2+}$ | - | 1.24 | 2.3 | - |
| | | $Fe^{3+}$ | - | 0.36 | 0.45 | - |
| Goodman et al. (1978) | Clinochlore | $Fe^{2+}$ | - | 1.13 | 2.69 | 0.28 |
| | | $Fe^{2+}$ | - | 1.13 | 2.46 | 0.41 |
| | | $Fe^{3+}$ | - | 0.39 | 0.57 | 0.24 |
| | | $Fe^{3+}$ | - | 0.34 | 0.82 | 0.76 |
| | Clinochlore | $Fe^{2+}$ | - | 1.13 | 2.68 | 0.28 |
| | | $Fe^{2+}$ | - | 1.15 | 2.30 | 0.30 |
| | | $Fe^{3+}$ | - | 0.28 | 0.78 | 0.78 |
| | Penninite | $Fe^{2+}$ | - | 1.13 | 2.72 | 0.29 |
| | | $Fe^{2+}$ | - | 1.15 | 2.38 | 0.38 |
| | | $Fe^{3+}$ | - | 0.27 | 0.53 | 0.71 |
| | | $Fe^{3+}$ | - | 0.40 | 1.40 | 0.80 |
| | Penninite | $Fe^{2+}$ | - | 1.13 | 2.72 | 0.26 |
| | | $Fe^{2+}$ | - | 1.14 | 2.41 | 0.34 |
| | | $Fe^{2+}$ | - | 0.25 | 0.70 | 0.79 |
| | Mg Chlorite | $Fe^{2+}$ | - | 1.13 | 2.70 | 0.25 |
| | | $Fe^{2+}$ | - | 1.13 | 2.51 | 0.36 |
| | | $Fe^{3+}$ | - | 0.32 | 0.58 | 0.27 |

| Source | Mineral | Oxidation state | Lattice position | Isomer shift (mm/sec) | Quadrupole splitting (mm/sec) | Half width (mm/sec) |
|---|---|---|---|---|---|---|
| | Clinochlore | $Fe^{2+}$ | - | 1.13 | 2.71 | 0.28 |
| | | $Fe^{2+}$ | - | 1.14 | 2.37 | 0.34 |
| | | $Fe^{3+}$ | - | 0.24 | 0.66 | 0.75 |
| | Thuringite | $Fe^{2+}$ | - | 1.14 | 2.67 | 0.35 |
| | | $Fe^{2+}$ | - | 1.15 | 2.39 | 0.55 |
| | | $Fe^{3+}$ | - | 0.36 | 1.10 | 0.85 |
| | Chamosite | $Fe^{2+}$ | - | 1.13 | 2.71 | 0.28 |
| | | $Fe^{2+}$ | - | 1.12 | 2.42 | 0.39 |
| | | $Fe^{3+}$ | - | 0.37 | 0.61 | 0.41 |
| | | $Fe^{3+}$ | - | 0.47 | 1.07 | 0.61 |
| | Daphnite | $Fe^{2+}$ | - | 1.13 | 2.69 | 0.28 |
| | | $Fe^{2+}$ | - | 1.12 | 2.35 | 0.42 |
| | | $Fe^{2+}$ | - | 0.26 | 0.72 | 0.61 |
| | | $Fe^{2+}$ | - | 0.37 | 1.06 | 0.52 |
| Malden & Meads (1967) | Kaolinite | $Fe^{2+}$ | - | - | ~2.25 | - |
| | | $Fe^{3+}$ | - | 0.39 | 0.50 | - |

# APPENDIX 5

Description and listing of Fortran program INTCORRECT.

Appendix 5.

Description and listing of FORTRAN program INTCORRECT.

The samples used in the palaeomagnetic studies of the nine-metre Delft core were not of the normal dimensions required for the Digico magnetometer, that is cylinders with a diameter and long axis of 2.54mm. Instead small microboxes made from plastic were used with internal dimensions of 19 x 19 x 14 mm. The computer program supplied with the Digico magnetometer is only capable of correcting for sample size variations in the Z direction. Therefore, a simple seperate FORTRAN program, INTCORRECT, has been written to correct the measured intensities of magnetization. A listing of the program follows this description. The formula used in the correction is,

$$INT_c = \sqrt{((X*R1)^2+(Y*R2)^2+(Z*R3)^2)}$$

where, $INT_c$ is the corrected intensity of magnetization in μG.

X,Y, and Z are the components of magnetization measured in the three orthogonal directions by the Digico magnetometer.

R1,R2, and R3 are the ratios of the assumed dimensions of the sample (2.54 mm in each orthogonal direction) to the actual dimensions of the sample in the X, Y, and Z directions respectively.

Similar symbols are used in the FORTRAN program to identify the various variables and constants. Initially, a card or a line is input with the number of samples to be corrected. Next the dimensions of the sample (D1, D2, and D3) are input corresponding to the X, Y, and Z directions of the sample (using the "Digico"

convention). Finally, a series of cards or lines, are input, one for each sample, with the measured components of magnetization of the sample, as measured by the magnetometer in the order X, Y, and Z.

The output lists the corrected intensity of magnetization, in $\mu G$, with the dimensions of the sample and its initial measured components of magnetization in each of the X, Y, and Z directions.

Listing of FORTRAN program INTCORRECT.

```
0000          MASTER INTCORRECT
0001 C      N IS THE NUMBER OF CORRECTIONS TO BE MADE
0002 C      D1 D2 AND D3 ARE THE DIMENSIONS OF THE SAMPLE
0003 C      X Y Z ARE THE MEASURED COMPONENTS OF MAGNETIZATION
0004          READ(1,10)N
0005          READ(1,20)D1,D2,D3
0006          WRITE(2,25)D1,D2,D3
0007          R1=2.54/D1
0008          R2=2.54/D2
0009          R3=2.54/D3
0010          DO 100 I=1,N
0011          READ(1,30)X,Y,Z
0012          WRITE(2,35)X.Y,Z
0013          X1=(X*R1)**2.0
0014          Y1=(Y*R2)**2.0
0015          Z1=(Z*R3)**2.0
0016          CINT=SQRT(X1+Y1+Z1)
0017          WRITE(2,15)CINT
0018      100 CONTINUE
0019          STOP
0020       10 FORMAT(I0)
0021       15 FORMAT(23HO CORRECTED INTENSITY =,F8.3)
0022       20 FORMAT(3F0.0)
0023       25 FORMAT(28HO DIMENSIONS OF SAMPLES ARE ,3F8.3)
0024       30 FORMAT(3F0.0)
0025       35 FORMAT(23HO X Y Z COMPONENTS ARE ,3F8.3)
0026          END
0027          FINISH
0028          ****
```

# APPENDIX 6

Description and listings of the Fortran programs DECSEC and INCSEC.

Appendix 6.

Description and listings of the FORTRAN programs DECSEC and INCSEC.

The FORTRAN programs DECSEC and INCSEC perform running mean smoothing of palaeomagnetic data for declination and inclination measurements respectively. Modifications of the program INCSEC may be used to smooth intensity and susceptibility measurements. The programs have been developed from the subroutines of Davies (1973).

The programs have been specifically designed for processing data recovered from the Delft cores, although with minor modification can be used for results from any coring method. In addition to performing running mean smoothing the program DECSEC calculates the mean declination of each one-metre core-section and uses that value as a fiducial line enabling orientation of core-sections with respect to one another. No orietation of the inclination results is necessary. A facility is also provided which eneables filtering of the data, so that data which varies by greater than plus or minus a chosen constant from the mean declination or inclination is removed from the calculations, by linear interpolation between adjacent data points.

The data for each run of the program is listed, together with its format, at the top of the listings of the two programs. Listings of DECSEC and INCSEC follow this description.

Graph plotting subroutines are used to plot the data in the form of a log. The resulting diagram, scaled to an A4 format, shows the raw data plotted as crosses, the smoothed data plotted as a continuous line and also the standard deviation

plotted as "tram lines". The standard deviation for each smoothed data point is calculated so that it represents the standard deviation of the raw data used to obtain it.

Listings of any of the results may be output, as described in the listing of the programs, by calling subroutine PRINTM. Examples of the graphical output are shown in appendix 7.

Listing of FORTRAN program DECSEC.

```
      MASTER DECSEC
      DIMENSION XIN(450),XOUT(450),XSTD(450),XINA(450)
      DIMENSION Y(450),Y2(450),XSTD1(450),XSTD2(450)
C     RUNNING MEAN SMOOTHING OF DECLINATION DATA OBTAINED FROM
C     ONE METRE CORE SECTIONS IS PERFORMED. IT IS ASSUMED THAT
C     THE CORE SECTIONS ARE NOT ORIENTED WITH RESPECT TO ONE
C     ANOTHER.
C     1ST CARD  SMOOTHING FACTOR AND FILTER (IO,FO.O)
C     2ND CARD  THE NUMBER OF CORE SECTIONS (IO)
C     3RD CARD  NUMBER OF SPECIMENS FROM FIRST CORE SECTION (2IO)
C     THE SECOND FIGURE IS ALWAYS (1).
C     4TH AND SUBSEQUENT CARDS ARE THE DECLINATION VALUES (FO.O)
C     REPEAT FROM CARD THREE FOR FURTHER CORE SECTIONS.
C     NOTE:  THE SMOOTHING FACTOR MUST BE AN ODD INTEGER.
C            THE FILTER (AFILT) IS USED TO REMOVE DATA WHICH DIFFER
C            BY GREATER THAN PLUS OR MINUS AFILT FROM THE MEAN
C            DECLINATION.
C   LISTINGS OF THE RAW, THE SMOOTHED AND FILTERED DATA OR THE
C   STANDARD DEVIATION DATA MAY BE OBTAINED BY CALLING SUBROUTINE
C   PRINTM
C   E.G. INSERT  CALL PRINTM(XOUT,IE,450,1)
C    WOULD PRODUCE A LISTING OF THE ORIENTED AND SMOOTHED DATA.
      READ(1,1000)M,AFILT
      READ(1,1006)NUM,SINC
      N=0
      N2=1
      N3=0
      S=0.0
      NUMB=FLOAT(NUM)
      CALL OPENGINOGP
      DO 10 L=1,NUM
      CALL READM(XIN,NN,NM,450,1)
      L4=1
      N2=N2+N
      N3=N3+NN
      SUMX=0.0
      DO 104 L2=1,N
      SUMX=SUMX+XIN(L2)
  104 CONTINUE
C     AMEAN IS THE MEAN OF EACH CORE SECTION
      AMEAN=SUMX/FLOAT(N)
      ADIV=1.0/FLOAT(N)
      DO 105 L3=N2,N3
      XINA(L3)=XIN(L4)
      IF(XINA(L3).GT.SINC)GOTO 20
      IF(XINA(L3).LT.SINC)GOTO 21
   20 BFILT=XINA(L3)-AFILT
      IF(BFILT.GT.SINC)GOTO 22
      GOTO 23
   21 CFILT=XINA(L3)+AFILT
      IF(CFILT.LT.SINC)GOTO 22
      GOTO 23
   22 XINA(L3)=SINC
```

```
  23 Y(L3)=S+ADIV
     S=Y(L3)
     L4=L4+1
C    XINA IS THE NORMALISED DECLINATION ARRAY.
 105 CONTINUE
  10 CONTINUE
     IE=N3-M+1
     ADIV2=NUMB/FLOAT(IE)
     S2=0.0
     DO 100 I=1,IE
     SUM=0.0
     SUMX1=0.0
     Y2(I)=S2+ADIV2
     S2=Y2(I)
     DO 101 J=1,M
     K=I+J-1
     SUM=SUM+XINA(K)
     SUMX1=SUMX1+XINA(K)*XINA(K)
C    XOUT IS THE SMOOTHED AND NORMALISED ARRAY
 101 CONTINUE
     XOUT(I)=SUM/FLOAT(M)
     VAR=(FLOAT(M)*SUMX1-SUM*SUM)/FLOAT(M*(M-1))
C    XSTD IS THE STANDARD DEVIATION OF THE (M) SAMPLES USED TO
C    OBTAIN XOUT.
     XSTD(I)=SQRT(VAR)
     XSTD1(I)=XOUT(I)+XSTD(I)
     XSTD2(I)=XOUT(I)-XSTD(I)
 100 CONTINUE
     CALL SHIFT2(70.0,50.0)
     CALL AXIPOS(0,0.0,75.0,200.0,1)
     CALL AXIPOS(1,0.0,0.0,150.0,2)
     CALL AXISCA(3,NUM,0.0,9.0,1)
     CALL AXISCA(3,12,-90.0,90.0,2)
     CALL CHASIZ(3.0,3.5)
     CALL AXIDRA(1,0,1)
     CALL AXIDRA(-1,-1,2)
     CALL MOVTO2(-20.0,60.0)
     CALL CHAANG(90.0)
     CALL CHAHOL(13HDECLINATION*.)
     CALL CHAANG(0.0)
     CALL CHASIZ(2.0,2.0)
      CALL GRAPOL(Y2,XSTD1,IE)
      CALL GRAPOL(Y2,XSTD2,IE)
     CALL PENSEL(2,0.0,0)
      CALL GRAPOL(Y2,XOUT,IE)
     CALL PENSEL(7,0.0,0)
      CALL GRASYM(Y,XINA,N3,4,0)
     CALL DEVEND
1000 FORMAT(IO,FO.0)
1006 FORMAT(IO,FO.0)
     STOP
     END
C
     SUBROUTINE READM(A,N,M,N1,M1)
     DIMENSION A(N1,M1)
     READ(1,1000)N,M
     DO 100 I=1,N
```

```
      READ(1,1001)N,M
  100 CONTINUE
      RETURN
 1000 FORMAT(2I0)
 1001 FORMAT(10F0.0)
      END
C
      SUBROUTINE PRINTM(A,N,M,N1,M1)
      DIMENSION A(N1,M1)
      DO 100 IB=1,M,10
      IE=IB+9
      IF(IE-M)2,2,1
    1 IE=M
    2 WRITE(2,2000)(I,I=IB,IE)
      DO 101 J=1,N
      WRITE(2,2001) J,(A(J,K),K=IB,IE)
  101 CONTINUE
  100 CONTINUE
      RETURN
 2000 FORMAT(1H1,1X,10I12)
 2001 FORMAT(1H0,I5,10F8.2)
      END
      FINISH
****
```

Listing of Fortran program INCSEC.

```
      MASTER INCSEC
      DIMENSION XIN(450),XOUT(450),XSTD(450),XINA(450)
      DIMENSION Y(450),Y2(450),XSTD1(450),XSTD2(450)
C   RUNNING MEAN SMOOTHING OF INCLINATION DATA OBTAINED FROM ONE-
C   METRE CORE SECTIONS IS PERFORMED. THE CORE SECTIONS ARE
C   ASSUMED TO BE ORIENTED VERTICALLY AND THUS NO ORIENTATION
C   CORRECTIONS ARE MADE.
C   1ST CARD  SMOOTHING FACTOR AND FILTER (IO,FO.O)
C   2ND CARD  THE NUMBER OF CORE SECTIONS AND THE INCLINATION OF
C   THE PRESENT EARTHS FIELD AT THE CORING SITE. (IO,FO.O)
C   3RD CARD NUMBER OF SPECIMENS FROM THE FIRST CORE SECTION (2IO)
C   THE SECOND FIGURE IS ALWAYS ONE.
C   4TH AND SUBSEQUENT CARDS ARE THE INCLINATION VALUES (FO.O)
C   REPEAT FROM CARD THREE FOR FURTHER CORE SECTIONS.
C   NOTE:  THE SMOOTHING FACTOR MUST BE AN ODD INTEGER.
C          THE FILTER (AFILT) IS USED TO REMOVE DATA WHICH DIFFER
C          BY GREATER THAN PLUS OR MINUS AFILT FROM THE PRESENT
C          INCLINATION.
C   LISTINGS OF THE RAW, THE SMOOTHED AND FILTERED DATA OR THE
C   STANDARD DEVIATION DATA MAY BE OBTAINED BY CALLING SUBROUTINE
C   PRINTM
C   E.G. INSERT  CALL PRINTM(XOUT,IE,450,1)
C   WOULD PRODUCE A LISTING OF THE FILTERED AND SMOOTHED DATA
      READ(1,1000)M,AFILT
      READ(1,1006)NUM,SINC
      N=0
      N2=1
      N3=0
      S=0.0
      NUMB=FLOAT(NUM)
      CALL OPENGINOGP
      DO 10 L=1,NUM
      CALL READM(XIN,NN,NM,450,1)
      L4=1
      N2=N2+N
      N3=N3+NN
      SUMX=0.0
      DO 104 L2=1,N
      SUMX=SUMX+XIN(L2)
  104 CONTINUE
C     AMEAN IS THE MEAN OF EACH CORE SECTION
      AMEAN=SUMX/FLOAT(N)
      ADIV=1.0/FLOAT(N)
      DO 105 L3=N2,N3
      XINA(L3)=XIN(L4)
      IF(XINA(L3).GT.SINC)GOTO 20
      IF(XINA(L3).LT.SINC)GOTO 21
   20 BFILT=XINA(L3)-AFILT
      IF(BFILT.GT.SINC)GOTO 22
      GOTO 23
   21 CFILT=XINA(L3)+AFILT
      IF(CFILT.LT.SINC)GOTO 22
      GOTO 23
   22 XINA(L3)=SINC
```

```
   23 Y(L3)=S+ADIV
      S=Y(L3)
      L4=L4+1
C     XINA IS THE FILTERED INCLINATION ARRAY
  105 CONTINUE
   10 CONTINUE
      IE=N3-M+1
      ADIV2=NUMB/FLOAT(IE)
      S2=0.0
      DO 100 I=1,IE
      SUM=0.0
      SUMX1=0.0
      Y2(I)=S2+ADIV2
      S2=Y2(I)
      DO 101 J=1,M
      K=I+J-1
      SUM=SUM+XINA(K)
      SUMX1=SUMX1+XINA(K)*XINA(K)
C     XOUT IS THE SMOOTHED AND FILTERED ARRAY.
  101 CONTINUE
      XOUT(I)=SUM/FLOAT(M)
      VAR=(FLOAT(M)*SUMX1-SUM*SUM)/FLOAT(M*(M-1))
C     XSTD IS THE STANDARD DEVIATION OF THE (M) SAMPLES USED TO
C     OBTAIN XOUT.
      XSTD(I)=SQRT(VAR)
      XSTD1(I)=XOUT(I)+XSTD(I)
      XSTD2(I)=XOUT(I)-XSTD(I)
  100 CONTINUE
      CALL SHIFT2(70.0,50.0)
      CALL AXIPOS(0,0.0,0.0,200.0,1)
      CALL AXIPOS(1,0.0,0.0,150.0,2)
      CALL AXISCA(3,NUM,0.0,9.0,1)
      CALL AXISCA(3,9,0.0,90.0,2)
      CALL CHASIZ(3.0,3.5)
      CALL AXIDRA(-1,-1,2)
      CALL AXIDRA(1,0,1)
      CALL MOVTO2(-20.0,60.0)
      CALL CHAANG(90.0)
      CALL CHAHOL(13HINCLINATION*.)
      CALL CHAANG(0.0)
      CALL CHASIZ(2.0,2.0)
       CALL GRAPOL(Y2,XSTD1,IE)
       CALL GRAPOL(Y2,XSTD2,IE)
      CALL PENSEL(2,0.0,0)
       CALL GRAPOL(Y2,XOUT,IE)
      CALL PENSEL(7,0.0,0)
       CALL GRASYM(Y,XINA,N3,4,0)
      CALL DEVEND
 1000 FORMAT(IO,FO.0)
 1006 FORMAT(IO,FO.0)
      STOP
      END
C
      SUBROUTINE READM(A,N,M,N1,M1)
      DIMENSION A(N1,M1)
      READ(1,1000)N,M
      DO 100 I=1,N
```

```
      READ(1,1001)N,M
  100 CONTINUE
      RETURN
 1000 FORMAT(2I0)
 1001 FORMAT(10F0.0)
      END
C
      SUBROUTINE PRINTM(A,N,M,N1,M1)
      DIMENSION A(N1,M1)
      DO 100 IB=1,M,10
      IE=IB+9
      IF(IE-M)2,2,1
    1 IE=M
    2 WRITE(2,2000)(I,I=IB,IE)
      DO 101 J=1,N
      WRITE(2,2001) J,(A(J,K),K=IB,IE)
  101 CONTINUE
  100 CONTINUE
      RETURN
 2000 FORMAT(1H1,1X,10I12)
 2001 FORMAT(1H0,I5,10F8.2)
      END
      FINISH
****
```

# APPENDIX 7.

Plots of DECSEC and INCSEC for the odd and even data sets from core D1.

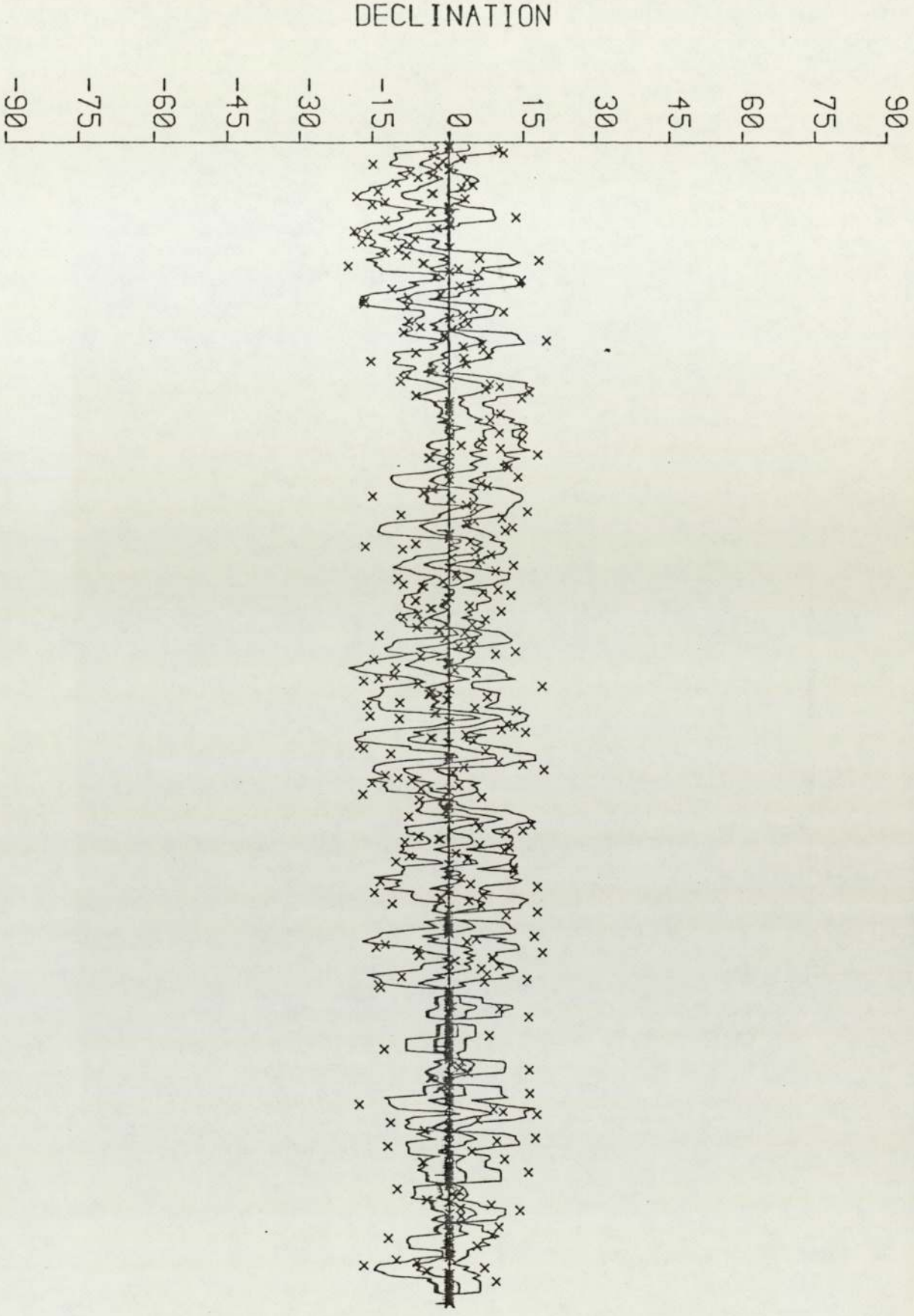


Core D1, even data set, five-term smoothing with a 20° filter.

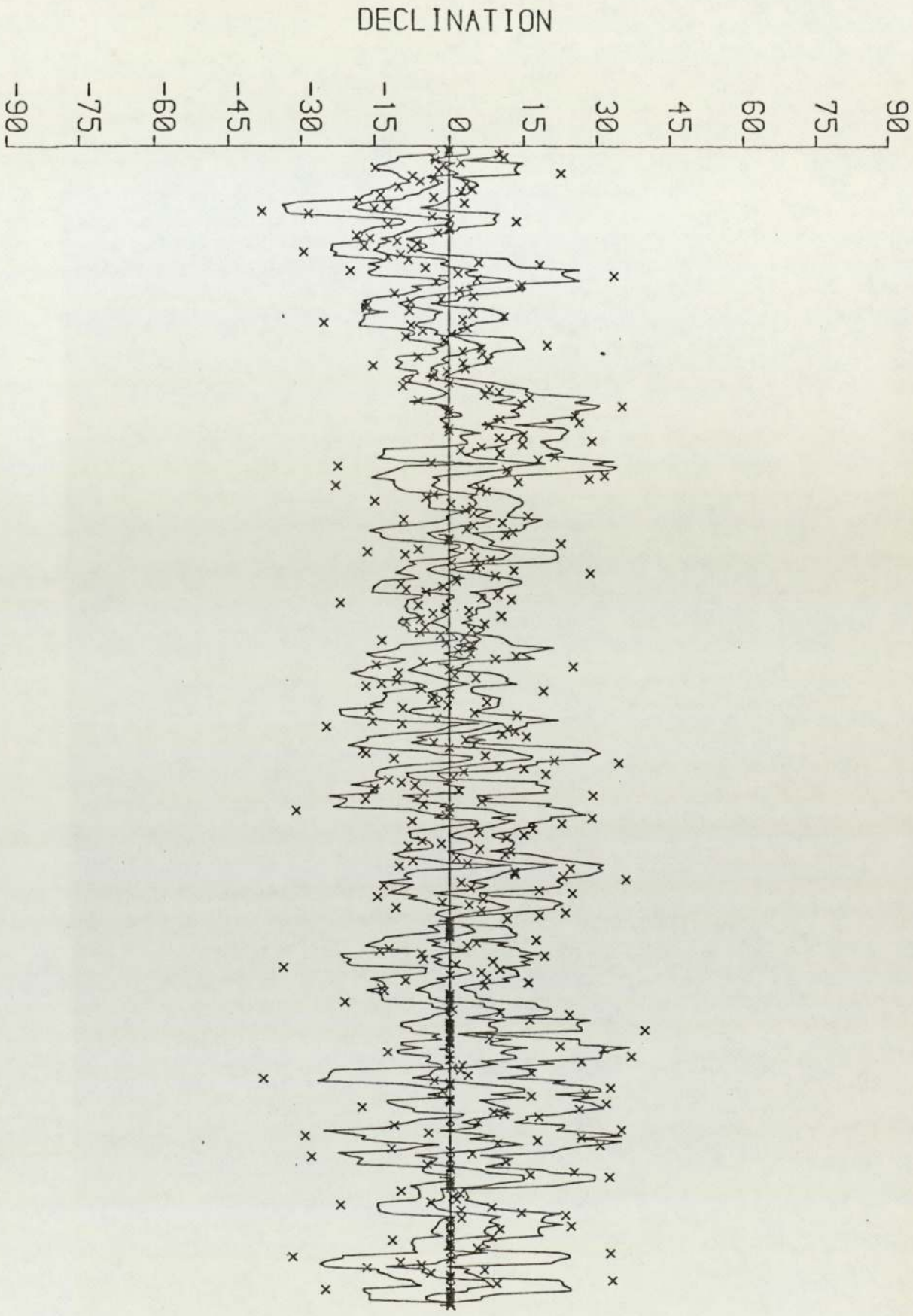


Core D1, even data set, five term smoothing with a 40° filter.

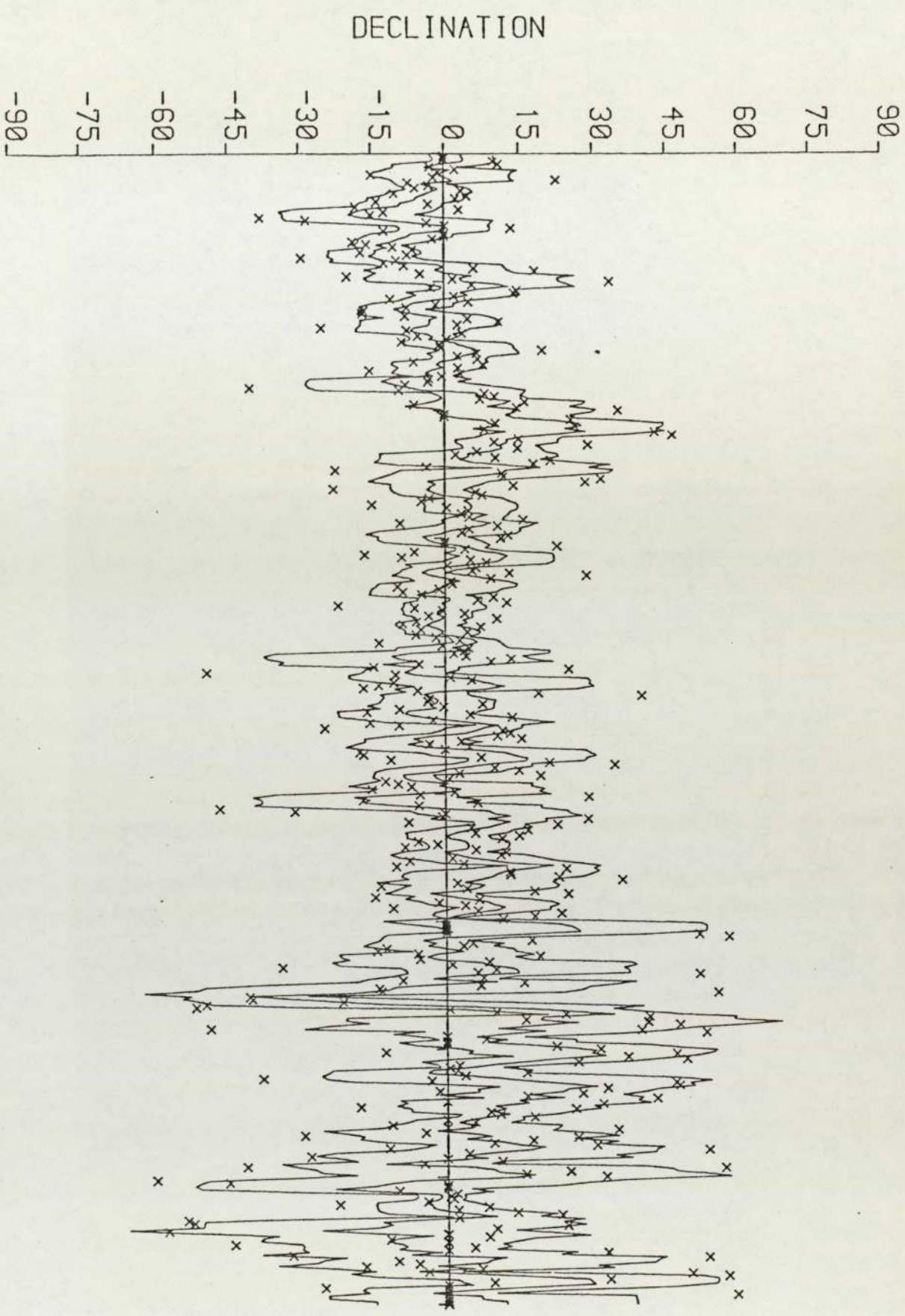


Core D1, even data set, five-term smoothing with a 60° filter.

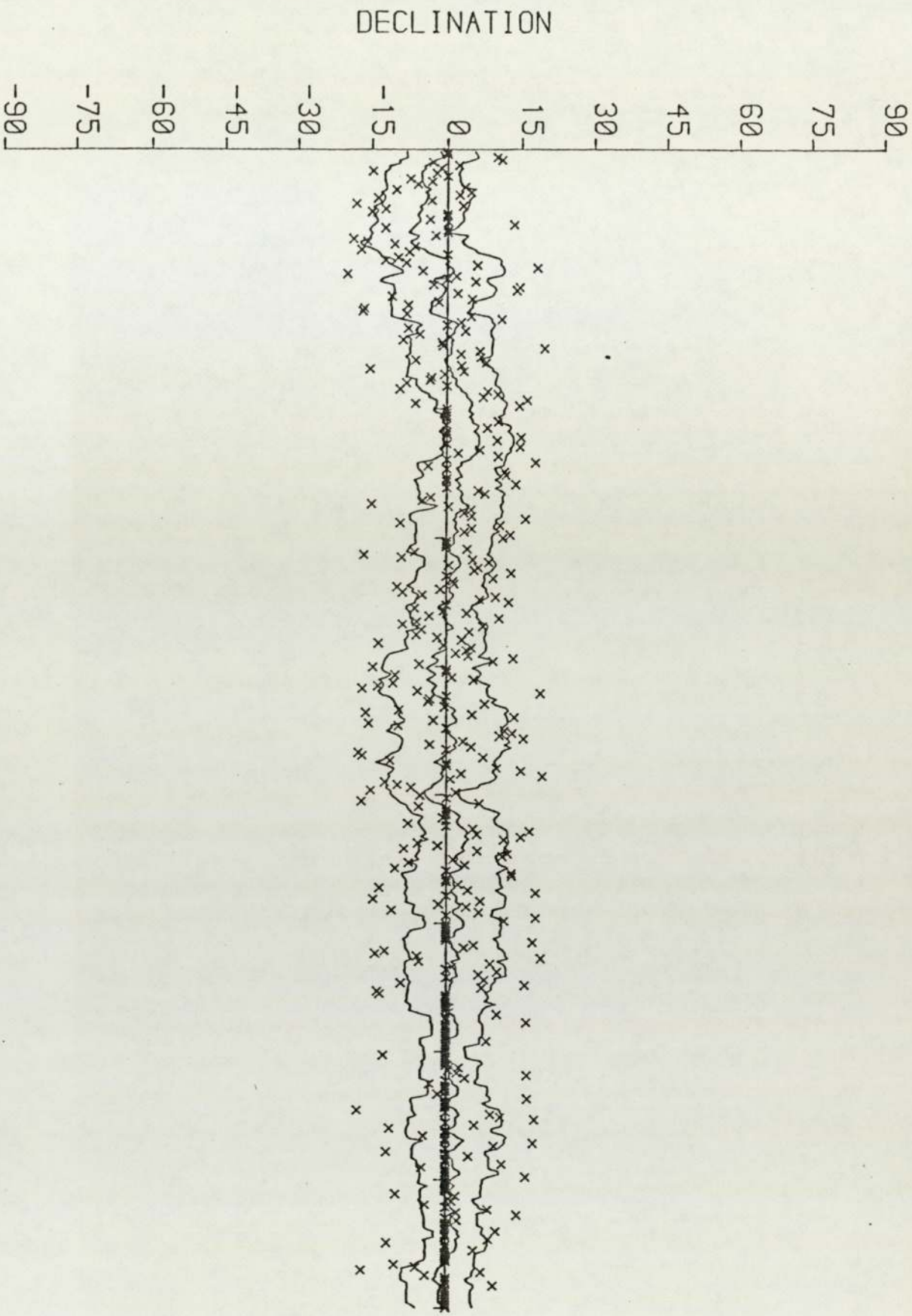


Core D1, even data set, fifteen-term smoothing with a 20° filter.

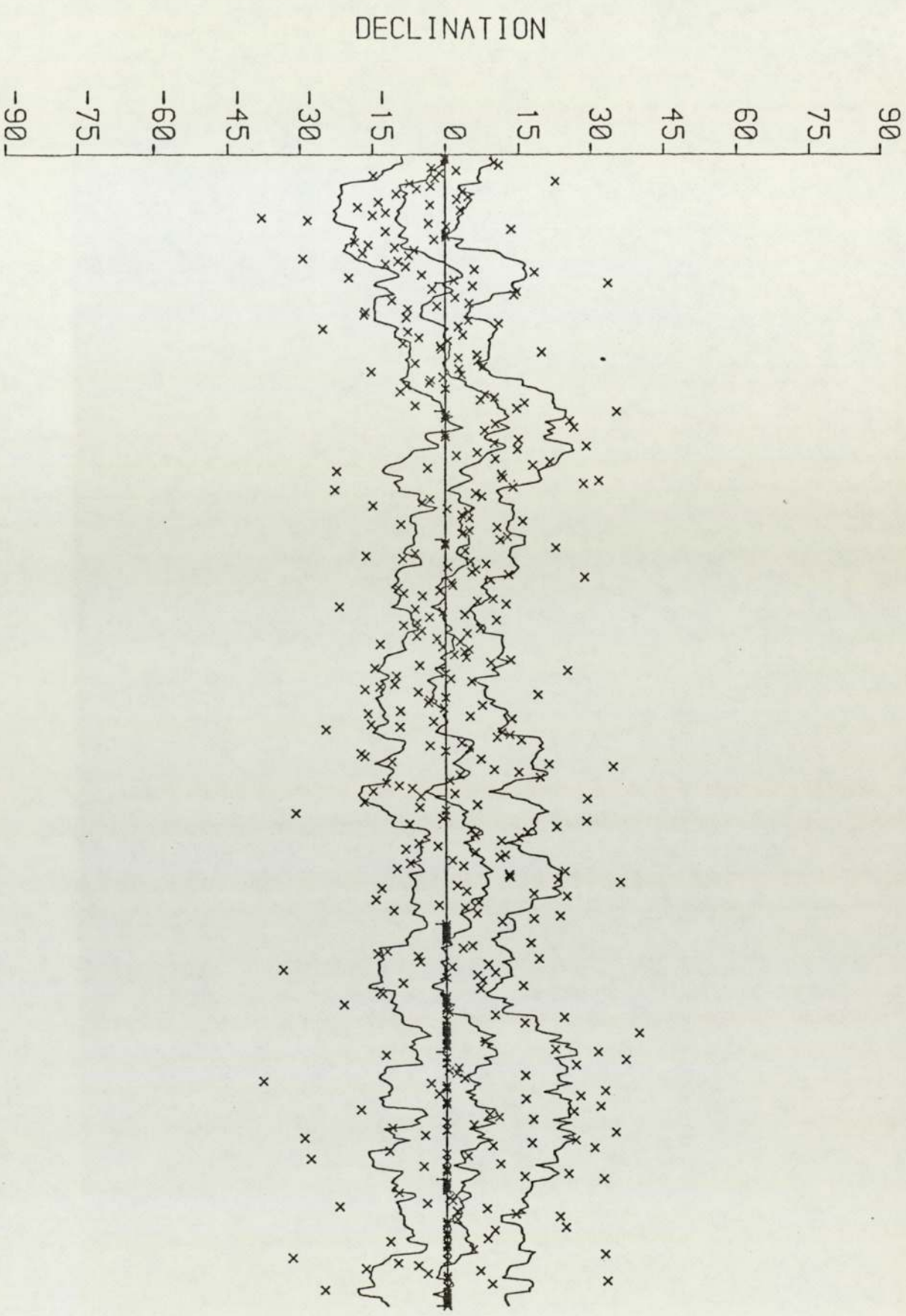


Core D1, even data set, fifteen-term smoothing with a 40° filter.

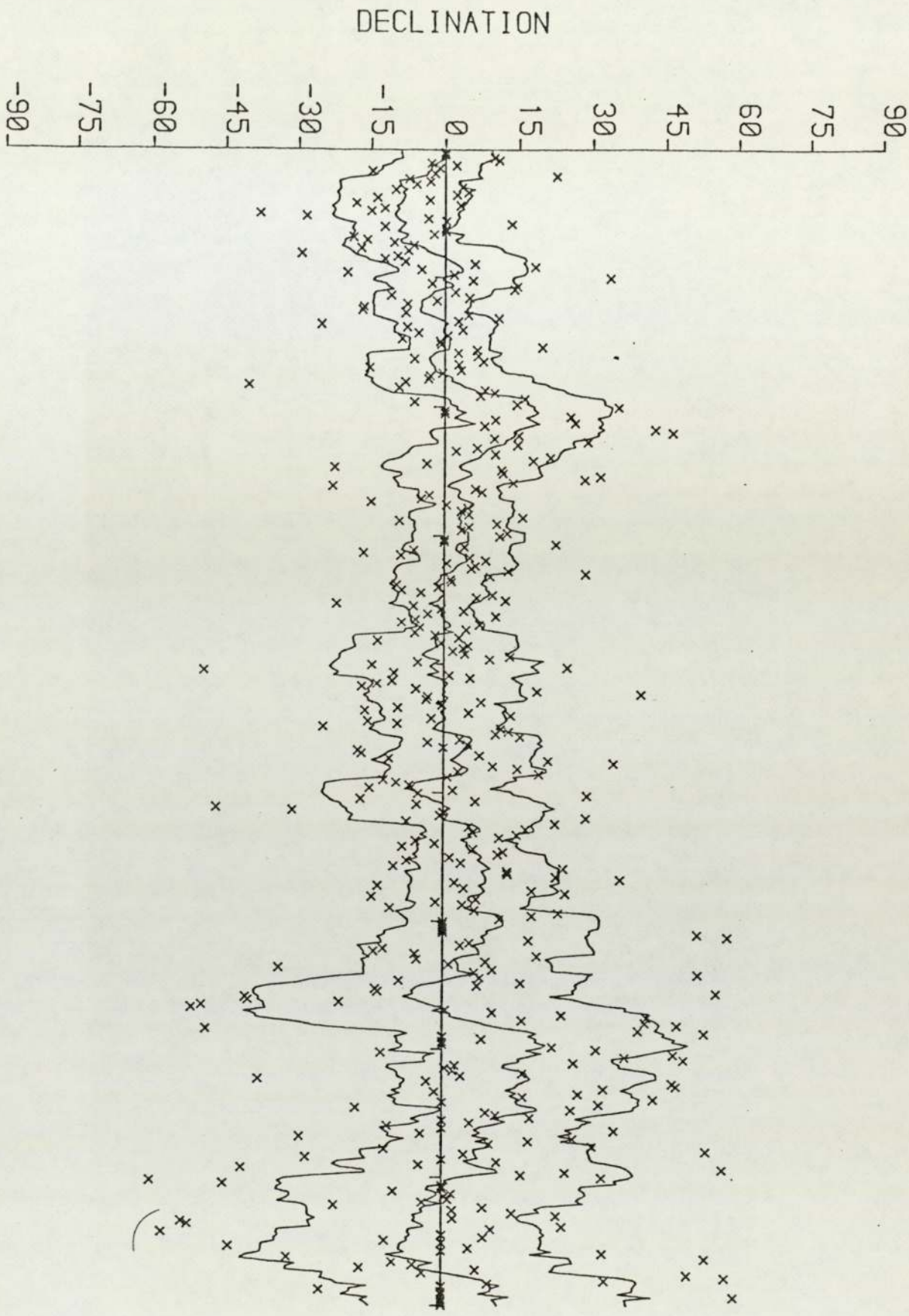


Core D1, even data set, fifteen-term smoothing with a 60° filter.

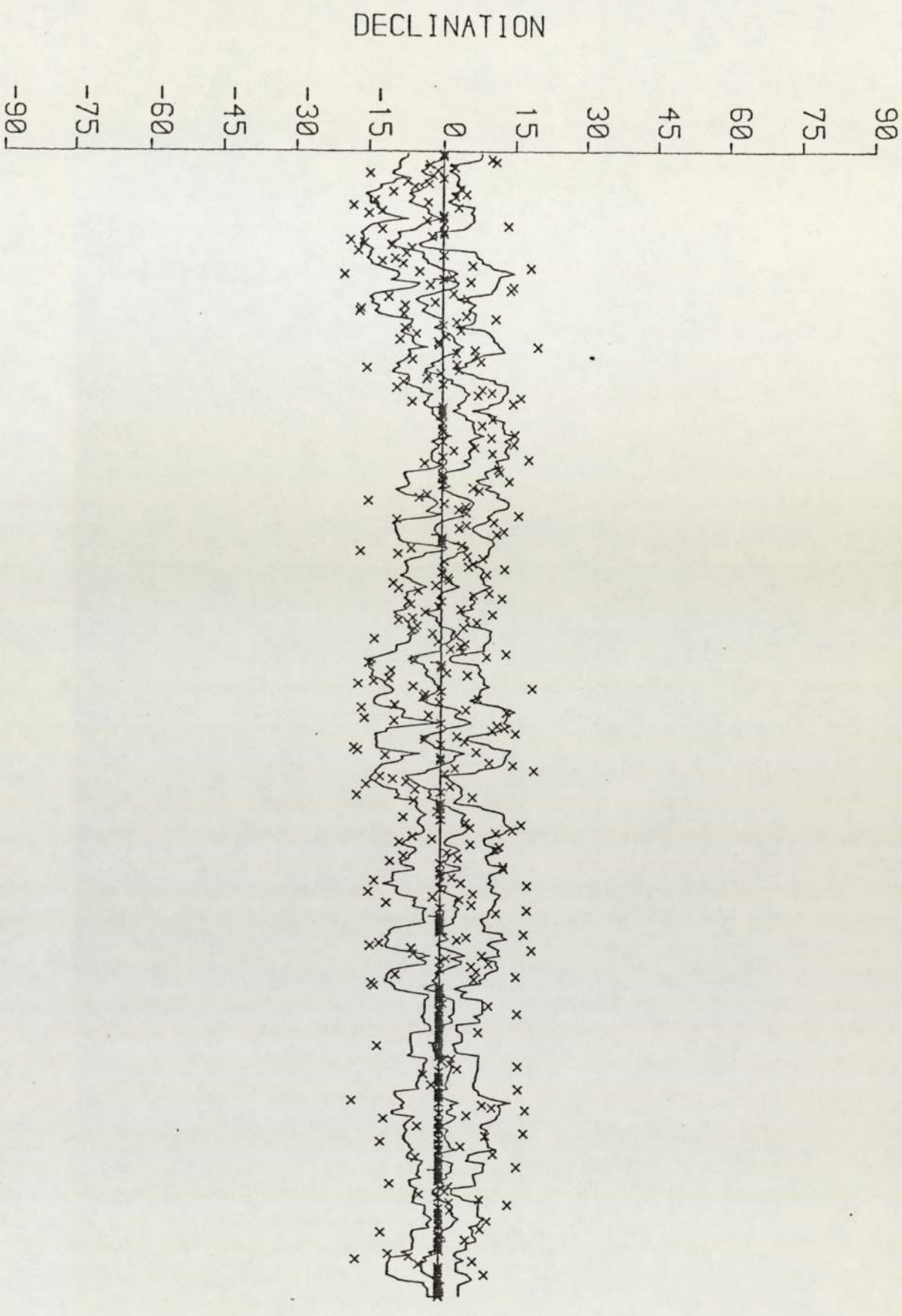


Core D1, even data set, nine-term smoothing with a 20° filter.

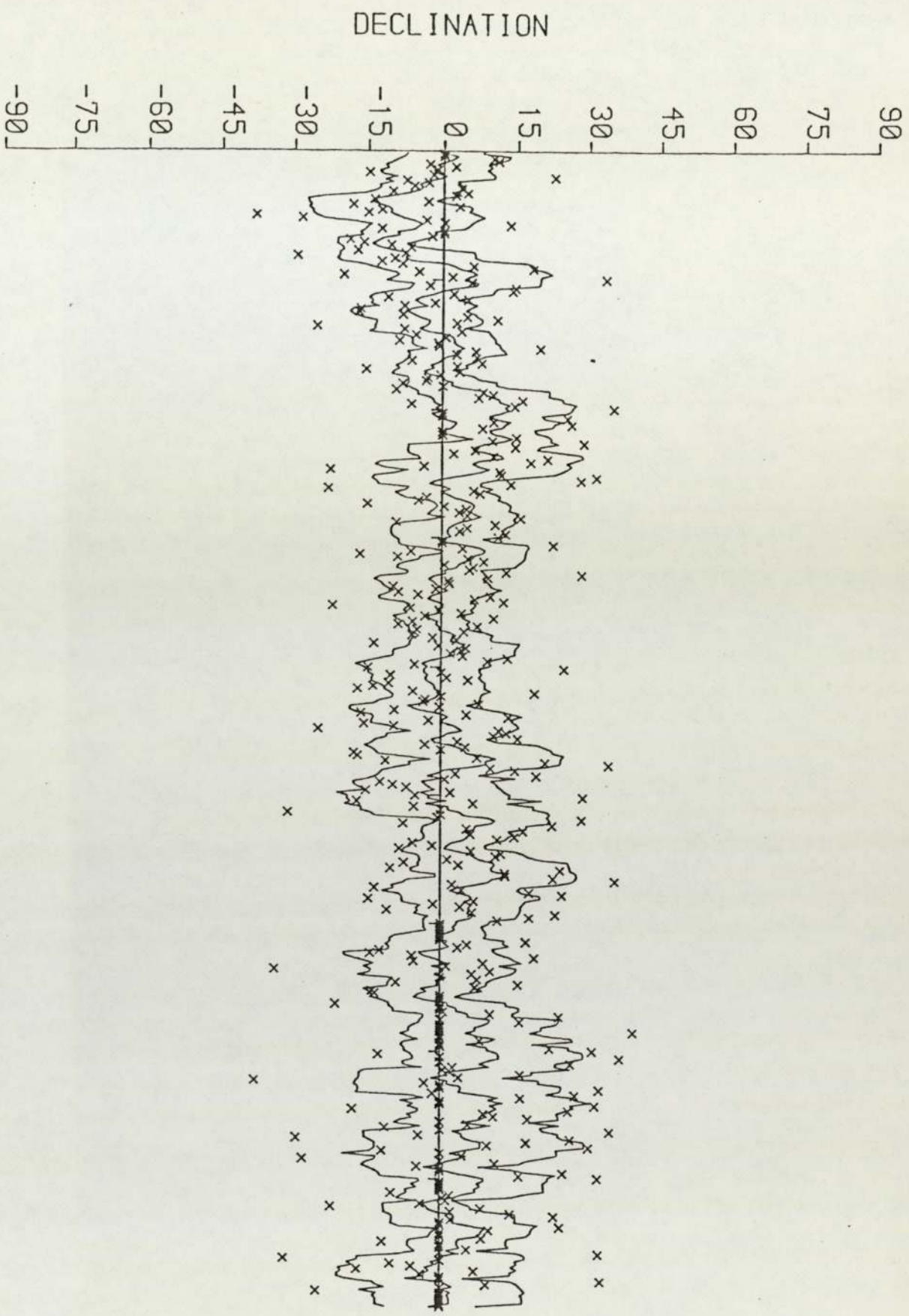


Core D1, even data set, nine-term smoothing with a 40° filter.

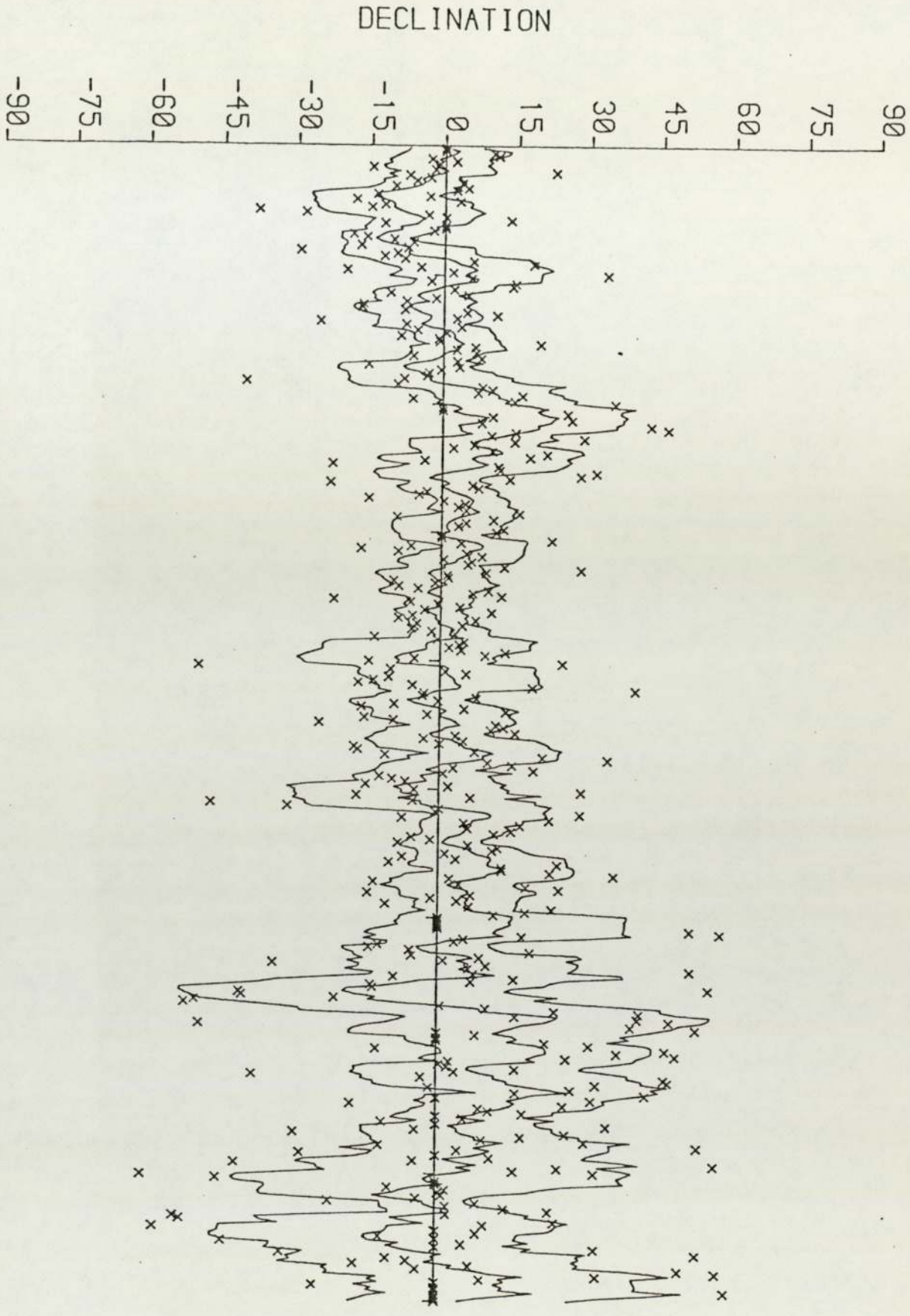


Core D1, even data set, nine-term smoothing with a 60° filter.

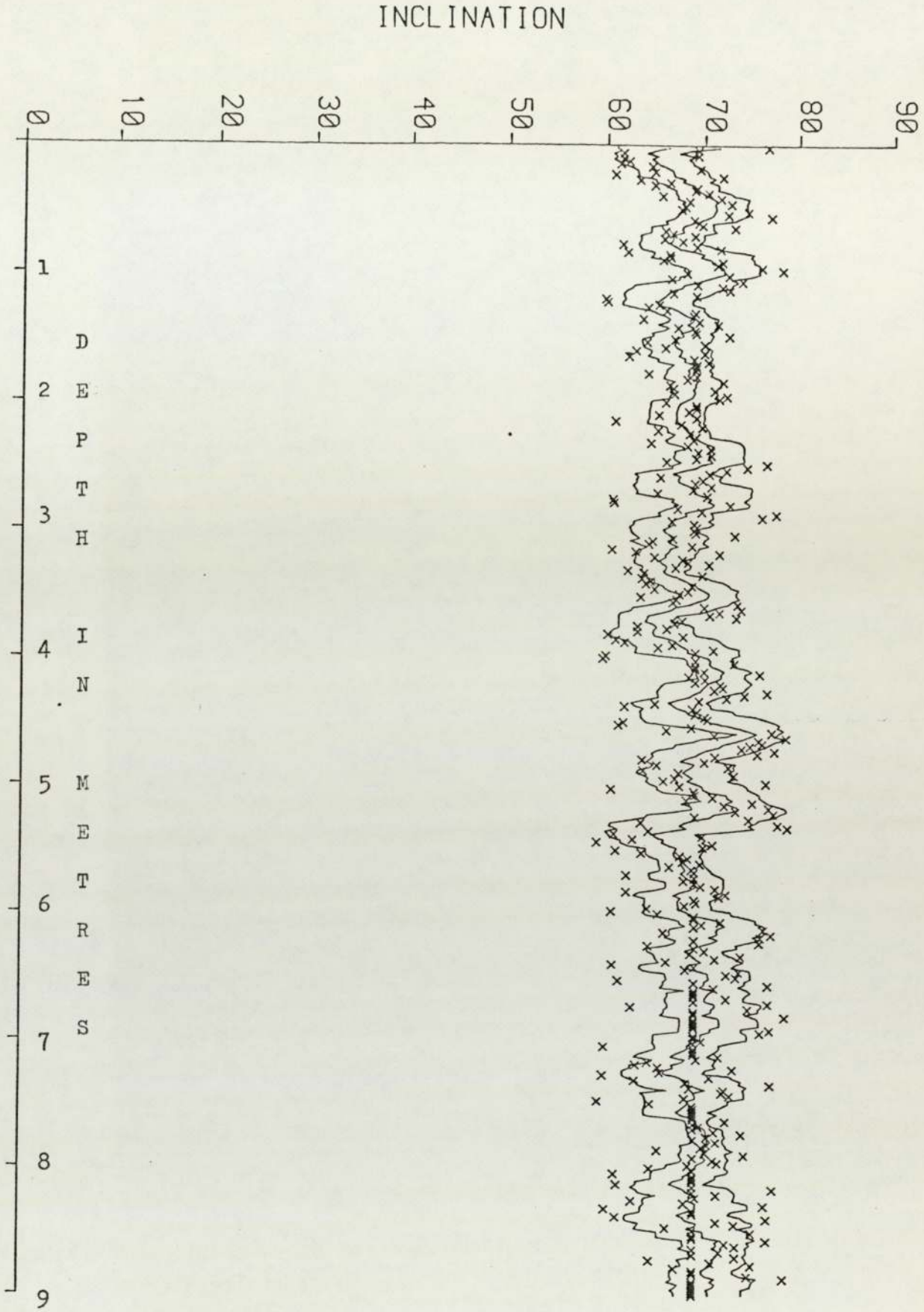


Core D1, odd data set, nine-term smoothing with a 10° filter.

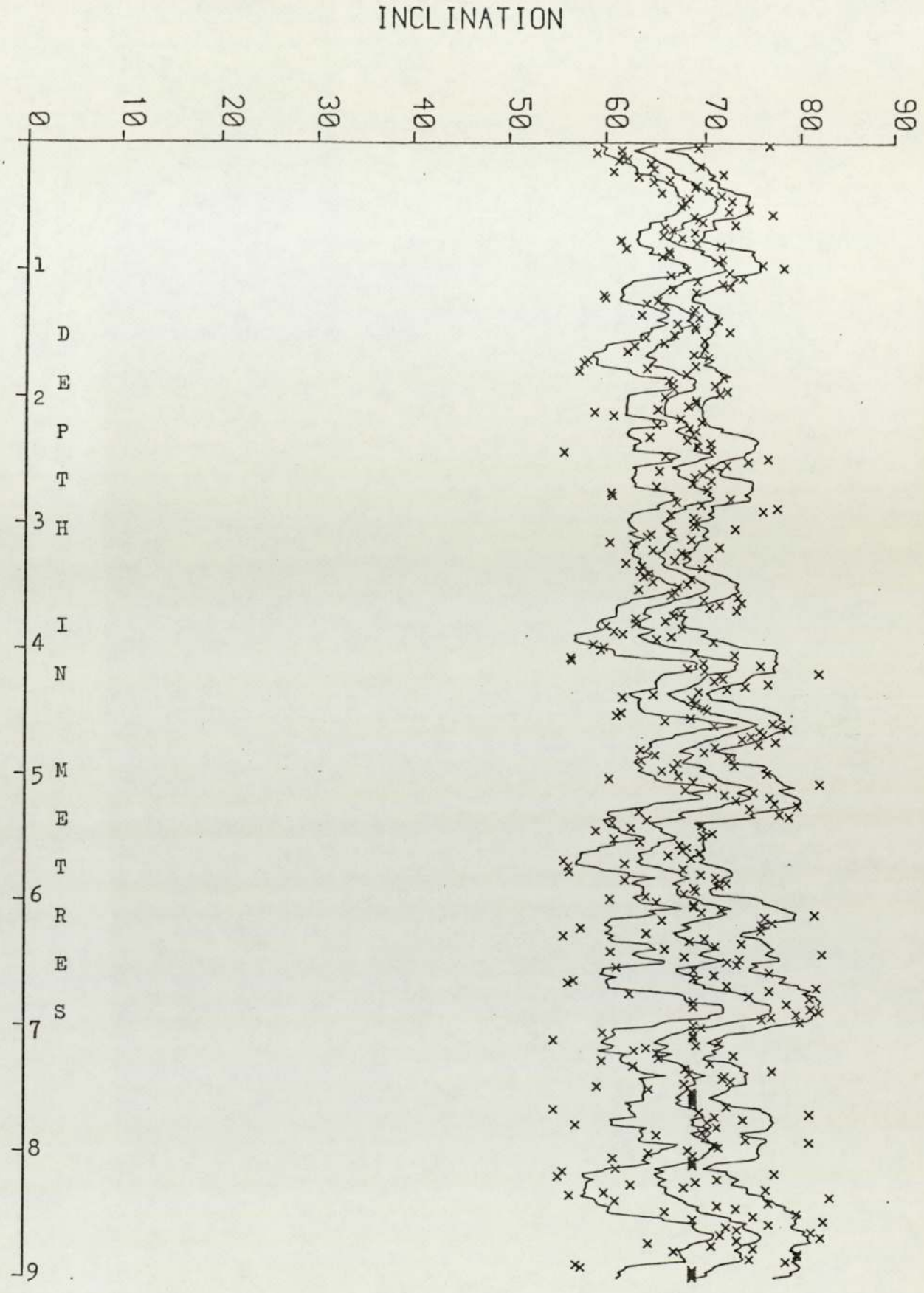


Core D1, odd data set, nine-term smoothing with a 15° filter.

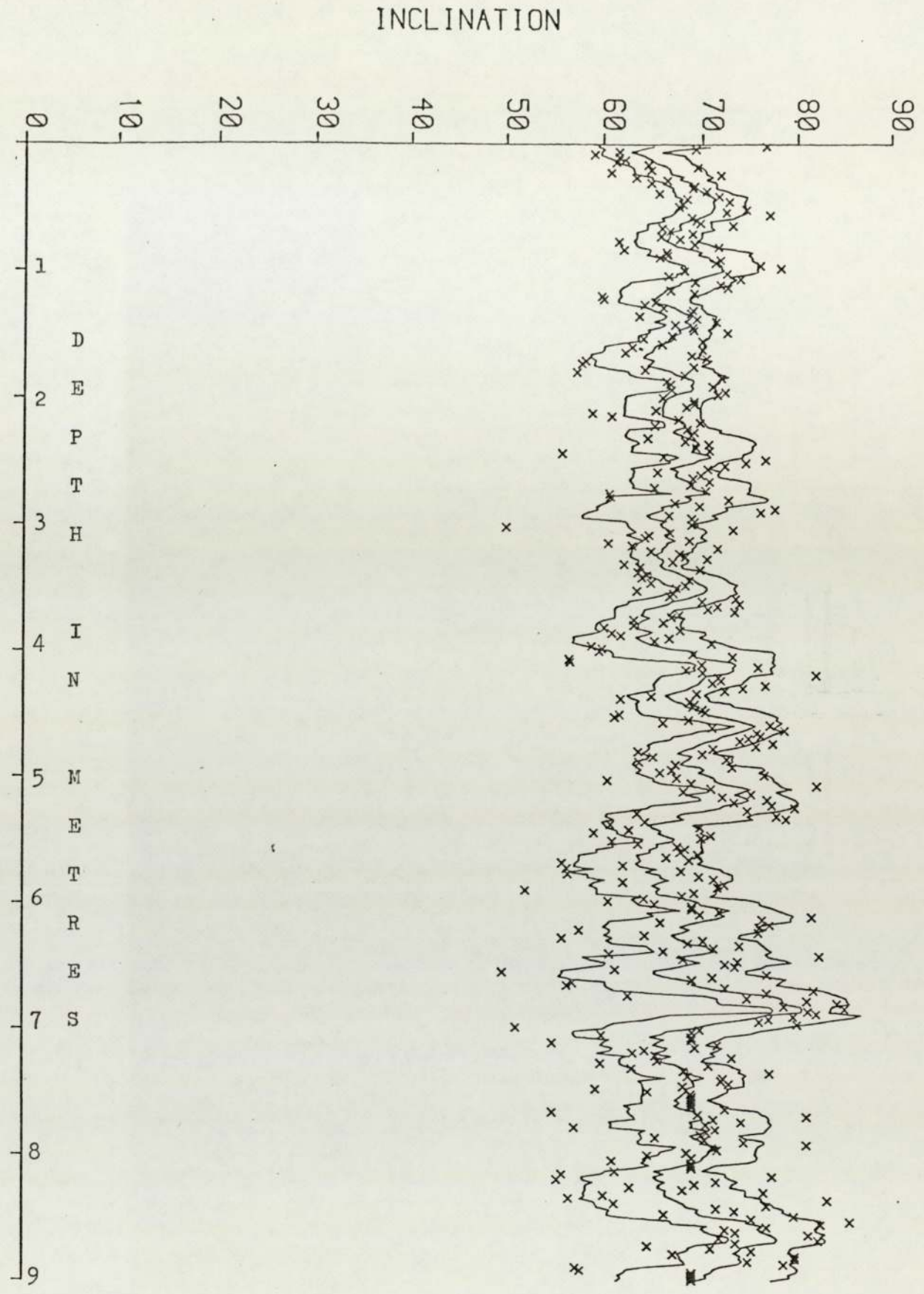


Core D1, odd data set, nine-term smoothing with a 20° filter.

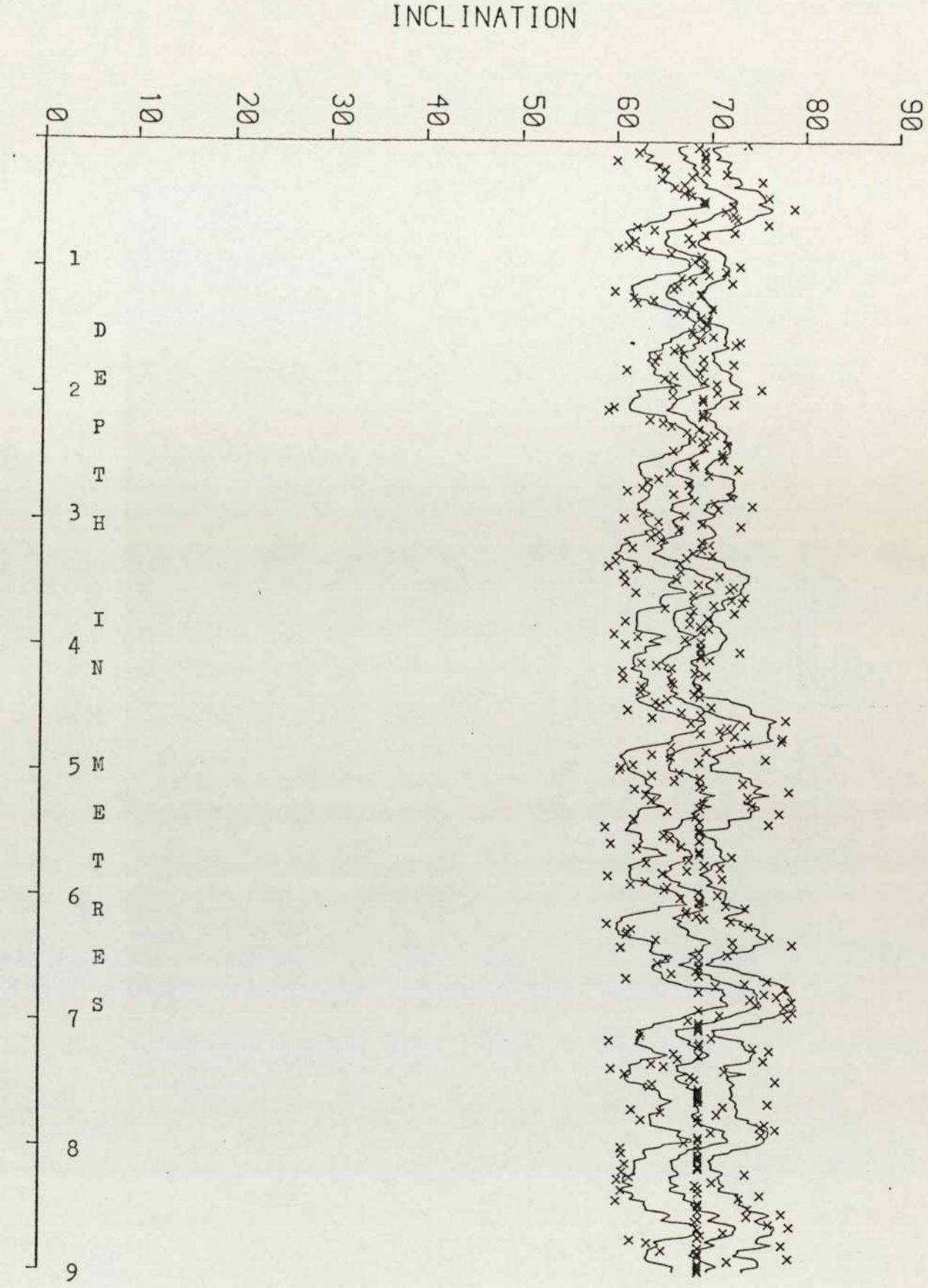


Core D1, even data set, nine-term smoothing with a 10° filter

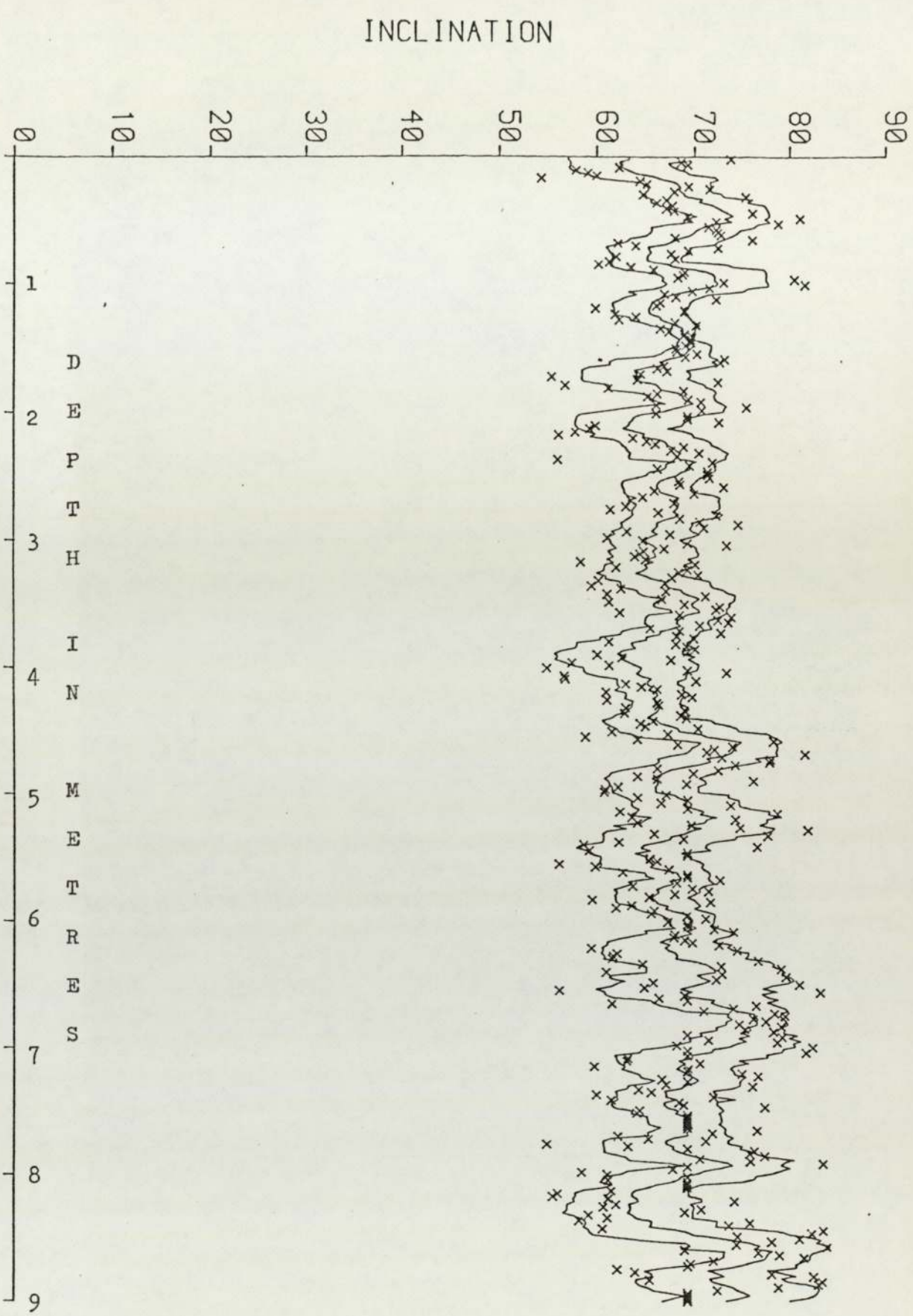


Core D1, even data set, nine-term smoothing with a 15° filter.

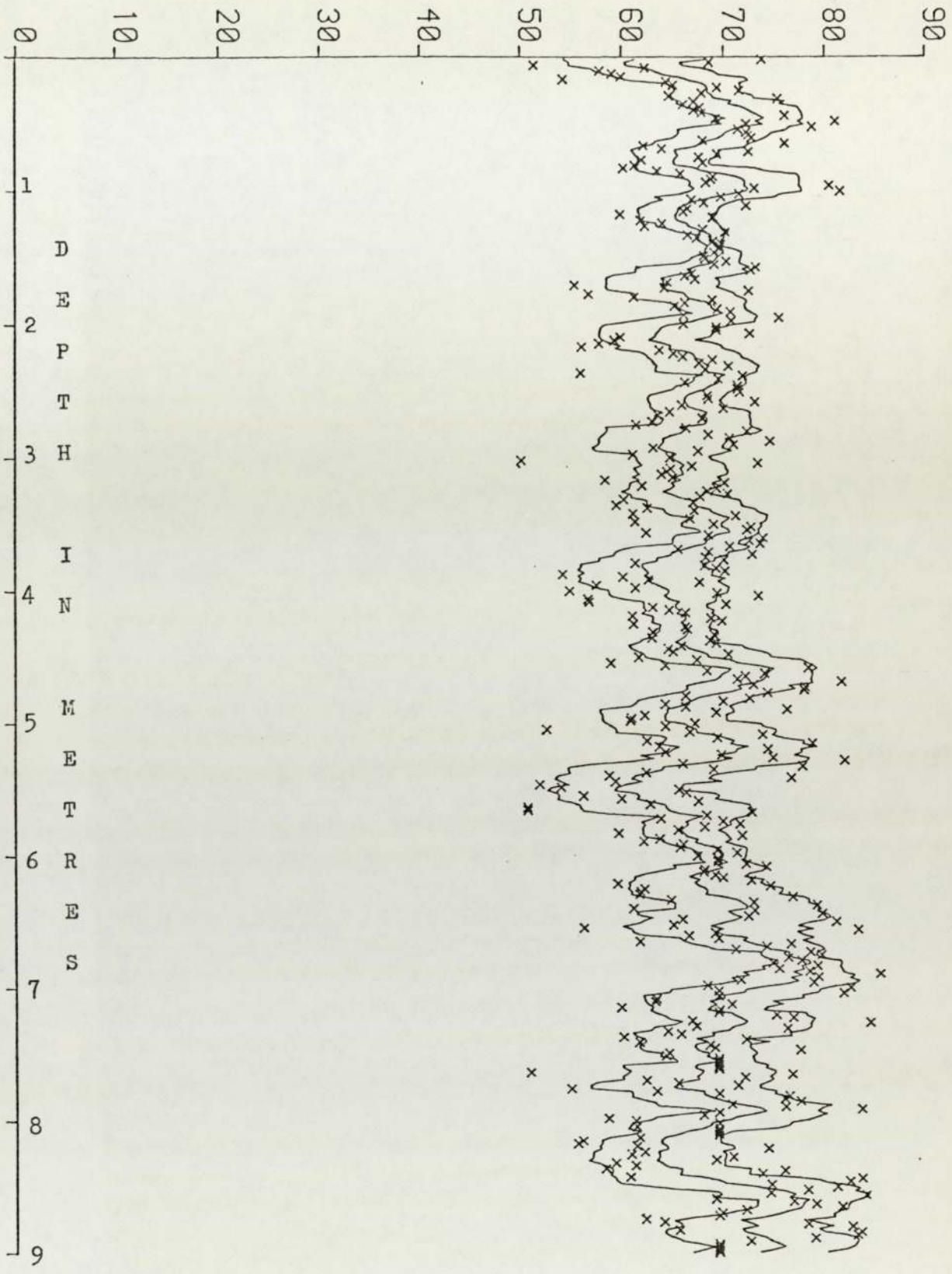


Core D1, even data set, nine-term smoothing with a 20° filter.

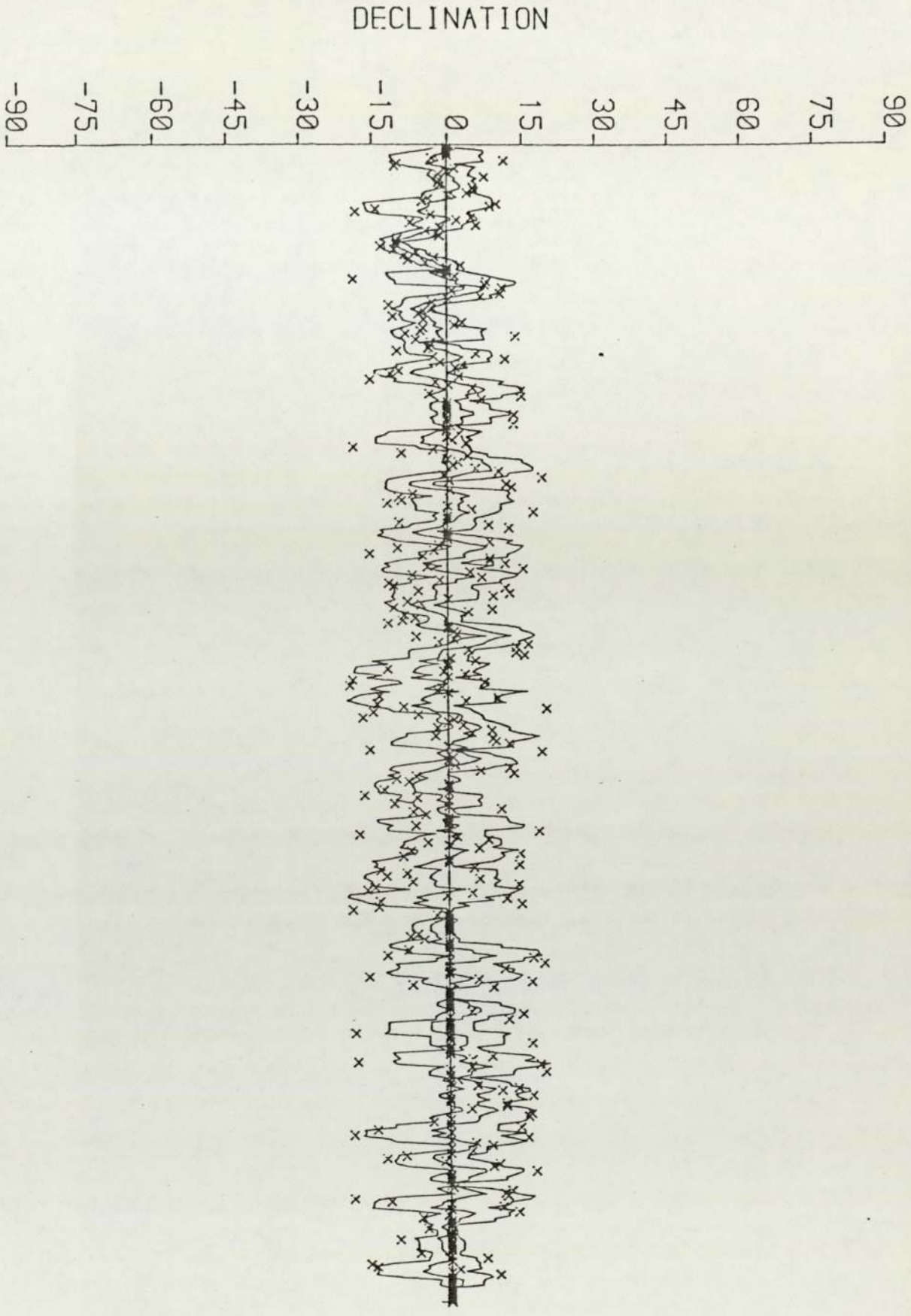


Core D1, odd data set, five-term smoothing with a 20° filter.

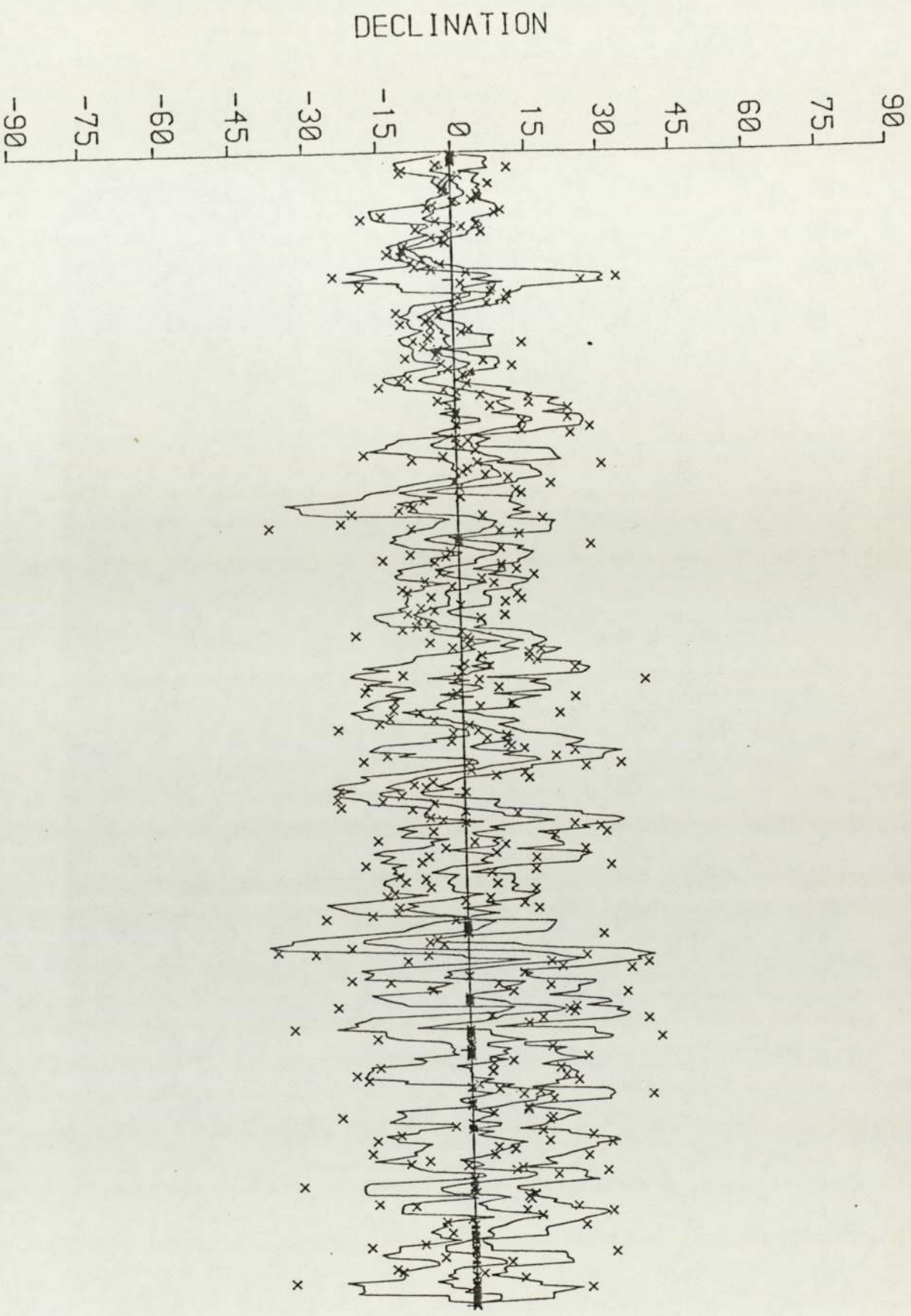


Core D1, odd data set, five-term smoothing with a 40° filter.

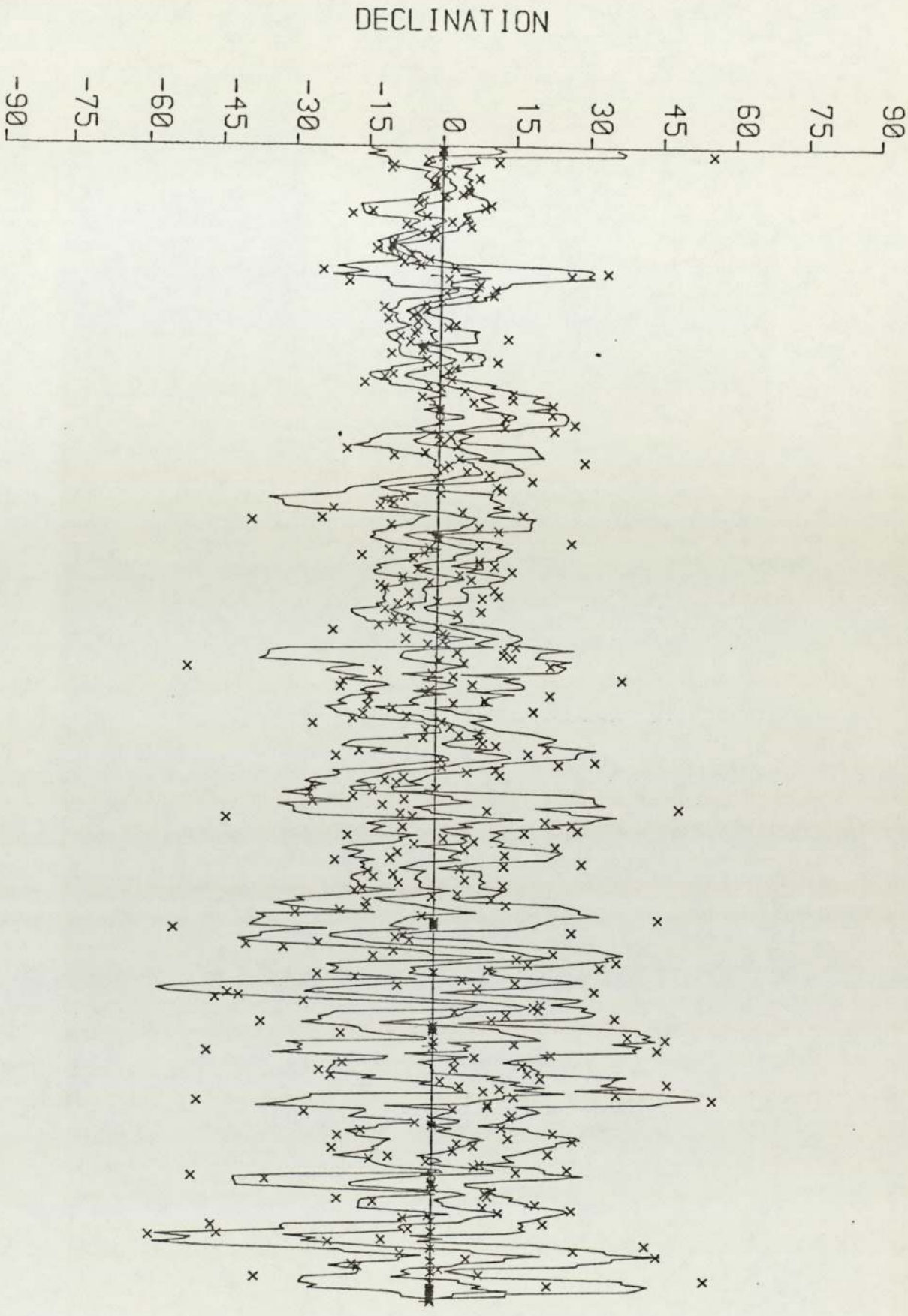


Core D1, odd data set, five term smoothing with a 60° filter.

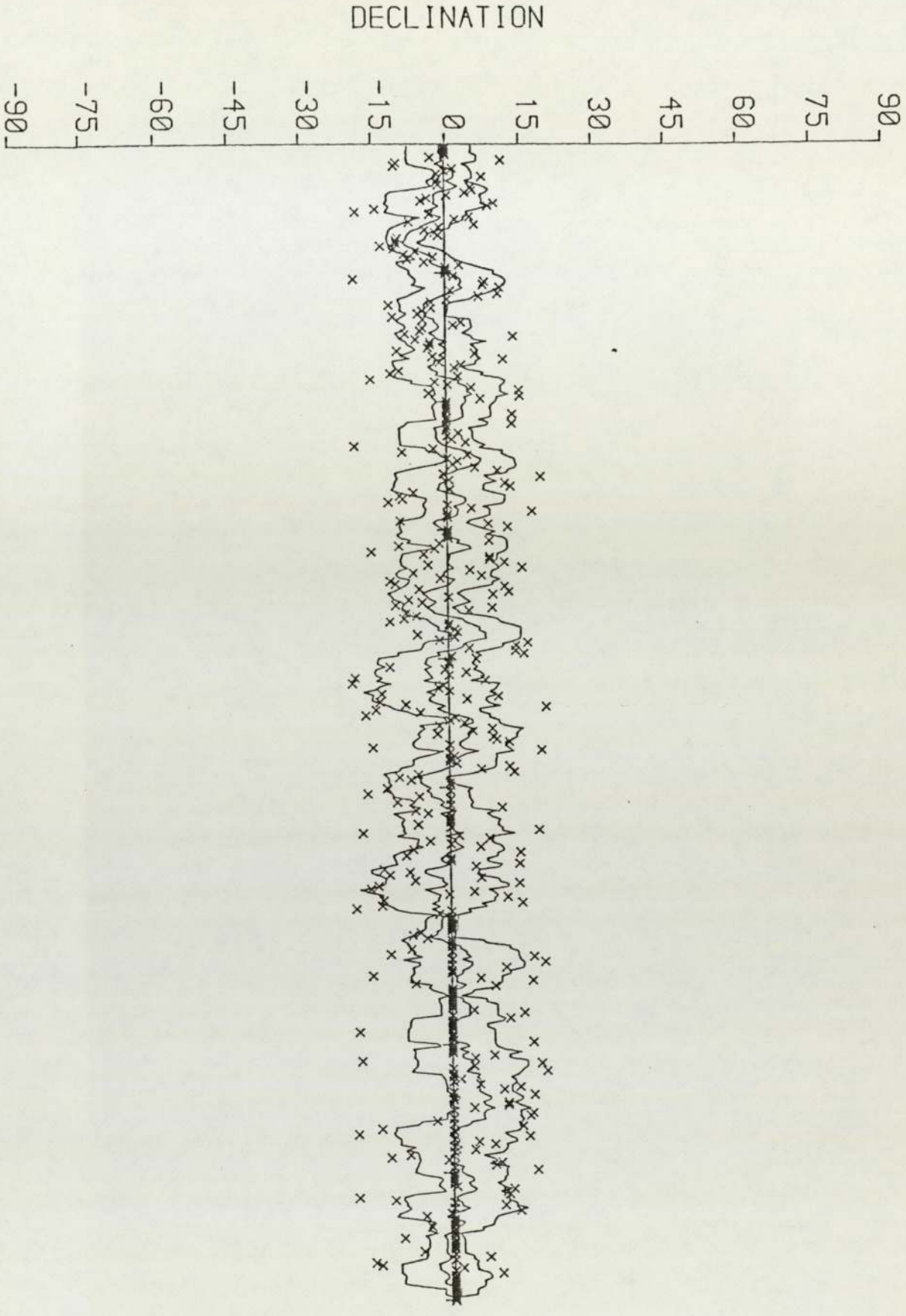


Core D1, odd data set, nine-term smoothing with a 20° filter.

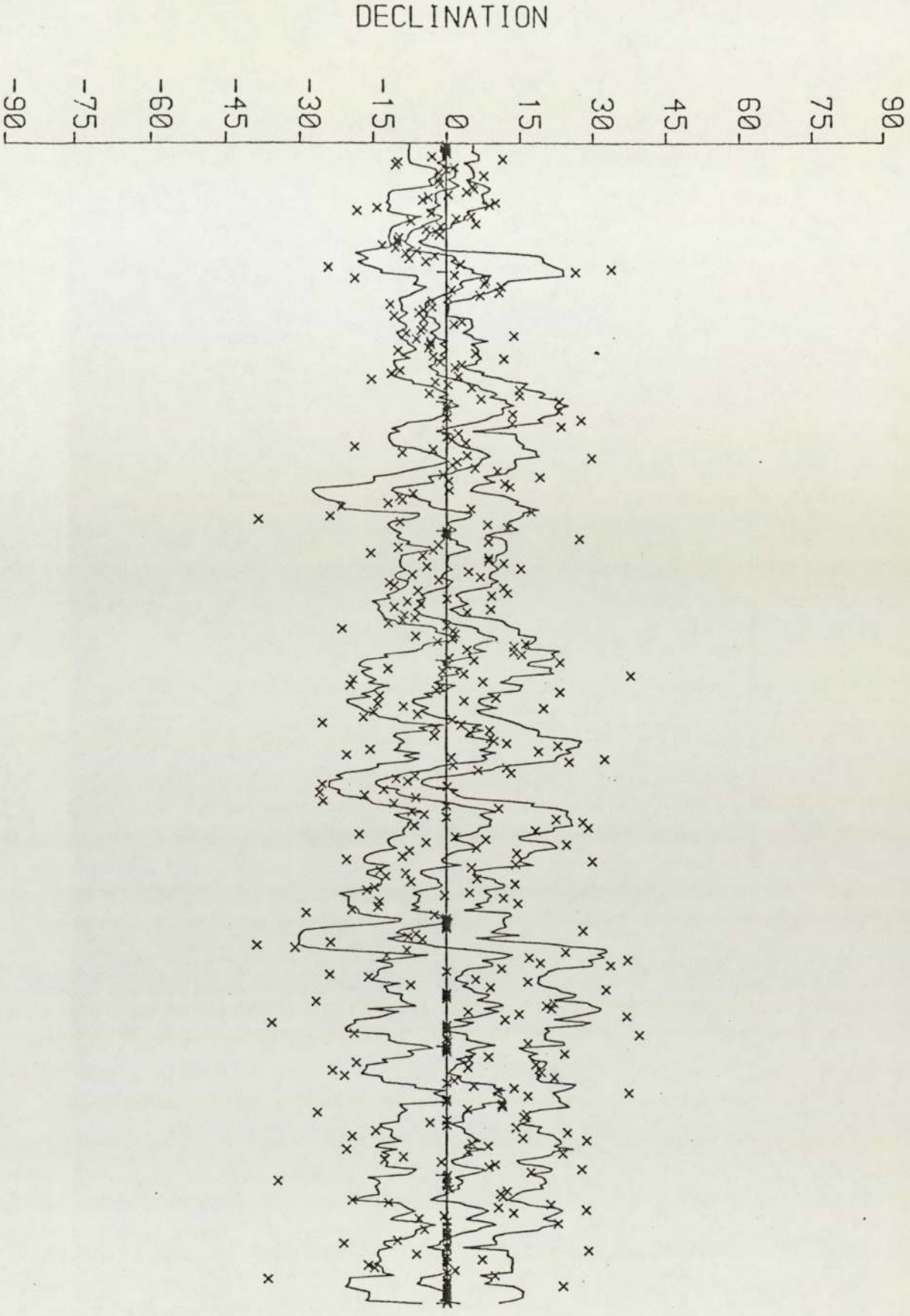


Core D1, odd data set, nine-term smoothing with a 40° filter.

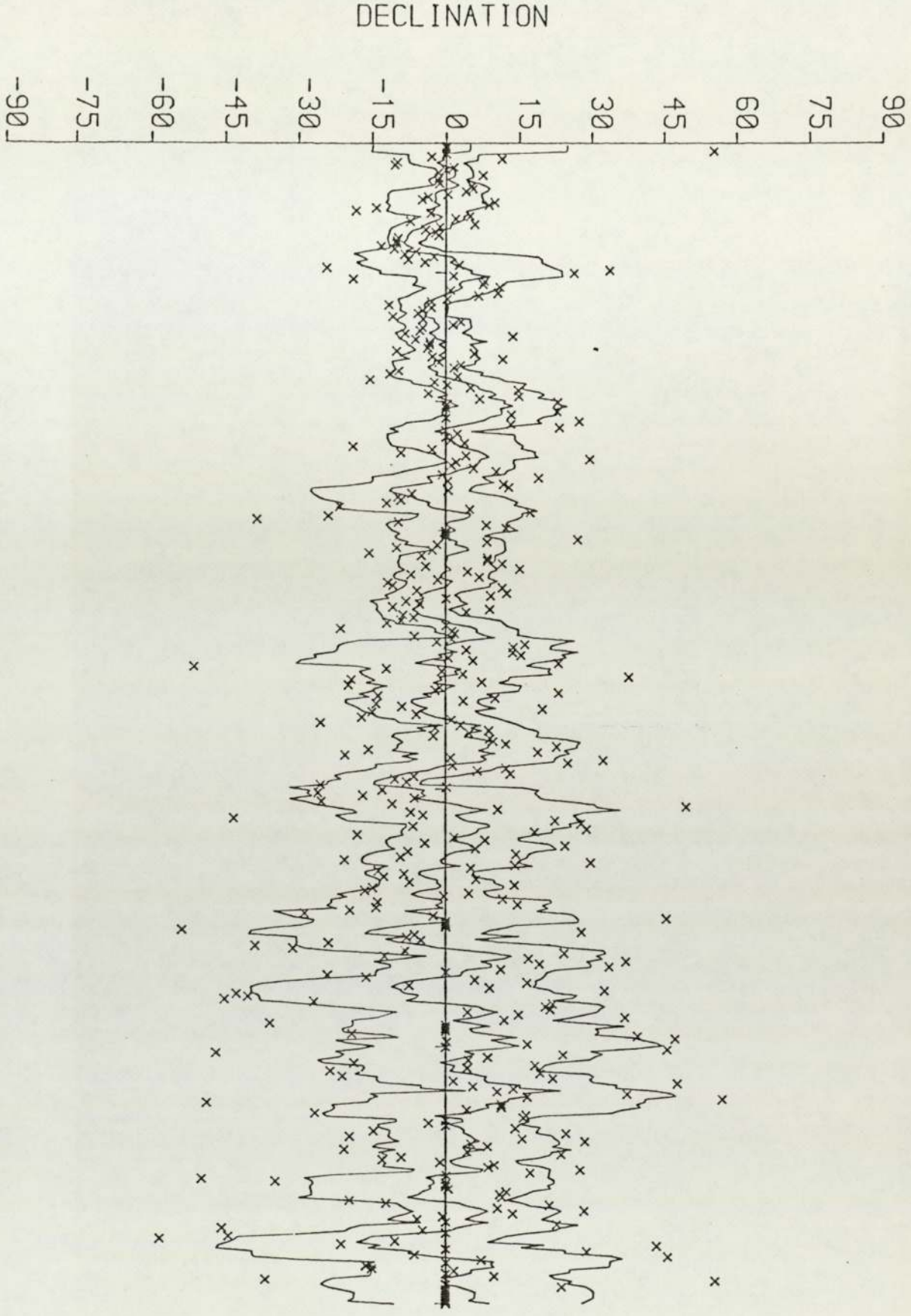


Core D1, odd data set, nine-term smoothing with a 60° filter.

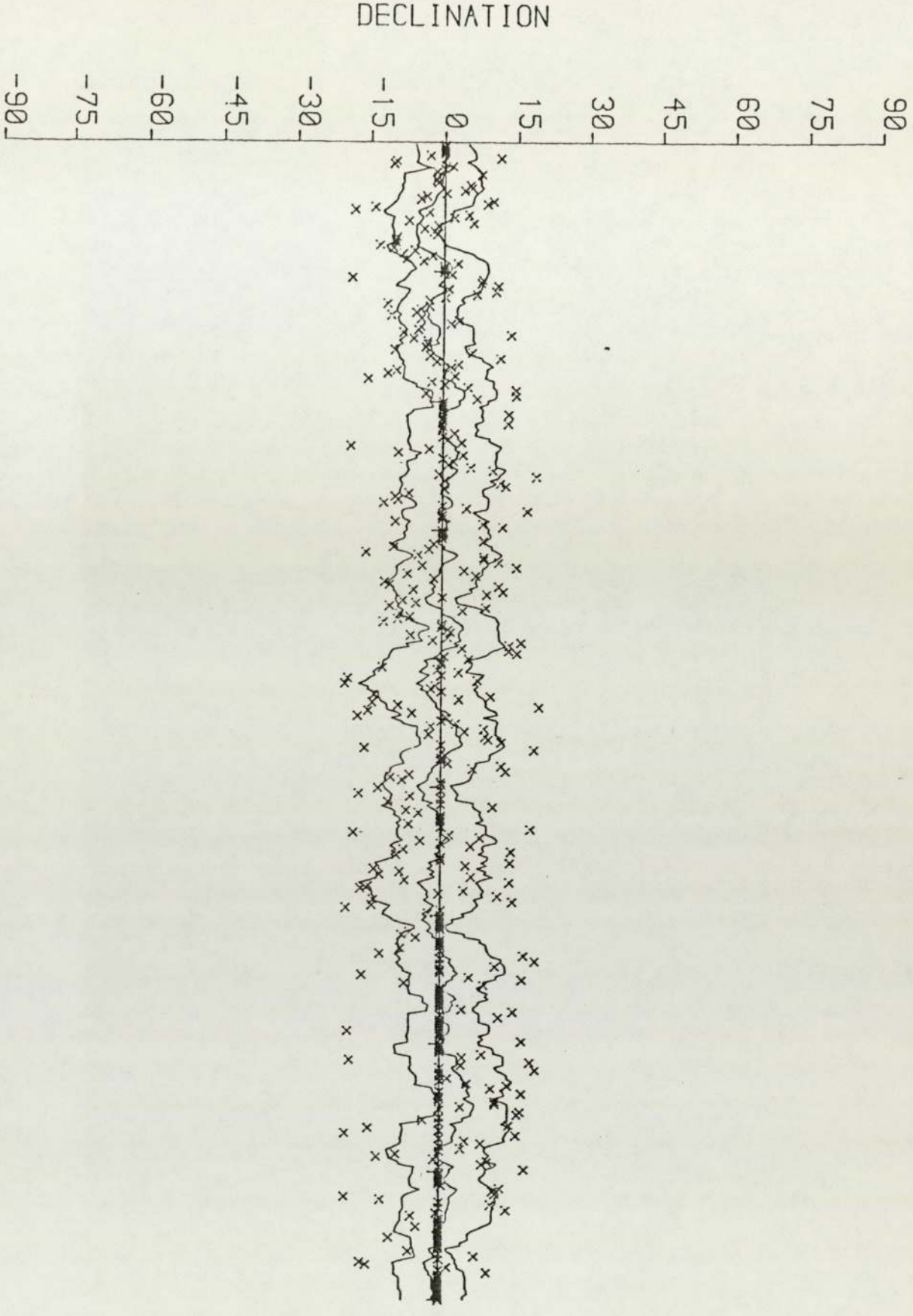


Core D1, odd data set, fifteen-term smoothing with a 20° filter.

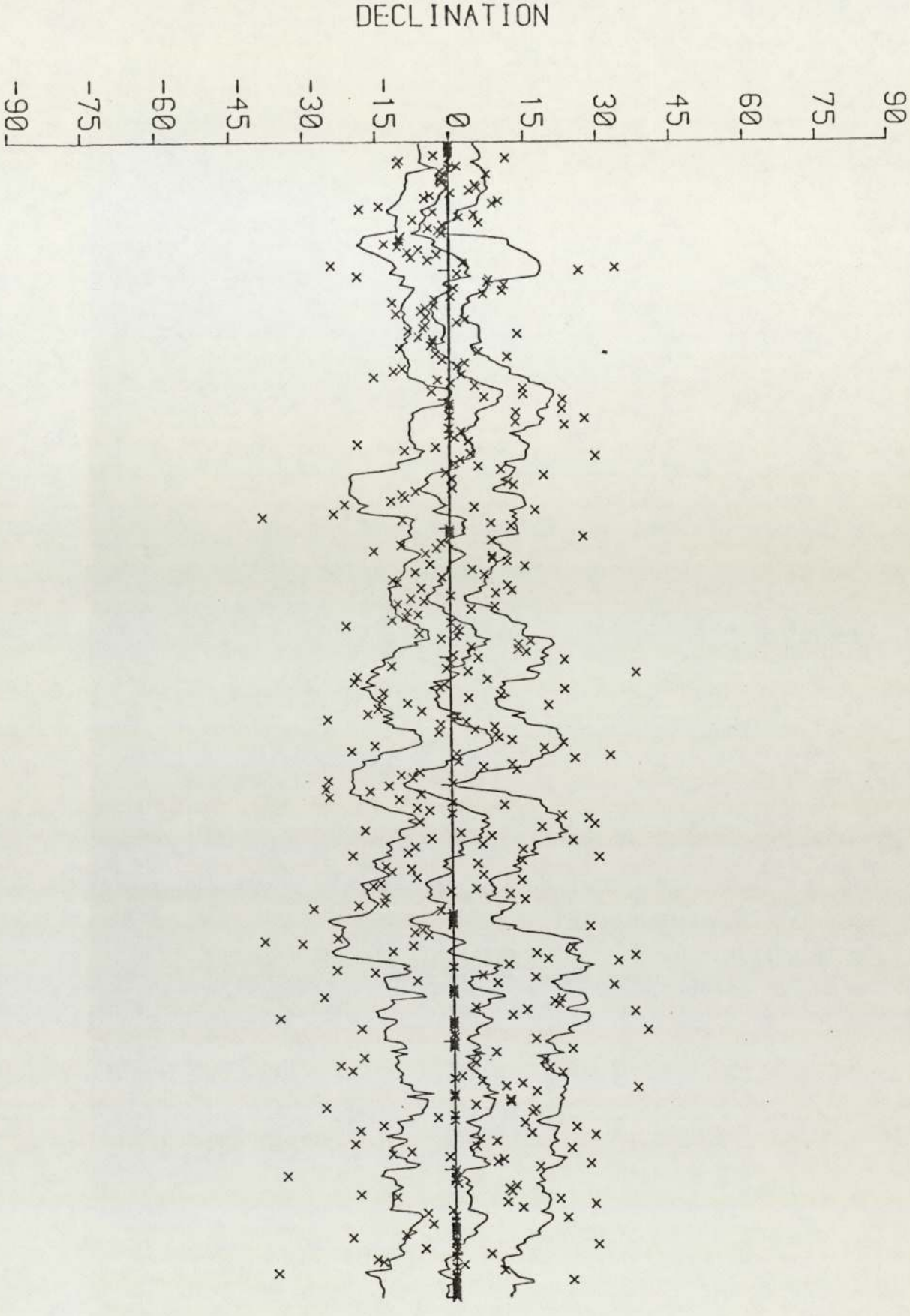


Core D1, odd data set, fifteen-term smoothing with a 40° filter.

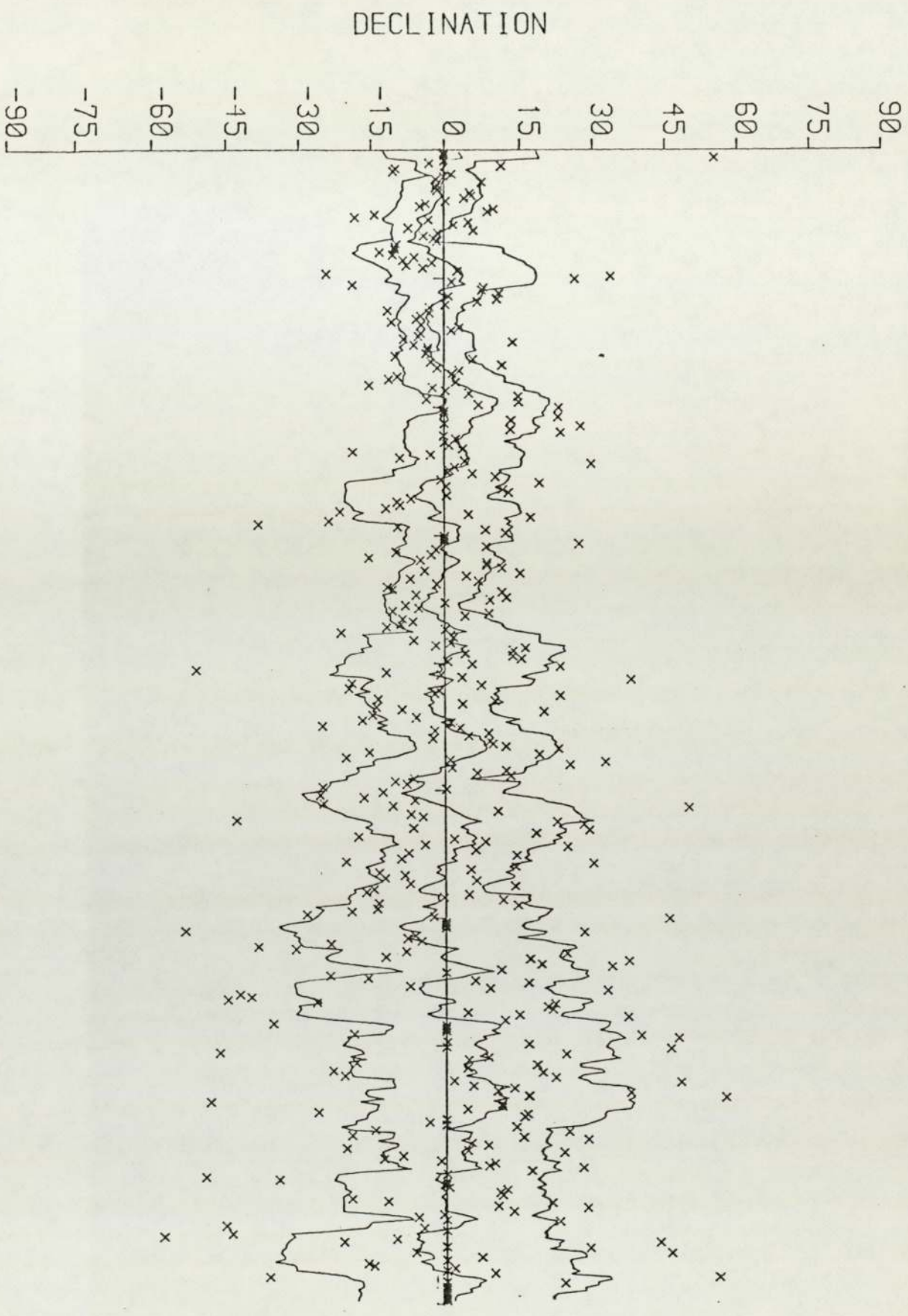


Core D1, odd data set, fifteen-term smoothing with a 60° filter.

REFERENCES.

Admiralty tide tables (1980) European waters, Vol 1. Published by The Hydrographer of the Navy.

Aitken, M.J. (1970) Dating by archaeomagnetic and thermoluminescent methods. Philos. Trans. R. Soc. Lond. 269, 77-88.

Amos, C.L. (1974) Recent sediments of the intertidal zone of the Wash. Unpublished PhD thesis, University of London.

Anderson, E.B., Fenger, J., and Rozen-Hansen, J., (1975) Determination of $Fe^{2+}/Fe^{3+}$ ratios in arfvedsonite by Mössbauer spectroscopy. Lithos, 8 237-246.

Bancroft, G.M., (1973) Mössbauer spectroscopy: An introduction for inorganic chemists and geochemists. McGraw Hill London. 240pp.

Bancroft, G.M., Maddock, A.G., Ong, W.K., Prince, R.H., and Stone, A.J., (1967) Mössbauer spectra of iron III diketone complexes. J. Chem. Soc. 1976, 1966-1971.

Bancroft, G.M., Sham, T.K., Riddle, C., Smith, T.E., and Turek, A. (1977) Ferric/Ferrous-iron ratios in bulk rock samples by Mössbauer spectroscopy - The determination of standard rock samples G-2, W-1 and mica-Fe. Chemical Geology. 19, 277-284.

Banerjee, S.K., O'Reilly, W., Gibb, T.C., and Greewood, N.N. (1967) The behaviour of ferrous ions in iron-titanium spinels. J. Phys. Chem. Solids, 28, 1323-1335.

Bauer, L.A., (1897) On the secular motion of a free magnetic needle II. Physical Review, 3, 34-48.

Berner, R.A., (1964a) Stability fields of iron minerals in anaerobic marine sediments. J.Geol. 72, 826-34.

Berner, R.A. (1964b) Iron sulphides formed from aqueous solution at low temperatures and atmospheric pressure. J.Geol., 72

293-306.

Berner, R.A. (1964c) Distribution and diagenesis of sulphur in some sediments from the Gulf of California. Marine Geology, 1, 117-140.

Berner, R.A. (1967) Thermodynamic stability of sedimentary iron sulphides. Am.J. Sci., 265, 773-785.

Berner, R.A. (1969) Migration of iron and sulphur within anaerobic sediments during early diagenesis. Am. J. Sci. 267, 19-42

Berner, R.A. (1970) Pleistocene sea levels possibly indicated by buried black sediments in the Black Sea. Nature, 227, 700.

Berner, R.A. (1971) Principles of Chemical Sedimentology. McGraw-Hill, New York. 256pp.

Berner, R.A. (1974) Iron sulphides in Pleistocene deep Black Sea sediments and their palaeo-oceanographic significance. In: The Black Sea, its Geology, Chemistry and Biology, edited by Degens, E.T., and Ross, D.A., Mem. Amer. Assoc. Pet. Geol.

Bishop, A.W. (1948) A new sampling tool for use in cohesionless sands below water level. Geot. 1, 125-131.

Bishop, P. (1975) The palaeomagnetism of muddy sediment cores from the Inner Sound, north west Scotland, and the glacial and post glacial history of sedimentation in the area. Earth Planet. Sci. Lett., 27, 51-56.

Blatt, H., Middleton,G., and Murray, R. (1972) Origin of Sedimentary Rocks, Prentice-Hall Inc., New Jersey. 634pp.

Blow, R.A. and Hamilton, N. (1974) Geomagnetic secular variation in recent sediments from the Tyrrhenian Sea. Earth Planet. Sci. Lett., 22, 417-422.

Bowen, L.H., Weed, S.B., and Stevens, J.G. (1969) Mössbauer study of micas and their potassium-depleted products. Am. Min., 54, 72-84.

Brindley, G.W. (1961) In: Brown, G. The X-ray identification and crystal structures of clay minerals. Min. Soc. (Clay Minerals Group) London.

Burst, J.F. (1959) Post diagenetic clay mineral environmental relationships in the Gulf Coast Eocene. Clays and Clay Minerals, 6, 327-341

Burst, J.F. (1969) Diagenesis of Gulf Coast clayey sediments and its possible relation to petroleum migration. Bull. Am. Assoc. Petrol. Geologists, 53, 73-93.

Carrol, D. (1958) Role of clay minerals in the transportation of iron. Geochim. et Cosmochim. Acta, 14, 1-27.

Carrol, D. (1970) Clay minerals: A guide to their X-ray identification. Geol. Soc. Am., Spec. Paper. 126, 80pp.

Chang, S.C. (1971) A study of the heavy minerals of the coastal sediments of the Wash and adjacent area. Unpublished M. Phil. thesis, University of London.

Clarke, R.M. (1976) Non-parametric estimation of a smooth regression function. J. R. stat. Soc. 39, 107-113.

Coey, J.M.D. (1975) Iron in a post-glacial lake sediment, a Mössbauer effect study. Geochim. et Cosmochim. Acta, 39, 401-415.

Coey, J.M.D., Schindler, D.W. and Weber, F. (1974) Iron compounds in lake sediments. Can. J. Earth Sci. 11, 1489-1491.

Coey, J.M.D., Spender, M.R., and Morrish, A.M. (1970) The magnetic structure of the spinel, $Fe_3S_4$. Solid State Comm. 8, 1605-1608.

Creer, K.M. (1974) Geomagnetic variations for the interval 7000-25000 yr B.P. as recorded in a core of sediment from station 1474 of the Black Sea Cruise of "Atlantis II". Earth Planet. Sci. Lett. 23, 34-42.

Creer, K.M., Thompson, R.? Molyneux, L., and Mackereth, F.J.H. (1972) Geomagnetic secular variation recorded in the stable magnetic remanence of recent sediments. Earth Planet. Sci. Lett. 14, 115-127.

Creer, K.M., Molyneux, L., Vernet, J.P., and Wagner, J.J. (1975) Palaeomagnetic dating of one-metre cores of sediment from Lake Geneva. Earth Planet. Sci. Lett. 28, 127-132

Creer, K.M., Anderson, T.W., and Lewis, C.F.M. (1976) Late Quaternary geomagnetic stratigraphy recorded in Lake Erie sediments. Earth. Planet. Sci. Lett. 31, 37-47.

Creer, K.M., Gross, D.L. and Lineback, J.A. (1976) Origin of regional geomagnetic vatiations recorded by Wisconsinian and Holocene sediments from Lake Michigan, USA., and Lake Windermere, England. Geol. Soc. Am. Bull. 87, 531-540.

Creer, K.M. and Kopper, J.S. (1976) Secular oscillations of the geomagnetic field recorded by sediments deposited in caves in the Mediterranean region. Geophys. J. R. astr. Soc. 45, 35-58.

Creer, K.M., Hogg, E., Malkowski, Z., Mojski, J.E., Niedziolka-Krol, E., Readman, P.W. and Tucholka, P. (1979) Paleomagnetism of Holocene lake sediments from north Poland. Geophys. J. R. astr. Soc. 59, 287-313.

Davies, J.C. (1973) Statistics and data analysis in geology. Wiley, New York. 550pp.

Deer, W.A., Howie, R.A. and Zussman, J. (1966) An introduction to the rock forming minerals. Longman, London.

Dickson, J.H., Stewart, D.A., Thompson, R., Turner, G., Baxter, M.S., Drndarsky, N.D., and Rose, J. (1978) Palynology, palaeomagnetism and radiometric dating of Flandrian marine and freshwater sediments of Loch Lomond. Nature 274, 548-553.

Doyle, L.J., Hopkins, T.L. and Betzer, P.R. (1976) Black magnetic spherule fallout in the eastern Gulf of Mexico. Science 194, 1157-1159.

Doyle, R.W. (1968) Identification and stability of iron sulphide in anaerobic lake sediment. Am.J.Sci. 266, 980-994.

Dunlop, D.J. (1972) Magnetic mineralogy of unheated and heated red sediments by coercivity spectrum analysis. Geophys. J. R. astro. Soc. 27, 37-55.

Durrance, E.M., Meads, D.E., Ballard, C.B.B. and Walsh, L.N. (1978) Oxidation state of iron in the Littleham Mudstone Formation of the New Red Sandstone Series (Permian-Triassic) of southeast Devon, England. Geol. Soc. Am. Bull. 89, 1231-1240.

Evans, B.J. and Haffner, S.S (1969) $^{57}Fe$ hyperfine fields in magnetite ($Fe_3O_4$). J. Appl. Phys. 40, 1411-1413.

Evans, G. (1965) Intertidal flat sediments and their environments of deposition in the Wash. Q. J. Geol Soc. Lond. 121, 209-245.

Evans, G. and Collins, M.B. (1975) The transportation and deposition of suspended sediment over the inter-tidal flats of the Wash. In: Nearshore Sediment Dynamics and Sedimentation. edited by Hall, J.,Wiley. London p273-306.

Folk, R.L. and Ward, W.C. (1957) Brazos river bar: A study in the significance of grain size parameters. J. Sed. Pet., 27, 3-27.

Forsyth, J.B., Hedley, I.G., and Johnson, C.E. (1968) The magnetic structure and hyperfine field of goethite ( FeOOH). J. Phys. (Proc. Phys. Soc.) 1, 179-194

Gary, M., McAfee, R., and Wolf, C.L. (editors) (1972) Glossary of Geology. Amer. Geol. Inst. Washington.

Gibbs, R.J. (1965) Error due to segregation in quantitative clay mineral X-ray diffraction techniques. Am. Min. 50, 741-751.

Gifford, J.A. (1969) An hydraulic corer for use in a water saturated sediment. J. Sed. Pet. 39, 1619-1621.

Giovanoli, F. and Kelts, K. (1980) Magnetic properties and formation of Mackinawite (FeS) in 11,000 year old mud turbidites from Lake Zurich. Abstracts of the 7th Annual meeting of the E.G.S., Budapest.

Godwin, H and Clifford, M.H. (1938) Studies of the post-glacial history of British vegetation. I Origin and stratigraphy of Fenland deposits near Woodwalton, Hunts. II Origin and Stratigraphy of deposits in the southern Fenland. Phil. Trans. 229, 323-406.

Goodman, B.A. and Bain, D.C. (1978) Mössbauer spectra of chlorites and their decomposition products. In: International Clay Conference 1978. Developments in Sedimentology No. 27. Edited by M.M Mortland and V.C. Farmer. p65-74. Elsevier, Amsterdam.

Graham, S. (1974) Remanent magnetization of Modern tidal flat sediments from San Francisco Bay, California. Geology, 2, 223-226.

Greenwood, N.N., and Gibb, T.C. (1971) Mössbauer spectroscopy. Chapman and Hall Ltd, London 659pp.

Griffin, G.M. (1971) Quantitative analysis of clay minerals: In Proceedures in Sedimentary Petrology (edited by R.E. Carver) Wiley Interscience, p531-539.

Hantzschel, W. (1955) Tidal flat deposits. In: Recent marine sediments. Tulsa, Oklahoma. (A.A.P.G.)

Hardy, F. (1920) The mineral composition of the modern Fenland silt, with special reference to carbonate minerals. Geol. Mag. 57, 543-551.

Hayes, M.O. (1976) Morphology of sand accummulation in estuaries: An introduction to the symposium. In: Esturine Research. Vol. II : Geology and Engineering, (edited by Gronin, L.E.) Academic Press, London, p3-22.

Hayes, M.O. and Kana, T.W. (1976) Terrigenous clastic depositional environments - some modern examples. II-184, Tech. Rept. II-CRD. Coastal Res. Div., Univ. S. Carolina. p 1-131.

Hedley, I.G. and Vandievoet, E. (1980) Magnetic mineralogy of a Mediterranean Sea core. Abstracts of the 7th Annual meeting of the E.G.S., Budapest.

Hogg, C.S. and Meads, R.E. (1970) The Mössbauer spectra of several micas and related minerals. Min. Mag. 37, 606-614.

Hutchinson, G.E. (1957) A treatise on limnology, vol. 1, Geography, physics, and chemistry. Wiley, New York.

Hydraulics Research (1958) The Wash, Hydraulic Research Station, 35-42.

Imbert, J.E., Gerard, A., and Wintenberger, M. (1963) Etude des sulfure arseniosulfure et arseniure de fer naturels par effect Mössbauer. C. R. 256, 4391-4393.

Inglis, G.C and Kestner, F.J.T. (1958) Changes in the Wash as affected by training walls and reclaimation works. Proc. Inst. Civ. Engin., II: 435-466.

Irving, E and Major,A (1964) Post-depositional detrital remanent magnetization in a synthetic sediment. Sedimentology 3, 135-143.

Johnson, H.P., Lowrie, W. and Kent, D.V. (1975) Stability of anhysteritic remanent magnetization in fine and coarse magnetite and maghemite particles. Geophys. J.R. astro. Soc. 41, 1-10.

Jowsey, P.C. (1966) An improved peat sampler. New Phytol. 65, 245-248.

Kaplan, I.R., Emery, K.O. and Rittenburg, S.C. (1963). The distribution and isotropic abundances of sulphur in Recent marine sediments off southern California. Geochim. et Cosmochim. Acta. 27, 297-332.

Kent, D.V. and Lowrie, W. (1974) Origin of magnetic instability in sediment cores from the central North Pacific. J. Geophys. Res. 79, 2987-3000.

Kestner, F.J.T. (1962) The old coastline of the Wash. Geogr. J. 128, 457-478.

Kjellman, W., Kallstenius, T. and Wager, O. (1950) Soil sampler with metal foils. Device for taking undisturbed samples of very great length. R. Swed. Geotech. Inst. Proc. 1.

Kundig, W. and Hargrove, R.S. (1969) Electron hopping in magnetite. Solid. State. Comm. 7, 223-227.

Littlewood, D.D. and Postgate, J.R. (1967) Sodium chloride and the growth of Desulphovibrio desulphuricans. J. Gen Biol. 17, 378-383.

Loon, J.C, van, and Parisis, C.M. (1969) Scheme of silicate analysis based on the lithium metaborate fusion technique followed by atomic absorption spectrophotometry. The Analyst, 94, 1057-1168

Lowrie, W. and Fuller, M. (1971) On the alternating field demagnetization characteristics of multidomain thermoremanent magnetization in magnetite. J. Geophys. Res. 76, 6339-6349.

Love, L.G. (1967) Early diagenetic iron sulphide in Recent sediments of the Wash (England). Sedimentology 9, 327-352.

McElhinney, M.W. (1973) Palaeomagnetism and Plate Tectonics. Camb. Earth Sci. Series. Cambridge Univ, Press. 358pp.

McElhinney, M.W. and Opdyke, N.D. (1973) Remagnetic study of the Trenton Limestone, New York State. Geol. Soc. Am. Bull. 84, 3697-3708.

Mackereth, F.J.H. (1958) A portable core sampler for lake deposits. Limnology and Oceanography 3, 181 - 191.

Mackereth, F.J.H. (1971) On the variation in the direction of the horizontal component of remanent magnetization in lake sediments. Earth Planet. Sci. Lett. 12, 332-338.

Malden, P.J. and Meads, R.E. (1967) Substitution by iron in kaolinite. Nature, 215, 844-846.

Manning, P.G. and Ash, L.A. (1978) Mössbauer studies of pyrite, ferric and high-spin ferrous distributions in sulphide-rich sediments from Moira Lake, Ontario. (in press).

Manning, P.G., Williams, J.D.H., Charlton, M.N., Ash, L.A., and Birchall, T. (1979) Mössbauer spectral studies of the diagenesis of iron in a sulphide-rich sediment core. Nature 280, 135-137.

Millot, G. (1970) Geology of Clays. Springer-Verlag, New York, 429pp.

Morice, J.A., Rees, L.V.C. and Rickard, D.T. (1969). Mössbauer studies of iron sulphides. J. inorg. nucl. Chem. 31, 3797-3802.

Murad, E. (1970) Mössbauer spectra of goethite: evidence for structural imperfections. Min. Mag. 43, 355-361.

Murray, R.G. (1956) Recent sediments of three Wisconsin lakes. Geol. Soc. Amer. Bull. 67, 883-910.

Noel, M (1975) The palaeomagnetism of varved clays from Blekinge southern Sweden. Geologiska Foreningens i Stockholm Forhandlingar, 97, 357-367.

Oldfield, F, Thompson, R. and Barker, K.E. (1978) Changing atmospheric fallout of magnetic particles in Recent ombrotropic peat sediments. Science, 199, 679-680.

O'Reilly, W. and Readman, P.W. (1971) The preparation and unmixing of cation deficient titanomagnetites. Zeitschriftfür Geophysik, 37, 321-327.

Palmer, D.F., Henyey, T.L., and Dodson, R.E. (1979) Palaeomagnetic and sedimentological studies at Lake Tahoe, California, Nevada. Earth Planet. Sci. Lett. 46, 125-137.

Parkin, D.W., Phillips, D.R. and Sullivan, R.A.L. (1970) Airborne dust collections over the north Atlantic. J. Geophys. Res. 75, 1782-1793.

Perry, E. and Hower, J. (1970). Burial diagenesis in Gulf Coast pelitic sediments. Clays and Clay Mins. 18, 165-177.

Postgate, J. (1958) The chemical physiology of the sulphate reducing bacteria. Producers Monthly, 22, 12-16.

Powers, M.C. (1957) Adjustment of land derived clays to the marine environment. J. Sed. Pet. 27, 355-372.

Preston, H. (1921) Sectional Officers Reports. Trans. Linc. Nat. Union. 160-161.

Raclavsky, K., Sitek, J., and Lipka,J. (1975) Mössbauer spectroscopy of iron in clay minerals. In: 5th Int. Conf. Mössbauer spect., Proc. Part 2, 368-371.

Rees, A.I., and Frederick, D. (1974) The magnetic fabric of samples from the deep sea drilling project, Legs I-VI. J.Sed. Pet. 44, 655-662.

Reineck, H.E. (1975) German North Sea tidal flats. In: Tidal Deposits (edited by R.N. Ginsburg) Springer-Verlag, Berlin.

Reineck, H.E. and Singh, I.B. (1975) Depositional sedimentary environments. Springer-Verlag, Berlin 439pp.

Rickard, D.T. (1969) The chemistry of iron sulphide formation at low temperatures. Stockholm Contributions in Geology Vol XX: 4.

Rickard, D.T. (1975) Kinetics and mechanism of pyrite formation at low temperatures. Amer. J. Sci., 275, 636-652.

Rozenson, I. and Heller-Kallai, L. (1977) Mössbauer spectra of dioctahedral smectites. Clays and Clay Mins., 25, 94-101.

Shapiro, J. (1964) Effect of yellow organic acids on iron and other metals in water. Am. Water Works Ass. J. 56, 1062.

Shaw, H.F. (1973) Clay mineralogy of Quaternary sediments in the Wash embayment, eastern England. Marine Geology, 14, 29-45.

Shishkinia, O.V. (1961) Sulfaty vilovykh vodakh Chernogo morya (Sulphate in the pore waters of the Black Sea sediments). Akad. Nauk. SSR Inst. Okeanologii Trudy, 33, 178-193.

Stephenson, A. and Collinson, D.W. (1974) Lunar magnetic field palaeointensities determined by an anhysteritic remanent magnetization method. Earth Planet. Sci. Letts. 23, 220-228.

Stevens, J.G. and Stevens, V.E. (1958-1976) Mössbauer Effect Data Index. Plenum Press.

Stober, J.C. and Thompson, R. (1977) Palaeomagnetic secular variation of Finnish lake sediment and the carriers of remanence. Earth Planet. Sci. Letts. 37, 139-144.

Straaten, L.M.J.U., van, (1952a) Biogene textures and the formation of shell beds in the Dutch Wadden Sea (I). Proc. Koninkl. Ned. Akad. Wetenschap. 55, 500-508.

Straaten, L.M.J.U., van, (1952b) Biogene textures and the formation of shell beds in the Dutch Wadden Sea (II). Proc. Koninkl. Ned. Akad. Wetenschap. 55, 509-516.

Straaten, L.M.J.U., van, (1954) Composition and structure of Recent marine sediments in the Netherlands. Leid. geol. Meded. 19, 1-110.

Straaten, L.M.J.U., avn, (1961) Sedimentation in tidal flat areas. Jour. Alberta Soc. Pet. geol. 9, 203-213.

Suttill, R.J. (1980a) Post-depositional remanent magnetization in Recent tidal flat sediments. Earth Planet. Sci. Letts. 49, 132-140.

Suttill, R.J. (1980b) Water content: its role in the acquisition and fixation of post-depositional remanence in Recent tidal flat sediments. Abstracts of the 7th annual meeting of the E.G.S., Budapest.

Suttill, R.J., Turner, P. and Vaughan, D.J. (1982) The geochemistry of iron in Recent tidal-flat sediments of the Wash area, England: A mineralogical, Mössbauer, and magnetic study. (in press).

Sweeney, R.E. and Kaplan, I.R. (1973) Pyrite framboid formation: laboratory synthesis and marine sediments. Econ. Geol. 68, 618-634.

Tarling, D.H. (1971) Principles and applications of palaeomagnetism. Chapman and Hall. 164pp.

Taylor, G.L., Ruotsala, A.P. and Keeling, R.D.J.R. (1968). Analysis of iron in layer silicates by Mössbauer spectroscopy. Clays and clay minerals. 16, 381-391.

Temperley, A.A. and Lefevre, H.W. (1966) The Mössbauer effect in marcasite structure iron compounds. J. Phys. Chem. Solids. 27, 85-92

Thellier, E. Geophysique, Encyclopedie de la Pleiade (1971) 236-376.

Thompson, R. (1977) Stratigraphic consequences of palaeomagnetic studies of Pleistocene and Recent sediments. J.Geol Soc. Lond. 133, 51-59.

Thompson, R. (1978) European palaeomagnetic secular variation 13,000-0 BP. Polskie Archiwum Hydrobiologh 25 413-418.

Thompson, R. and Berglund, B (1976) Late Weichselian geomagnetic 'reversal' as a possible example of reinforcement syndrome. Nature 263, 490-491.

Thompson, R., and Kelts K, (1974) Holocene sediments and magnetic stratigraphy from Lakes Zug and Zurich, Switzerland. Sedimentology 21, 577-596.

Thompson, R. and Turner, G.M. (1979) British geomagnetic master curve 10000-0 yr BP for dating European sediments. Geophys. Res. Letts. 6, 249-252.

Trudinger, P.A. (1976) Experimental geomicrobiology in Australia. Earth Sci. Reviews. 12, 259-278.

Vaughan, D.J. (1971) Aspects of structure and bonding in the iron sulphides and related minerals. Unpublished thesis, University of Oxford.

Vaughan, D.J. and Craig, J.R. (1978) Mineral Chemistry of Metal Sulphides. Cambridge University Press, 493pp.

Vaughan, D.J. and Linskill, M. (1979) Computer fitting of Mössbauer spectra. University of Aston in Birmingham. 33pp.

Vaughan, D.J. and Ridout, M. S. (1971) Mössbauer studies of some sulphide minerals. J. inorg. nucl. Chem. 33, 741-746.

Verosub, K.L. (1977) Depositional and post depositional processes in the magnetization of sediments. Rev. Geophys. Space Phys. 15, 129-143.

Weaver, C.E., Wampler, J.M., and Pecuil, T.E. (1967) Mössbauer analysis of iron in clay minerals. Science 156, 504-508.

Wedepohl, K.H. (1969) Handbook of Geochemistry. Springer-Verlag Berlin.

Wentworth, C.K. (1922) A scale of grade and class terms for clastic sediments. J. Geol. 30, 377-392.